https://ntrs.nasa.gov/search.jsp?R=19820024507 2020-03-21T06:17:22+00:00Z

NASA CR-165149

3 1176 00161 4974

NASA CR-165149
PWA-5594-92

NASA-CR-165149
19820024507

FOR EARLY DOMESTIC DISSEMINATION

Because of its significant early commercial potential, this information, which has been developed under a U.S. Government program, is being disseminated within the United States in advance of general publication. This information may be duplicated and used by the recipient with the express limitation that it not be published. Release of this information to other domestic parties by the recipient shall be made subject to these limitations.

Foreign release may be made only with prior NASA approval and appropriate export licenses. This legend shall be marked on any reproduction of this information in whole or in part.

Review for general release OCT 1981

ENERGY EFFICIENT ENGINE
HIGH-PRESSURE TURBINE UNCOOLED
RIG TECHNOLOGY REPORT

Prepared
by

W. B. Gardner, Program Manager
Energy Efficient Engine Component
Development and Integration Program

UNITED TECHNOLOGIES CORPORATION
Pratt & Whitney Aircraft Group
Commercial Products Division

LIBRARY COPY

NOV 10 1980

LANGLEY RESEARCH CENTER
LIBRARY, NASA
HAMPTON, VIRGINIA

Because of their possible significant early commercial value, these data developed under a U.S. Government contract are being disseminated within the U.S. in advance of general publication. These data may be duplicated and used by the recipient with the expressed limitations that the data will not be published nor will they be released to foreign parties without permission of Pratt & Whitney Aircraft Group and appropriate export licenses. Release of these data to other domestic parties by the recipient shall only be made subject to the limitations contained in NASA Contract NAS3-20646. These limitations shall be considered void after two (2) years after date of such data. This legend shall be marked on any reproduction of these data in whole or in part.

Prepared for
NATIONAL AERONAUTICS AND SPACE ADMINISTRATION
NASA-Lewis Research Center
Contract NAS3-20646

NF02430

BEST

AVAILABLE

COPY

1 Report No	2 Government Accession No	3 Recipient's Catalog No
NASA-CR-165149		

4 Title and Subtitle	5 Report Date
Energy Efficient Engine - High-Pressure Turbine Uncooled Rig Technology Report	October 1979
	6 Performing Organization Code
7 Author(s)	8 Performing Organization Report No
W.B.Gardner, et al	PWA-5594-92
	10 Work Unit No
9 Performing Organization Name and Address	
United Technologies Corporation Pratt & Whitney Aircraft Group - CPD East Hartford, Connecticut 06108	11 Contract or Grant No NAS3-20646
	13 Type of Report and Period Covered Technology Report
12 Sponsoring Agency Name and Address National Aeronautics and Space Administration Lewis Research Center 21000 Brookpark Road, Rocky River, OH 44135	14 Sponsoring Agency Code

15 Supplementary Notes
NASA Project Manager, Mr.N.T.Saunders, NASA-Lewis Research Center

16 Abstract

Results obtained from testing five performance builds (three vane cascades and two rotating rigs of the Energy Efficient Engine uncooled rig have established the uncooled aerodynamic efficiency of the high-pressure turbine at 91.1 percent. This efficiency level was attained by increasing the rim speed and annulus area (AN^2), and by increasing the turbine reaction level. The increase in AN^2 resulted in a performance improvement of 1.15 percent. At the design point pressure ratio, the increased reaction level rig demonstrated an efficiency of 91.1 percent. The results of this program have verified the aerodynamic design assumptions established for the Energy Efficient Engine high-pressure turbine component.

17 Key Words (Suggested by Author(s))	18 Distribution Statement
Uncooled Rig Reaction Level Annular Cascade Annulus area Stress Testing Rotating Rig	

19 Security Classif (of this report)	20 Security Classif (of this page)	21 No of Pages	22 Price*
		242	

* For sale by the National Technical Information Service, Springfield, Virginia 22161

NASA-C-168 (Rev 10-75)

N81-71514 #

This Page Intentionally Left Blank

FOREWORD

The Energy Efficient Engine Component Development and Integration Program is being conducted under parallel National Aeronautics and Space Administration contracts to Pratt & Whitney Aircraft Group and General Electric Company. The overall project is under the direction of Mr. Neal T. Saunders. Mr. John W. Schaefer is the NASA Assistant Project Manager for the Pratt & Whitney Aircraft effort under NASA Contract NAS3-20646, and Mr. Michael Vanco is the NASA Project Engineer responsible for the portion of the project described in this report. Mr. William B. Gardner is manager of the Energy Efficient Engine Project at Pratt & Whitney Aircraft Group.

This Page Intentionally Left Blank

TABLE OF CONTENTS

TABLE OF CONTENTS (Cont'd)

LIST OF ILLUSTRATIONS

LIST OF ILLUSTRATIONS (Cont'd)

LIST OF ILLUSTRATIONS (Cont'd)

LIST OF ILLUSTRATIONS (Cont'd)

LIST OF TABLES

This Page Intentionally Left Blank

LIST OF SYMBOLS

A annulus area, in^2
bx axial chord, in
cx axial flow velocity, fps
g force-mass conversion constant, 32.174 f/s^2
h specific enthalpy, Btu/lb

J work equivalent, $\frac{\text{ft-lbs}}{\text{Btu}}$

M Mach number
N mechanical speed, RPM
P pressure, in of mercury
T temperature, ^{o}F or ^{o}R
U tangential wheel speed, fps
W mass flow, lbs/sec
x axial distance, in.
y tangential distance, in.
α absolute angle, degree
β relative angle, degrees

Subscripts

a air
AA area-averaged
m metal
MA mass-averaged
S static condition
T total state

1.0 SUMMARY

To achieve the goal efficiency for the Energy Efficient Engine high-pressure turbine component, a single stage turbine was designed to produce a high ratio of wheel speed to specific work, velocity ratio, and a low ratio of through flow to wheel speed (Cx/U). This aerodynamic concept was limited structurally by allowable blade stress, typified by parameter AN^2 (product of annulus area and wheel speed squared). This design reduced turbine Mach numbers at the expense of airfoil turning, and was predicted to increase high-pressure turbine performance by 1.1 percent. The actual performance improvement, 1.15 percent, is in excellent agreement with the predicted value.

In addition to high velocity ratio and low Cx/U feature, design trade studies indicated that a 0.5 percent increase in turbine efficiency could be attained by increasing the turbine reaction level from a balanced Mach number design to a design with a subsonic vane. At the design point pressure ratio, the increased reaction level rig demonstrated an efficiency of 91.1 percent, 0.8 percent higher than the lower reaction rig.

The results obtained by canting the vane 13 degrees in the direction of rotation showned that the canted vane configuration had the lowest mass averaged total loss of all of the airfoils tested.

These results have established the uncooled aerodynamic efficiency of the high-pressure turbine at 91.1 percent and have verified the feasibility of the Energy Efficient Engine high-pressure turbine aerodynamic design concepts.

2.0 INTRODUCTION

The objective of the NASA Energy Efficient Engine Development and Integration program is to develop, evaluate, and demonstrate the technology for achieving lower installed fuel consumption and lower operating costs in future commercial turbofan engines. NASA has set minimum goals of 12 percent reduction in thrust specific fuel consumption (TSFC), 5 percent reduction in direct operating cost (DOC), and 50 percent reduction in performance degradation for the Energy Efficient Engine (flight engine) relative to the JT9D-7A reference engine. In addition, environmental goals on emissions (meet the proposed EPA 1981 regulation) and noise (meet FAR 36-1978 standards) have been established.

The Pratt & Whitney Aircraft Energy Efficient Engine high-pressure turbine is a single-stage design. A single-stage design has certain advantages when compared to its multi-stage counterpart. Single stage turbines require no interstage seals, require fewer cooled airfoils, and contain fewer leakage paths. The inherent design simplicity of the single stage reduces engine initial cost, maintenance material cost, and overall engine weight.

The purpose of the Energy Efficient Engine high-pressure turbine uncooled rig program was to (1) establish the uncooled aerodynamic efficiency base for the high-pressure turbine component and (2) verify the aerodynamic design assumptions for this component. The program was conducted to ensure timely interaction with the high-pressure turbine component effort, as summarized in Figure 1. The efficiency goals are presented in Table 1, and the major test configurations are summarized in Table 2.

Five performance builds (three vane cascades and two rotating rigs) of the uncooled turbine rig were tested to establish the Energy Efficient Engine turbine efficiency base and to verify the advanced aerodynamic design concepts of the program. The first rotating rig (Build 1) and its companion cascade had a design reaction level of 35 percent and examined the effects of high AN^2 (low Cx/U and high velocity ratio) on turbine efficiency. The second rotating rig (Build 2) and its companion cascade examined the effects of stage reaction on stage efficiency. This build of the rotating rig was also used to evaluate blade vibratory stress levels. The tests with the third annular cascade rig investigated the effects of a 13-degree vane tangential cant on cascade losses.

This report describes the design of the two transonic single stage turbines and the test results obtained in the annular cascade and rotating rig test programs.

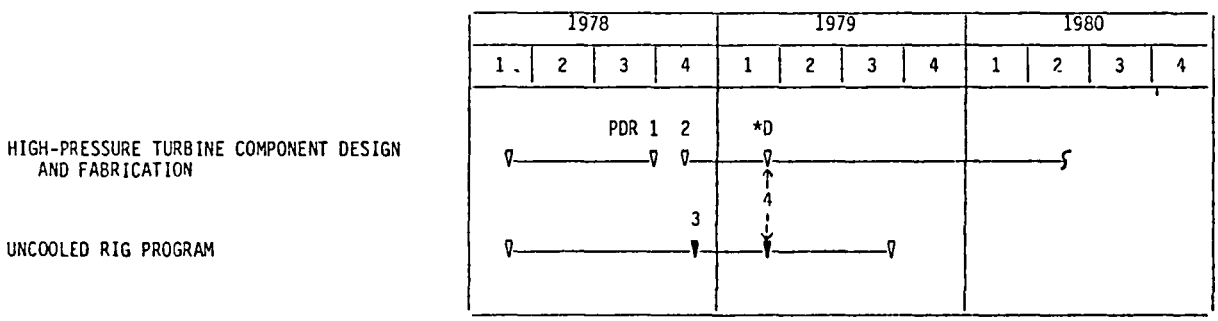

*D Program critical decision point

1 Component preliminary design effort completed, preliminary design review (PDR) held.

2 Component detailed design effort initiated on non-aerodynamic activities.

3 Build 1 rotating stage tests completed. Results establish feasibility of advanced aerodynamic concepts

4 Build 2 rotating stage tests completed Results enable decision to be made on best vane and blade aerodynamic configuration. Component detailed design effort continues, incorporating aerodynamic activities

Figure 1 Interaction of Uncooled Rig Supporting Technology Program With the High-Pressure Turbine Component Effort - The un- cooled rig program was conducted to ensure timely interac- tion with the high-pressure turbine component effort.

TABLE 1

EFFICIENCY GOALS OF THE UNCOOLED RIG PROGRAM

	Build 1 Rotating Stage	Build 2 Rotating Stage
AN^2 (in.-rpm)^2	49×10^9	49×10^9
Rim Speed, Redline (ft/sec)	1730	1730
Reaction (percent)	35	43
Uncooled Efficiency (percent)	90.3	90.8

TABLE 2

MAJOR TEST CONFIGURATIONS OF THE HIGH-PRESSURE TURBINE UNCOOLED RIG

Vane Cascades	
Build 1	35-Percent Reaction, "Zero" Vane Cant Angle
Build 2	43-Percent Reaction, "Zero" Vane Cant Angle
Build 3	43-Percent Reaction, 13-Degree Vane Cant Angle
Rotating Stages	
Build 1	35-Percent Reaction (vane and blade), "Zero" Vane Cant Angle
Build 2	43-Percent Reaction (vane and blade), "Zero" Vane Cant Angle
	Blade Vibratory Stress Level Testing of the 43-Percent Reaction (vane and blade), "Zero" Vane Cant Angle

3.0 ANALYSIS AND DESIGN

3.1 Aerodynamic Design

Turbine design studies indicated that to meet the goal efficiency, advanced aerodynamic concepts which achieve a high ratio of wheel speed to specific work (velocity ratio) and a low ratio of through-flow velocity to wheel speed (Cx/U) are required. These aerodynamic design concepts are limited by structural considerations typified by the parameter AN^2 (product of annulus area to wheel speed squared). By designing the Energy Efficient Engine high-pressure turbine to an AN^2 level of 49×10^9, an increase of 1.1 percent in turbine efficiency was predicted relative to state-of-the-art single-stage turbines. Design trade studies also indicated that turbine efficiency could be improved by increasing the reaction level from a balanced Mach number design to a design featuring a subsonic vane. However, as turbine stage reaction increases, rearward thrust across the turbine is increased and, therefore, bearing thrust balance can become a limiting factor. In the Energy Efficient Engine design, this limit was reached at about 43 percent reaction (see Figure 2).

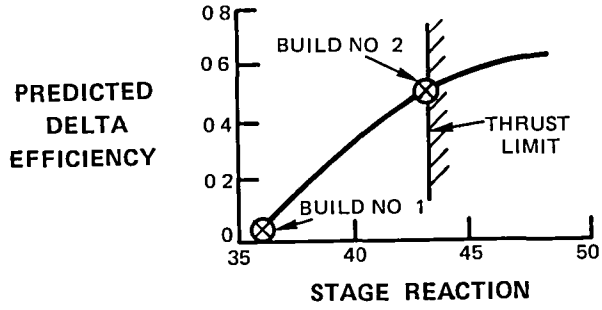

Figure 2 Reaction Level Versus Turbine Efficiency - Maximum turbine reaction was limited by the engine rotor thrust balance.

As a result of these studies, two high AN^2 turbines with reaction levels of 35 and 43 percent were designed for uncooled rig performance evaluation. The turbine parameters for these two designs are listed in Table 3.

In addition to the two full stage designs, a third set of vanes was designed, incorporating a 13-degree cant angle in the direction of rotation. This design imparts radial body loads to the gas flow and, according to published literature, has been shown to reduce the inner diameter endwall losses. The aerodynamics for the three vane designs are summarized in Table 4.

TABLE 3
PRELIMINARY TURBINE DESIGN PARAMETERS

	Build 1	Build 2
No. of Stages	1	1
Pressure Ratio	4.0	4.0
Mean Velocity Ratio, $\frac{U}{\sqrt{2gJ\Delta h}}$	0.56	0.56
Work Factor, $\frac{(Jg\Delta h)}{U^2}$	1.59	1.59
AN^2 (SLTO), $(cm\text{-}rps)^2((in\text{-}rpm)^2)$	$8.24 \times 10^7 (46 \times 10^9)$	$8.24 \times 10^7 (46 \times 10^9)$
AN^2(Redline), $(cm\text{-}rps)^2((in\text{-}rpm)^2)$	$8.79 \times 10^7 (49 \times 10^9)$	$8.79 \times 10^7 (49 \times 10^9)$
Rim Speed (SLTO), m/sec (ft/sec)	511.0 (1677)	511.0 (1677)
Rim Speed (Redline), m/sec (ft/sec)	527.0 (1730)	527.0 (1730)
Inlet Speed Parameter, $N/\sqrt{T}$	252.1	252.1
Inlet Flow Parameter, $W\sqrt{T}/P$	17.69	17.69
Specific Work, $\Delta h/T$	0.0729	0.0729
Blade Tip Clearance, cm (in.)	0.051 (0.020)	0.051 (0.020)
Mean Reaction Level	0.35	0.43
Mean Blade Turning	125°	117.8°
Goal Cooled Turbine Efficiency, %	88.2	88.2

Specific procedures followed in the turbine aerodynamic design included a meanline analysis, streamline analysis, airfoil design, airfoil pressure distribution, and boundary layer analysis. Meanline analysis was performed to determine flowpath areas. Primary considerations during the streamline analysis were inlet and exit Mach triangles and gas turning angles. This analysis generated radial profiles using both two- and three-dimensional analytical procedures to produce suitable airfoil pressure distributions. This analysis also determined the radial distribution of aerodynamic properties. Boundary layer calculations were then used to verify the low loss characteristics of the airfoils. Through this approach, a comprehensive turbine design study was conducted, and criteria were established for the design of both the vane and blade.

The vane airfoil sections were designed so that the flow was accelerated past the gage point (throat) with low, smooth backend diffusion. Durability constraints set the minimum thickness for the airfoil. The uncovered turning and exit wedge angle were optimized to minimize the two-dimensional loss. Based on previous single-stage turbine design correlations, an existing exit angle deviation system and a radial work distribution were applied to the design of the Energy Efficient Engine. The blade airfoil sections were designed to the same pressure distribution criteria as the vane. The blade uncovered turning and exit wedge angle were further optimized to reduce trailing edge shock losses. The blade leading edge diameter was set by durability considerations. The uncooled rig was scaled to match the engine Mach number triangles and vane exit Reynolds number. This aerodynamic scaling, coupled with the constraints of using existing uncooled rig hardware, resulted in a scale factor of 0.7325 between rig and engine turbines.

TABLE 4
AERODYNAMIC PROPERTIES

Vane	Build 1	Build 2	Build 3
α Exit (degrees)	10.4	10.4	10.4
M_{Exit}	1.01	0.93	0.93
Gap/Chord	0.90	0.90	0.90
Blade Mean			
Reaction	0.35	0.43	
Turning (degrees)	125	117.8	
Load Coefficient	0.92	0.95	
M_{Exit}	1.15	1.23	
Cx/u	0.328	0.320	
Gap/Chord	0.90	0.96	
Blade Root			
Reaction	0.29	0.36	
Turning (degrees)	133.3	133.9	
Load Coefficient	0.78	0.81	
Gap/Chord	0.88	1.01	
Blade Tip			
Reaction	0.42	0.49	
Turning (degrees)	111.3	87.5	
Load Coefficient	1.13	1.16	
Gap/Chord	0.92	0.91	

Reaction = Static Pressure drop across the rotor ratioed to the static pressure drop across the stage.

$$\frac{Ps_2 - Ps_{1.5}}{Ps_2 - Ps_1}$$

$$\text{Load Coefficient} = \frac{2\tau}{b_x} \sin^2 \alpha_2 \left[\frac{Cx1}{Cx2} \operatorname{ctn} \alpha_1 + \operatorname{ctn} \alpha_2\right]$$

The flight engine flowpath was scaled to rig size (see Figure 3). Mach numbers and velocity triangles were made to correspond to those required in actual operating conditions (see Figures 4 and 5). The uncooled flowpath dimensions were reduced to maintain design reactions without cooling air.

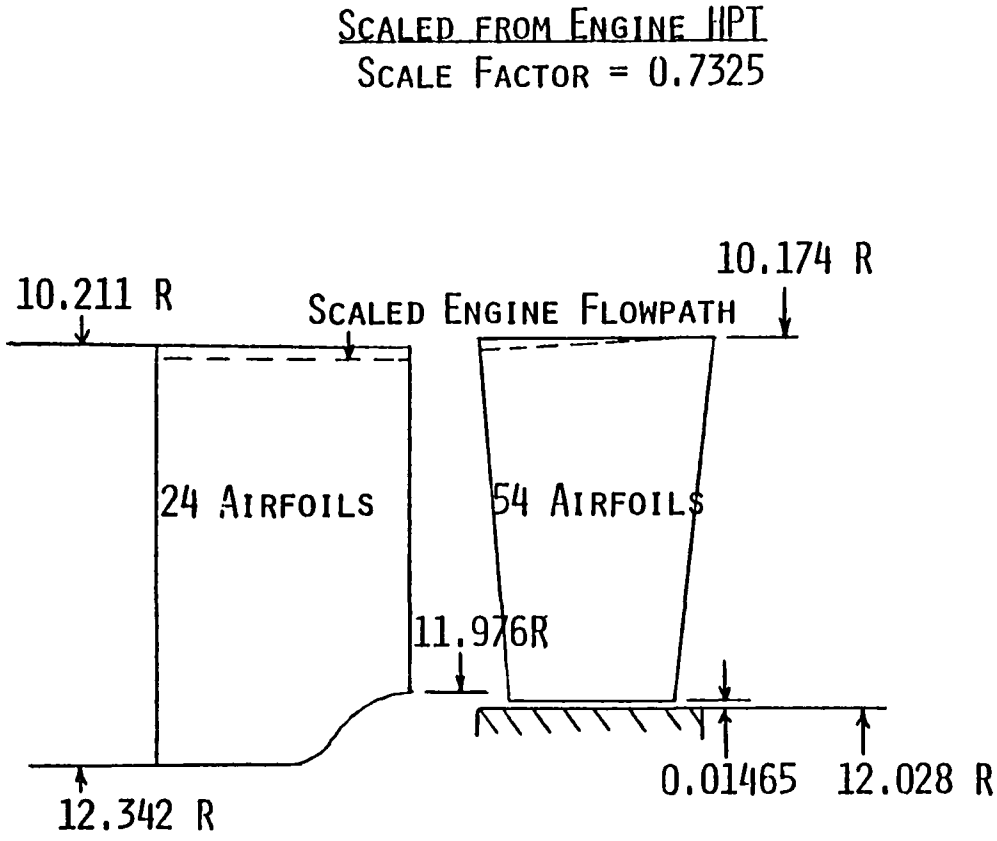

Figure 3 Uncooled Rig Flowpath

An iterative procedure using a computer interactive airfoil design system was used to design the external contours of the airfoils, and to establish the desired airfoil static pressure distribution. Figures 6 through 20 show the resultant airfoil shapes and surface pressure distributions of the three vane cascades and the two blade designs. Figures 6 through 8 show the Build 1 vane; 9 through 11, the Build 1 blade; 12 through 14, the Build 2 vane; 15 through 17, the Build 2 blade; and 18 through 20, the Build 3 vane. A set of coordinates for these airfoils is presented in Appendix A.

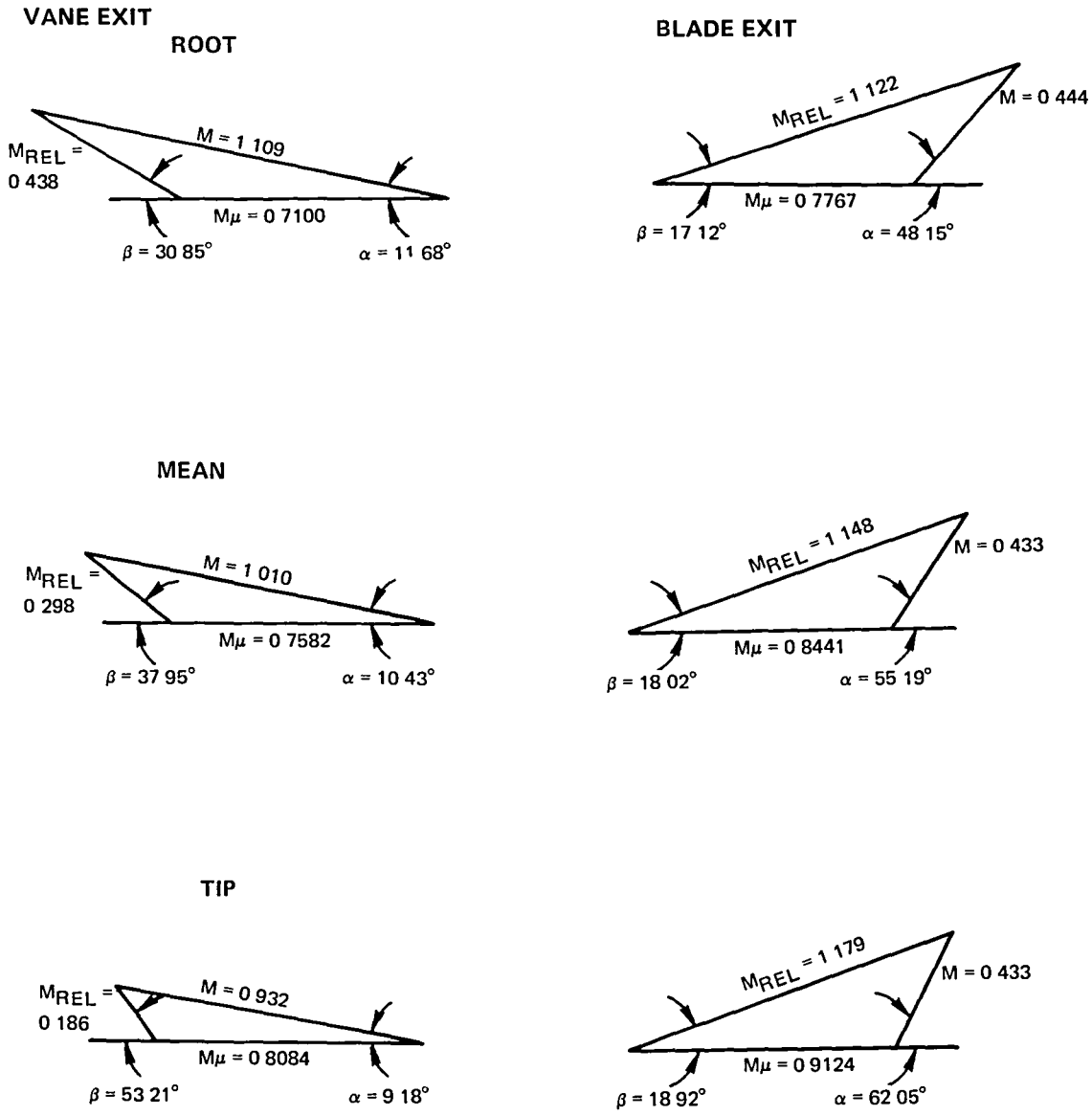

Figure 4 Build 1 Velocity Triangles

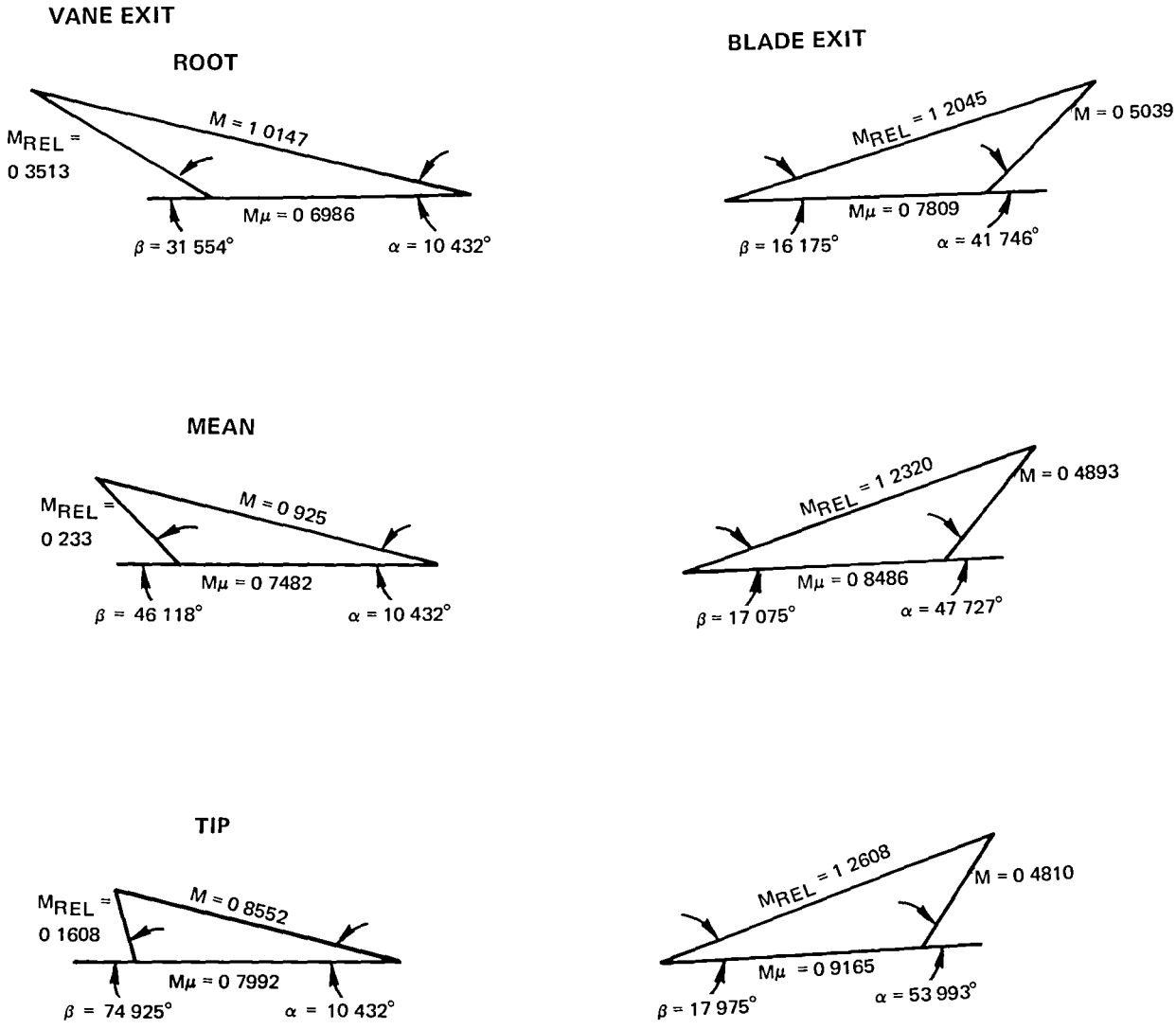

Figure 5 Build 2 Velocity Triangles

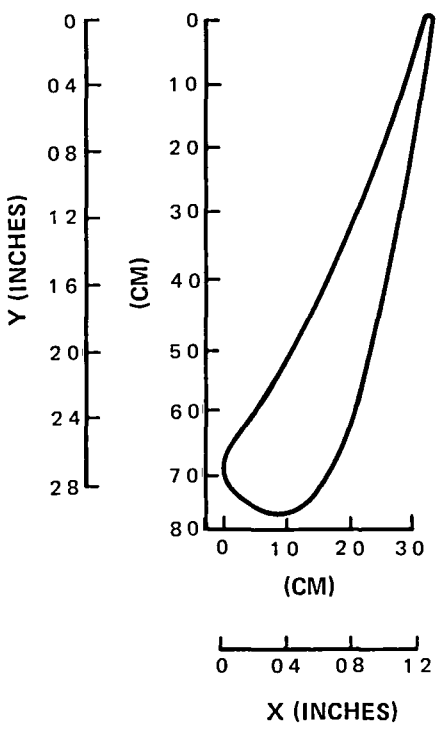

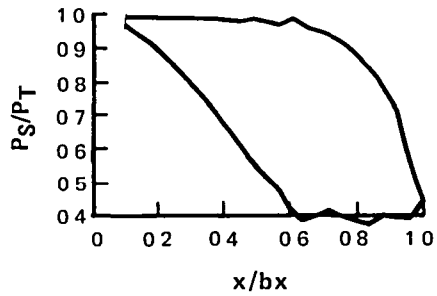

RADIUS	25 94 cm (10 211 in)
# FOILS	24
AXIAL CHORD	3 24 cm (1 275 in)
LE DIA	1 02 cm (0 400 in)
TE DIA	0 10 cm (0 040 in)
UNCOVERED TURNING	8°
EXIT WEDGE ANGLE	4°
FOIL INLET β	90°
FOIL EXIT β	11 68°
Max Mn s s	1 257

Figure 6 Build 1 Vane Root Section

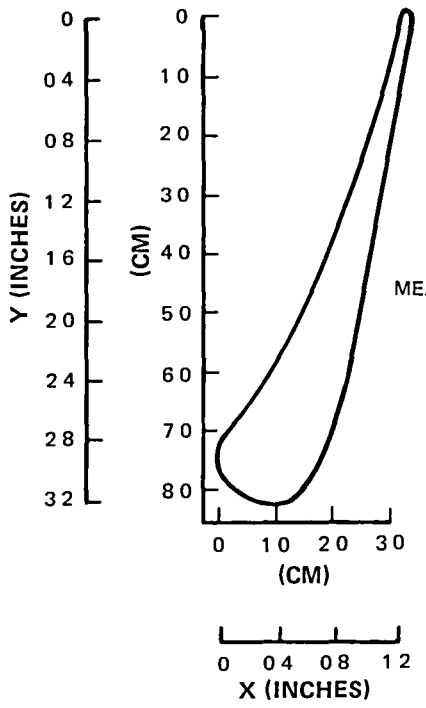

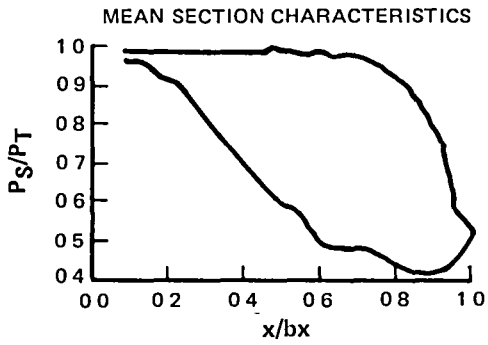

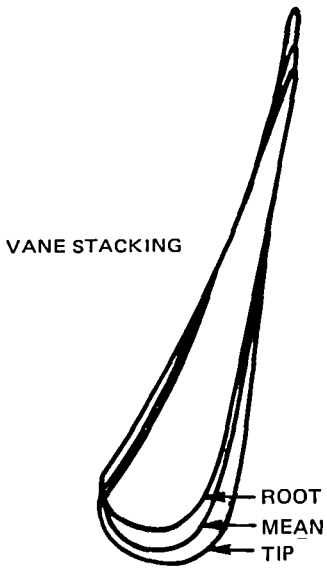

PRESSURE DISTRIBUTION

RADIUS	28 18 cm (11 094 in)
# FOILS	24
AXIAL CHORD	3 24 cm (1 275 in)
LE DIA	1 02 cm (0 400 in)
TE DIA	0 10 cm (0 040 in)
UNCOVERED TURNING	9°
EXIT WEDGE ANGLE	4°
FOIL INLET β	90°
FOIL EXIT β	10 44°
Max Mn s s	1 196

Figure 7 Mean Section Build 1 Vane

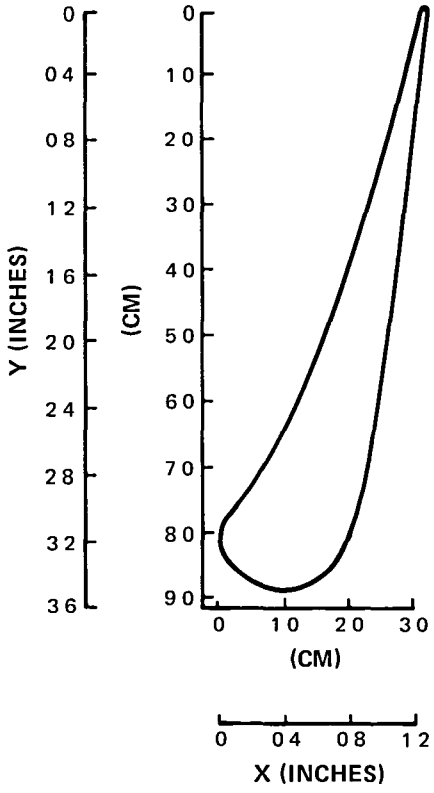

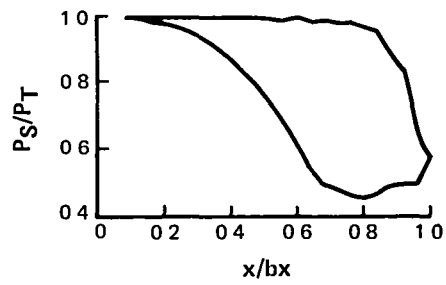

RADIUS	31 35 cm (12 342 in)
# FOILS	24
AXIAL CHORD	3 24 cm (1 275 in)
LE DIA	1 02 cm (1 275 in)
TE DIA	0 10 cm (0 040 in)
UNCOVERED TURNING	10°
EXIT WEDGE ANGLE	4°
FOIL INLET β	90°
FOIL EXIT β	8 69°
Max Mn s s	1 136

Figure 8 Build 1 Vane Tip Section

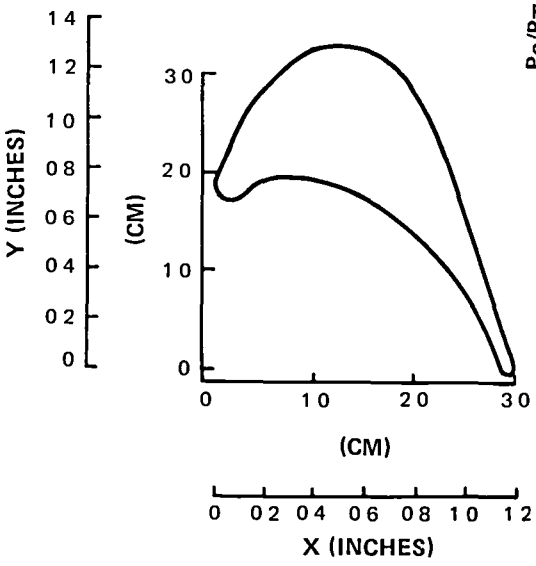

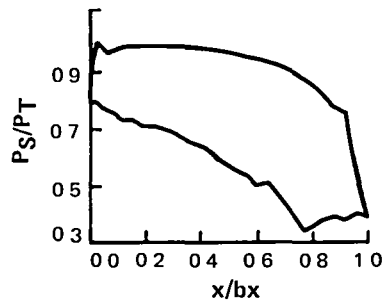

RADIUS	25 84 cm (10 174 in)
# FOILS	54
AXIAL CHORD	3 015 cm (1 187 in)
LE DIA	0 30 cm (0 117 in)
TE DIA	0 10 cm (0 040 in)
UNCOVERED TURNING	10°
EXIT WEDGE ANGLE	2°
FOIL INLET β	29 57°
FOIL EXIT β	17 12°
Max Mn s s	1 359

Figure 9 Build 1 Blade Root Section

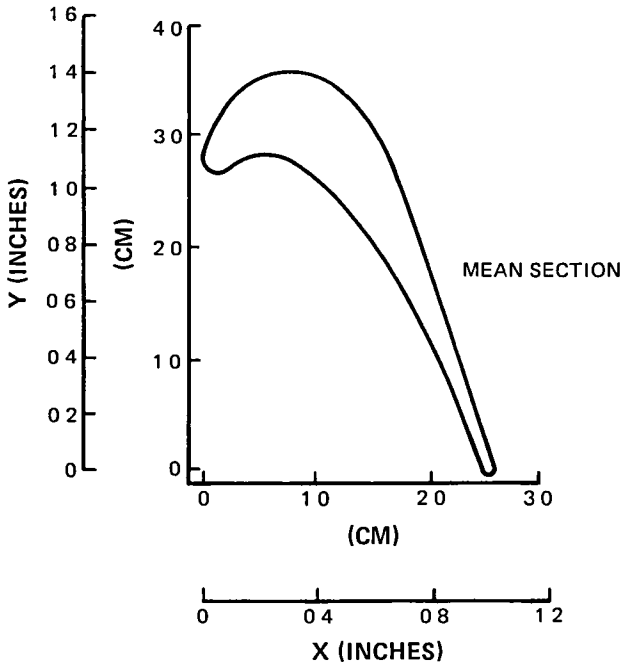

MEAN SECTION CHARACTERISTICS

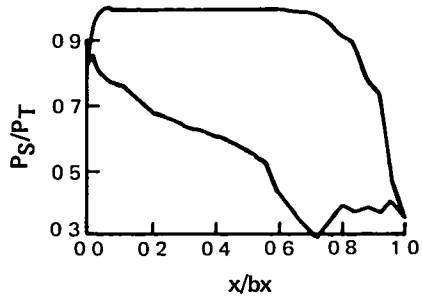

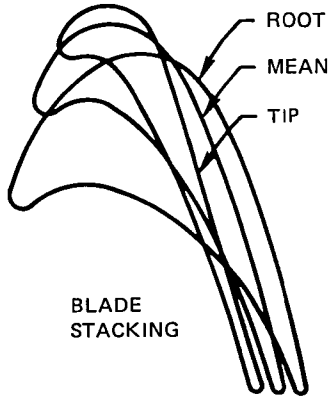

PRESSURE DISTRIBUTION

RADIUS	28 17 cm (11 093 in)
# FOILS	54
AXIAL CHORD	2 58 cm (1 015 in)
LE DIA	0 30 cm (0 117 in)
TE DIA	0 10 cm (0 040 in)
UNCOVERED TURNING	8°
EXIT WEDGE ANGEL	2°
FOIL INLET β	32 03°
FOIL EXIT β	18 02°
Max Mn s s	1 461

Figure 10 Build 1 Blade Mean Section

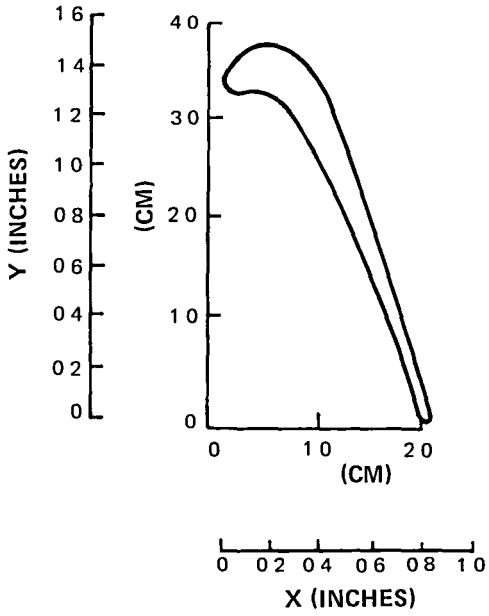

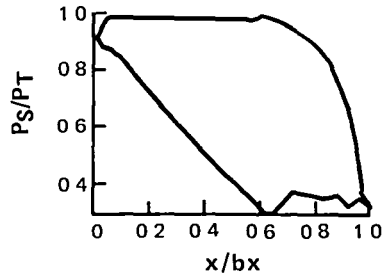

RADIUS	30 51 cm (12 012 in)
# FOILS	54
AXIAL CHORD	2 14 cm (0 842 in)
LE DIA	0 30 cm (0 117 in)
TE DIA	0 10 cm (0 040 in)
UNCOVERED TURNING	4°
EXIT WEDGE ANGLE	2°
FOIL INLET β	44 74°
FOIL EXIT β	18 92°
Max Mn s s	1 442

Figure 11 Build 1 Blade Tip Section

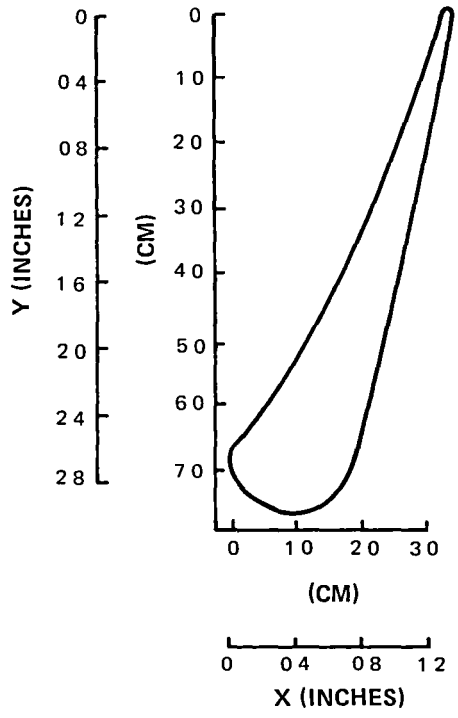

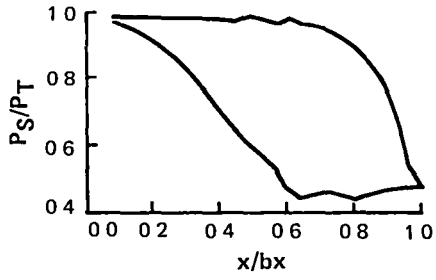

RADIUS	25 94 cm (10 211 in)
# FOILS	24
AXIAL CHORD	3 24 cm (1 275 in)
LE DIA	1 02 cm (0 400 in)
TE DIA	0 10 cm (0 040 in)
UNCOVERED TURNING	8°
EXIT WEDGE ANGLE	4°
FOIL INLET β	90°
FOIL EXIT β	10 43°
Max Mn s s	1 131

Figure 12 Build 2 Vane Root Section

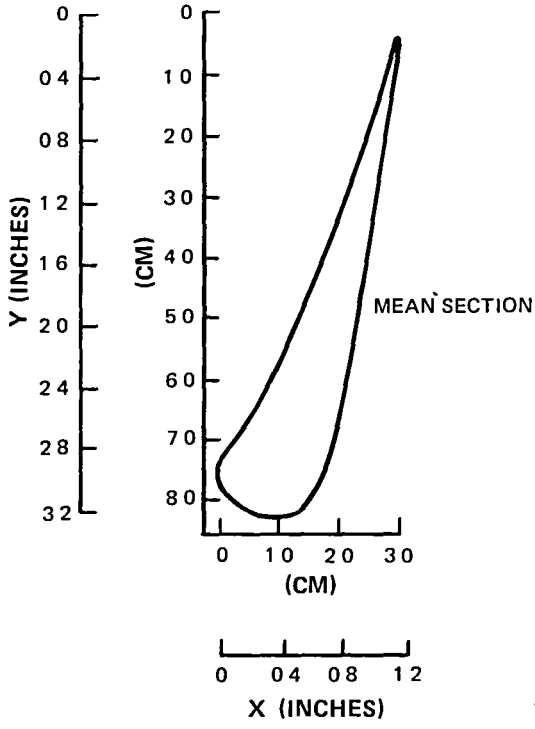

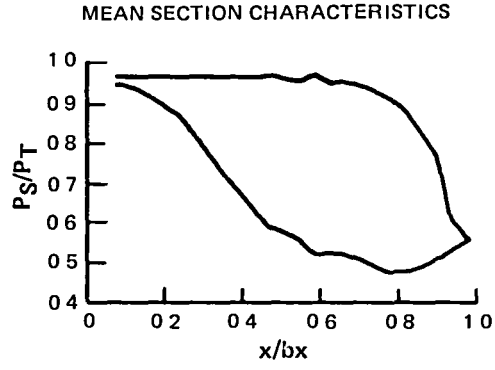

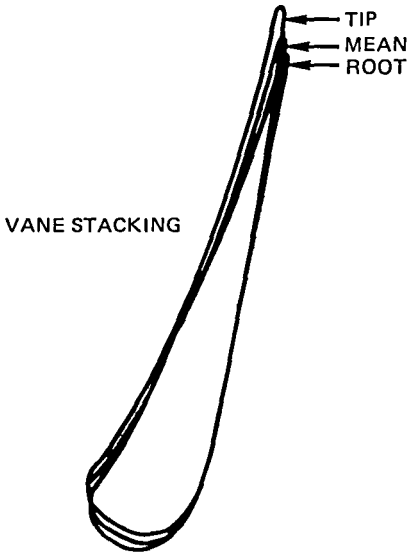

PRESSURE DISTRIBUTION

RADIUS	28 18 cm (11 094 in)
# FOILS	24
AXIAL CHORD	3 24 cm (1 275 in)
LE DIA	1 02 cm (0 400 in)
TE DIA	0 10 cm (0 040 in)
UNCOVERED TURNING	10°
EXIT WEDGE ANGLE	4°
FOIL INLET β	90°
FOIL EXIT β	10 43°
Max Mn s s	1 074

Figure 13 Build 2 Vane Mean Section

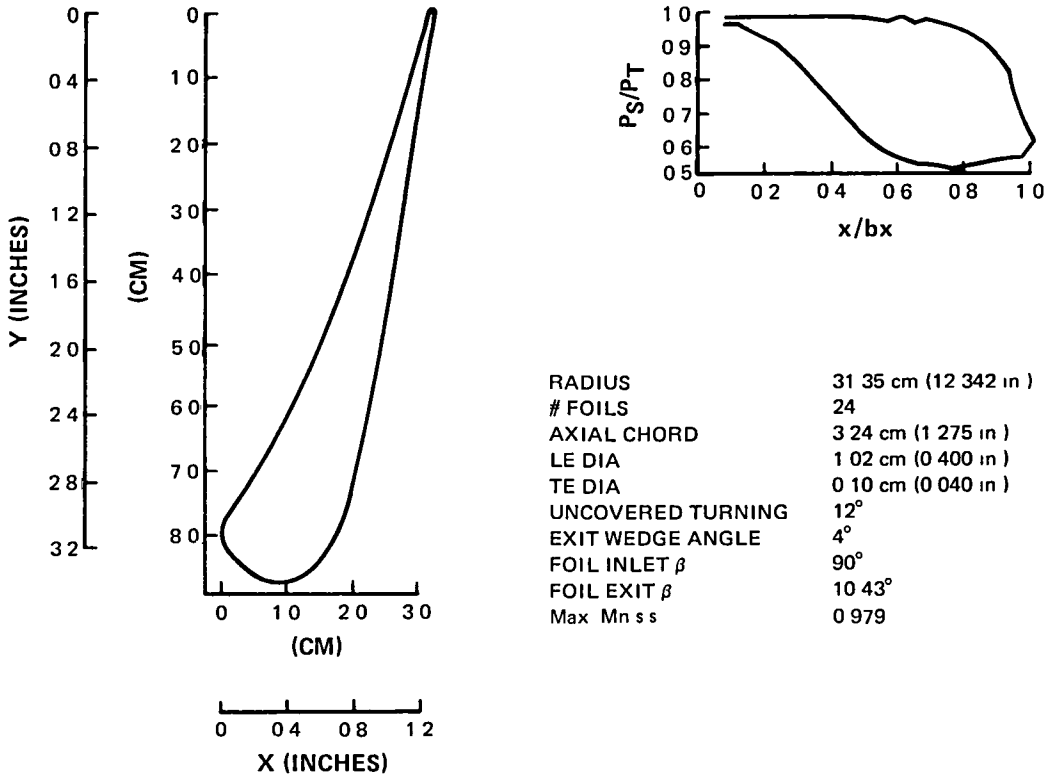

RADIUS	31 35 cm (12 342 in)
# FOILS	24
AXIAL CHORD	3 24 cm (1 275 in)
LE DIA	1 02 cm (0 400 in)
TE DIA	0 10 cm (0 040 in)
UNCOVERED TURNING	12°
EXIT WEDGE ANGLE	4°
FOIL INLET β	90°
FOIL EXIT β	10 43°
Max Mn s s	0 979

Figure 14 Build 2 Vane Tip Section

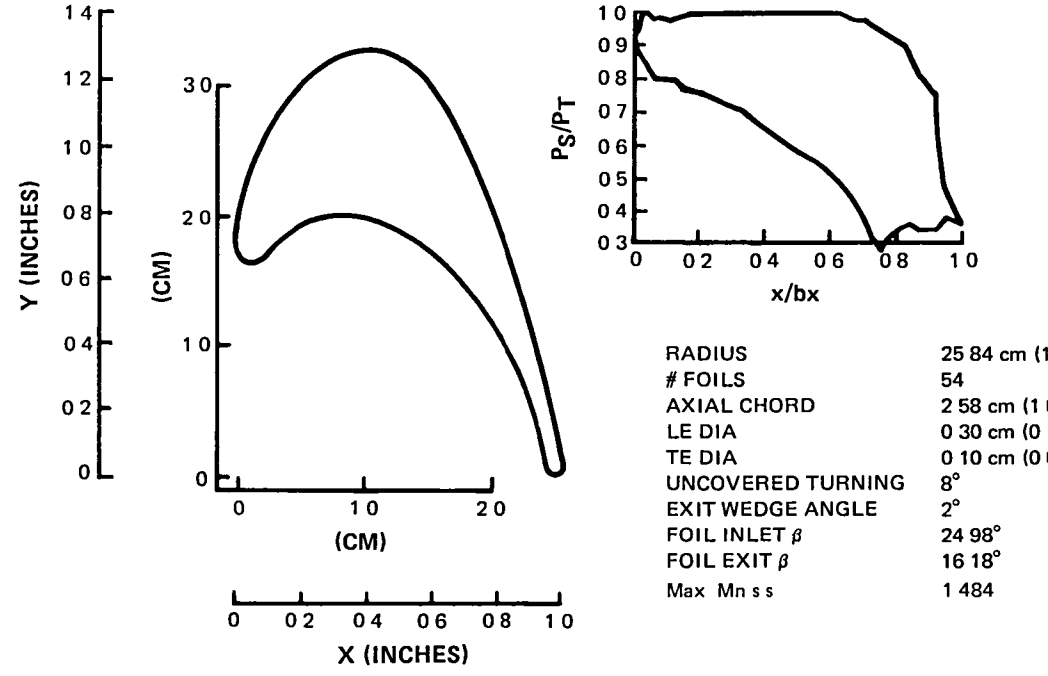

RADIUS	25 84 cm (10 174 in)
# FOILS	54
AXIAL CHORD	2 58 cm (1 018 in)
LE DIA	0 30 cm (0 117 in)
TE DIA	0 10 cm (0 040 in)
UNCOVERED TURNING	8°
EXIT WEDGE ANGLE	2°
FOIL INLET β	24 98°
FOIL EXIT β	16 18°
Max Mn s s	1 484

Figure 15 Build 2 Blade Root Section

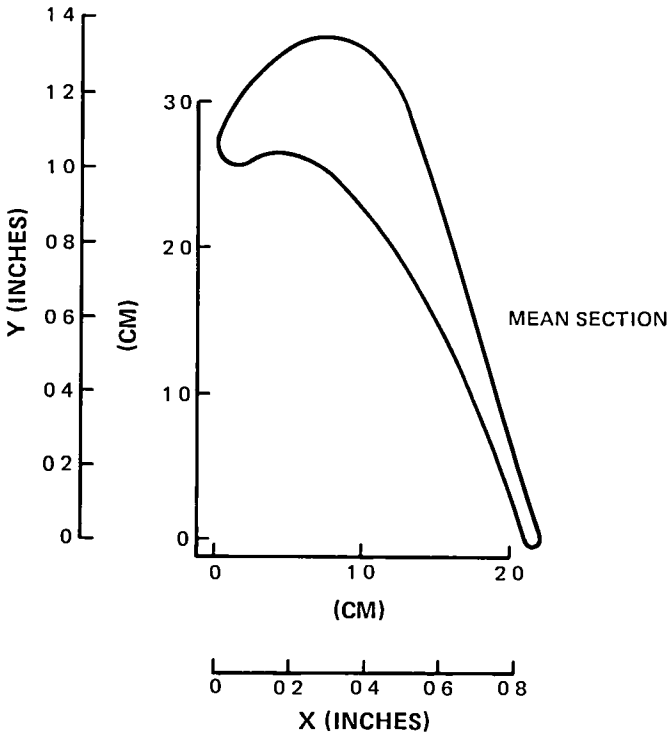

MEAN SECTION CHARACTERISTICS

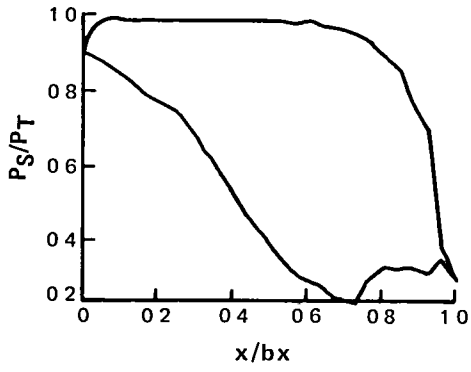

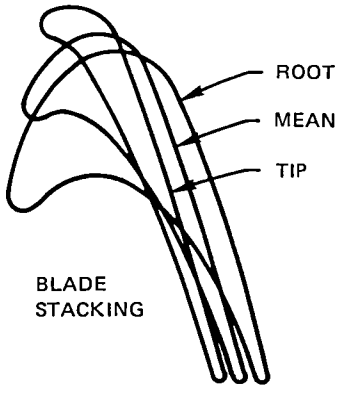

PRESSURE DISTRIBUTION

RADIUS	28 18 cm (11 093 in)
# FOILS	54
AXIAL CHORD	2 22 cm (0 875 in)
LE DIA	0 30 cm (0 117 in)
TE DIA	0 10 cm (0 040 in)
UNCOVERED TURNING	6°
EXIT WEDGE ANGLE	2°
FOIL INLET β	40 15°
FOIL EXIT β	17 08°
Max Mn s s	1 577

Figure 16 Build 2 Blade Mean Section

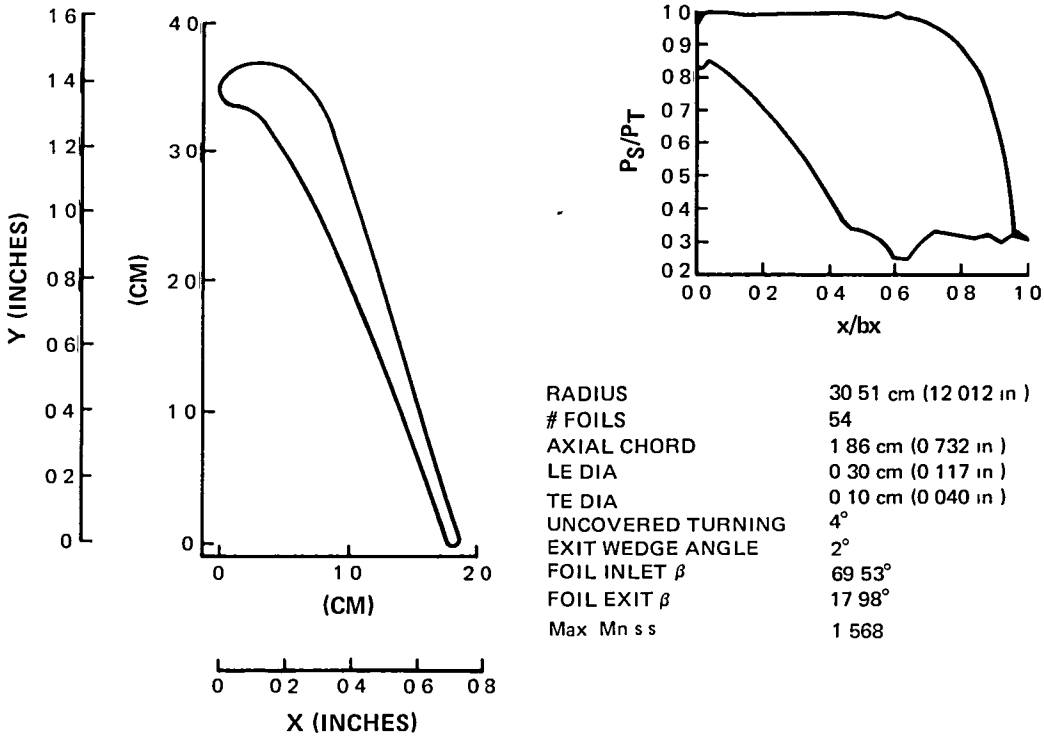

RADIUS	30 51 cm (12 012 in)
# FOILS	54
AXIAL CHORD	1 86 cm (0 732 in)
LE DIA	0 30 cm (0 117 in)
TE DIA	0 10 cm (0 040 in)
UNCOVERED TURNING	4°
EXIT WEDGE ANGLE	2°
FOIL INLET β	69 53°
FOIL EXIT β	17 98°
Max Mn s s	1 568

Figure 17 Build 2 Blade Tip Section

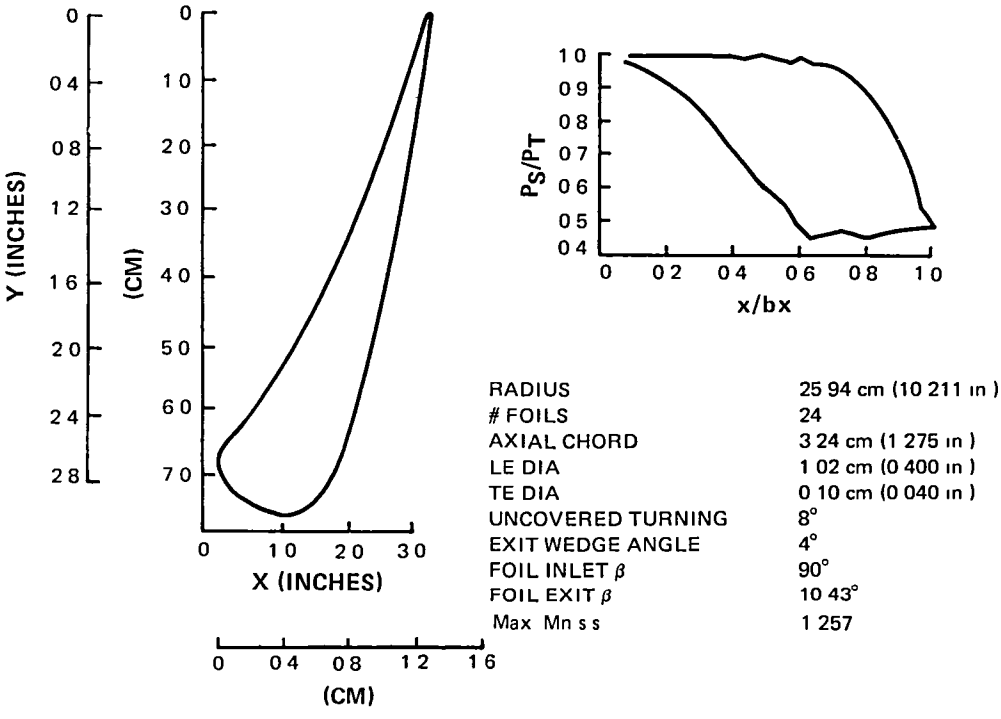

RADIUS	25 94 cm (10 211 in)
# FOILS	24
AXIAL CHORD	3 24 cm (1 275 in)
LE DIA	1 02 cm (0 400 in)
TE DIA	0 10 cm (0 040 in)
UNCOVERED TURNING	8°
EXIT WEDGE ANGLE	4°
FOIL INLET β	90°
FOIL EXIT β	10 43°
Max Mn s s	1 257

Figure 18 Build 3 Vane Root Section

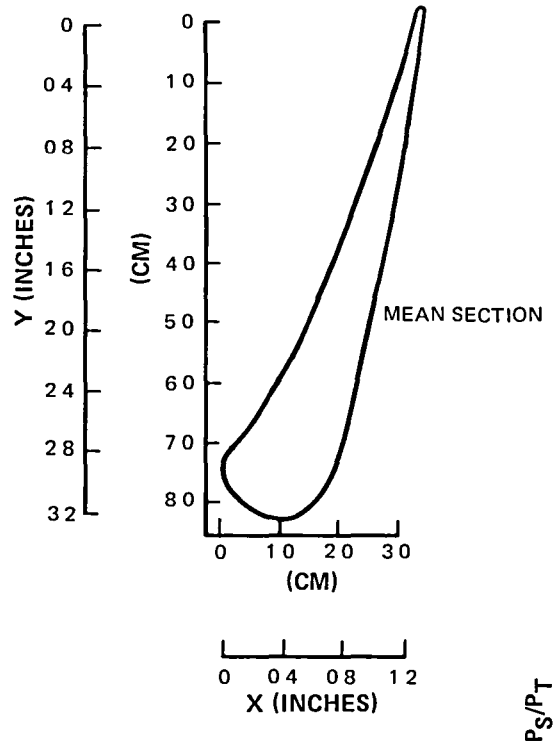

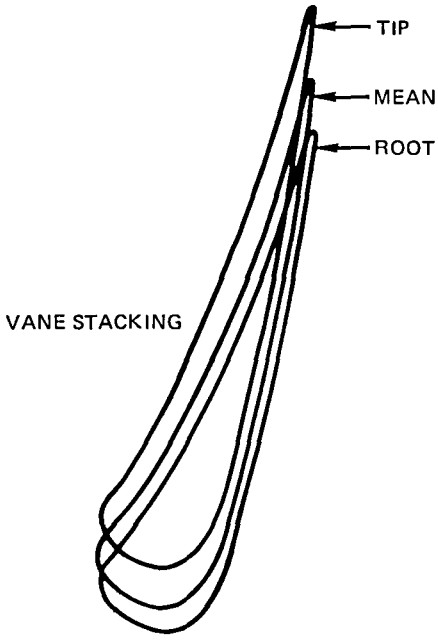

MEAN SECTION CHARACTERISTICS

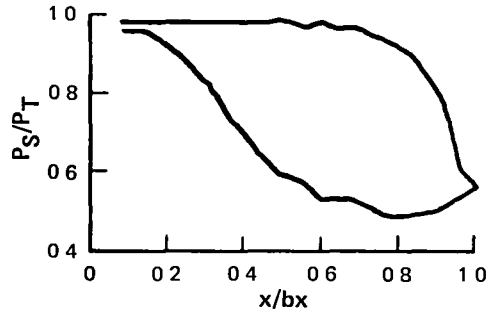

PRESSURE DISTRIBUTION

RADIUS	28 18 cm (11 094 in)
# FOILS	24
AXIAL CHORD	3 24 cm (1 275 in)
LE DIA	1 02 cm (0 400 in)
TE DIA	0 10 cm (0 040 in)
UNCOVERED TURNING	10°
EXIT WEDGE ANGLE	4°
FOIL INLET β	90°
FOIL EXIT β	10 43°
Max Mn s s	1 196

Figure 19 Build 3 Vane Mean Section

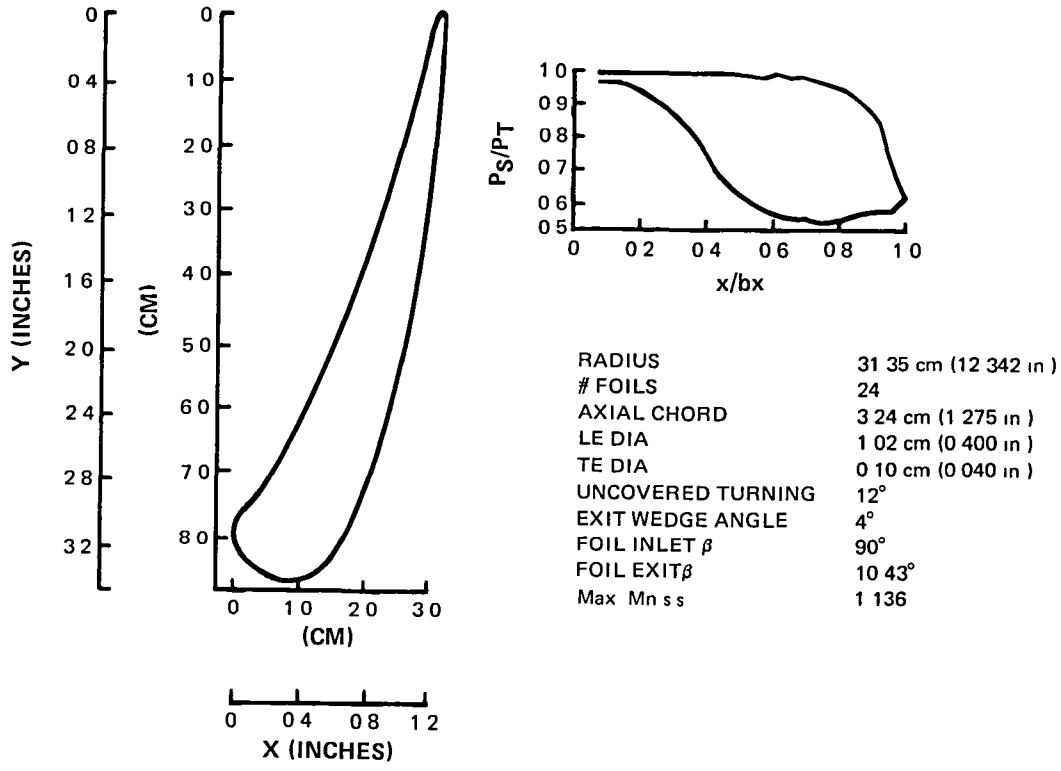

Figure 20 Build 3 Vane Tip Section

3.2 Mechanical Design

3.2.1 Design of Rig Subsystems

Disk

The rotor disk was conservatively designed for a nominal 30-percent burst margin above maximum anticipated operating speed. Computer analysis ensured that the stress levels in this disk were consistent with structural design criteria.

Blade and Disk Attachments

Blade and disk attachments were designed to keep stresses well within design margins. Potential vibratory stress problems were avoided by "tuning" the disk design to provide a frequency margin at 24E vane passing exitation for both the low and high reaction blades at maximum speed and to keep the occurrence of low order resonances well above maximum speed (see Figures 21 and 22). Fixed inlet rakes were aerodynamically configured and located sufficiently upstream to minimize any potential exitation from this source. Blade and

disk-coupled vibration characteristics were analyzed by a conventional beam analysis and a more rigorous NASTRAN finite element vibration analysis. Blade dampers controlled the levels of buffeting and resonant response.

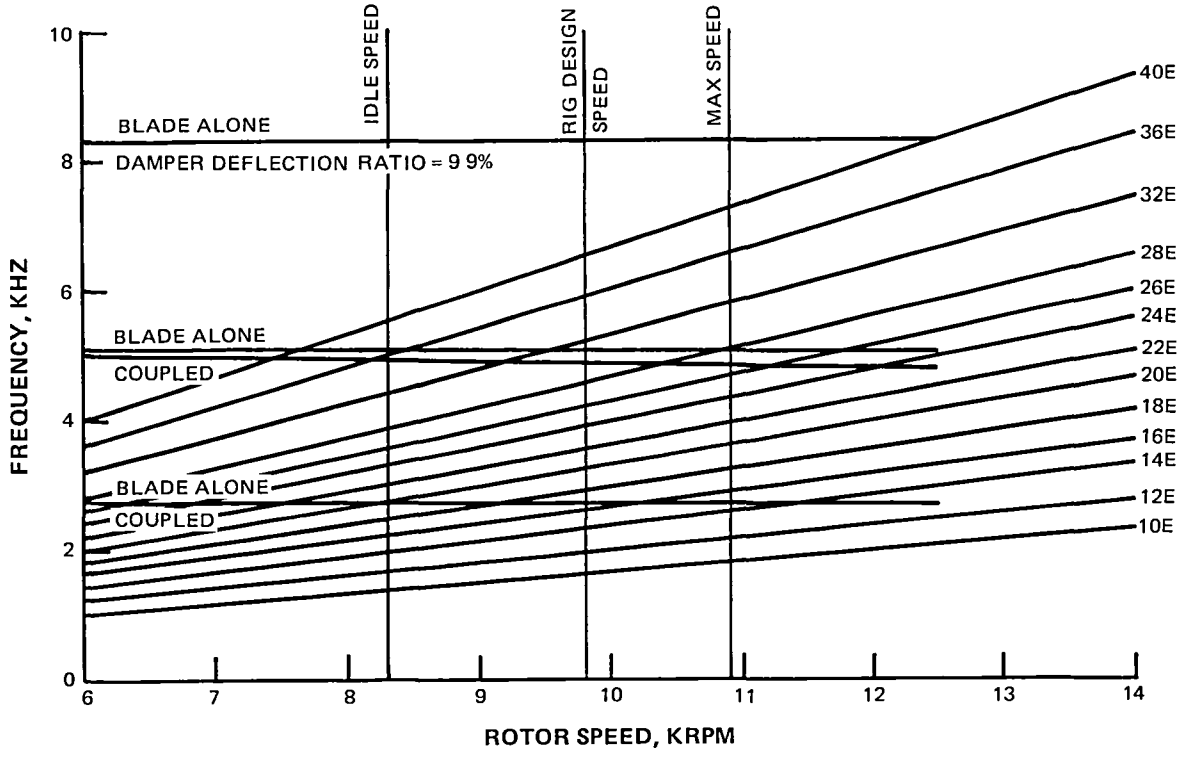

Figure 21 Uncooled Rig Resonance Diagram (Build 1 Low Reaction Blade) - Results of an initial beam deck analysis with disk rim and blade root changes made to avoid first or second mode resonances with the number of nozzle vanes (24) in the rig operating range.

Bearing Arrangements

Bearing arrangements were established on the basis of rotor stiffness, weight, and speed. The optimized bearing arrangement ensured that the operating range was free of vibrational modes that could otherwise cause premature hardware failure.

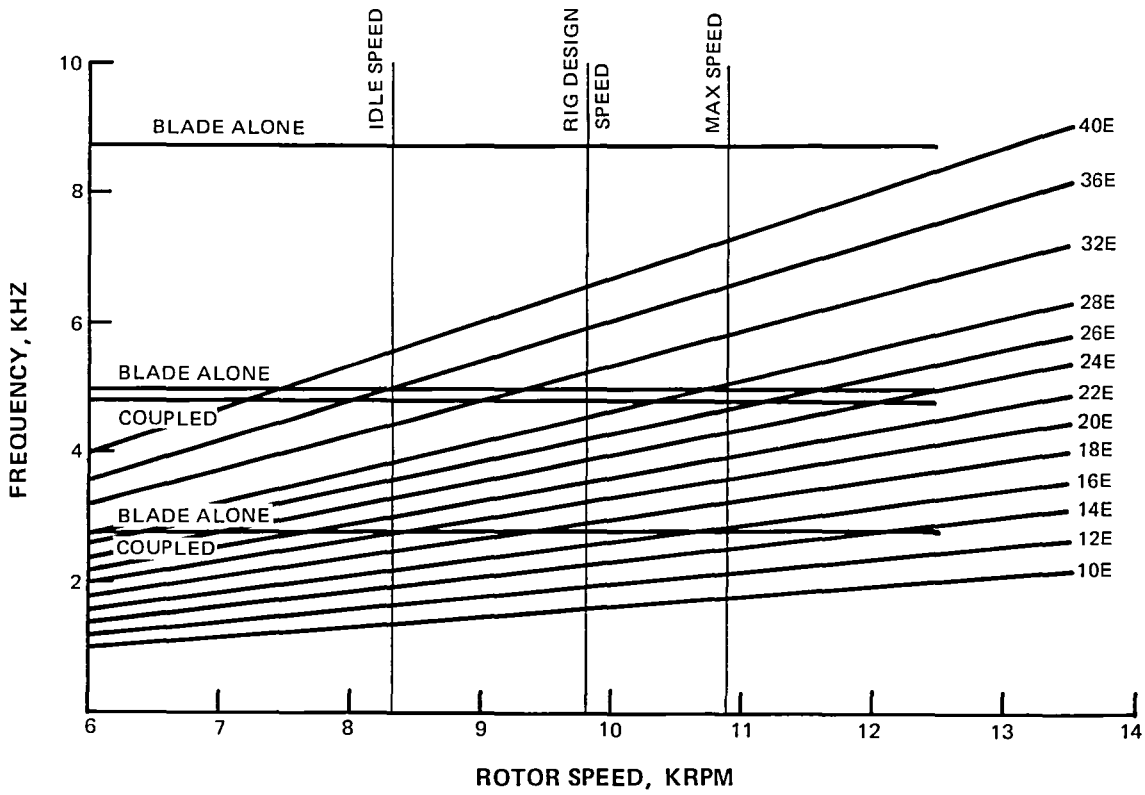

Figure 22 Uncooled Rig Resonance Diagram (Build 2 High Reaction Blade) - This diagram is based on the same calculation procedure and requirements as the Build 1 design (see Figure 21).

3.2.2 Design of Test Rig

The test rig, illustrated in Figure 23, was used both for the vane annular cascade testing and full-stage (rotating rig) testing. A unique feature of the rig was the circumferentially traversing instrumentation ring, which permitted pressure, temperature, and six angle measurements both radially and circumferentially in the flowpath. The total range of circumferential travel for a given sensor mounted on the ring was 30 degrees (corresponding to two vane pitches). This flowpath scanning capability is illustrated in Figure 24.

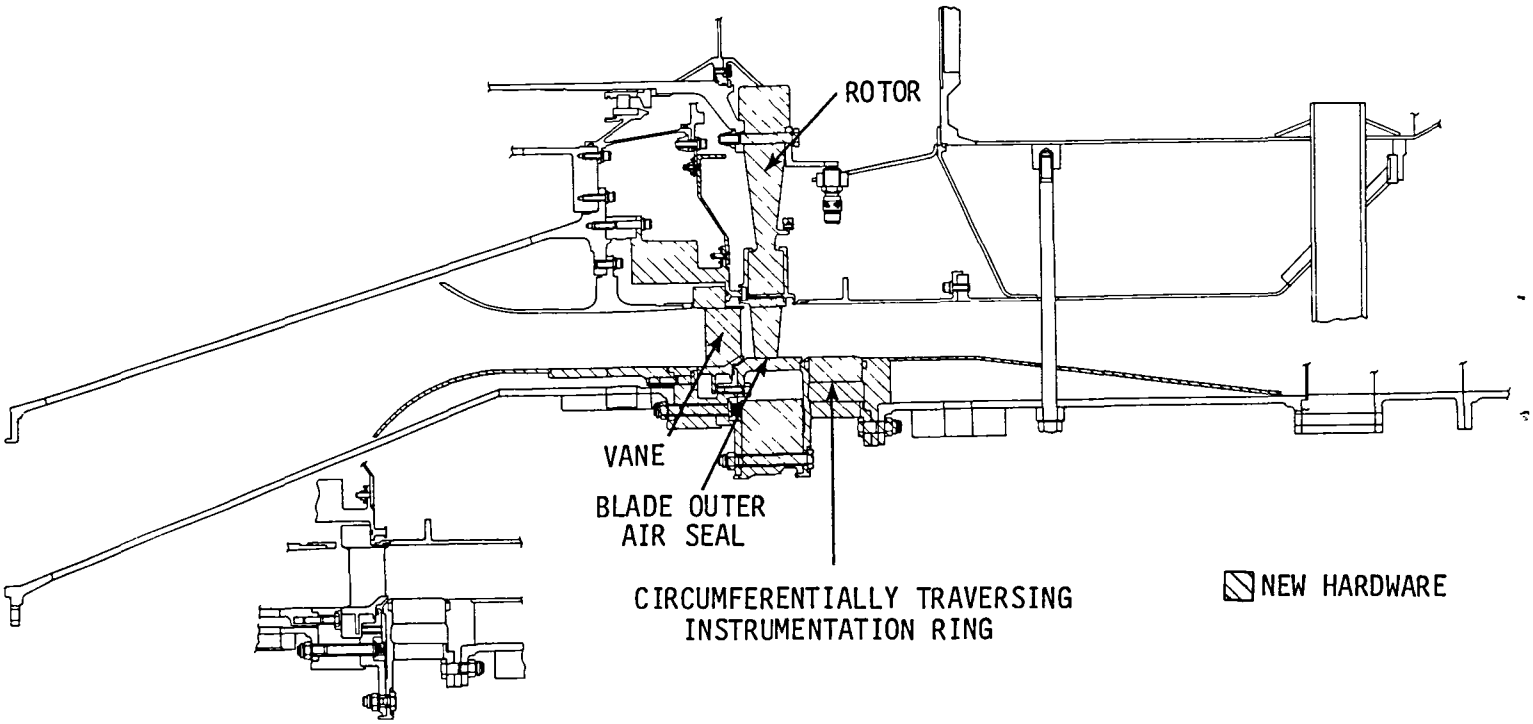

Figure 23 Energy Efficient Engine High-Pressure Turbine Uncooled Rig - A unique feature of the rig is the circumferentially traversing instrumentation ring which permits pressure, temperature, and air angle measurements both radially and circumferentially in the flowpath.

The test rig was adapted to annular cascade testing as shown in Figure 25. Filler pieces were installed in the rig flowpath to cover the steps in the flowpath that originally contributed to endwall losses. In addition, the rotor and blade outer air seal assemblies were removed, and the inner and outer diameter exit flowpath ducts and instrumentation ring were moved forward to the exit instrumentation plane.

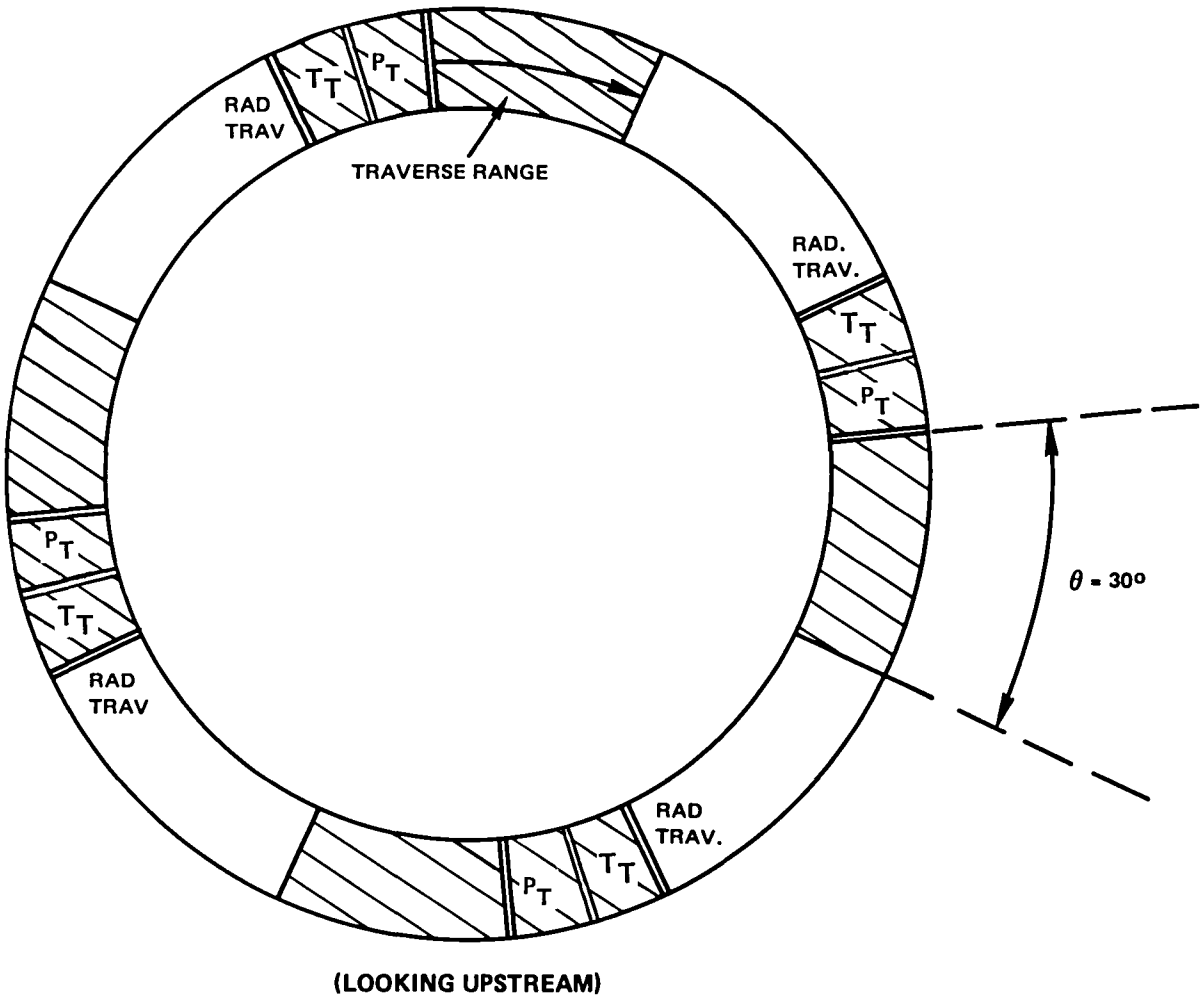

Figure 24 Circumferentially Traversing Exit Instrumentation Ring - The total range of circumferential travel for a given sensor mounted on the ring is 30 degrees (corresponding to two vane pitches).

Structural design criteria and mechanical constraints consistent with experimental hardware were used to establish the design configuration of the test rig. Computer programs helped determine airfoil stresses and deflections caused by centrifugal force, gas bending loads, and foil-to-platform transitions. Computer analysis also established the proper running clearance in order to simulate the tight clearances required by the full scale component.

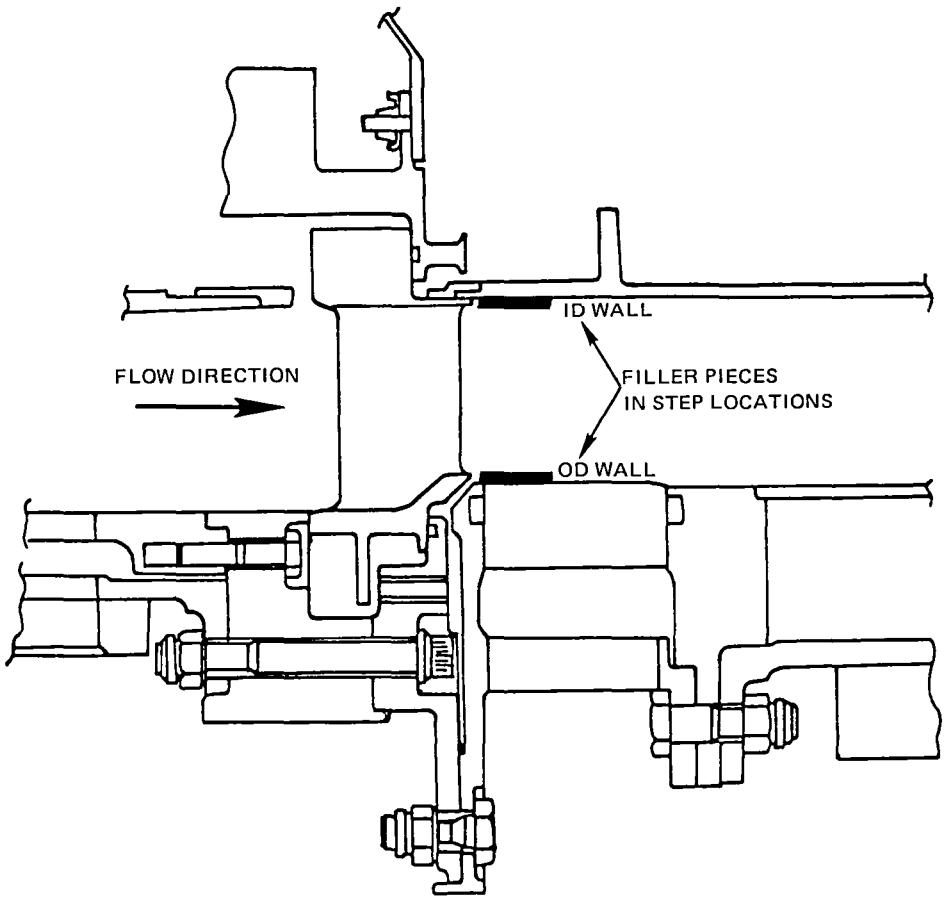

Figure 25 Uncooled Rig Modifications Required for Annular Cascade Testing - For vane annular cascade testing, the rotor and blade outer air seal assembles were removed and the inner and outer diameter exit flow path ducts and instrumentation ring moved forward to the exit instrumentation plane of the vane annular cascade.

A rotor dynamics analytical model of the rig was constructed and the critical speed analysis was run to predict system resonances and mode shapes. The analysis of rig critical speed characteristics (Figure 26) demonstrated that the inherent stiff bearing margin of 100 percent was sufficient to compensate for any potential high strain energy modes that might occur in the rig running range. Trim balance capability was incorporated into the rig to provide additional margin. In addition, the rig speed control system was set to allow a 2000 rpm margin of safety between maximum overspeed and burst speed in case of a water brake failure.

In order to reduce cost, the rig utilized many parts from an existing Pratt & Whitney Aircraft single-stage rig. Hardware designed and fabricated to adapt

that rig for testing is shown in the shaded areas of Figure 23. The major items designed for this program were:

- o inlet cases
- o vane airfoil and inner and outer shrouds
- o the rotor (including disk, blade airfoils, sideplates, dampers, and speed pickup ring)
- o the blade outer air seal
- o the circumferentially traversing instrumentation ring
- o exit outer cases interfacing with the rotor rim seals
- o instrumentation.

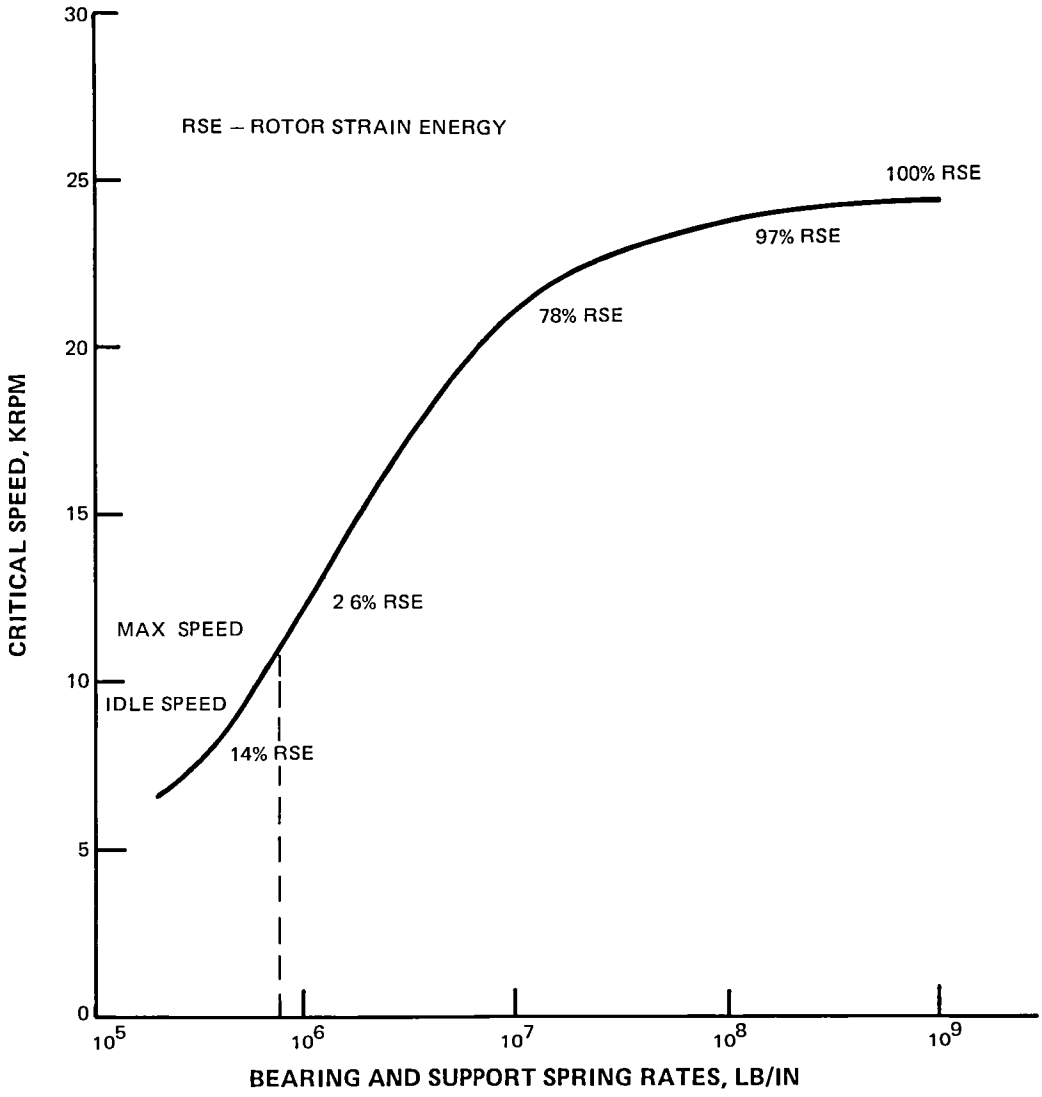

Figure 26 Critical Speed Characteristics - A stiff bearing critical speed margin of 100 percent is sufficient to guarantee no modes with high levels of rotor strain energy in the engine operating range.

This Page Intentionally Left Blank

4.0 FABRICATION AND ASSEMBLY

4.1 Fabrication

In this task, hardware was procured and fabricated based on the specifications established in the analysis and design task. AMS 5613 material was used in all of the major parts.

The fabrication procedures used for each of the rig sub-assemblies (blades, vanes, disks and sideplates, cases, and shaft and main bearings) were structured to maximize the use of existing hardware and established machining procedures. Fabrication procedures are discussed in sections 4.1.1 through 4.1.5.

4.1.1 Blades

Two sets of blades (one set for each of the builds of the rotating stages) were fabricated. Each set incorporated the different aerodynamic configurations defined in Table 2 (see page 4). As the blades were fabricated, provisions were made for the necessary instrumentation.

The blade airfoil sections for Build 1 testing were electrochemically machined; the blade platform, trailing edge, and fillet radii were conventionally machined. The electrochemical machining process used in Build 1 blade fabrication was judged too costly and too time consuming for Build 2 blade fabrication; therefore, the Build 2 blades were conventionally machined.

To ensure that blade contours were within established tolerances, each blade was shadowgraphed at the mean section, and every sixth blade was shadowgraphed at the root, mean, and tip sections. Seventy-two shadowgraphs were made for each build.

4.1.2 Vanes

Three sets of vanes were fabricated (each set fabricated for use in the vane cascades was later reused in the rotating stage tests). Each set incorporated the different aerodynamic configurations defined in Table 2 (see page 4). Provisions were made for the necessary instrumentation as the vanes were fabricated.

The vane airfoil sections for Build 1 testing were electrochemically machined and the endwalls were finished by a computer controlled milling machine operation. The vanes were difficult to secure during machining because of their longer chord geometry. The conventional techniques were modified to provide the rigid support needed to hold the vanes in place during the machining process.

The electrochemical machining process used in Build 1 vane fabrication was judged too time consuming for Build 2 and Build 3 vane fabrication; therefore, the Build 2 and Build 3 vanes were conventionally machined. The 13-degree canted vane did not cause any unusual machining problems. Each vane was shadow-

graphed at the root, mean, and tip sections to ensure that vane contours were within established tolerances. Two hundred and sixteen shadowgraphs were taken for the three builds.

4.1.3 Disks and Sideplates

Disks and sideplates were fabricated from raw material using standard machining practices.

4.1.4 Cases

Inlet and exhaust cases were made available from an existing in-house rig. The cases required only minor modifications to accommodate the dimensional standards of the rig flowpath. Inner and outer diameter rings for the vane assembly were fabricated from raw material by standard machining practices.

4.1.5 Shaft and Main Bearings

The main shaft, stub shaft, bearing housings, and oil jets were made available from in-house hardware. Vendors, following Pratt & Whitney Aircraft specifications, fabricated the No. 4 and No. 5 bearings and the No. 4 and No. 5 carbon seals.

4.2 Assembly

Following fabrication, the hardware was assembled into the required configurations using normal bench assembly procedures. These procedures, as applied to each of the rig subassemblies, are discussed in sections 4.2.1 through 4.2.5.

4.2.1 Vanes

A typical vane assembly is illustrated in Figure 27. Each assembly contained 24 vanes. Six vanes were instrumented with surface static pressure taps and with mid-gap chordwise and trailing edge gapwise wall static pressure taps. Each vane was secured at the outer diameter by two pins and at the inner diameter by one pin. The two vanes equipped with surface static instrumentation at the tip section were held in place without the bolt. The seal lands in the vane inner diameter shrouds were machined rough while the vanes were being finished machined. Following this procedure, the seal lands were built up with epoxy to ensure that they were dimensionally concentric.

Gaging dimensions were measured at three locations along the gaging plane. Actual gaging areas were calculated from these dimensions and compared with the design areas. Agreement between design gaging areas and actual areas is shown in Table 5. Trailing edge mid-span angles and flowpath diameters were also measured.

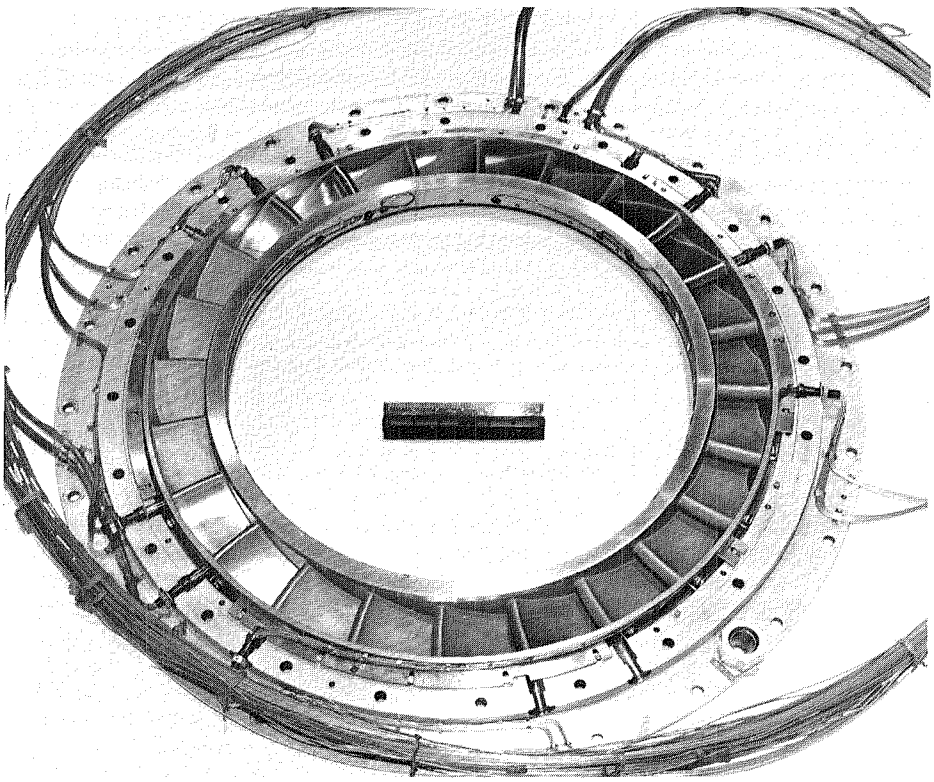

Figure 27 Uncooled Rig Vane Assembly

TABLE 5

VANE THROAT AREA

	Design (cm sq. (in. sq.))		Actual cm sq. (in. sq.))	
Build 1	138.19	(21.418)	137.14	(21.256)
Build 2	143.20	(22.194)	141.16	(21.878)
Build 3	143.20	(22.194)	145.94	(22.619)

4.2.2 Rotor

A typical rotor assembly is illustrated in Figure 28. Each assembly contained 54 blades. Nine blades were instrumented with surface static pressure taps and immersion thermocouples. Strain gages were placed on four blades of the first build of the rig and on three blades of the second build. To ensure dimensional concentricity, the blade tips, seal lands, and knife edge seals were machined to their final diameters while assembled in the disk. The blade outer air seal was also machined during assembly so that it would be concentric with the inside diameter of the rear main bearing housing. Wire seals were axially positioned in grooves at the edge of the blade platform to control radial leakage. Blade dampers were also included.

Figure 28 Uncooled Rig Rotor Assembly

Blade instrumentation was led out through rivet holes and through openings created by drilling into the rear sideplate. The leads were then routed along the rear face of the disk and out to the base of the driveshaft.

Gaging dimensions were measured at three radial locations of 42 blades (instrumented blades were not included in this measurement). Actual gaging areas were then calculated from these dimensions and compared to the design gaging areas. Agreement between design values and actual values is shown in Table 6. Flowpath dimensions and blade tip diameters were also measured.

TABLE 6
BLADE THROAT AREA

	Design (cm sq (in. sq.))		Actual (cm sq. (in. sq.))	
Build 1	239.92	(37.185)	240.53	(37.280)
Build 2	223.79	(34.685)	225.68	(34.979)

4.2.3 Cases

Many of the inlet and exhaust cases used in this program were made available from in-house hardware supplies. These cases required only the following modifications to conform to program requirements: (1) the case flanges had to be modified to accommodate required dimensions of the rig flowpath and (2) the radial step of the exhaust case had to be leveled by adding filler rings. This same exhaust case was used in both the cascade and the rotating rig tests (the filler rings were removed before the rotating rig tests).

The rig exit plane instrumentation case was adapted to program requirements from readily available parts. To permit circumferential traversing, the case was axially positioned on a Teflon-coated surface with eight bearings. Four additional bearings radially supported the case. Two "pusher" type traverse cans were used to circumferentially rotate the case. Flat-faced, spring-loaded Teflon seals prevented leakage.

4.2.4 Shaft and Main Bearings

The main shaft, stub shaft, bearing housings, and oil jets were also made available from in-house hardware supplies. The No. 4 and No. 5 carbon seals and the No. 4 and No. 5. bearings were new parts.

Bearing compartments were assembled in accordance with established procedures. The duplex bearing was assembled in a tandem arrangement to increase bearing life. Critical measurements verified that the assembly met design specifications. The oil jets were examined to ensure that they provided the desired oil flow patterns. No additional modifications were required for incorporating thrust balance air.

4.2.5 Stand Instrumentation

Provisions were made for specialized instrumentation (in addition to the previously discussed instrumentation). This instrumentation included accelerometers, vibration pickups, thermocouples, and optical proximity probes. Accelerometers were positioned vertically and horizontally on the front and rear bearing housings. Vibration pickups were located vertically and horizontally on the outer inlet and exit cases. Thermocouples were placed at the No. 4 and No. 5 bearings and at the No. 4 and No. 5 carbon seal locations. The three optical proximity probes, positioned in the blade outer air seal, recorded blade tip clearances at each performance condition. These probes were backed up by three rub buttons, also built into the blade outer air seal. The blade surface static pressure instrumentation was recorded by the data system via a rotating scanivalve system.

5.0 TESTING

5.1 General Description

A test program was established and conducted to substantiate the program objectives described in section 3.1. This included (1) use of a test facility designed to simulate an engine operational testing environment over the range of test parameters evaluated, (2) test rigs designed for low cost but retaining the capability to accurately duplicate the full-size high-pressure turbine design definition, (3) instrumentation specifically selected or designed to maximize data acquisition capability without unduly perturbating the flow characteristics of the rig, (4) time tested procedures and equipment for data acquisition and recording plus "real-time" data reduction capability, permitting rapid and accurate assessment of test results, and (5) test conditions and parameters chosen to provide the most effective range of data with which to accurately determine rig performance. Specific details of this test program are described in the following sections.

5.1.1 Test Facility

All testing was conducted at the Pratt & Whitney Aircraft X-212 test stand. The test turbine was mounted on an open bedplate and connected to the inlet air collector and exhaust duct. Air was supplied by laboratory compressors. The power generated by the turbine was absorbed by a waterbrake, and exit conditions were varied using flow exhausters. All controls and instrumentation required to operate and monitor the testing were located in a room adjacent to the test cell.

For emergency purposes, an explosive-actuated burst disk was located in the inlet duct to enable the rapid discharge of high-pressure air. If an emergency had arisen, the explosive would have been detonated within 50 milliseconds after receiving a signal from the overspeed limiter.

5.1.2 Test Rigs

Each of the hardware subassemblies described in section 4.2 was incorporated into the completed test rig and mounted in the test stand. Figure 29 shows a vane cascade test rig; Figure 30 shows a rotating test rig mounted for testing. The exhaust cases have been pulled back to expose details of the flowpath hardware.

Figure 31 identifies the locations of the primary instrumentation used in the rigs. A detailed description of the instrumentation used in the test program is presented in section 5.2.

5.2 Instrumentation

5.2.1 Annular Cascade Instrumentation

The primary performance instrumentation for the rig consisted of inlet total temperature and inlet and exit total pressure rakes (see Table 7). Additional instrumentation was used to measure primary and secondary flow rates, exit flow angle, static pressures (airfoil, flowpath, and cavity), cavity air temperatures, and metal temperatures.

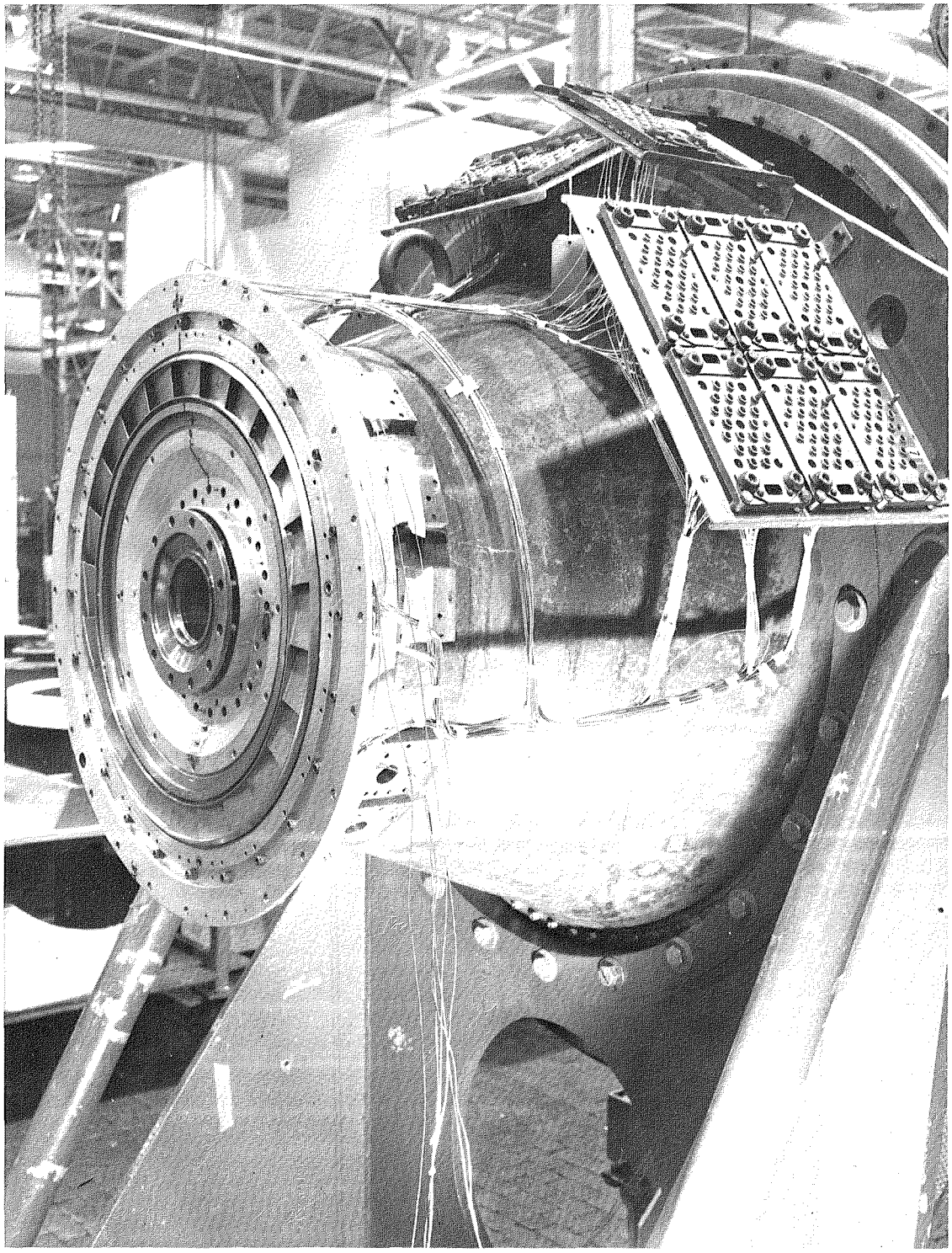

Figure 29 Annular Cascade Rig

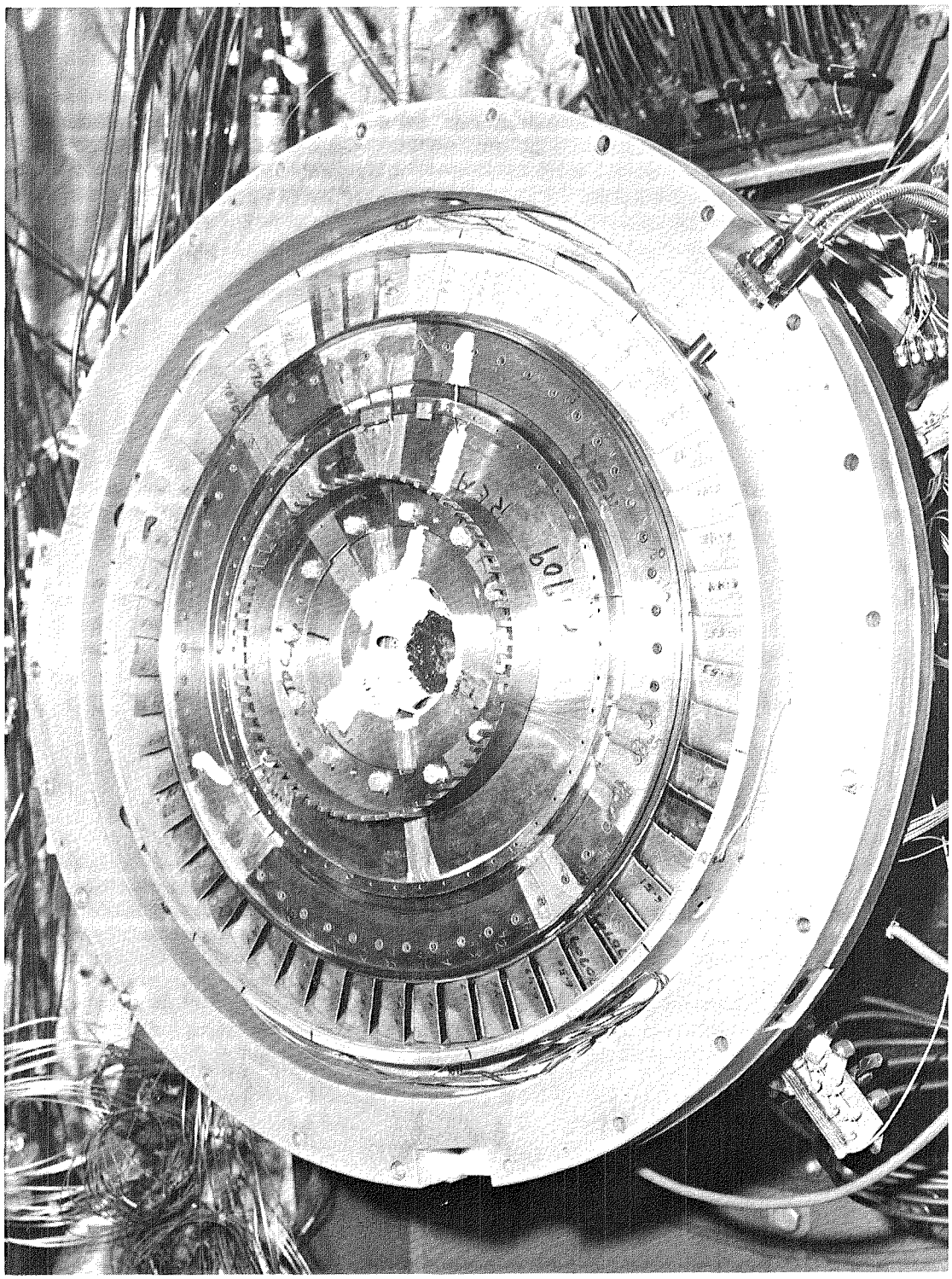

Figure 30 Rotating Rig

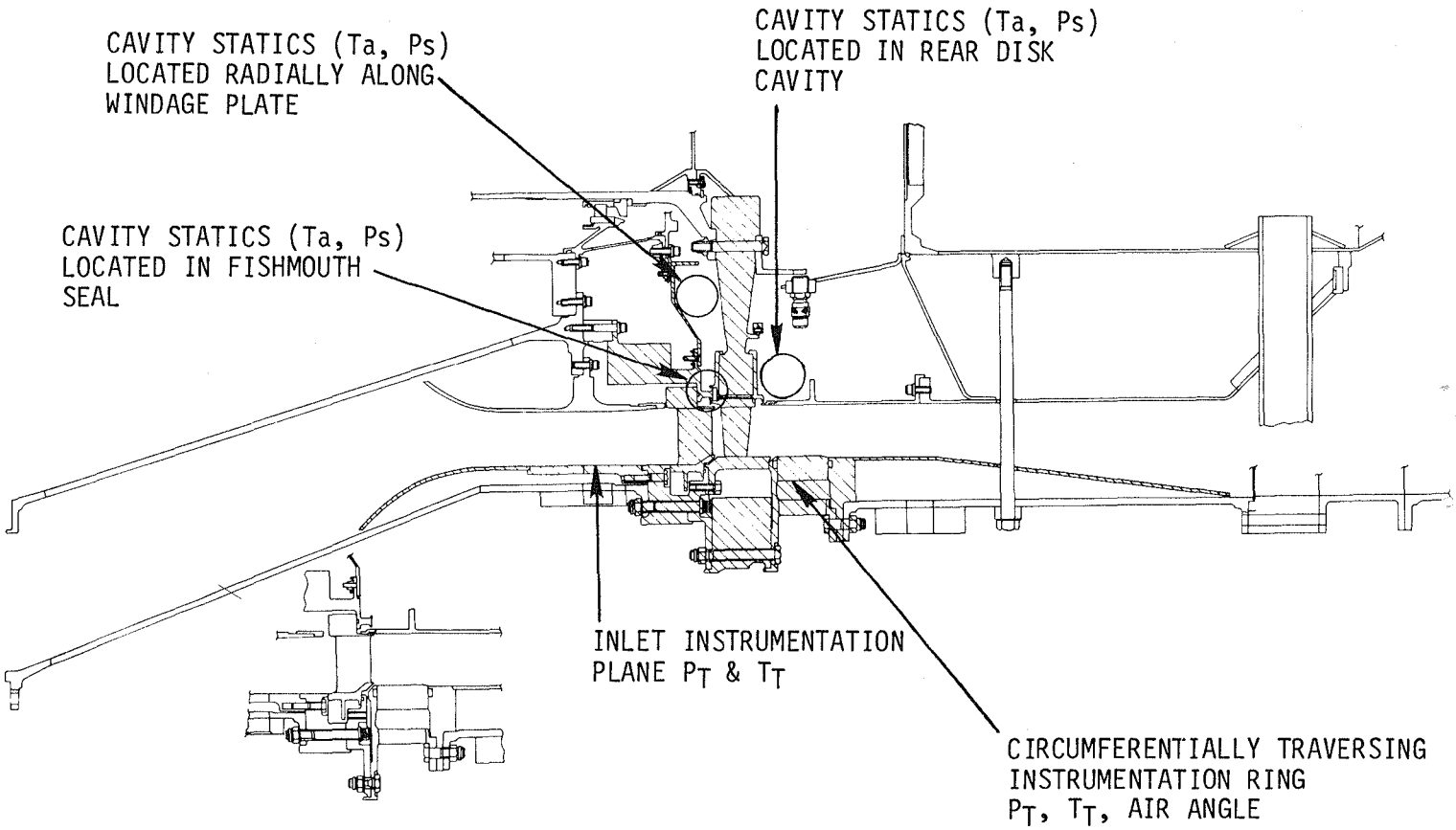

Figure 31 Uncooled Rig Primary Performance Instrumentation

Exit instrumentation was mounted on a circumferentially traversing instrumentation ring supported on the outer diameter. The instrumentation ring contained 4 radially fixed total pressure rakes and 4 radially traversing air angle probes. The traversing ring rotated through 30 degrees; therefore, the four probes mapped 120 degrees of the exit circumference.

5.2.2 Rotating Rig Instrumentation

For the rotating rig test, the ring contained 4 radially fixed total pressure rakes, 4 radially fixed total temperature rakes, 1 radially traversing concentric temperature/pressure probe, and 3 radially traversing air angle probes. The total range of circumferential travel for a given sensor mounted on a ring was 30 degrees (corresponding to two vane pitches). The instrumentation used in the rotating rig tests is summarized in Table 8.

TABLE 7

ANNULAR CASCADE TEST INSTRUMENTATION

Location	Type	Quantity
Inlet	P_t, T_t	4 P_t Rakes, 8 T_t Rakes (10 Sensors per Rake)
Inlet	P_s	12 Total, 6 Each on the Inner and Outer Flowpath Walls
Vane Surface	P_s	51 Total, on the Pressure and Suction Surfaces at Three Radial Locations
Vane Endwalls	P_s	42 Total, on the OD and ID Vane Channels
Exit	P_t	4 Rakes (10 Sensors per Rake) Mounted on the Outer Diameter Supported Circumferentially Traversing Instrumention Ring
Exit	Air Angle, P_t	4 Radially Traversing Probes Mounted on the Circumferentially Traversing Instrumentation Ring
Exit	P_S	12 total, 6 each in the inner and outer vane cavities
Exit	P_s	20 Total, 12 on the Inner Diameter Flowpath and 8 on the Outer Diameter Flowpath
Exit	P_s	10 Total Along the Inner Diameter Flowpath Inner Liner to Exhaust Dump

The primary performance instrumentation for the rig consisted of inlet and exit total temperature and total pressure rakes (see Table 8). Additional instrumentation was used to measure primary and secondary flow rates, speed, exit flow angle, static pressures (airfoil, flowpath, and cavity), cavity air temperatures, metal temperatures, and blade tip clearance.

5.3 Test Procedures

5.3.1 Annular Cascade Test Conditions

The annular cascade test consisted of operating points covering a range of vane pressure ratios (exit Mach numbers). Inlet conditions were held constant and the cascade exit static pressure was varied using exhausters. The annular cascade test program is summarized in Table 9.

TABLE 8

ROTATING RIG TEST INSTRUMENTATION

Location	Type	Quantity
Inlet	P_t, T_t	4 P_t Rakes, 8 T_t Rakes (10 Sensors per Rake)
Inlet	P_s	12 Total, 6 Each on the Inner and Outer Flow path Walls
Vane Surface	P_s	54 Total, on the Pressure and Suction Surfaces at Three Radial Locations
Vane Endwalls	P_s	42 Total, on the OD and ID Vane Channels
Vane Exit	P_s	12 Total, 6 Each in the Inner and Outer Vane Cavities
Blade Surface	P_s	35 Total, on the Pressure and Suction Surface at Three Radial Locations
Exit	P_t, T_t	4 P_t Rakes, 4 T_t (12 Sensors per Rake) Mounted on the Outer Diameter Supported Circumferentially Traversing Instrumention Ring
Exit	Air Angle, P_t	3 Radially Traversing Probes Mounted on the Circumferentially Traversing Instrumentation Ring
Exit	Concentric, P_t, T_t	1 Radially Traversing Probe Mounted on the Circumferentially Traversing Instrumentation Ring
Exit	P_S	12 total, 6 each in the inner and outer blade cavities
Exit	P_s	20 Total, 12 on the Inner Diameter Flow path and 8 on the Outer Diameter Flow path
Various Cavities	P_s, T_a	48 P_s, 48 T_a for Diagnosis
Disk Blade	T_m	12 T_m at 4 Radial Locations for Tip Clearance Analysis and Rotating Static Corrections
Rotor Casing	T_m	9 T_m for Tip Clearance Analyses
Rotor Casing	Proximity Probe	3 Laser Probes for Tip Clearance Measurement

TABLE 9

TYPICAL RUN FOR ANNULAR CASCADE TESTING

Operating Point	Exit Mach No.	P_T inlet PSIA	T_T inlet Degrees R	P_S exit/P_T inlet
1	0.70	57.42	775	0.70
2	0.80	57.42	775	0.64
3	0.92	57.42	775	0.56
4	1.01	57.42	775	0.49
5	1.13	57.42	775	0.41

5.3.2 Rotating Rig Test Conditions

The rotating rig test covered approximately 12 operating conditions, consisting of a range of turbine speed parameters, pressure ratios, and front disk flow rates. The values that were determined included the sensitivity of the blade-to-incidence angle, Mach number, and the injection of the front disk leakage flow. Inlet conditions were held constant, and the turbine conditions were varied by exit flow exhausters and a power absorbing waterbrake. Flow was injected into the primary flow stream at varying rates. This flow was directed through the front disk cavity at the pressure ratio and speed parameter of the design point. The rotating rig test program is summarized in Figure 32.

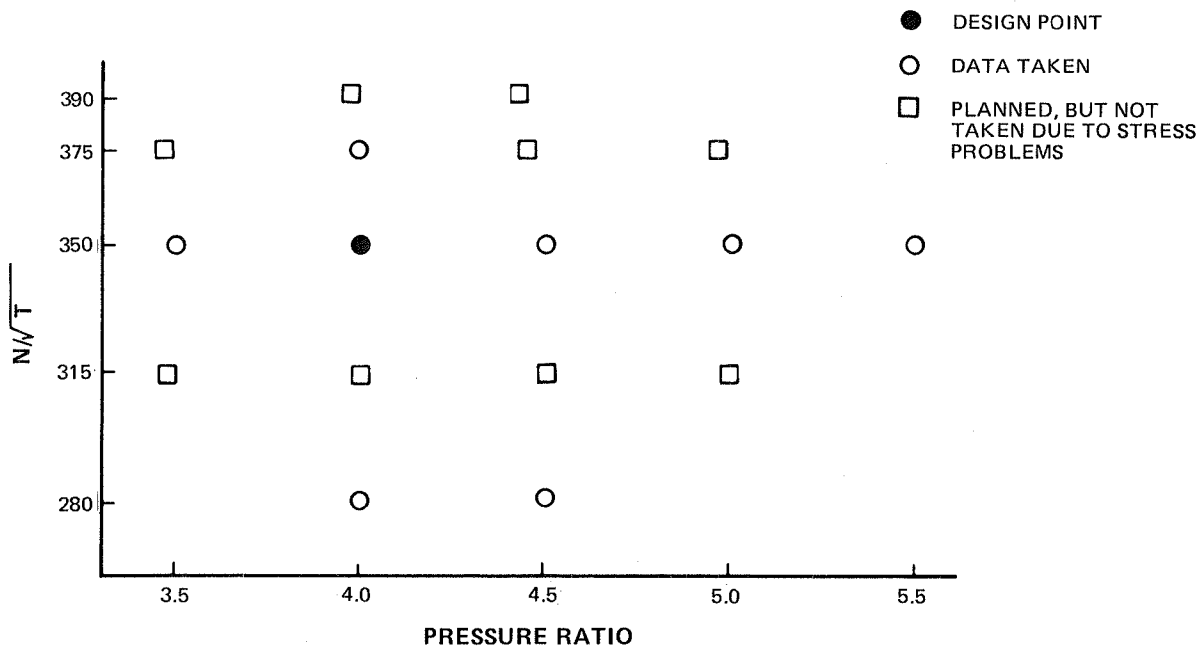

Figure 32 Typical Run For Rotating Rig Testing - Additional testing was conducted to determine the effect of leakage by injecting air into the front disk cavity at the design point conditions.

5.3.3 Data Acquisition

Annular cascade and rotating rig data were acquired in a planned sequence for all of the test conditions.

5.3.4 Data Recording

All test data were automatically recorded by a time sharing computer (Sigma 8) via a remote batch terminal located at the test stand. Pressure data were acquired by scanivalves using high precision transducers with negligible hysteresis. Thermocouples were "hooked into" Universal Temperature Reference boxes with unbroken leads to copper buses before the signal went to the digital voltmeter. Pressure and temperature data proceeded through a high accuracy digital voltmeter to the remote batch terminal. The data were then processed through the Sigma 8 computer, converted into engineering units, and either displayed at the test stand or printed.

5.3.5 Data Reduction

Data from the annular cascade test were reduced to row total pressure loss, which was calculated from the measured spanwise and circumferential inlet and exit total pressure traverses. Measured vane exit air angle profiles, airfoil static pressure distributions, and endwall static pressures were also determined from the data.

Rotating rig efficiency was calculated using the measured inlet and exit total temperatures and pressures. Stage exit air angle profiles, vane and blade static pressure distributions, endwall static pressures, cavity static pressures and air temperature, flows, mechanical speeds, clearances, and metal temperatures were measured, recorded, and presented. Data was then analyzed and compared with the predictions.

5.3.6 Shakedown Testing

During assembly, instrumentation was first installed and connected and was later checked for identification and leakage. The shakedown procedure consisted of obtaining a complete data point to substantiate the mechanical integrity of the test rig and to verify the performance of the instrumentation and data acquisition systems. The testing resumed after it was ascertained that all instrumentation and systems were operating properly.

5.3.7 Rotating Rig Stress Testing

Four blades of the Build 1 rotating rig were eac' instrumented with one strain gage (see Figure 33) to monitor vibratory stresses during performance testing. During the initial attempt to acc erate to design speed (nominal 9800 rpm), a first mode 24E resonance was encountered at 8900 rpm with blade stresses reaching 18 ksi. These stresses were higher than normal test limits, so a review of the running program was instituted. To reduce these stresses, thereby allowing accelerations to design speed, rig inlet pressure was

decreased and the rig was rapidly accelerated through the 24E resonance. The combination of increased rate of acceleration and reduced inlet pressure resulted in acceptable airfoil stress levels which allowed performance testing at the higher speeds.

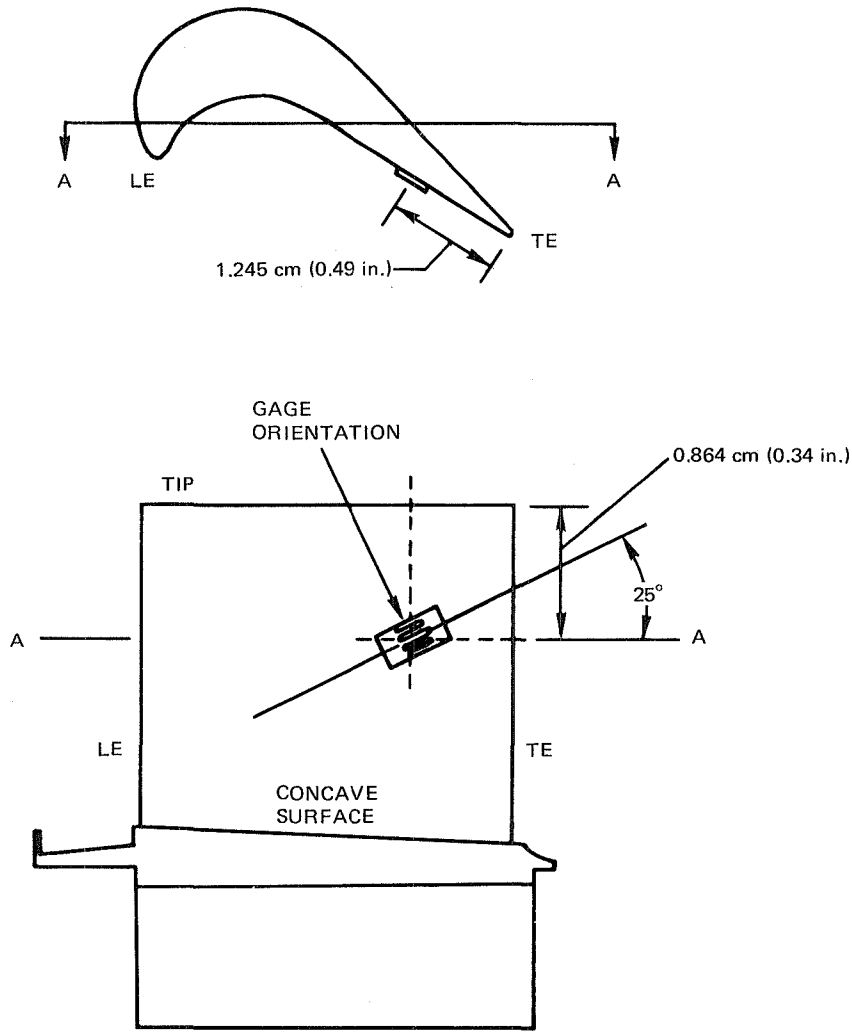

Figure 33 Strain Gage Location (Build 1)-Installed to monitor vibratory stresses during performance testing.

The experience gained in Build 1 with the low reaction blading and the similarity of resonant characteristics between low and high reaction blading indicated that the Build 2 high reaction blading should be equipped with strain gages. Three blades of the Build 2 rig were instrumented with 4 gages on each blade to better define the dynamic stress distribution in the modes of response. During Build 2 testing, high stresses again occurred in the first mode 24E resonance at approximately 8800 rpm, reaching a maximum of 34 ksi. Again, rig inlet pressure was reduced and the rig rapidly accelerated through the 24E resonance so that performance data could be acquired at higher speeds.

The high 24E first mode stresses of Builds 1 and 2 were thought to be associated with a higher than predicted resonant speed coupled with inadequate mechanical damping. The rig incorporated a wire seal, positioned between the platforms of adjacent blades for sealing, plus a damper, located under the platforms for minimizing resonant response (see Figure 34). The indications from both Builds 1 and 2 were that either the wire seal, the damper, or both, were "locked up." This condition would produce higher frequences and minimal mechanical damping. Since the wire seal and damper were parts unique to the rig, an abbreviated test plan was formulated to evaluate the frequency and stress response of the Build 2 high reaction blades. For this test, a lighter weight design was created by removing the wire seal and reducing the damper thickness.

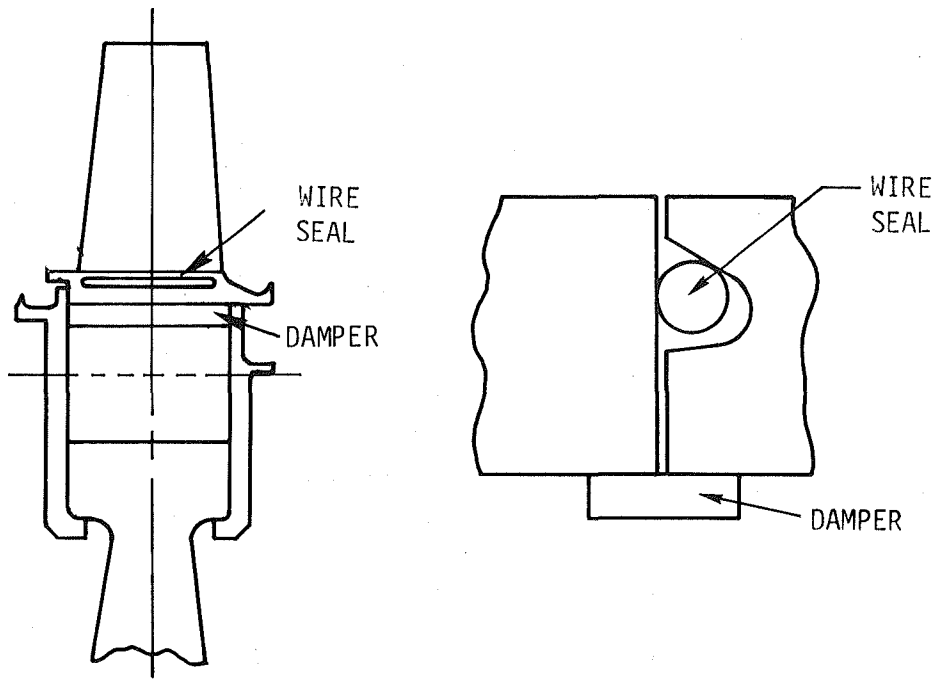

Figure 34 Rig Wire Seal and Damper-Wire seals were used to prevent leakages between adjacent platforms and dampers were used to minimize resonant response.

5.3.7.1 Test Program

The primary objectives of this program were to (1) determine how the removal of the wire seal and the reduction of the size of the damper seal would affect the resonant frequencies and (2) determine how effective a platform damper is in minimizing dynamic response.

Bench Testing

Four low reaction blades were tested in the holography laboratory to define mode shapes and frequencies. Each blade was held in a broach block that was uniformly squeezed from the sides. The broach block loading was sufficient to prevent attachment slippage and maintained at a constant level for each blade. Typical holograms are shown for the first five modes in Figure 35 where significant chordwise bending motion can be noted even in the first flap mode. These mode shapes required the use of additional strain gages in the rotating rig test to adequately define actual airfoil stress distribution in the various modes of response.

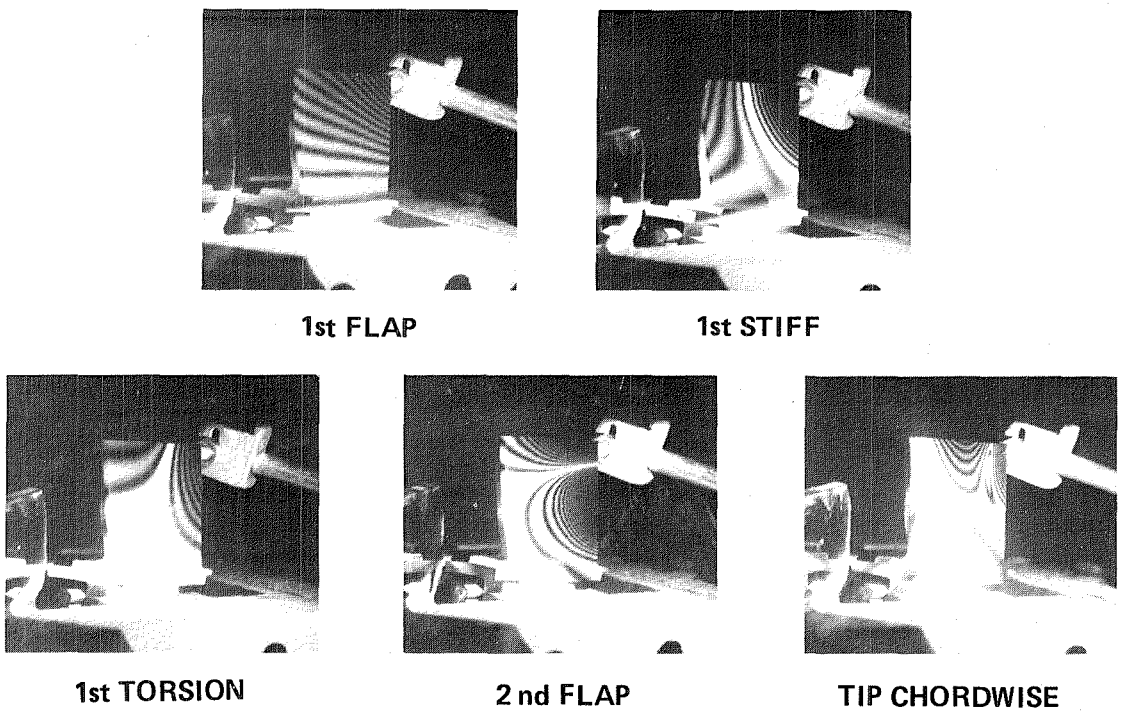

Figure 35 Vibrational Holographic Analysis of the Energy Efficient Engine Cold Flow Rig Turbine Blade

The three high reaction blades previously instrumented in Build 2 were re-instrumented with eight strain gages per blade (see Figure 36).These gages were located at expected areas of high stress for the 5 modes previously identified. Bench testing was then performed at room temperature to define the vibratory stress distribution in each of these first five modes. Figure 37 shows the level of stress for each gage location in terms of a percentage of maximum for the first two modes.

- EIGHT 40.64 cm (1/16 IN.) DYNAMIC STRAIN GAGES PER BLADE
- THREE BLADES (SN 43, 49 & 56)

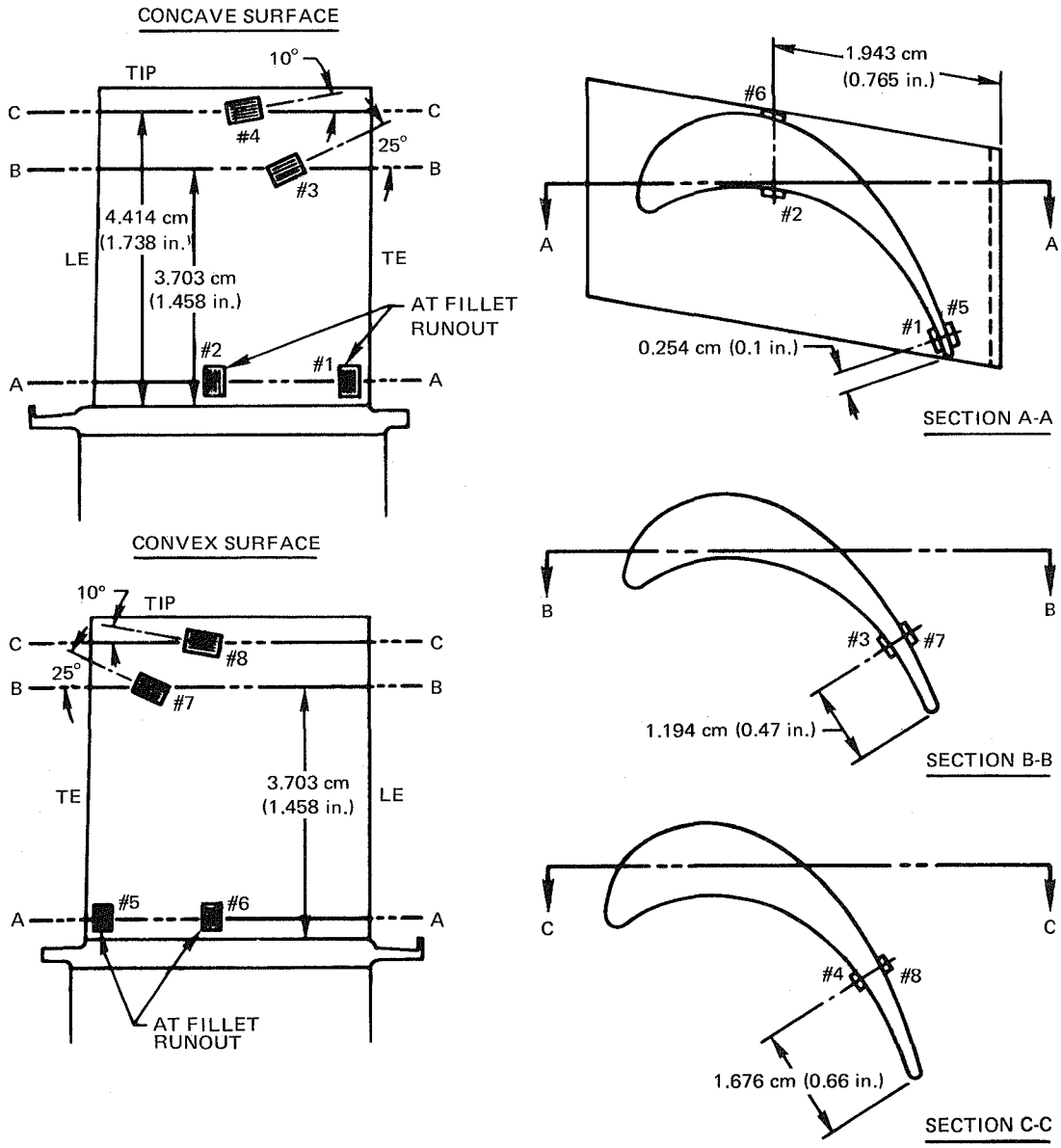

Figure 36 Strain Gage Location (Stress Test and Bench Test)

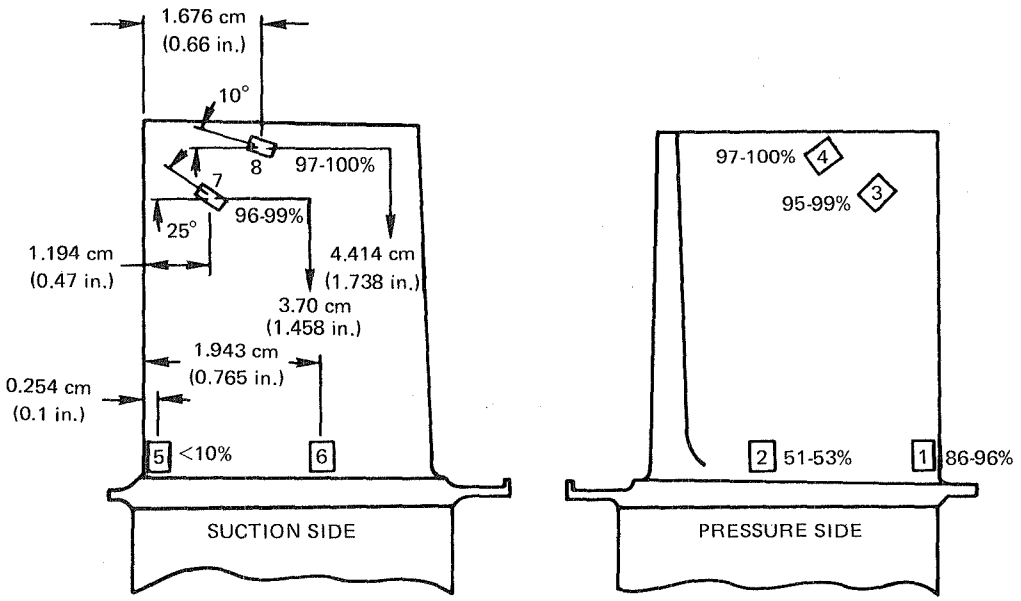

1ST MODE

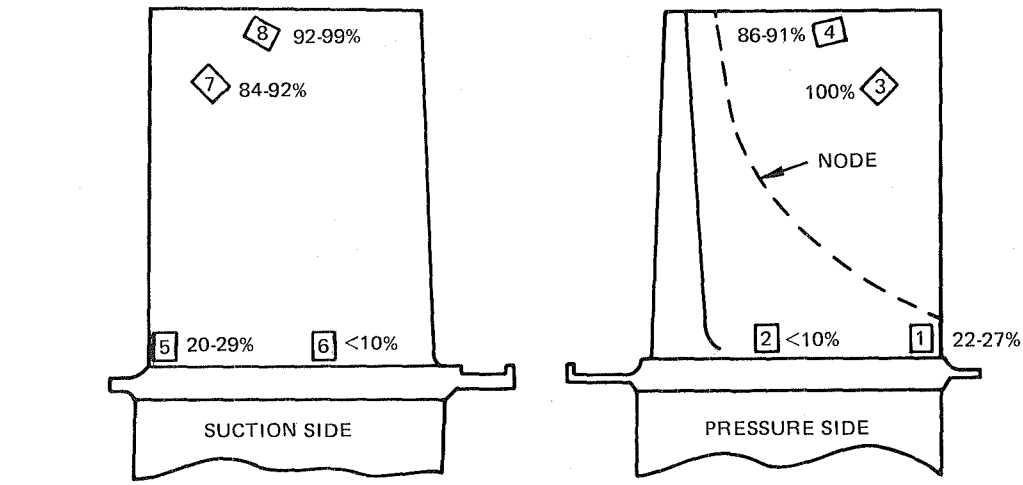

2ND MODE

Figure 37 Stress Ratios From Blade Bench Tests

Rig Testing

A slow acceleration was run to 11,000 rpm followed by a slow deceleration. Stress levels for all three blades were recorded during this running for all 24 strain gages. The previously recorded 24E first mode resonance from Build 2 was noted to be approximately 1000 rpm lower and responded at about 25 percent of the stress level. These two facts met the primary objectives of the test by showing that removing the wire seal and reducing the size of the damper did lower the first mode frequency as well as show that this mode could be effectively damped at the under platform location.

5.3.7.2 Results and Conclusions

Test results confirmed that lower stresses were obtained when the rig-unique wire seal and damper design were replaced with a modified lighter weight damper. This type will be used in the engine. Also, the frequency information gathered from the bench and rotating rig testing was used to adjust the NASTRAN analysis for the component design (see Figure 38).

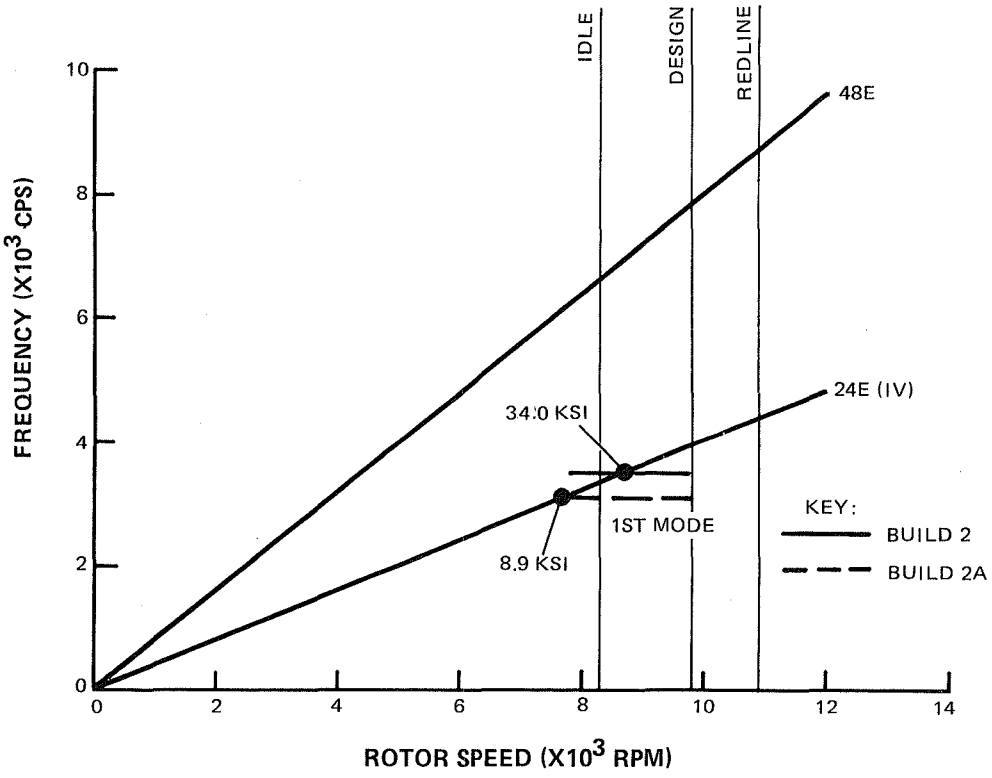

Figure 38 Rig Blade Resonance Diagram - 24E first mode response shows the effect of wire seal removal and damper size reduction on frequency and stress.

As a result of this test program, the component rotor design effort will include evaluation of lighter weight design concepts for the damper located under the blade platforms.

6.0 RESULTS

6.1 Annular Cascades

6.1.1 Performance Discussion

6.1.1.1 Loss Comparison

Vane losses, which include span mass averaged total loss, endwall loss, and profile loss from the three annular cascade tests, are shown in Figures 39 and 40 for the wedge probes and the exit rakes. On each figure, all losses are plotted against mass averaged Mach number; the endwall loss (or secondary loss) is derived by subtracting the profile loss from the total vane loss. The wedge probes were in the axial plane of the blade leading edge (about 0.46 in. axially from the vane trailing edge). The exit rake kiel heads were further downstream (about 0.84 in. axially). Therefore, increased mixing losses cause the losses measured by the rakes to be higher than losses measured by the probes.

The testing of three different vanes in annular cascades has substantiated the low loss predictions established for the uncooled rig. The trends with profile loss are in excellent agreement with predicted values. A comparison of the data at the blade leading edge location shows the canted vane to have the lowest mass averaged total losses. The Build 1 vane had the next lowest losses, and the Build 2 vane had the highest losses.

6.1.1.1.1 Data Presentation

The contour plots for the three builds of the annular cascade show a clean low loss core flow and higher loss endwall and wake regions (see Figures 41 through Figure 43). These data were acquired from the radial circumferential traversing of the exit probes.

The low loss core region is also shown by circumferentially area averaging the vane loss contours and plotting the results spanwise (see Figure 44). The comparison between the data from the probes and rakes shows the additional mixing loss at the rake station to be predominately at the inner diameter. A spanwise comparison of the probe data shows the Build 1 vane to have higher loss at the inner diameter and lower loss at the outer diameter than the Build 2 vane. The figure also shows additional reduction in loss at the inner diameter and increased loss at the outer diameter caused by canting the Build 2 vane 13 degrees in Build 3.

The comparison of total losses, generated by mass averaging the spanwise losses with the results from the air angle traverse, showed the lower loss at the outer diameter for Build 1 outweighs the higher loss at the inner diameter, thereby giving the Build 1 vane a lower mass averaged total loss than the Build 2 vane at the same Mach number (see Figure 39). The results of the canted vane tests showed the reduced loss at the inner diameter outweighed the increased loss at the outer diameter to give the canted vane the lowest mass averaged total loss of the three airfoils tested.

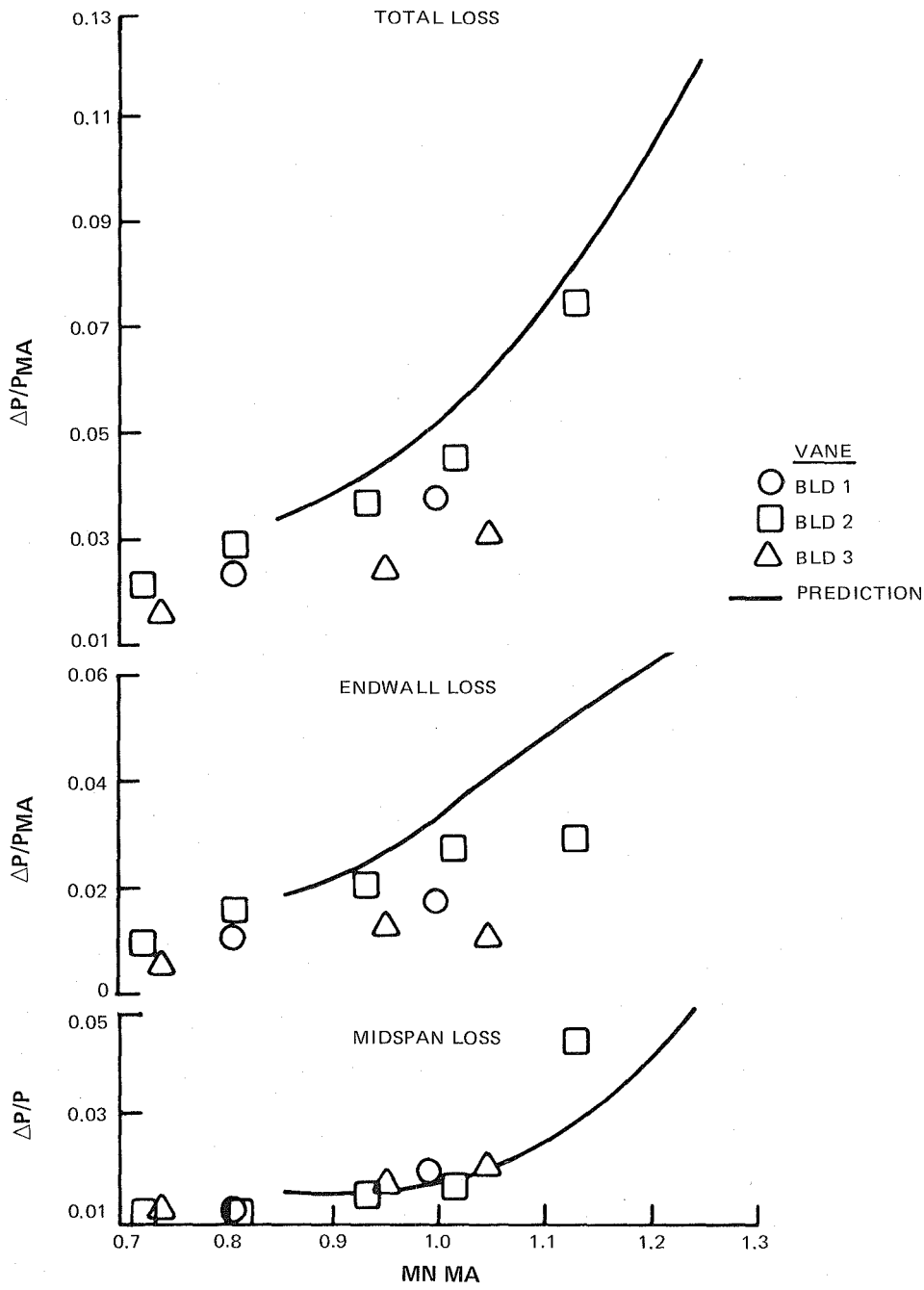

Figure 39 Annular Cascade Pressure Loss vs Mach Number

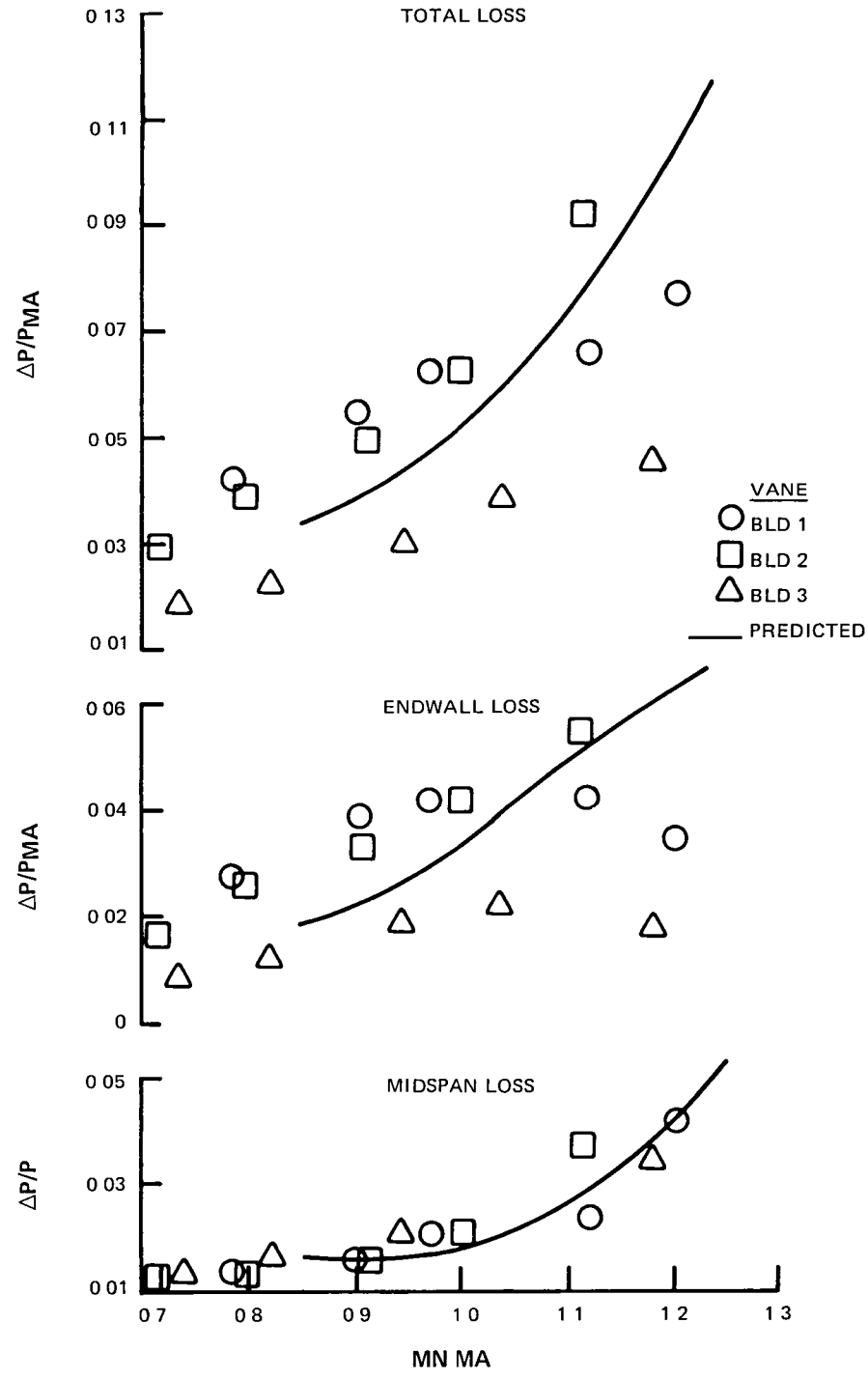

Figure 40 Annular Cascade Pressure Loss vs Mach Number

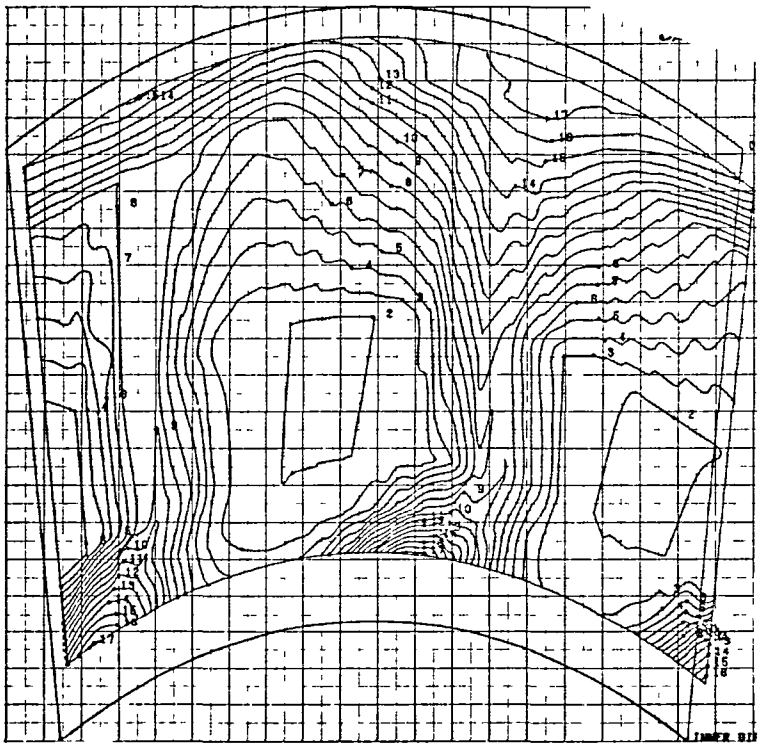

Curve Label	Curve Value Δ P/P
2	0.0
3	0.01000
4	0.02000
5	0.03000
6	0.04000
7	0.05000
8	0.06000
9	0.07000
10	0.08000
11	0.09000
12	0.10000
13	0.11000
14	0.12000
15	0.13000
16	0.14000
17	0.15000

Build 1 Mn_{ma} = 0.997

Figure 41 Typical Vane Loss Contours at Design - This plot represents circumferential traverse data over two vane gaps at 8 radial positions.

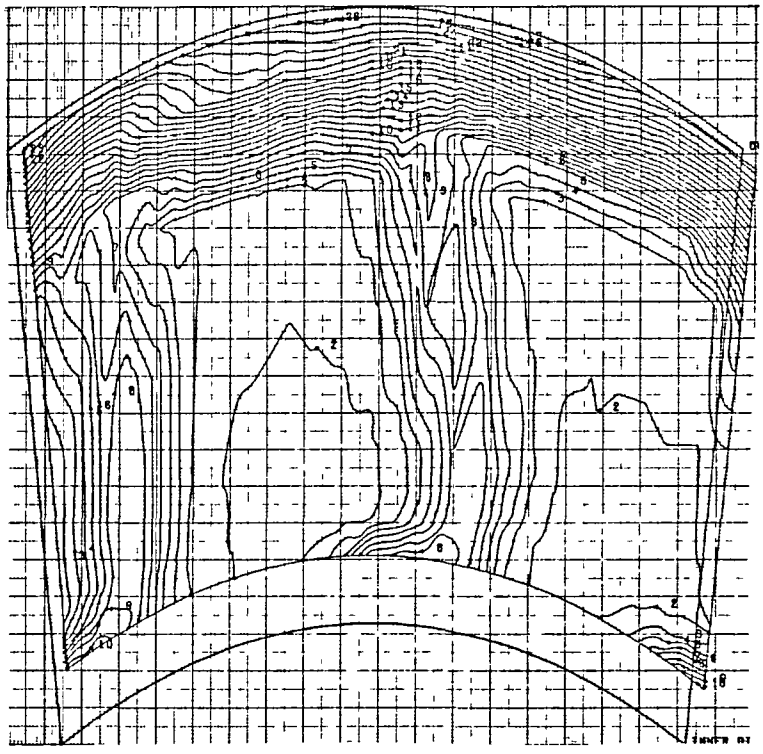

Curve Label	Curve Value ΔP/P
2	0.0
3	0.01000
4	0.02000
5	0.03000
6	0.04000
7	0.05000
8	0.06000
9	0.07000
10	0.08000
11	0.09000
12	0.10000
13	0.11000
14	0.12000
15	0.13000
16	0.14000
17	0.15000
18	0.16000
19	0.17000
20	0.18000
21	0.19000
22	0.20000
23	0.21000
24	0.22000
25	0.23000
26	0.24000
27	0.25000

Build 2 Mn_{ma} = 0.932

Figure 42 Typical Vane Loss Contours at Design - This plot represents circumferential traverse data over two vane gaps at 10 radial positions.

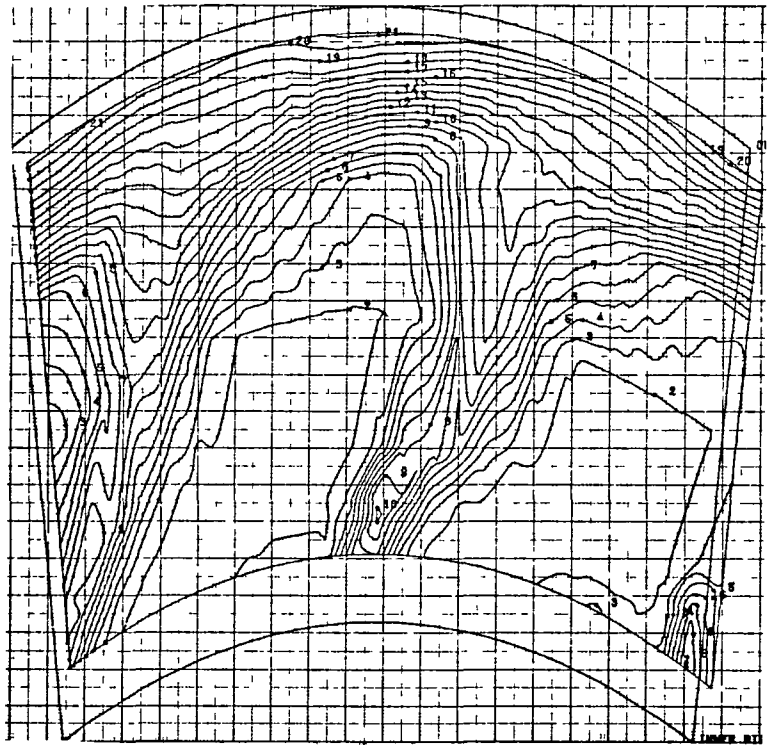

Curve Label	Curve Value ΔP/P
2	0.0
3	0.01000
4	0.02000
5	0.03000
6	0.04000
7	0.05000
8	0.06000
9	0.07000
10	0.08000
11	0.09000
12	0.10000
13	0.11000
14	0.12000
15	0.13000
16	0.14000
17	0.15000
18	0.16000
19	0.17000
20	0.18000
21	0.19000

Build 3 Mn_{ma} = 0.951

Figure 43 Typical Vane Loss Contours at Design - This plot represents circumferential traverse data over two vane gaps at 9 radial positions.

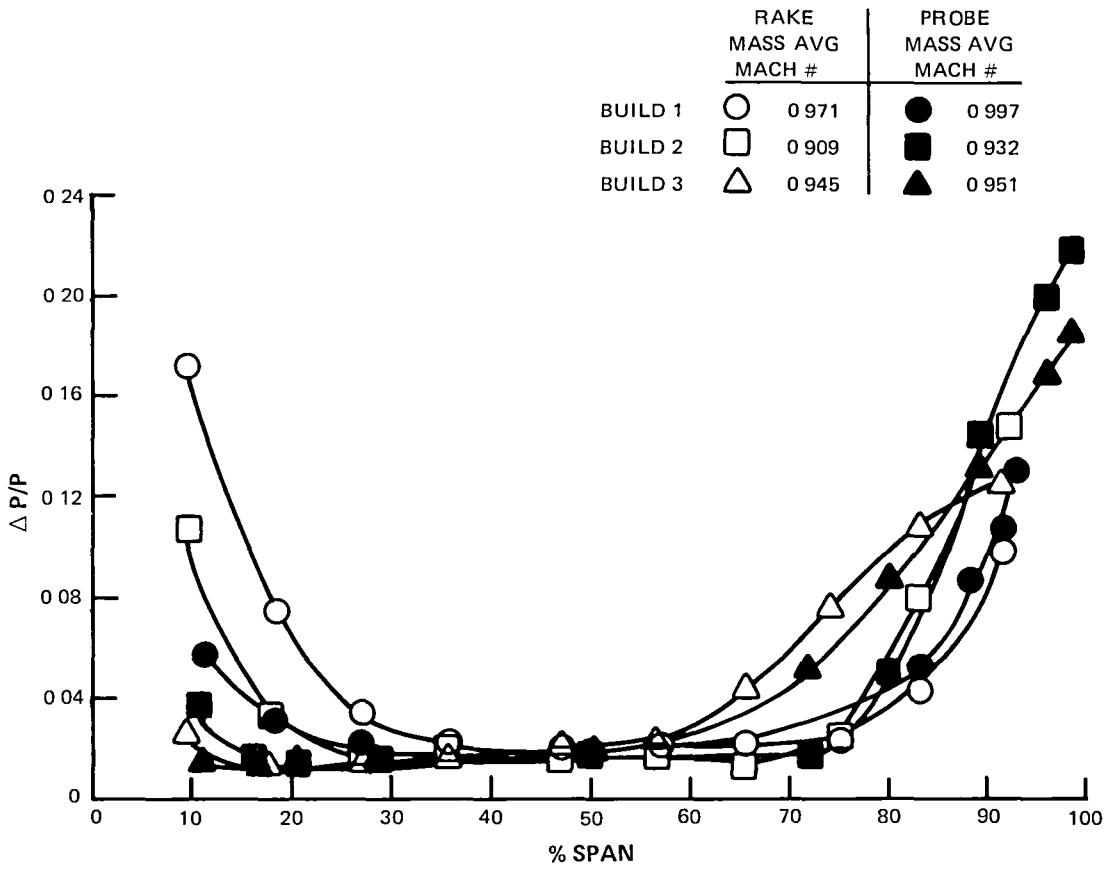

Figure 44 Vane Loss vs Percent Span - The low loss core region is indicated by circumferentially averaging the vane loss and plotting the results spanwise.

The mass-averaged total losses for Builds 1, 2 and 3 were .0376, .0369 and 0.0245, respectively, at the design conditions as measured by the exit probe.

Vane gas exit angle is important for good performance, because blade inlet conditions, incidence distribution, and flow distribution are functions of vane exit angle and wheel speed. Design point vane exit angle spanwise data are shown in Figure 45. The level of the measured data, acquired with a radial traverse at mid-gap, was adjusted to match continuity. The data shows the angle skews, with higher angles near the inner diameter and lower angles near the outer diameter. Build 3 has the largest skew, Build 1, the next largest, and Build 2, the least. Although the angle skew was not predicted, good overall rotating rig performance for Build 1 and Build 2 suggests that the incidence and flow distribution shown in the annular cascade were not the same in the rotating rig because of a redistribution of flow caused by the rotor. The Build 3 vane was not tested in a rotating rig; therefore, it is not known if its larger angle skew would cause a performance penalty. For this reason, the Build 3 vane will not be used in the engine design without additional rig work. Therefore, the Build 1 vane, having proven air angle distribution and lower loss than the Build 2 vane at comparable Mach numbers, will be used for the engine design. Additional data for the annular cascade tests for Builds 1, 2 and 3 are presented in Appendices B, C, and D, respectively.

6.1.2 Analysis Discussion

6.1.2.1 Deviation

Airfoil deviation is defined as the difference between the exit air angle and the gage plane (throat) air angle. The calculation of the deviation becomes important because it is a factor in setting the flow through the cascade. The average deviation for the three builds of the annular cascade was calculated based on continuity and measured geometry and is compared to the design system used for each build. Figure 46 shows this comparison. At the cascade design point, the Build 1 results indicate an approximate 0.3-degree difference; the Build 2 results, an approximate 0.85-degree difference; and the Build 3 results, an approximate 0.80-degree difference. Therefore, the Build 1 design system was in better agreement with the experimental deviation than the system used for Builds 2 and 3.

The measured and predicted flow parameters are shown as a function of exit Mach number in Figure 47. The flow parameter measurements used here were calculated with rig inlet flows measured with choked venturis. The predicted flow parameters were based on an analysis that was performed with averaged data using the measured throat areas and a deviation system similar to that used for the Build 1 design. Table 10 compares the predicted and measured flow for the high Mach numbers where the flow is choked. Build 1 shows the best agreement with the design system. This may be caused by the margin of error in measuring the airflow or throat area, the deviation system, and possible leakage between the rig and the sonic venturi.

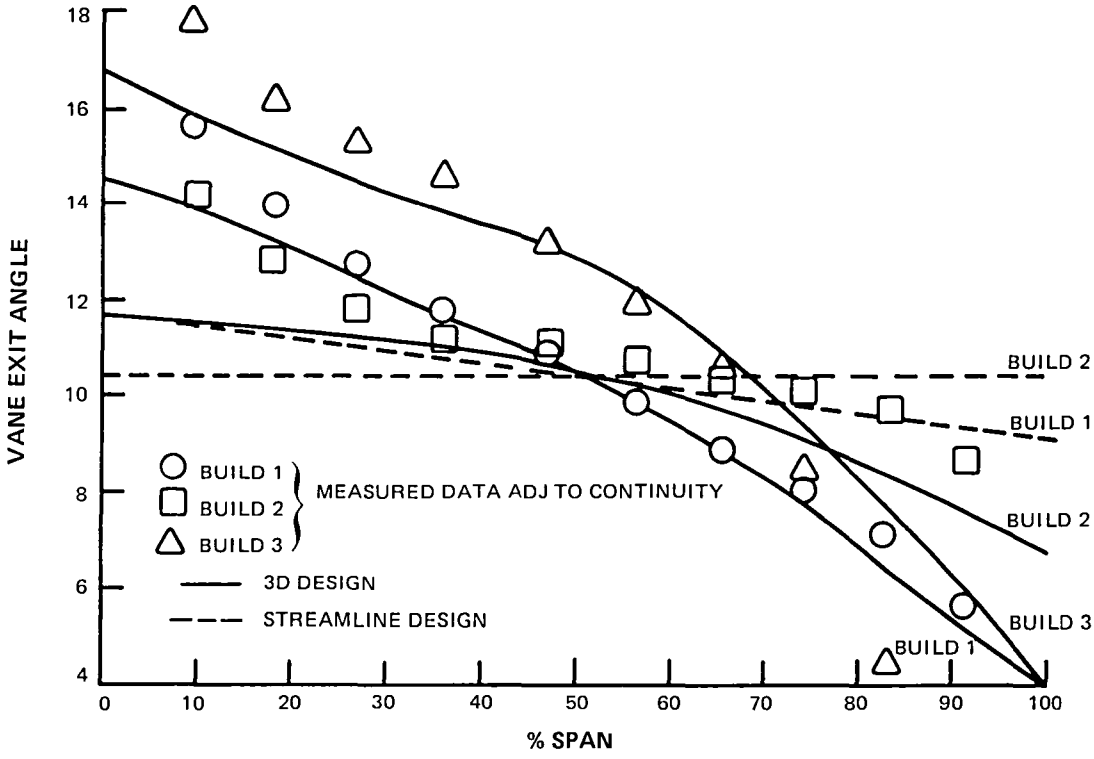

Figure 45 Vane Exit Angle Distribution - Higher angles near the inner diameter and lower angles near the outer diameter were measured.

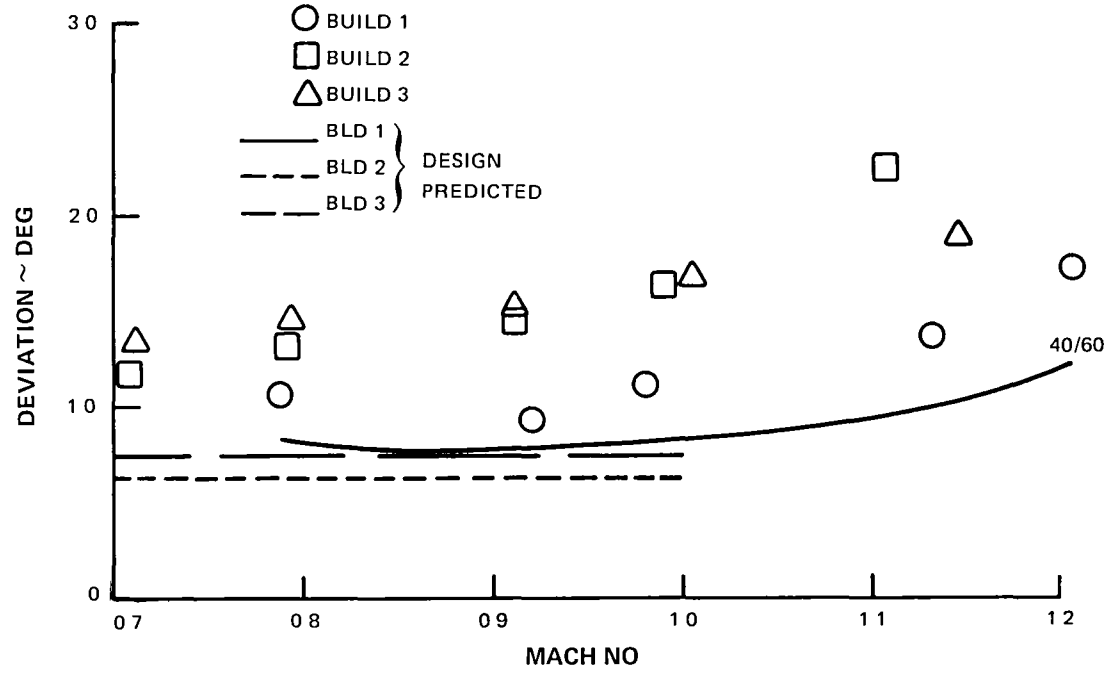

Figure 46 Deviation vs Mach Number - The deviation prediction system used for the Build 1 design gave better agreement than the system used for Build 2 or Build 3.

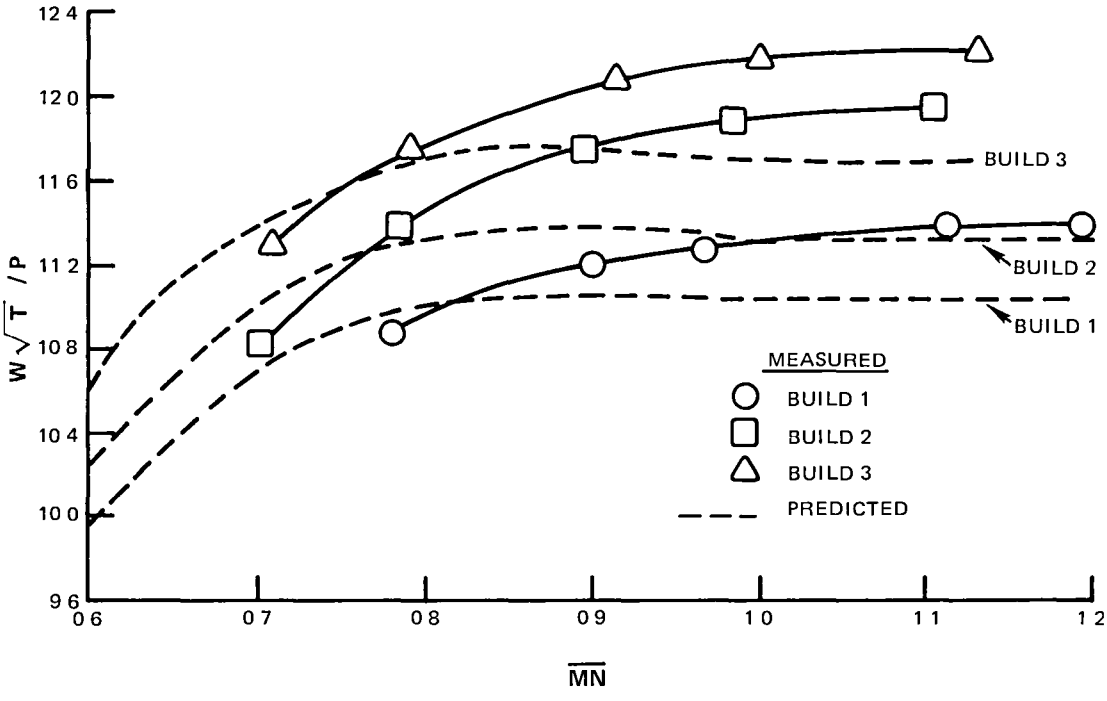

Figure 47 Flow Parameters Mach Number - At high Mach numbers, the rig exhibits a higher flow parameter than predicted.

TABLE 10

FLOW COMPARISON

	Measured $w\sqrt{T/P}$	Predicted $w\sqrt{T/P}$	Percent Difference
Build 1	11.39	11.04	3.1
Build 2	11.95	11.32	5.6
Build 3	12.22	11.68	4.6

6.1.2.2 Pressure Distribution Discussion

Low loss vane performance is attained by maintaining a desirable airfoil surface pressure distribution. Effects of adverse pressure gradients and shock losses are minimized by appropriate loading distributions. Mean section vane surface static pressures at design are compared for all three builds in Figure 48. This figure shows the airfoil static pressure, non-dimensionalized by the average inlet total pressure, plotted against percent of axial chord. Loading distributions from front to rear are similar, yet vary from build to build. Predicted distributions qualitatively match the data, which verify design procedures. Predictions accurately follow the changes from build to build. The prediction, a two-dimensional calculation at a given radius, uses a streamtube radial height ratio between the airfoil leading edge and trailing edge to model the flow over the airfoil sections. Consequently, the Build 3 canted vane configuration, which has identical sections to Build 2, can have different pressure distributions from Build 2 only because of radial forces caused by the vane cant, and other 3-dimensional flow effects. Airfoil surface pressure distributions for both the cascade and stage tests are presented in Appendices B through F at various radial sections.

6.2 Rotating Rig

6.2.1 Performance Discussion

6.2.1.1 Efficiency Comparison

An efficiency gain of 1.1 percent was predicted at the design point by increasing AN^2 from 34×10^9 to 49×10^9 $(\text{in-RPM})^2$. This increase in AN^2 allowed the Energy Efficient Engine high-pressure turbines to run at a lower Cx/U ratio and a higher velocity ratio. The experimental gain in efficiency is shown in Figure 49 where the area averaged efficiency of Build 1 of the uncooled rig is compared to the state-of-the-art AN^2 level at the Build 1 reaction level. At the design point, the efficiency gain was 1.15 percent, which agrees with the predicted value of 1.1 percent.

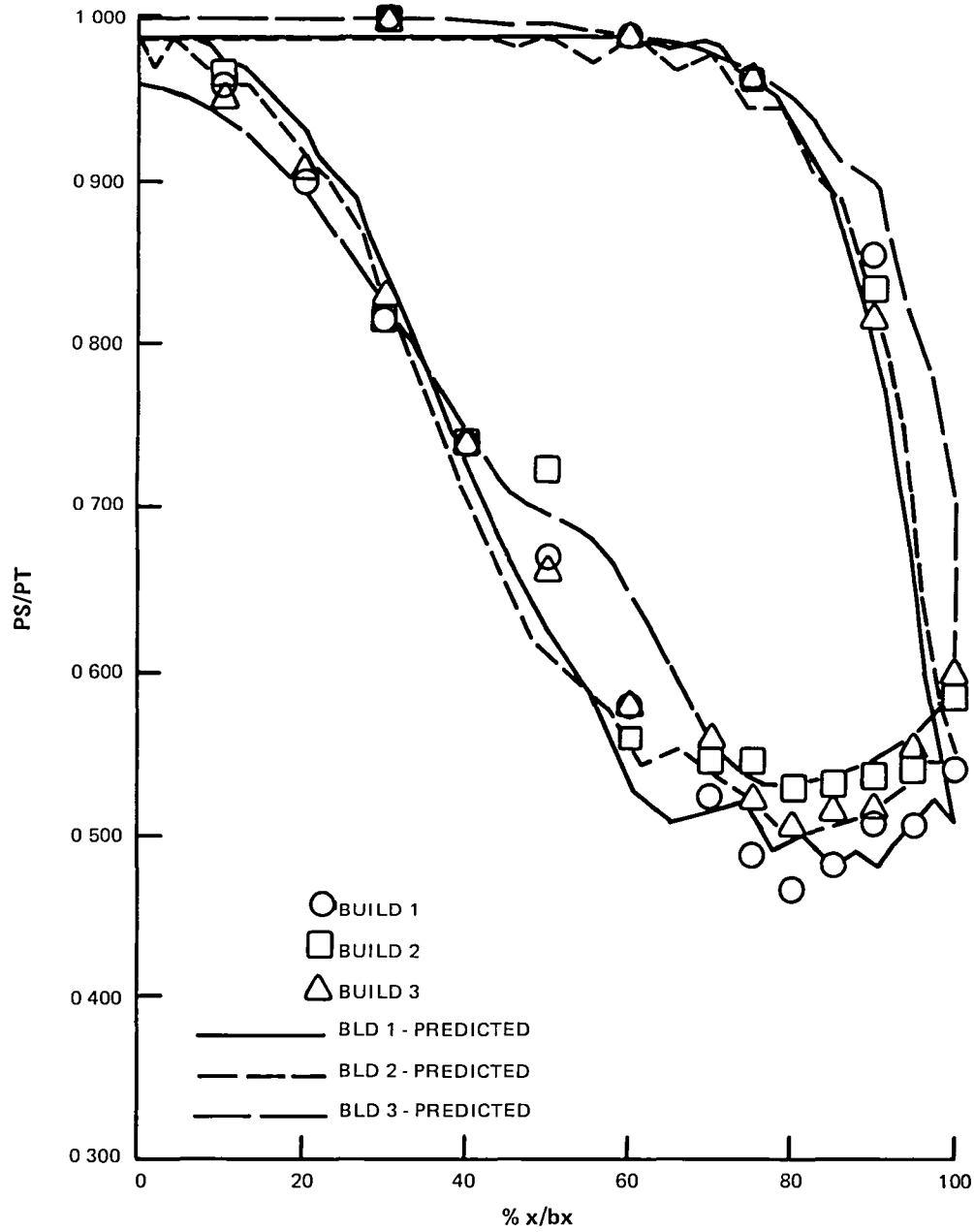

Figure 48 Vane Surface Statics (50 percent span) - Low loss vane performance is achieved by maintaining a desirable pressure distribution.

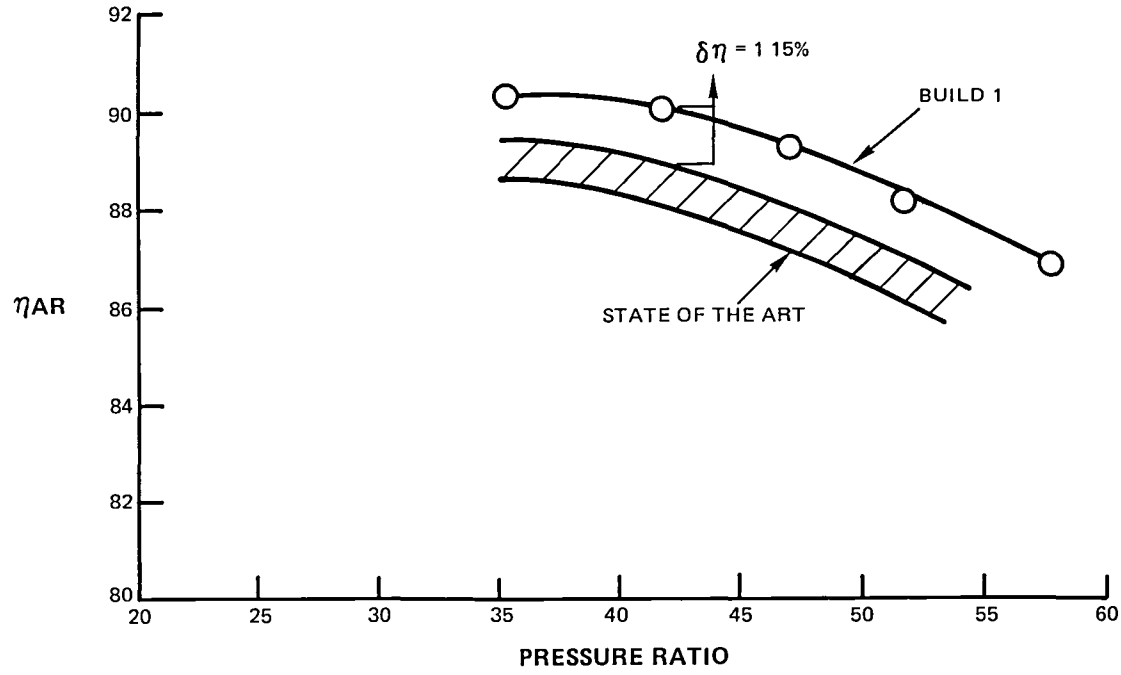

Figure 49 AN^2 Increase - A net area-averaged efficiency gain of 1.15 percent was achieved by increasing the AN^2 parameter.

A comparison of low reaction and high reaction rig performance is shown in Figure 50. The high reaction turbine demonstrates a 0.8-percent higher efficiency than the low reaction turbine at the design point. This exceeds the predicted efficiency gain of 0.5 percent. This benefit for high reaction decreased as the turbine was run off-design (see Figure 50). The Build 1 test data agree with predicted values at lower pressure ratios, but at the higher pressure ratio points efficiency is overpredicted. For Build 2, the measured efficiency exceeded the prediction at the design point, but at the higher pressure ratio points, efficiency is overpredicted. The lower corrected speed (280) data are overpredicted, and the high corrected speed (375) data are underpredicted. The design point data are summarized in Table 11 and in Figure 50.

TABLE 11

DESIGN POINT PERFORMANCE
(Corrected to 0.0145 in. tip clearance)

Build	Reaction (percent) Predicted	Reaction (percent) Test	Mass Averaged Efficiency (percent) Predicted	Mass Averaged Efficiency (percent) Test
1	36	33	90.3	90.3
2	43	37	90.8	91.1

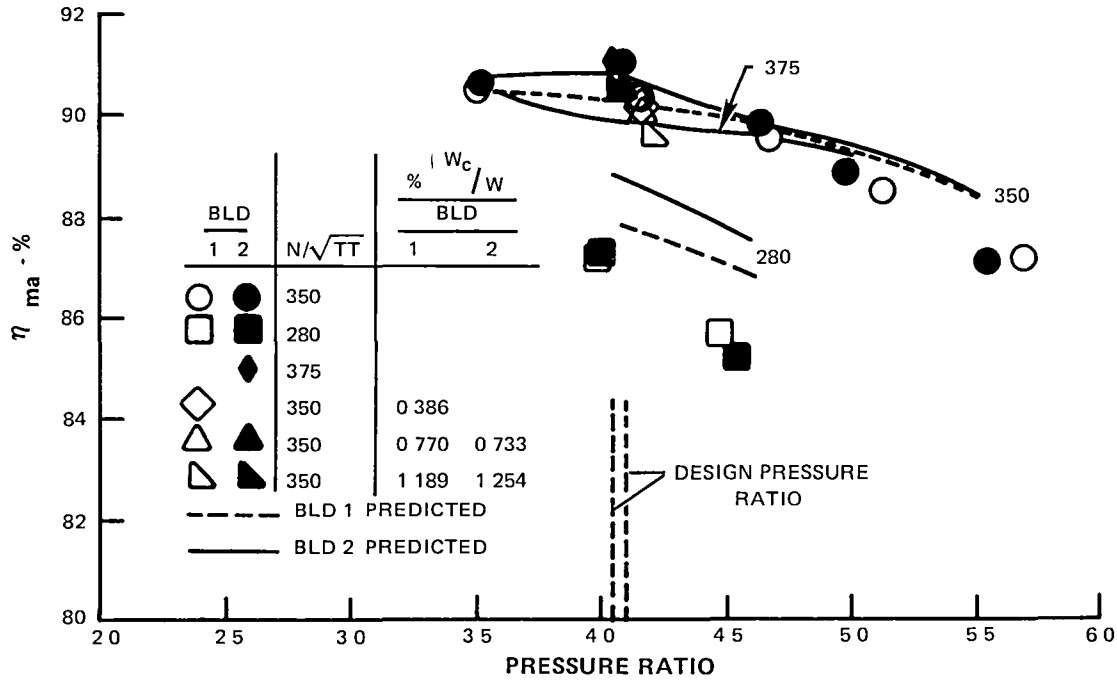

Figure 50 Mass-Averaged Efficiency vs Pressure Ratio - The high reaction level rotating rig performed better than the low reaction rig at the design pressure ratio.

Efficiency of the uncooled rigs was calculated using inlet and exit measurements of pressure, temperature, and air angle. Fixed temperature and pressure rakes were used to measure inlet conditions. Temperature and pressure rakes that traversed through the same 15-degree arc (1 vane gap) were used to measure conditions at the exit plane. The efficiency values over the 15-degree arc were circumferentially area averaged and radially mass averaged with the results from the radial air angle traverse.

The measured efficiency data were adjusted for variations in tip clearance caused by speed changes and temperature changes of the disk due to front disk leakage flows. The sensitivity of the change in efficiency to tip clearance was arrived at by correlation of running clearances from three sources. These included readings made by the laser optical probes located at two circumferential locations, measurement of mechanical rub buttons installed at three circumferential locations, and from analytical calculations based on disk, outer air seal, and case metal temperatures. Once the tip clearance was established, the change in local efficiency at the outer diameter was determined as a function of clearance (Figure 51). To adjust the stage

efficiency to the design clearance, these data were applied to the spanwise efficiency. Study of the spanwise efficiency profiles showed that the loss caused by tip clearance migrated to 65 percent of the span, resulting in a spanwise average adjustment of 0.079 percent in efficiency for 0.0025 cm (0.001 in.) in tip clearance.

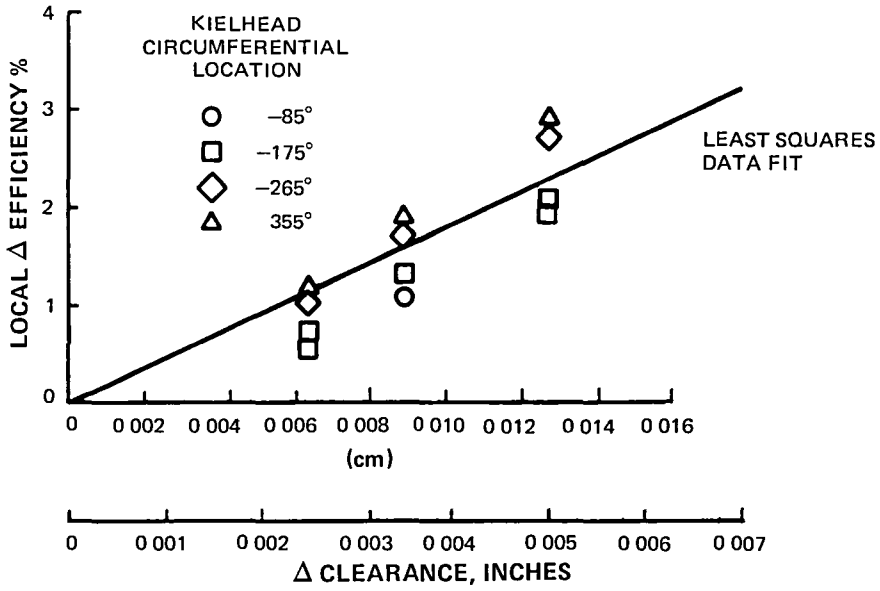

Figure 51 Outer Diameter Kielhead Efficiency Change - Study of the spanwise efficiency profiles showed that the loss caused by tip clearance migrated to 65 percent of the span, resulting in a spanwise average adjustment of 0.079 percent in efficiency for 0.0025 cm (0.001 in.) in tip clearance.

Reaction for the rotating rigs was defined as a ratio of the static pressure drop across the rotor to the static pressure drop across the stage. The results of the tests on the two rotating rigs are shown in Figure 52, where reaction is plotted against pressure ratio. The cooling flow points are not presented because the inner diameter cavity static pressure taps were affected by the disk leakage flow and did not read the correct flowpath pressure. The measured reaction was lower than predicted as shown in Table 11. This was caused by three factors: (1) fabrication tolerances on the airfoil throat areas, (2) the differences between the measured and predicted deviations for the vane and blade, and (3) the predicted versus measured losses for the vane and blade.

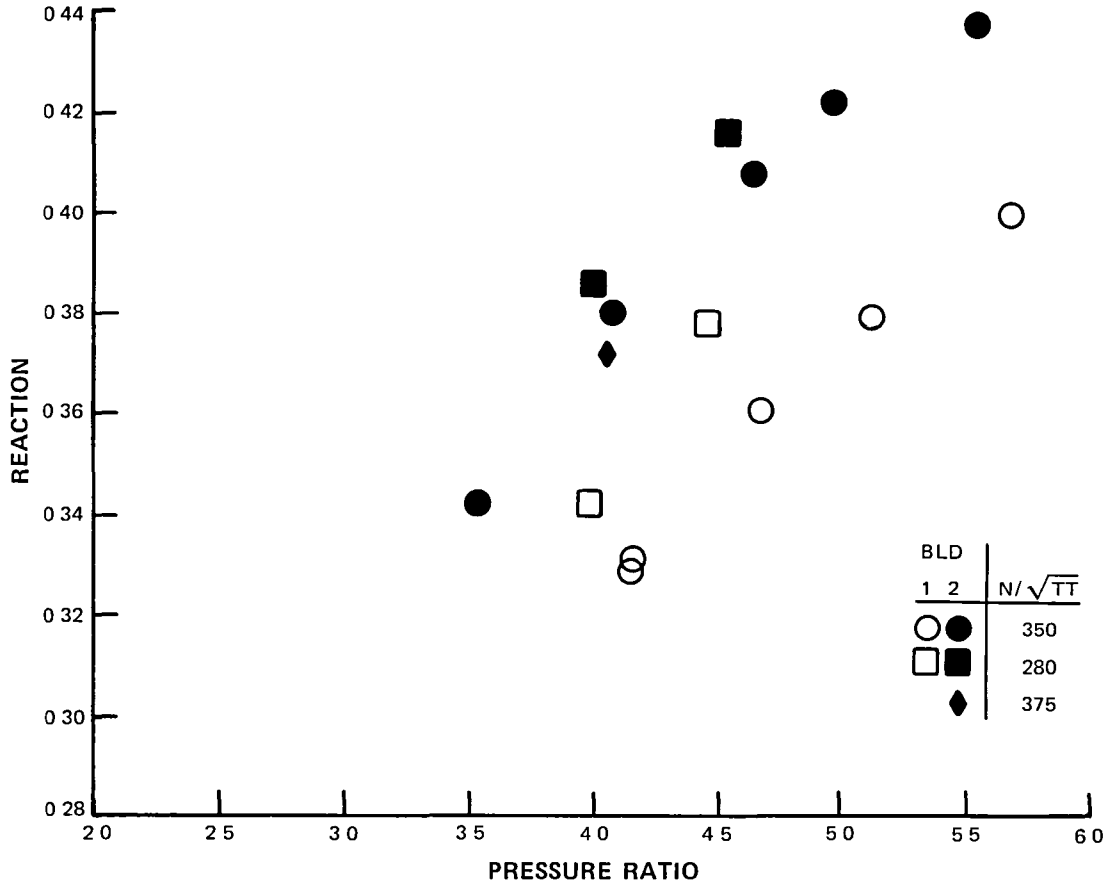

Figure 52 Reaction vs Pressure Ratio - The measured reaction for both builds was lower than design values.

6.2.1.1.1 Data Presentation

During the design efforts, attempts were made to maintain high efficiency in core regions and to minimize endwall losses. In practice, endwall flow regions and wake regions generally have lower efficiency than core flow regions, as shown by the contour plots at design in Figure 53 and Figure 54. This plot shows the efficiency contour lines over one vane gap for Builds 1 and 2. The data were then circumferentially area averaged as shown in Figure 55. The shapes of the efficiency curves for the low and high reaction Builds are similar, with the high reaction turbine showing greater midspan efficiency.

Blade exit absolute air angle, which was used to mass average the efficiency data, is shown in Figure 56. The level of the measured data was adjusted to match continuity. For Build 1, original design point data (350) and repeat design point data (344) are shown. Build 2 angles are lower than Build 1 angles, as predicted by the streamline design. Additional stage performance data for both the lower reaction Build 1 and higher reaction Build 2 are presented in Appendices E and F.

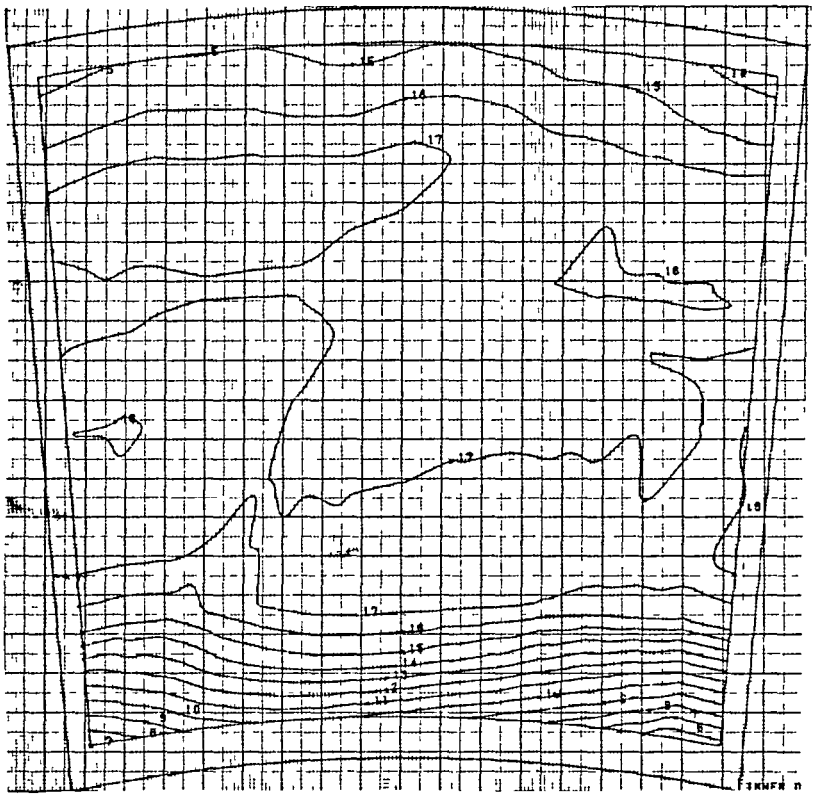

Curve Label	η
6	0.81000
7	0.82000
8	0.83000
9	0.84000
10	0.85000
11	0.86000
12	0.87000
13	0.88000
14	0.89000
15	0.90000
16	0.91000
17	0.92000
18	0.93000

Build 1 N/sq. rt. T_T = 351.4
PR_{ma} = 4.088

Figure 53 Efficiency Contour

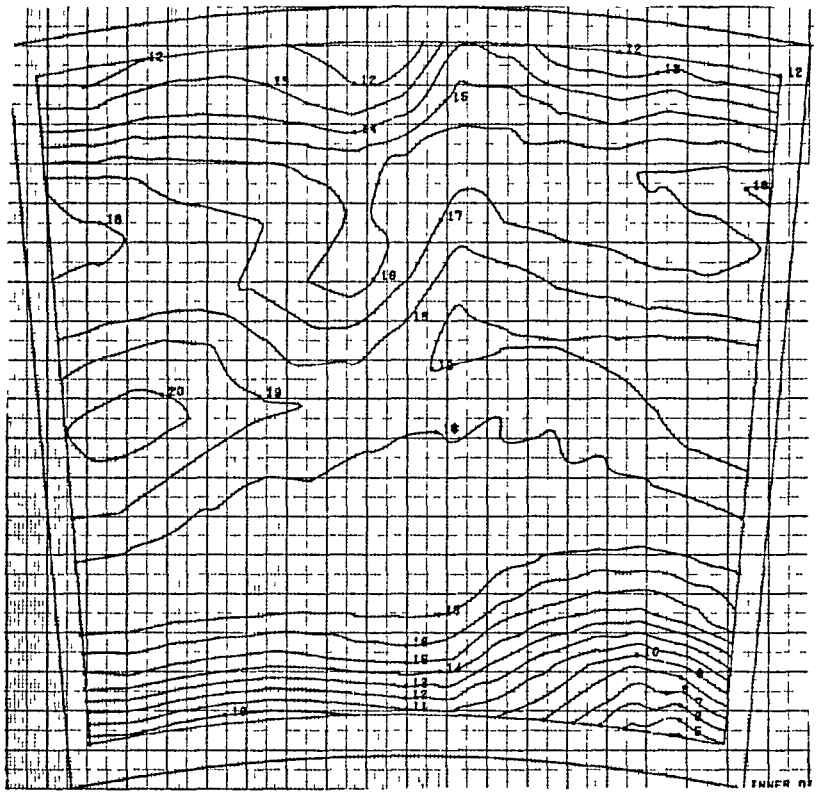

Curve Label	η
5	0.80000
6	0.81000
7	0.82000
8	0.83000
9	0.84000
10	0.85000
11	0.86000
12	0.87000
13	0.88000
14	0.89000
15	0.90000
16	0.91000
17	0.92000
18	0.93000
19	0.94000
20	0.95000

Build 2 N/sq. rt. T_T = 350.8
PR_{ma} = 4.149

Figure 54 Efficiency Contour

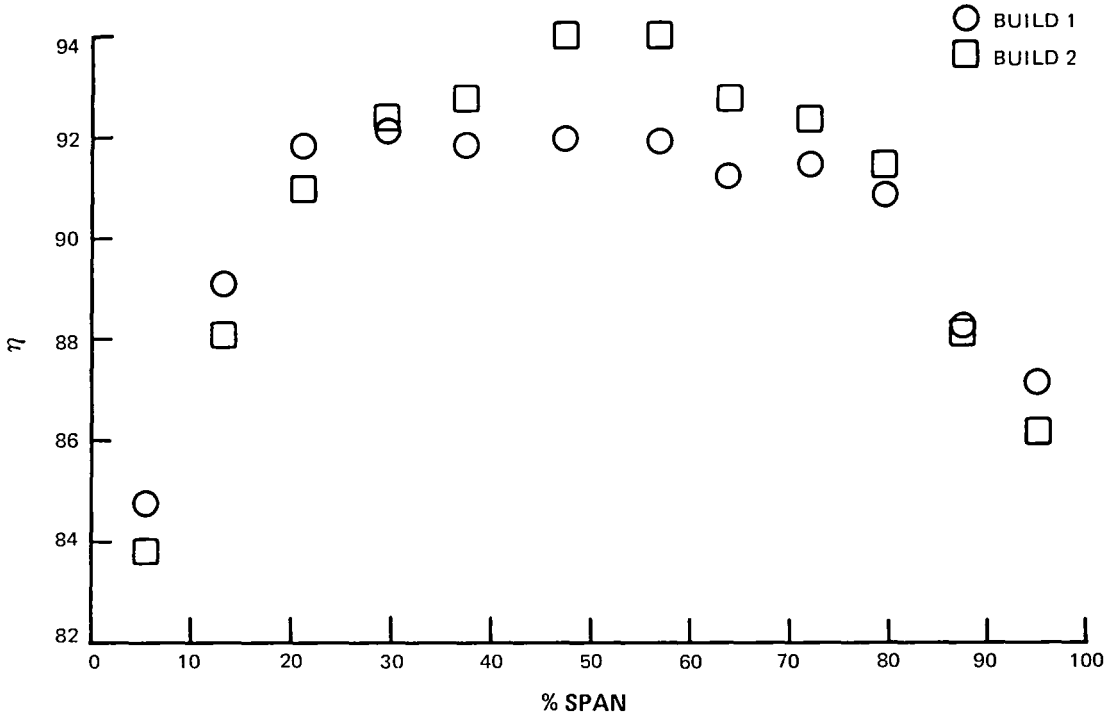

Figure 55 Efficiency vs Percent Span - The shapes of the efficiency curves for the low and high reaction builds are similar, with the high reaction turbine showing greater midspan efficiency.

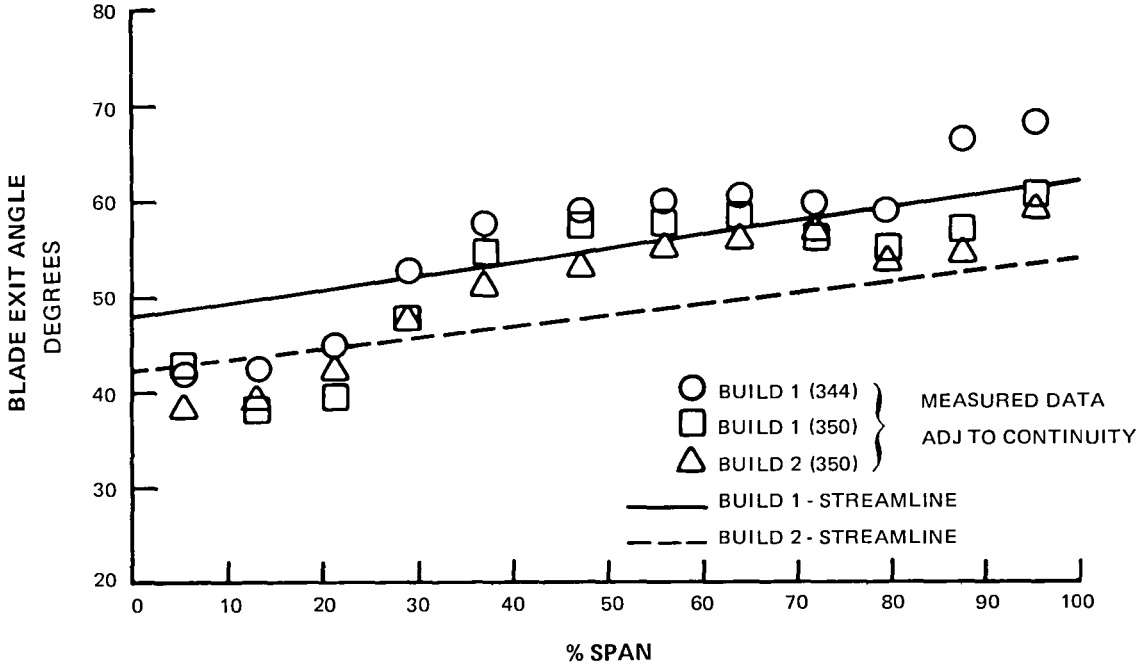

Figure 56 Blade Exit Angle - The predicted angles have the trend of lower inner diameter angles and higher outer diameter angles shown by the data.

6.2.2 Blade Analysis Discussion

6.2.2.1 Blade Pressure Loss

The high reaction Build 2 rig demonstrated lower losses at design pressure ratio and design speed (see Figure 57). The blade total loss was calculated with a meanline analysis using the mass average vane loss and efficiency (the calculation did not consider losses caused by blade tip clearance as being separate from the foil). Off design, Build 1 and Build 2 losses were generally comparable. Large losses were associated with low speed (positive incidence), but there were no increased losses for the higher speed (negative incidence) Build 2 design. Low speed losses were underpredicted, and high speed losses were overpredicted. Build 1 predicted loss values matched the test data at design, but were too low for off-design conditions. Generally, the test data for Build 2 were lower than the predicted values, except at the high-pressure ratio.

The meanline analysis used for the blade losses was also used to calculate the actual Mach triangles for Build 1 and Build 2 of the rotating rig. The Mach triangles presented in Figure 58 are compared with the design Mach triangles (see Figure 4 and Figure 5) in Table 12. The Build 1 and Build 2 vane Mach numbers are higher than the design intent, and Build 1 and Build 2 blade Mach numbers are lower than the design intent. The reason for this difference is that the reaction level of the rigs was lower than the design reaction level.

TABLE 12

COMPARISON OF DESIGN AND EXPERIMENTAL MACH NUMBERS

	Design Build 1	Experimental Build 1	Design Build 2	Experimental Build 2
Vane Mn	1.017	1.061	0.932	0.999
Blade Mn	1.150	1.127	1.232	1.193

6.2.2.2 Deviation

The blade deviation for Build 1 and Build 2 is shown in Figure 59 for the design corrected speed of 350. The experimental deviation (air angle at the exit plane minus the gage plane air angle) was calculated from continuity and the exit plane measured conditions. The predicted deviation was calculated using the design system updated for the measured areas and test conditions. The prediction follows the trend of the data; however, the level is low.

6.2.2.3 Pressure Distribution

Due to instrumentation system malfunctions, no valid blade surface pressure distributions were measured for Build 1.

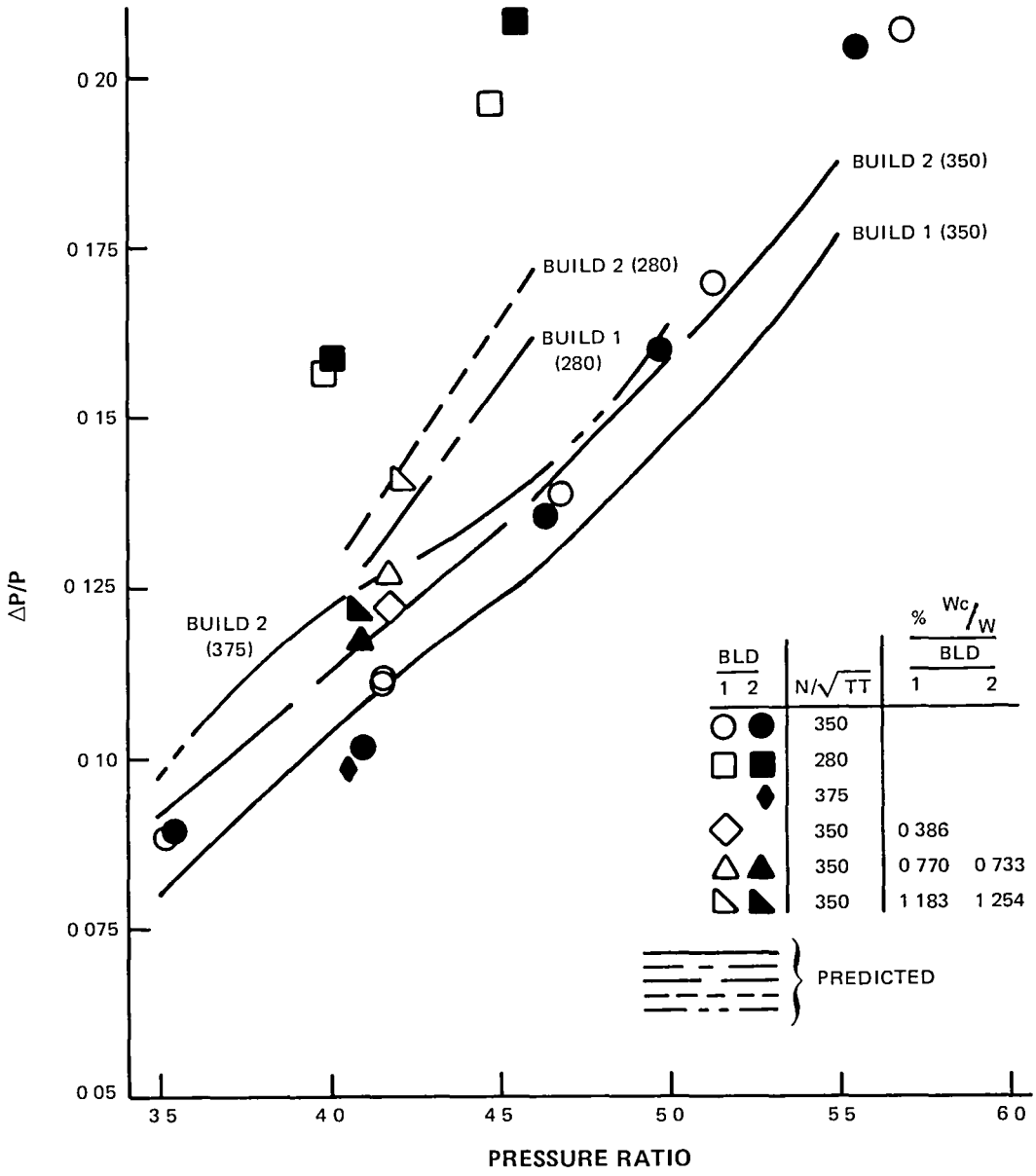

Figure 57 Mass-Averaged Blade Total Loss vs Pressure Ratio - The high reaction Build 2 rig demonstrated lower losses at design pressure ratio and design speed.

Build 2 blade pressure distributions are shown in Figure 60 for all spans at design. The blade relative inlet total pressure was approximated by using the measured 30-percent axial chord, pressure side static pressure in calculating the PS/PT ratio. Good performance was maintained because the adverse pressure gradients at all spans occured well back on the foil. Also, the pressure increases caused by shock waves were relatively small. The design prediction qualitatively matches 50-percent span data, but is not a good match at other spans.

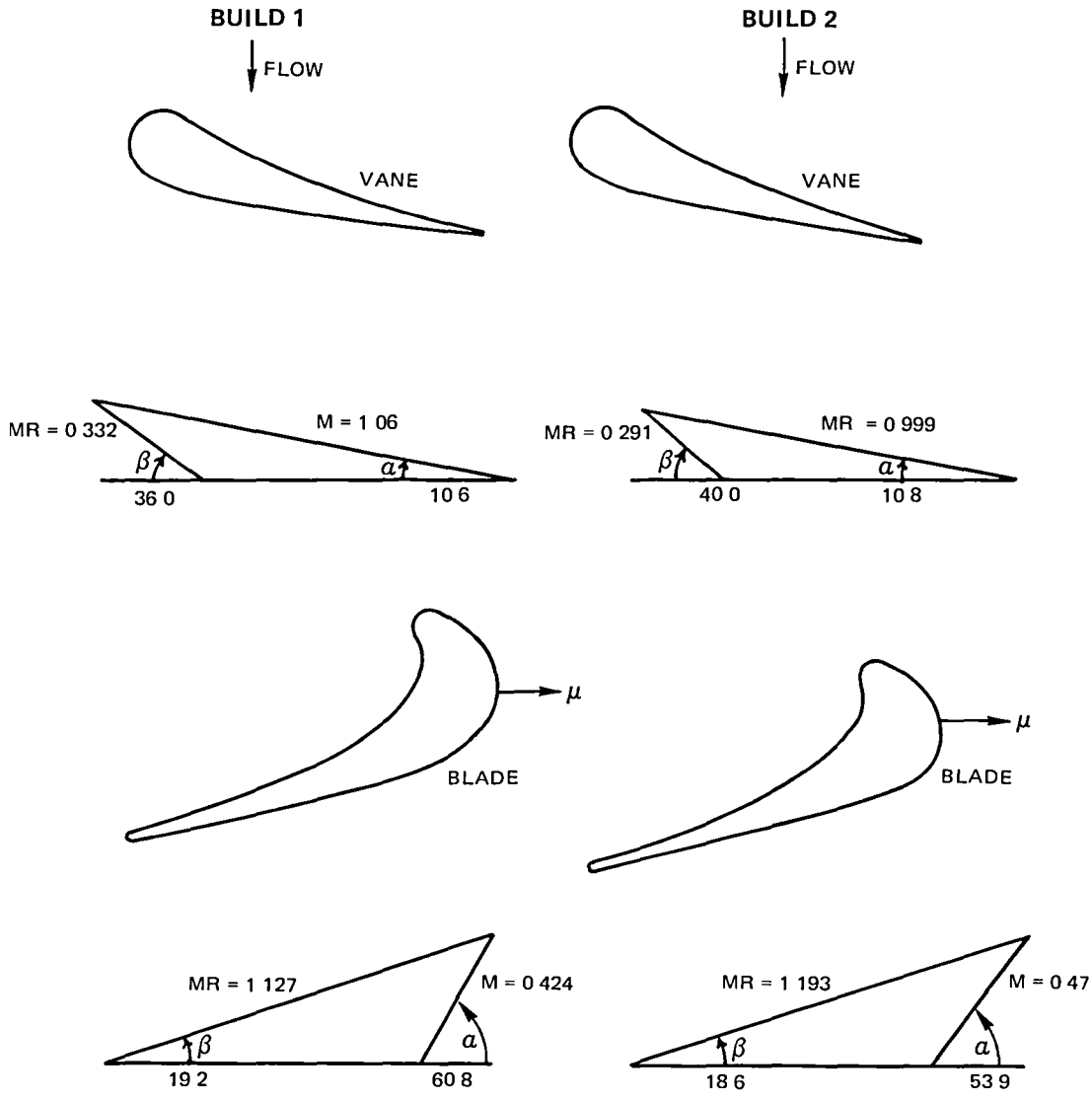

Figure 58 Mach Triangles - Experimental Design Point Mach Triangles for Build 1 and Build 2.

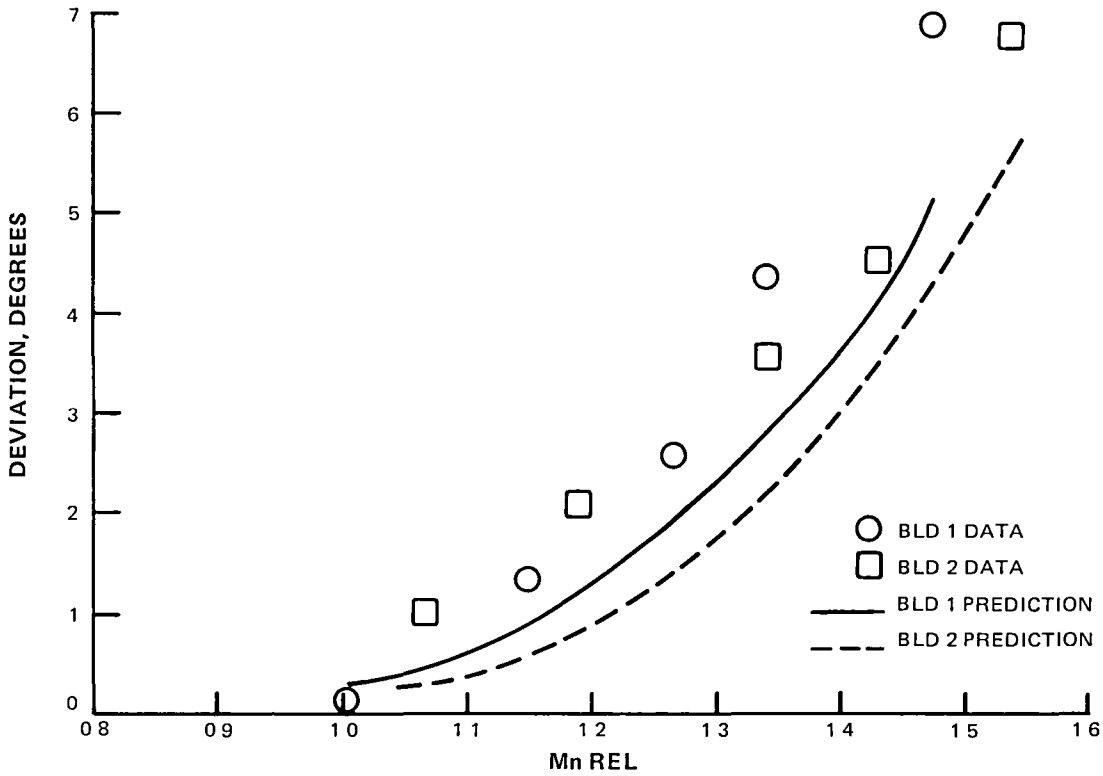

Figure 59 Total Blade Deviation (Air angle at the exit plane minus the gage plane air angle) -

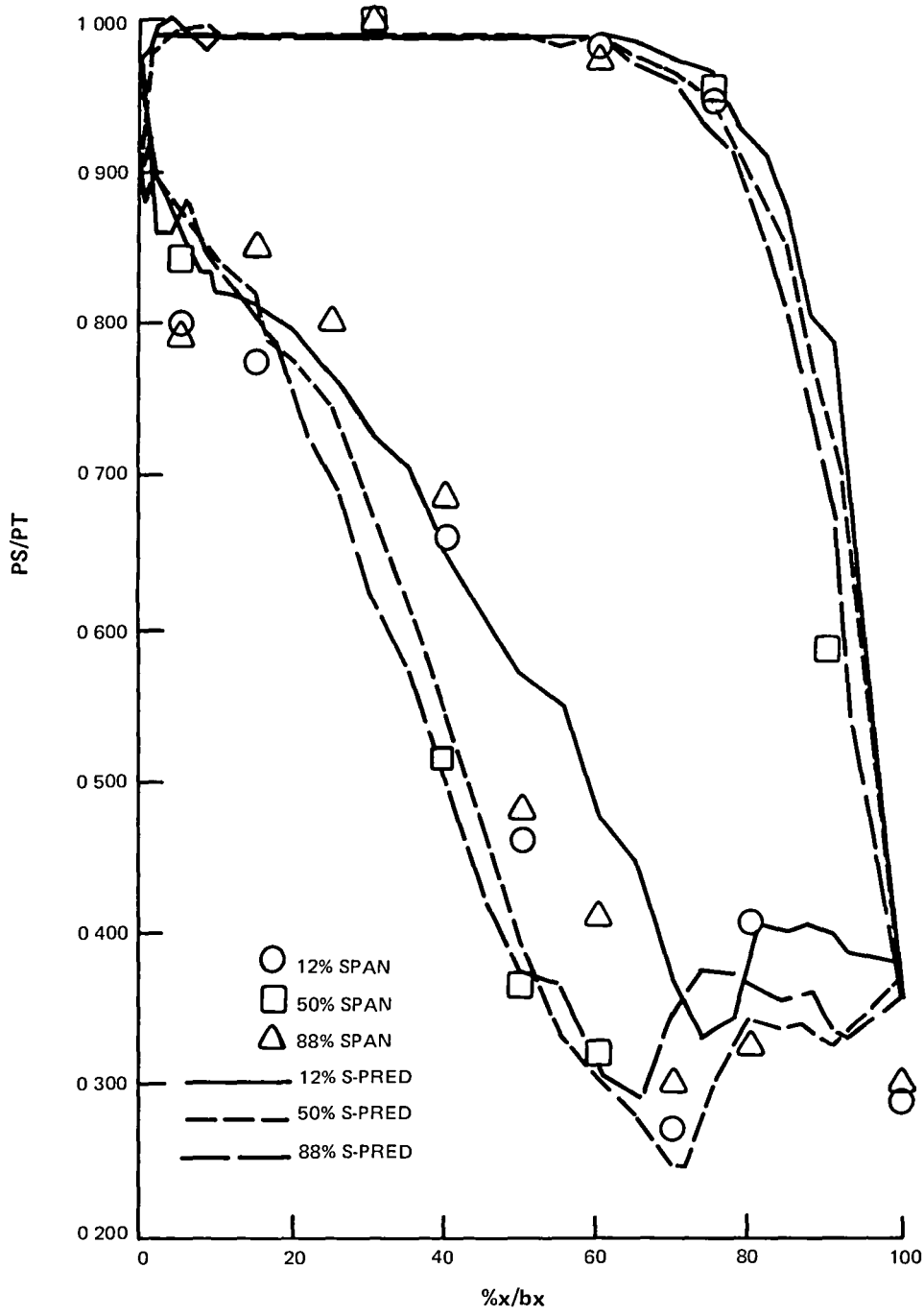

Figure 60 Blade Surface Statics - All distributions successfully delay the start of adverse pressure gradients until well back on the foil.

6.2.2.4 Disk Cooling Flow Penalty

The presence of leakage and cooling air in the engine environment will create a performance penalty relative to the uncooled rig environment. In the uncooled rig, leakage flowed outward along the front of the blade disk, where mixing with gas path flow caused an efficiency reduction. The performance penalty caused by blade disk leakage flow is summarized in Figure 61. The figure, showing span mass averaged efficiency corrected to design clearance, shows the change in efficiency caused by the mixing of the cooling flow. The data agree reasonably with predicted values.

6.3 Summary

The results of the Energy Efficient Engine high-pressure turbine uncooled rig program have established the uncooled aerodynamic efficiency of the high-pressure turbine at 91.1 percent and have verified the feasibility of the Energy Efficient Engine high-pressure turbine aerodynamic design concepts.

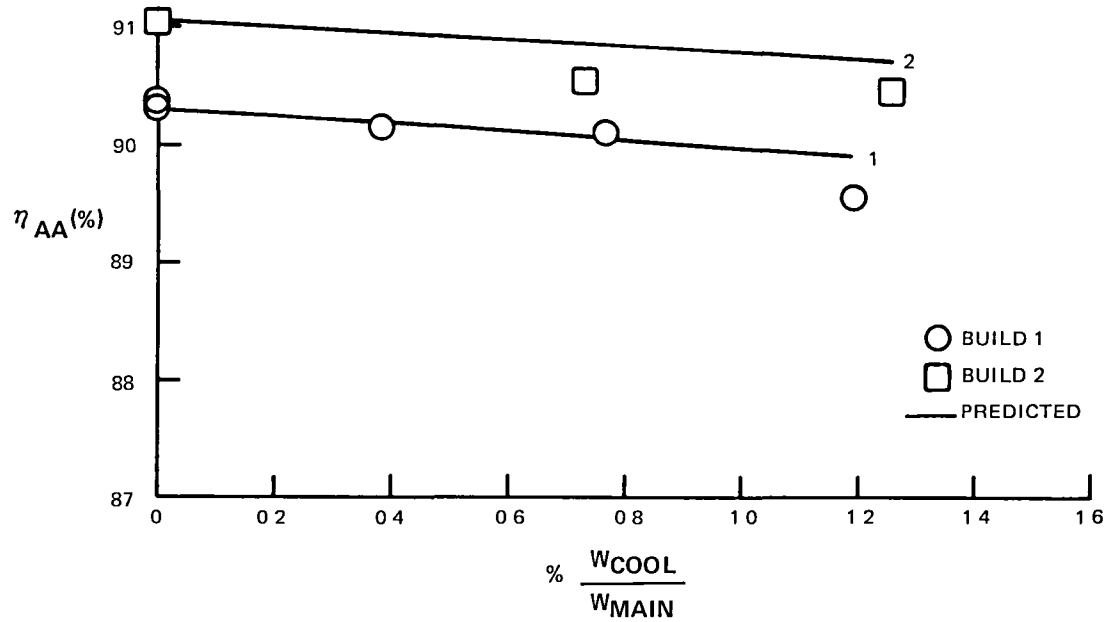

Figure 61 Effect of Leakage Flow on Efficiency - The change in efficiency because of mixing compares reasonably to predicted values.

The measured benefit of higher AN^2 is shown in Figure 62. This figure compares the area averaged efficiency of the current state-of-the-art single stage turbine with the area averaged Build 1 results and shows an improvement of 1.15 percent at the Energy Efficient Engine design point.

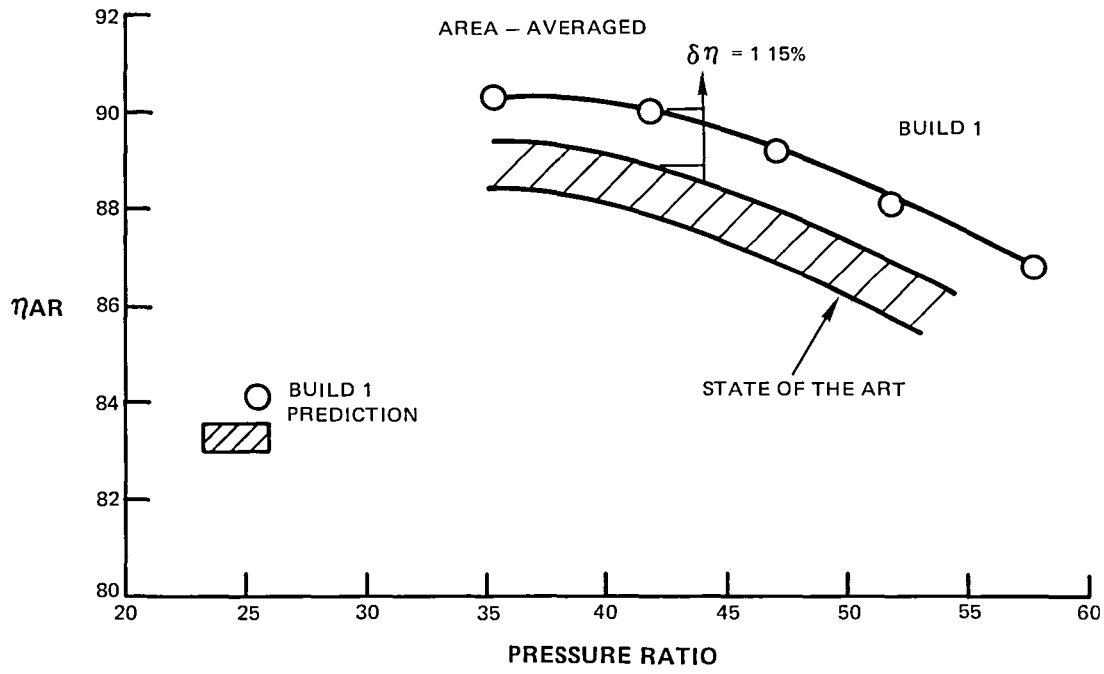

Figure 62 Area-Averaged Efficiency vs Pressure Ratio (Effect of AN^2 Increase) - An increase in AN^2 resulted in an increase in turbine efficiency.

The Build 2 rotating rig demonstrated a mass averaged efficiency of 91.1 percent, 0.8 percent higher than the lower reaction Build 1 rig. Build 1 was tested with a reaction level of 33 percent, and Build 2 was tested with a reaction level of 37 percent. Figure 63 shows the comparison of efficiency vs pressure ratio for these two builds.

Results also showed that the 13-degree canted vane configuration had the lowest mass averaged total loss of the three airfoils tested. The mass-averaged probe measurements indicated an overall pressure loss of 0.0245 as compared to 0.0369 for the radial Build 2 vane at the design point.

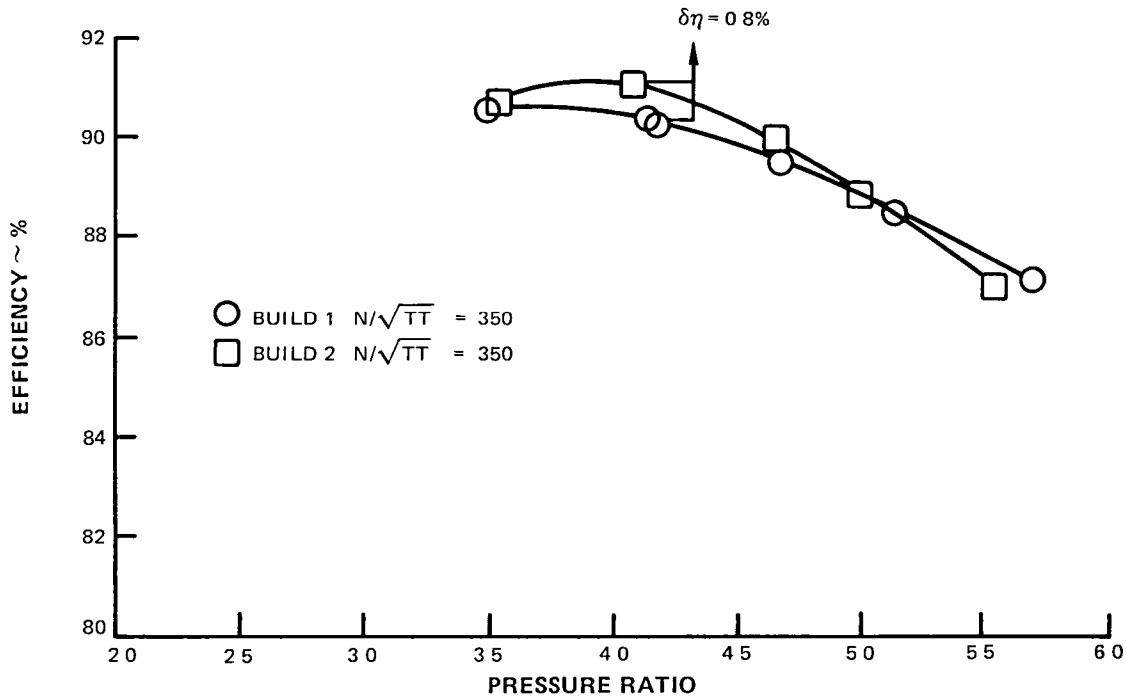

Figure 63 Mass-Averaged Efficiency vs Pressure Ratio (Effect of Reaction Level Increase) - An increase in reaction level resulted in an increase in turbine efficiency.

This Page Intentionally Left Blank

7.0 CONCLUSIONS

- The second build of the Energy Efficient Engine uncooled rig has verified that increased AN^2 and higher turbine reaction level lead to increased efficiency. The demonstrated uncooled efficiency was 91.1 percent.

- The Build 1 vane demonstrated the best compromise between low loss and a proven air angle distribution.

- The 13-degree canted vane configuration had the lowest performance loss of all the vanes tested.

- The Build 2 high reaction blade demonstrated lower losses than the Build 1 blade at the design point..

This Page Intentionally Left Blank

APPENDIX A - AIRFOIL COORDINATES

Figure	Title
A-1	Build 1 Vane Root Section
A-2	Build 1 Vane Mean Section
A-3	Build 1 Vane Tip Section
A-4	Build 1 Blade Root Section
A-5	Build 1 Blade 1/4 Root Section
A-6	Build 1 Blade Mean Section
A-7	Build 1 Blade 1/4 Tip Section
A-8	Build 1 Blade Tip Section
A-9	Build 2 Vane Root Section
A-10	Build 2 Vane Mean Section
A-11	Build 2 Vane Tip Section
A-12	Build 2 Blade Root Section
A-13	Build 2 Blade 1/4 Root Section
A-14	Build 2 Blade Mean Section
A-15	Build 2 Blade 1/4 Tip Section
A-16	Build 2 Blade Tip Section

This Page Intentionally Left Blank

A-1 Build 1 Vane Root Section

PERCENT X/bx	X	SUCTION SIDE Y TOP	PRESSURE SIDE Y BOT
0.0	0.00136	2.76641	2.58250
0.010	0.01408	2.78196	2.58219
0.020	0.02680	2.79679	2.57657
0.030	0.03952	2.81091	2.56778
0.040	0.05224	2.82435	2.55681
0.050	0.06496	2.83711	2.54420
0.060	0.07768	2.84924	2.53030
0.070	0.09040	2.86071	2.51536
0.080	0.10312	2.87157	2.49952
0.090	0.11584	2.88181	2.48291
0.100	0.12856	2.89145	2.46563
0.125	0.16036	2.91295	2.42000
0.150	0.19216	2.93086	2.37143
0.175	0.22396	2.94524	2.32051
0.200	0.25576	2.95613	2.26762
0.225	0.28755	2.96354	2.21299
0.250	0.31935	2.96746	2.15679
0.275	0.35115	2.9678	2.09919
0.300	0.38295	2.96460	2.04033
0.325	0.41475	2.95762	1.98026
0.350	0.44655	2.94672	1.91906
0.375	0.47835	2.93170	1.85678
0.400	0.51015	2.91229	1.79349
0.425	0.54195	2.88811	1.72917
0.450	0.57374	2.85869	1.66389
0.475	0.60554	2.82339	1.59764
0.500	0.63734	2.78135	1.53045
0.525	0.66914	2.73135	1.46227
0.550	0.70094	2.67159	1.39316
0.575	0.73274	2.59917	1.32304
0.600	0.76454	2.50885	1.25195
0.625	0.79634	2.39717	1.17980
0.650	0.82814	2.27172	1.10660
0.675	0.85993	2.13735	1.03225
0.700	0.89173	1.99650	0.95673
0.725	0.92353	1.85024	0.87989
0.750	0.95533	1.69954	0.80169
0.775	0.98713	1.54483	0.72191
0.800	1.01893	1.38659	0.64042
0.825	1.05073	1.22486	0.55692
0.850	1.08253	1.05995	0.47107
0.875	1.11433	0.89178	0.38231
0.900	1.14612	0.72053	0.28983
0.910	1.15884	0.65111	0.25148
0.920	1.17156	0.58117	0.21218
0.930	1.18428	0.51069	0.17171
0.940	1.19700	0.43966	0.12981
0.950	1.20972	0.36808	0.08602
0.960	1.22244	0.29592	0.03965
0.970	1.23516	0.22315	-0.01069
0.980	1.24788	0.14972	-0.05916
0.990	1.26060	0.07568	-0.10727
1.000	1.27332	0.00101	-0.15640

A-2 Build 1 Vane Mean Section

HUT RADIUS = 11.09400

PERCENT X/bx	X	SUCTION SIDE Y TOP	PRESSURE SIDE Y BOT
0.0	0.00149	2.88313	2.70955
0.010	0.01421	2.89776	2.70225
0.020	0.02693	2.91191	2.69328
0.030	0.03964	2.92560	2.68291
0.040	0.05236	2.93882	2.67132
0.050	0.06508	2.95157	2.65868
0.060	0.07779	2.96383	2.64509
0.070	0.09051	2.97562	2.63064
0.080	0.10323	2.98693	2.61543
0.090	0.11594	2.99776	2.59950
0.100	0.12866	3.00809	2.58292
0.125	0.16045	3.03176	2.53894
0.150	0.19225	3.05229	2.49174
0.175	0.22404	3.06959	2.44175
0.200	0.25583	3.08357	2.38931
0.225	0.28762	3.09412	2.33463
0.250	0.31941	3.10109	2.27789
0.275	0.35121	3.10434	2.21925
0.300	0.38300	3.10370	2.15886
0.325	0.41479	3.09893	2.09676
0.350	0.44656	3.08979	2.03304
0.375	0.47837	3.07599	1.96776
0.400	0.51017	3.05717	1.90099
0.425	0.54196	3.03289	1.83272
0.450	0.57375	3.00264	1.76303
0.475	0.60554	2.96575	1.69186
0.500	0.63733	2.92143	1.61928
0.525	0.66913	2.86856	1.54523
0.550	0.70092	2.80579	1.46975
0.575	0.73271	2.73111	1.39276
0.600	0.76450	2.64173	1.31427
0.625	0.79629	2.53428	1.23418
0.650	0.82809	2.41091	1.15250
0.675	0.85988	2.27482	1.06907
0.700	0.89167	2.12832	0.98387
0.725	0.92346	1.97286	0.89669
0.750	0.95525	1.80964	0.80747
0.775	0.98705	1.63946	0.71592
0.800	1.01884	1.46309	0.62185
0.825	1.05063	1.28093	0.52488
0.850	1.08242	1.09351	0.42460
0.875	1.11421	0.90106	0.32031
0.900	1.14601	0.70397	0.21113
0.910	1.15872	0.62387	0.16575
0.920	1.17144	0.54308	0.11922
0.930	1.18416	0.46158	0.07138
0.940	1.19687	0.37941	0.02196
0.950	1.20959	0.29656	-0.02933
0.960	1.22231	0.21305	-0.08294
0.970	1.23502	0.12889	-0.13951
0.980	1.24774	0.04410	-0.20017
0.990	1.26046	-0.04135	-0.26701
1.000	1.27317	-0.12741	-0.34486

A-3 Build 1 Vane Tip Section

HOT RADIUS = 12.34200

PERCENT X/bx	X	SUCTION SIDE Y TOP	PRESSURE SIDE Y BOT
0.0	0.00156	2.94352	2.77237
0.010	0.01428	2.95847	2.76425
0.020	0.02699	2.97285	2.75481
0.030	0.03970	2.98667	2.74419
0.040	0.05242	2.99995	2.73250
0.050	0.06513	3.01270	2.71985
0.060	0.07785	3.02493	2.70631
0.070	0.09056	3.03666	2.69194
0.080	0.10327	3.04791	2.67682
0.090	0.11599	3.05866	2.66098
0.100	0.12870	3.06894	2.64448
0.125	0.16049	3.09263	2.60053
0.150	0.19227	3.11351	2.55313
0.175	0.22406	3.13166	2.50262
0.200	0.25584	3.14711	2.44934
0.225	0.28763	3.15989	2.39350
0.250	0.31941	3.17000	2.33524
0.275	0.35120	3.17743	2.27474
0.300	0.38298	3.18212	2.21212
0.325	0.41477	3.18400	2.14746
0.350	0.44655	3.18298	2.08082
0.375	0.47834	3.17892	2.01227
0.400	0.51013	3.17165	1.94188
0.425	0.54191	3.16093	1.86963
0.450	0.57370	3.14648	1.79559
0.475	0.60548	3.12792	1.71972
0.500	0.63727	3.10476	1.64207
0.525	0.66905	3.07627	1.56256
0.550	0.70084	3.04150	1.48124
0.575	0.73262	2.99899	1.39799
0.600	0.76441	2.94646	1.31285
0.625	0.79619	2.87974	1.22566
0.650	0.82798	2.78978	1.13641
0.675	0.85976	2.66306	1.04495
0.700	0.89155	2.50659	0.95119
0.725	0.92333	2.32861	0.85491
0.750	0.95512	2.13409	0.75596
0.775	0.98690	1.92619	0.65404
0.800	1.01869	1.70726	0.54886
0.825	1.05047	1.47876	0.43996
0.850	1.08226	1.24207	0.32676
0.875	1.11404	0.99801	0.20842
0.900	1.14583	0.74748	0.08378
0.910	1.15854	0.64558	0.03176
0.920	1.17126	0.54275	-0.02175
0.930	1.18397	0.43905	-0.07693
0.940	1.19668	0.33449	-0.13411
0.950	1.20940	0.22916	-0.19365
0.960	1.22211	0.12298	-0.25607
0.970	1.23483	0.01603	-0.32220
0.980	1.24754	-0.09164	-0.39330
0.990	1.26026	-0.20007	-0.47175
1.000	1.27297	-0.30918	-0.56264

A-4 Build 1 Blade Root Section

HOT RADIUS = 10.17400

PERCENT X/bx	X	SUCTION SIDE Y TOP	PRESSURE SIDE Y BOT
0.0	0.0	0.74161	0.48400
0.010	0.01157	0.77465	0.51500
0.020	0.02374	0.80750	0.54350
0.030	0.03561	0.83470	0.57350
0.040	0.04748	0.86231	0.60000
0.050	0.05935	0.88942	0.62450
0.060	0.07122	0.91332	0.64600
0.070	0.08309	0.93496	0.66550
0.080	0.09496	0.95446	0.68300
0.090	0.10683	0.97090	0.69818
0.100	0.11870	0.98134	0.71094
0.125	0.14837	1.04544	0.73554
0.150	0.17805	1.09834	0.75250
0.175	0.20772	1.13760	0.76599
0.200	0.23740	1.16861	0.77425
0.225	0.26707	1.19267	0.77999
0.250	0.29675	1.21449	0.78182
0.275	0.32642	1.22672	0.78041
0.300	0.35610	1.23506	0.77750
0.325	0.38577	1.23707	0.77255
0.350	0.41545	1.23180	0.76467
0.375	0.44512	1.22129	0.75609
0.400	0.47480	1.20655	0.74461
0.425	0.50447	1.18750	0.73460
0.450	0.53414	1.16819	0.72102
0.475	0.56382	1.14143	0.70591
0.500	0.59350	1.11112	0.68970
0.525	0.62317	1.07788	0.67119
0.550	0.65285	1.04504	0.65159
0.575	0.68252	1.00484	0.63049
0.600	0.71220	1.00304	0.60786
0.625	0.74187	1.17188	0.58343
0.650	0.77155	1.14735	0.55789
0.675	0.80122	1.12117	0.53042
0.700	0.83090	1.09219	0.50119
0.725	0.86057	1.06184	0.47006
0.750	0.89025	0.91949	0.43692
0.775	0.91992	0.84167	0.40156
0.800	0.94960	0.76390	0.36373
0.825	0.97927	0.67436	0.32319
0.850	1.00895	0.58449	0.27977
0.875	1.03862	0.48837	0.23143
0.900	1.06830	0.39865	0.17871
0.925	1.09797	0.26134	0.15591
0.950	1.12764	0.23271	0.13192
0.960	1.13957	0.20177	0.10653
0.970	1.15150	0.17446	0.07847
0.980	1.16343	0.14496	0.04634
0.990	1.17536	0.11504	0.01158
1.000	1.18730	0.08482	-0.01691
		0.05277	-0.05763
		0.01877	-0.10824
		0.00282	-0.18988

A-5 Build 1 Blade 1/4 Root Section

HOT RADIUS = 10.63400

PERCENT X/bx	X	SUCTION SIDE Y TOP	PRESSURE SIDE Y BOT
0.0	0.04300	0.94975	0.65504
0.010	0.05401	0.98286	0.67439
0.020	0.06502	1.01248	0.73598
0.030	0.07603	1.03932	0.77636
0.040	0.08704	1.06386	0.80707
0.050	0.09805	1.08646	0.83191
0.060	0.10906	1.10737	0.85260
0.070	0.12007	1.12680	0.87018
0.080	0.13108	1.14491	0.88529
0.090	0.14209	1.16183	0.89838
0.100	0.15310	1.17765	0.90975
0.125	0.18062	1.21300	0.93214
0.150	0.20815	1.24309	0.94769
0.175	0.23567	1.26864	0.95789
0.200	0.26320	1.29015	0.96369
0.225	0.29072	1.30800	0.96574
0.250	0.31825	1.32244	0.96453
0.275	0.34577	1.33369	0.96041
0.300	0.37330	1.34189	0.95364
0.325	0.40082	1.34713	0.94446
0.350	0.42835	1.34947	0.93301
0.375	0.45587	1.34895	0.91943
0.400	0.48340	1.34555	0.90382
0.425	0.51092	1.33922	0.88628
0.450	0.53845	1.32990	0.86685
0.475	0.56597	1.31746	0.84559
0.500	0.59350	1.30172	0.82253
0.525	0.62102	1.28246	0.79770
0.550	0.64855	1.25936	0.77109
0.575	0.67607	1.23198	0.74270
0.600	0.70360	1.19973	0.71252
0.625	0.73112	1.16175	0.68051
0.650	0.75865	1.11674	0.64664
0.675	0.78617	1.06261	0.61084
0.700	0.81370	0.99808	0.57304
0.725	0.84122	0.92910	0.53313
0.750	0.86875	0.85524	0.49099
0.775	0.89627	0.77930	0.44646
0.800	0.92380	0.69887	0.39935
0.825	0.95132	0.61738	0.34939
0.850	0.97885	0.53406	0.29625
0.875	1.00637	0.44908	0.23949
0.900	1.03390	0.36260	0.17849
0.910	1.04491	0.32759	0.15272
0.920	1.05592	0.29237	0.12607
0.930	1.06693	0.25692	0.09844
0.940	1.07794	0.22127	0.06975
0.950	1.08895	0.18529	0.03983
0.960	1.09996	0.14931	0.00856
0.970	1.11097	0.11303	-0.02429
0.980	1.12198	0.07652	-0.05898
0.990	1.13299	0.03981	-0.09588
1.000	1.14400	0.00290	-0.13551

A-6 Build 1 Blade Mean Section

HOT RADIUS = 11.09300

PERCENT X/bx	X	SUCTION SIDE Y TOP	PRESSURE SIDE Y BOT
0.0	0.09630	1.11361	0.89847
0.010	0.09615	1.14536	0.91871
0.020	0.10670	1.17734	0.94250
0.030	0.11665	1.19588	0.96568
0.040	0.12640	1.21676	0.98533
0.050	0.13625	1.23550	1.00078
0.060	0.14600	1.25244	1.01932
0.070	0.15735	1.26786	1.03216
0.080	0.16720	1.28194	1.04448
0.090	0.17715	1.29485	1.05542
0.100	0.18710	1.30660	1.06511
0.125	0.21187	1.33323	1.08447
0.150	0.23635	1.35382	1.09782
0.175	0.26070	1.36920	1.10606
0.200	0.28500	1.38187	1.10982
0.225	0.30937	1.39118	1.10962
0.250	0.33375	1.39741	1.10583
0.275	0.35813	1.40071	1.09875
0.300	0.38250	1.40124	1.08867
0.325	0.40687	1.39905	1.07576
0.350	0.43125	1.39419	1.06020
0.375	0.45562	1.38667	1.04211
0.400	0.47990	1.37647	1.02163
0.425	0.50417	1.36341	0.99884
0.450	0.52835	1.34748	0.97382
0.475	0.55240	1.32868	0.94664
0.500	0.57650	1.30693	0.91735
0.525	0.60057	1.28201	0.88599
0.550	0.62465	1.25422	0.85259
0.575	0.64869	1.22450	0.81717
0.600	0.67280	1.17321	0.77974
0.625	0.69707	1.12401	0.74031
0.650	0.72175	1.06545	0.69887
0.675	0.74713	1.0114	0.65539
0.700	0.77355	0.95334	0.60987
0.725	0.80137	0.89376	0.56226
0.750	0.83095	0.83025	0.51251
0.775	0.86262	0.76671	0.46059
0.800	0.89670	0.70085	0.40642
0.825	0.93357	0.63453	0.34994
0.850	0.97375	0.56677	0.29055
0.875	1.01772	0.49919	0.22928
0.900	1.06600	0.42973	0.16550
0.910	1.08615	0.39672	0.13946
0.920	1.09613	0.36456	0.11147
0.930	1.10645	0.33329	0.08309
0.940	1.11710	0.30290	0.05548
0.950	1.12809	0.27340	0.02745
0.960	1.13940	0.24478	-0.00162
0.970	1.15105	0.21705	-0.03125
0.980	1.16303	0.19020	-0.06148
0.990	1.17535	0.16424	-0.09231
1.000	1.18800	0.13918	-0.12379

A-7 Build 1 Blade 1/4 Tip Section

HOT RADIUS = 11.55200

PERCENT X/bx	X	SUCTION SIDE Y TOP	PRESSURE SIDE Y BOT
0.0	0.12913	1.24157	1.06966
0.010	0.13842	1.26764	1.09942
0.020	0.14771	1.28950	1.10171
0.030	0.15699	1.30838	1.11175
0.040	0.16628	1.32496	1.12350
0.050	0.17557	1.33971	1.13543
0.060	0.18486	1.35291	1.14684
0.070	0.19414	1.36480	1.15751
0.080	0.20343	1.37553	1.16730
0.090	0.21272	1.38525	1.17612
0.100	0.22201	1.39402	1.18395
0.125	0.24522	1.41242	1.19937
0.150	0.26844	1.42641	1.20927
0.175	0.29166	1.43661	1.21414
0.200	0.31488	1.44341	1.21438
0.225	0.33810	1.44709	1.21039
0.250	0.36132	1.44787	1.20246
0.275	0.38453	1.44584	1.19091
0.300	0.40775	1.44110	1.17600
0.325	0.43097	1.43365	1.15794
0.350	0.45419	1.42348	1.13695
0.375	0.47741	1.41052	1.11319
0.400	0.50063	1.39462	1.08684
0.425	0.52384	1.37564	1.05801
0.450	0.54706	1.35324	1.02686
0.475	0.57028	1.32699	0.99347
0.500	0.59350	1.29626	0.95794
0.525	0.61672	1.25998	0.92037
0.550	0.63994	1.21825	0.88081
0.575	0.66315	1.17190	0.83935
0.600	0.68637	1.12039	0.79603
0.625	0.70959	1.06221	0.75090
0.650	0.73281	0.99642	0.70401
0.675	0.75603	0.92829	0.65537
0.700	0.77925	0.86049	0.60503
0.725	0.80246	0.79214	0.55302
0.750	0.82568	0.72303	0.49935
0.775	0.84890	0.65317	0.44406
0.800	0.87212	0.58273	0.38714
0.825	0.89534	0.51170	0.32865
0.850	0.91856	0.44019	0.26862
0.875	0.94178	0.36823	0.20709
0.900	0.96499	0.29596	0.14418
0.910	0.97428	0.26683	0.11864
0.920	0.98357	0.23770	0.09292
0.930	0.99286	0.20855	0.06704
0.940	1.00214	0.17935	0.04098
0.950	1.01143	0.15007	0.01480
0.960	1.02072	0.12077	-0.01150
0.970	1.03000	0.09138	-0.03789
0.980	1.03929	0.06200	-0.06443
0.990	1.04858	0.03256	-0.09124
1.000	1.05787	0.00306	-0.11971

A-8 Build 1 Blade Tip Section

HOT RADIUS - 12.01200

PERCENT X/bx	X	SUCTION SIDE Y TOP	PRESSURE SIDE Y BOT
0.0	0.17256	1.23577	1.16624
0.010	0.13002	1.35111	1.19091
0.020	0.13374	1.36507	1.19456
0.030	0.13776	1.37780	1.20720
0.040	0.20410	1.39044	1.21884
0.050	0.21410	1.40003	1.22942
0.060	0.22202	1.40984	1.23912
0.070	0.23144	1.41875	1.24779
0.080	0.23956	1.42669	1.25540
0.090	0.24838	1.43431	1.26222
0.100	0.25670	1.44104	1.26802
0.110	0.27775	1.44510	1.27347
0.120	0.28855	1.46553	1.28339
0.130	0.31835	1.47265	1.28305
0.140	0.34000	1.47665	1.27779
0.150	0.36105	1.48767	1.26792
0.160	0.3893 0	1.47580	1.25276
0.170	0.40405	1.47104	1.23565
0.180	0.42510	1.46244	1.21300
0.190	0.44615	1.45235	1.18977
0.200	0.44720	1.43919	1.16019
0.210	0.48825	1.42224	1.12959
0.220	0.50930	1.40173	1.09602
0.230	0.53035	1.37725	1.06009
0.240	0.55140	1.34830	1.02203
0.250	0.57245	1.31767	0.98199
0.260	0.59350	1.27719	0.94017
0.270	0.61455	1.23132	0.89671
0.280	0.63560	1.18082	0.85174
0.290	0.65665	1.12137	0.80540
0.300	0.67770	1.05956	0.75779
0.310	0.69875	0.97402	0.70903
0.320	0.71980	0.91102	0.65919
0.330	0.74085	0.84675	0.60839
0.340	0.76190	0.78329	0.55666
0.350	0.78295	0.71766	0.50411
0.360	0.80400	0.65284	0.45079
0.370	0.82505	0.58814	0.39674
0.380	0.84610	0.52327	0.34203
0.390	0.86715	0.45835	0.28671
0.400	0.88820	0.39340	0.23082
0.410	0.90925	0.32842	0.17439
0.420	0.93030	0.26340	0.11747
0.430	0.95135	0.19839	0.06007
0.440	0.97240	0.13337	0.00220
0.450	0.99345	0.06835	-0.05617
0.460	1.01450	0.00334	-0.11455

A-9 Build 2 Vane Root Section

HOT RADIUS = 10.21100

PERCENT X/bx	X	SUCTION SIDE Y TOP	PRESSURE SIDE Y BOT
0.0	0.00462	2.77029	2.60028
0.010	0.01727	2.78472	2.59138
0.020	0.02991	2.79871	2.58134
0.030	0.04256	2.81223	2.57032
0.040	0.05520	2.82531	2.55843
0.050	0.06785	2.83794	2.54576
0.060	0.08050	2.85011	2.53237
0.070	0.09314	2.86185	2.51834
0.080	0.10579	2.87312	2.50372
0.090	0.11843	2.88393	2.48855
0.100	0.13108	2.89430	2.47286
0.125	0.16269	2.91821	2.43163
0.150	0.19431	2.93922	2.38780
0.175	0.22593	2.95729	2.34170
0.200	0.25754	2.97234	2.29356
0.225	0.28916	2.98428	2.24356
0.250	0.32077	2.99302	2.19182
0.275	0.35239	2.99844	2.13846
0.300	0.38400	3.00038	2.08361
0.325	0.41562	2.99864	2.02729
0.350	0.44723	2.99303	1.96958
0.375	0.47885	2.98327	1.91050
0.400	0.51046	2.96904	1.85012
0.425	0.54208	2.94993	1.78844
0.450	0.57369	2.92547	1.72550
0.475	0.60531	2.89501	1.66126
0.500	0.63692	2.85774	1.59576
0.525	0.66854	2.81257	1.52896
0.550	0.70015	2.75802	1.46087
0.575	0.73177	2.69183	1.39143
0.600	0.76338	2.61085	1.32065
0.625	0.79500	2.50876	1.24840
0.650	0.82661	2.38576	1.17471
0.675	0.85823	2.25010	1.09941
0.700	0.88984	2.10651	1.02248
0.725	0.92146	1.95671	0.94373
0.750	0.95307	1.80189	0.86306
0.775	0.98469	1.64254	0.78019
0.800	1.01630	1.47910	0.69493
0.825	1.04792	1.31163	0.60686
0.850	1.07953	1.14025	0.51553
0.875	1.11115	0.96475	0.42019
0.900	1.14276	0.78477	0.31979
0.910	1.15541	0.71138	0.27781
0.920	1.16805	0.63721	0.23456
0.930	1.18070	0.56205	0.18980
0.940	1.19335	0.48597	0.14319
0.950	1.20599	0.40870	0.09426
0.960	1.21864	0.33028	0.04228
0.970	1.23129	0.25035	-0.01408
0.980	1.24393	0.16874	-0.07774
0.990	1.25658	0.08520	-0.15559
1.000	1.26922	-0.00093	-0.22302

A-10 Build 2 Vane Mean Section

HUT RADIUS = 11.09400

PERCENT X/bx	X	SUCTION SIDE Y TOP	PRESSURE SIDE Y BOT
0.0	0.00483	2.82634	2.65481
0.010	0.01747	2.84050	2.64625
0.020	0.03011	2.85428	2.63648
0.030	0.04275	2.86767	2.62565
0.040	0.05539	2.88069	2.61385
0.050	0.06803	2.89330	2.60120
0.060	0.08067	2.90551	2.58775
0.070	0.09331	2.91732	2.57358
0.080	0.10594	2.92870	2.55874
0.090	0.11858	2.93967	2.54329
0.100	0.13122	2.95021	2.52726
0.125	0.16282	2.97464	2.48485
0.150	0.19442	2.99622	2.43950
0.175	0.22601	3.01484	2.39151
0.200	0.25761	3.03032	2.34117
0.225	0.28921	3.04251	2.28867
0.250	0.32081	3.05123	2.23414
0.275	0.35240	3.05627	2.17775
0.300	0.38400	3.05739	2.11959
0.325	0.41560	3.05433	2.05973
0.350	0.44720	3.04678	1.99823
0.375	0.47879	3.03438	1.93514
0.400	0.51039	3.01675	1.87054
0.425	0.54199	2.99339	1.80439
0.450	0.57358	2.96374	1.73678
0.475	0.60518	2.92713	1.66766
0.500	0.63678	2.88273	1.59707
0.525	0.66838	2.82948	1.52496
0.550	0.69997	2.76613	1.45135
0.575	0.73157	2.69095	1.37617
0.600	0.76317	2.60164	1.29944
0.625	0.79477	2.49664	1.22102
0.650	0.82636	2.37778	1.14093
0.675	0.85796	2.24711	1.05902
0.700	0.88956	2.10617	0.97523
0.725	0.92115	1.95608	0.88938
0.750	0.95275	1.79780	0.80135
0.775	0.98435	1.63196	0.71088
0.800	1.01595	1.45922	0.61777
0.825	1.04754	1.27996	0.52159
0.850	1.07914	1.09467	0.42191
0.875	1.11074	0.90357	0.31799
0.900	1.14233	0.70704	0.20894
0.910	1.15497	0.62693	0.16353
0.920	1.16761	0.54600	0.11691
0.930	1.18025	0.46424	0.06889
0.940	1.19289	0.38167	0.01924
0.950	1.20553	0.29831	-0.03235
0.960	1.21817	0.21416	-0.08634
0.970	1.23081	0.12924	-0.14341
0.980	1.24345	0.04352	-0.20465
0.990	1.25609	-0.04294	-0.27213
1.000	1.26872	-0.13016	-0.35014

A-11 Build 2 Vane Tip Section

HOT RADIUS = 12.34200

PERCENT X/bx	X	SUCTION SIDE Y TOP	PRESSURE SIDE Y BOT
0.0	0.00504	2.87973	2.70205
0.010	0.01767	2.89441	2.69689
0.020	0.03030	2.90857	2.68930
0.030	0.04293	2.92221	2.67973
0.040	0.05556	2.93534	2.66852
0.050	0.06819	2.94797	2.65592
0.060	0.08082	2.96009	2.64211
0.070	0.09345	2.97171	2.62724
0.080	0.10608	2.98281	2.61141
0.090	0.11871	2.99340	2.59472
0.100	0.13134	3.00349	2.57724
0.125	0.16292	3.02651	2.53054
0.150	0.19449	3.04633	2.48010
0.175	0.22606	3.06292	2.42647
0.200	0.25764	3.07622	2.37007
0.225	0.28921	3.08616	2.31118
0.250	0.32079	3.09263	2.25001
0.275	0.35236	3.09551	2.18674
0.300	0.38394	3.09463	2.12157
0.325	0.41551	3.08981	2.05456
0.350	0.44709	3.08081	1.98579
0.375	0.47866	3.06733	1.91536
0.400	0.51023	3.04902	1.84332
0.425	0.54181	3.02544	1.76970
0.450	0.57338	2.99600	1.69456
0.475	0.60496	2.95995	1.61788
0.500	0.63653	2.91634	1.53970
0.525	0.66811	2.86379	1.45998
0.550	0.69968	2.80039	1.37877
0.575	0.73126	2.72311	1.29598
0.600	0.76283	2.62841	1.21164
0.625	0.79440	2.51581	1.12565
0.650	0.82598	2.38667	1.03801
0.675	0.85755	2.24261	0.94859
0.700	0.88913	2.08561	0.85733
0.725	0.92070	1.91743	0.76408
0.750	0.95228	1.73991	0.66874
0.775	0.98385	1.55447	0.57107
0.800	1.01542	1.36249	0.47088
0.825	1.04700	1.16497	0.36779
0.850	1.07857	0.96292	0.26146
0.875	1.11015	0.75695	0.15120
0.900	1.14172	0.54780	0.03627
0.910	1.15435	0.46332	-0.01129
0.920	1.16698	0.37844	-0.05993
0.930	1.17961	0.29317	-0.10980
0.940	1.19224	0.20753	-0.16105
0.950	1.20487	0.12156	-0.21394
0.960	1.21750	0.03527	-0.26882
0.970	1.23013	-0.05134	-0.32617
0.980	1.24276	-0.13822	-0.38665
0.990	1.25539	-0.22538	-0.45152
1.000	1.26802	-0.31279	-0.52292

A-12 Build 2 Blade Root Section

HOT RADIUS = 10.17400

PERCENT X/bx	X	SUCTION SIDE Y TOP	PRESSURE SIDE Y BOT
0.0	0.0	0.70967	0.48962
0.010	0.01018	0.76221	0.51336
0.020	0.02036	0.80548	0.53533
0.030	0.03054	0.84286	0.55574
0.040	0.04072	0.87604	0.57474
0.050	0.05090	0.90599	0.59247
0.060	0.06108	0.93336	0.60902
0.070	0.07126	0.95857	0.62450
0.080	0.08144	0.98195	0.63898
0.090	0.09162	1.00374	0.65253
0.100	0.10180	1.02411	0.66521
0.125	0.12725	1.06979	0.69343
0.150	0.15270	1.10914	0.71719
0.175	0.17815	1.14324	0.73698
0.200	0.20360	1.17279	0.75319
0.225	0.22905	1.19829	0.76614
0.250	0.25450	1.22010	0.77605
0.275	0.27995	1.23849	0.78313
0.300	0.30540	1.25364	0.78754
0.325	0.33085	1.26568	0.78939
0.350	0.35630	1.27471	0.78881
0.375	0.38175	1.28076	0.78587
0.400	0.40720	1.28383	0.78064
0.425	0.43265	1.28389	0.77317
0.450	0.45810	1.28088	0.76350
0.475	0.48355	1.27465	0.75166
0.500	0.50900	1.26505	0.73765
0.525	0.53445	1.25182	0.72148
0.550	0.55990	1.23462	0.70314
0.575	0.58535	1.21299	0.68260
0.600	0.61080	1.18627	0.65983
0.625	0.63625	1.15349	0.63477
0.650	0.66170	1.11315	0.60738
0.675	0.68715	1.06271	0.57755
0.700	0.71260	0.99952	0.54520
0.725	0.73805	0.92883	0.51020
0.750	0.76350	0.85423	0.47238
0.775	0.78895	0.77687	0.43157
0.800	0.81440	0.69732	0.38753
0.825	0.83985	0.61600	0.33996
0.850	0.86530	0.53306	0.28849
0.875	0.89075	0.44855	0.23265
0.900	0.91620	0.36264	0.17180
0.910	0.92638	0.32783	0.14587
0.920	0.93656	0.29278	0.11893
0.930	0.94674	0.25748	0.09091
0.940	0.95692	0.22197	0.06171
0.950	0.96710	0.18615	0.03121
0.960	0.97728	0.15006	-0.00071
0.970	0.98746	0.11367	-0.03422
0.980	0.99764	0.07703	-0.06951
0.990	1.00782	0.04000	-0.10684
1.000	1.01800	0.00265	-0.14653

A-13 Build 2 Blade 1/4 Root Section

HUT RADIUS = 10.63400

PERCENT X/bx	X	SUCTION SIDE Y TOP	PRESSURE SIDE Y BOT
0.0	0.02723	0.89211	0.69667
0.010	0.03670	0.92342	0.71601
0.020	0.04617	0.95185	0.73392
0.030	0.05564	0.97793	0.75053
0.040	0.06511	1.00204	0.76593
0.050	0.07458	1.02445	0.78022
0.060	0.08405	1.04538	0.79347
0.070	0.09352	1.06498	0.80576
0.080	0.10299	1.08340	0.81715
0.090	0.11246	1.10074	0.82768
0.100	0.12193	1.11708	0.83740
0.125	0.14560	1.15406	0.85844
0.150	0.16928	1.18614	0.87523
0.175	0.19295	1.21395	0.88819
0.200	0.21663	1.23792	0.89766
0.225	0.24030	1.25835	0.90390
0.250	0.26398	1.27548	0.90714
0.275	0.28765	1.28945	0.90756
0.300	0.31133	1.30039	0.90530
0.325	0.33500	1.30835	0.90049
0.350	0.35868	1.31335	0.89324
0.375	0.38235	1.31537	0.88362
0.400	0.40603	1.31436	0.87170
0.425	0.42970	1.31021	0.85755
0.450	0.45338	1.30278	0.84120
0.475	0.47705	1.29183	0.82269
0.500	0.50073	1.27707	0.80203
0.525	0.52440	1.25808	0.77925
0.550	0.54808	1.23426	0.75433
0.575	0.57175	1.20476	0.72728
0.600	0.59543	1.16828	0.69807
0.625	0.61910	1.12263	0.66669
0.650	0.64278	1.06471	0.63308
0.675	0.66645	0.99931	0.59720
0.700	0.69013	0.93053	0.55900
0.725	0.71380	0.85969	0.51838
0.750	0.73748	0.78721	0.47526
0.775	0.76115	0.71345	0.42952
0.800	0.78483	0.63858	0.38102
0.825	0.80850	0.56270	0.32960
0.850	0.83218	0.48585	0.27506
0.875	0.85585	0.40806	0.21714
0.900	0.87953	0.32928	0.15555
0.910	0.88900	0.29749	0.12980
0.920	0.89847	0.26559	0.10337
0.930	0.90794	0.23346	0.07624
0.940	0.91741	0.20114	0.04836
0.950	0.92688	0.16863	0.01970
0.960	0.93635	0.13591	-0.00979
0.970	0.94582	0.10304	-0.04015
0.980	0.95529	0.06987	-0.07145
0.990	0.96476	0.03642	-0.10374
1.000	0.97423	0.00273	-0.13709

A-14 Build 2 Blade Mean Section

HUT RADIUS = 11.09300

PERCENT X/bx	X	SUCTION SIDE Y TOP	PRESSURE SIDE Y BOT
0.0	0.05314	1.07601	0.87672
0.010	0.06169	1.09482	0.89931
0.020	0.07064	1.11244	0.91902
0.030	0.07939	1.12900	0.93634
0.040	0.08814	1.14459	0.95161
0.050	0.09689	1.15930	0.96510
0.060	0.10564	1.17319	0.97703
0.070	0.11439	1.18632	0.98755
0.080	0.12314	1.19874	0.99682
0.090	0.13189	1.21048	1.00494
0.100	0.14064	1.22160	1.01200
0.125	0.16251	1.24679	1.02559
0.150	0.18439	1.26860	1.03411
0.175	0.20626	1.28728	1.03828
0.200	0.22814	1.30304	1.03864
0.225	0.25001	1.31602	1.03560
0.250	0.27189	1.32631	1.02948
0.275	0.29376	1.33396	1.02054
0.300	0.31564	1.33899	1.00899
0.325	0.33751	1.34137	0.99499
0.350	0.35939	1.34104	0.97870
0.375	0.38126	1.33790	0.96021
0.400	0.40314	1.33179	0.93964
0.425	0.42501	1.32251	0.91706
0.450	0.44689	1.30975	0.89254
0.475	0.46876	1.29308	0.86612
0.500	0.49064	1.27192	0.83786
0.525	0.51251	1.24536	0.80779
0.550	0.53439	1.21200	0.77592
0.575	0.55626	1.16940	0.74228
0.600	0.57814	1.11411	0.70687
0.625	0.60001	1.05230	0.66969
0.650	0.62189	0.98805	0.63074
0.675	0.64376	0.92241	0.58999
0.700	0.66564	0.85565	0.54743
0.725	0.68751	0.78805	0.50301
0.750	0.70939	0.71975	0.45670
0.775	0.73126	0.65089	0.40844
0.800	0.75314	0.58137	0.35816
0.825	0.77501	0.51129	0.30578
0.850	0.79689	0.44066	0.25120
0.875	0.81876	0.36953	0.19431
0.900	0.84064	0.29769	0.13495
0.910	0.84939	0.26881	0.11048
0.920	0.85814	0.23981	0.08558
0.930	0.86689	0.21070	0.06023
0.940	0.87564	0.18147	0.03442
0.950	0.88439	0.15211	0.00813
0.960	0.89314	0.12261	-0.01867
0.970	0.90189	0.09295	-0.04597
0.980	0.91064	0.06303	-0.07382
0.990	0.91939	0.03300	-0.10222
1.000	0.92814	0.00282	-0.13122

A-15 Build 2 Blade 1/4 Tip Section

HOT RADIUS = 11.55200

PERCENT X/bx	X	SUCTION SIDE Y TOP	PRESSURE SIDE Y BOT
0.0	0.08359	1.25237	1.02672
0.010	0.09163	1.26350	1.06302
0.020	0.09967	1.27404	1.09122
0.030	0.10771	1.28400	1.11282
0.040	0.11575	1.29342	1.12902
0.050	0.12379	1.30232	1.14212
0.060	0.13183	1.31073	1.15282
0.070	0.13987	1.31865	1.16155
0.080	0.14791	1.32611	1.16912
0.090	0.15595	1.33312	1.17484
0.100	0.16399	1.33969	1.17901
0.125	0.18409	1.35427	1.18388
0.150	0.20419	1.36632	1.18244
0.175	0.22429	1.37593	1.17607
0.200	0.24439	1.38315	1.16567
0.225	0.26449	1.38801	1.15185
0.250	0.28459	1.39049	1.13507
0.275	0.30469	1.39057	1.11568
0.300	0.32479	1.38816	1.09394
0.325	0.34489	1.38315	1.07007
0.350	0.36499	1.37538	1.04424
0.375	0.38509	1.36462	1.01659
0.400	0.40519	1.35057	0.98723
0.425	0.42529	1.33280	0.95626
0.450	0.44539	1.31068	0.92376
0.475	0.46549	1.28328	0.88979
0.500	0.48559	1.24910	0.85441
0.525	0.50569	1.20543	0.81767
0.550	0.52579	1.15074	0.77960
0.575	0.54589	1.09238	0.74024
0.600	0.56599	1.03249	0.69960
0.625	0.58609	0.97151	0.65771
0.650	0.60619	0.90982	0.61458
0.675	0.62629	0.84754	0.57021
0.700	0.64639	0.78480	0.52461
0.725	0.66649	0.72162	0.47777
0.750	0.68659	0.65807	0.42969
0.775	0.70669	0.59416	0.38035
0.800	0.72679	0.52992	0.32973
0.825	0.74689	0.46533	0.27781
0.850	0.76699	0.40042	0.22456
0.875	0.78709	0.33516	0.16993
0.900	0.80719	0.26958	0.11387
0.910	0.81523	0.24326	0.09104
0.920	0.82327	0.21680	0.06797
0.930	0.83131	0.19035	0.04465
0.940	0.83935	0.16376	0.02107
0.950	0.84739	0.13717	-0.00275
0.960	0.85543	0.11051	-0.02683
0.970	0.86347	0.08369	-0.05119
0.980	0.87151	0.05686	-0.07581
0.990	0.87955	0.02994	-0.10072
1.000	0.88759	0.00289	-0.12591

A-16 Build 2 Blade Tip Section

HUT RADIUS = 12.01200

PERCENT X/bx	X	SUCTION SIDE Y TOP	PRESSURE SIDE Y BOT
0.0	0.11708	1.40015	1.27932
0.010	0.12570	1.40710	1.28672
0.020	0.13253	1.41339	1.29267
0.030	0.13985	1.41909	1.29802
0.040	0.14718	1.42423	1.30312
0.050	0.15450	1.42885	1.30722
0.060	0.16183	1.43297	1.31092
0.070	0.16915	1.43664	1.31342
0.080	0.17648	1.43986	1.31492
0.090	0.18380	1.44265	1.31521
0.100	0.19113	1.44504	1.31472
0.125	0.20944	1.44931	1.30791
0.150	0.22775	1.45126	1.29499
0.175	0.24607	1.45100	1.27748
0.200	0.26438	1.44860	1.25631
0.225	0.28269	1.44404	1.23215
0.250	0.30100	1.43732	1.20546
0.275	0.31932	1.42835	1.17658
0.300	0.33763	1.41700	1.14579
0.325	0.35594	1.40307	1.11328
0.350	0.37425	1.38628	1.07925
0.375	0.39257	1.36620	1.04381
0.400	0.41088	1.34214	1.00710
0.425	0.42919	1.31301	0.96921
0.450	0.44750	1.27673	0.93022
0.475	0.46582	1.22953	0.89021
0.500	0.48413	1.17581	0.84923
0.525	0.50244	1.12025	0.80734
0.550	0.52075	1.06373	0.76459
0.575	0.53907	1.00661	0.72102
0.600	0.55738	0.94905	0.67666
0.625	0.57569	0.89122	0.63155
0.650	0.59400	0.83304	0.58572
0.675	0.61232	0.77463	0.53920
0.700	0.63063	0.71603	0.49200
0.725	0.64894	0.65730	0.44415
0.750	0.66725	0.59837	0.39567
0.775	0.68557	0.53930	0.34657
0.800	0.70388	0.48015	0.29688
0.825	0.72219	0.42082	0.24659
0.850	0.74050	0.36140	0.19573
0.875	0.75882	0.30187	0.14431
0.900	0.77713	0.24227	0.09233
0.910	0.78445	0.21842	0.07139
0.920	0.79178	0.19451	0.05036
0.930	0.79910	0.17063	0.02925
0.940	0.80643	0.14669	0.00804
0.950	0.81375	0.12279	-0.01325
0.960	0.82108	0.09883	-0.03462
0.970	0.82840	0.07490	-0.05607
0.980	0.83573	0.05091	-0.07762
0.990	0.84305	0.02695	-0.09924
1.000	0.85038	0.00297	-0.12095

APPENDIX B - BUILD 1 ANNULAR CASCADE DATA

TABLE B-1
DATA SUMMARY

UNCOOLED RIG - BLD #1
ANNULAR CASCADE DATA SUMMARY

OPERATING POINT #	PT-IN PSIA	TT-IN °R	W-MAIN LBM/S	AREA WTD MACH #	RAKE AREA WTD TOTAL PT/PT	MID-SPAN PT/PT	AREA WTD MACH #	PROBE AREA WTD TOTAL PT/PT	MID-SPAN PT/PT
1	57.42	775	22.55	0.779	0.0415	0.0131	0.787	0.0330	0.0125
2	57.42	775	23.09	0.899	0.530	0.0165			
3*	57.42	775	23.31	0.967	0.0600	0.0185	0.979	0.0459	0.0190
4	57.42	775	23.39	1.116	0.0625	0.0255			
5	57.42	775	23.49	1.194	0.0765	0.0405			

*Design Point

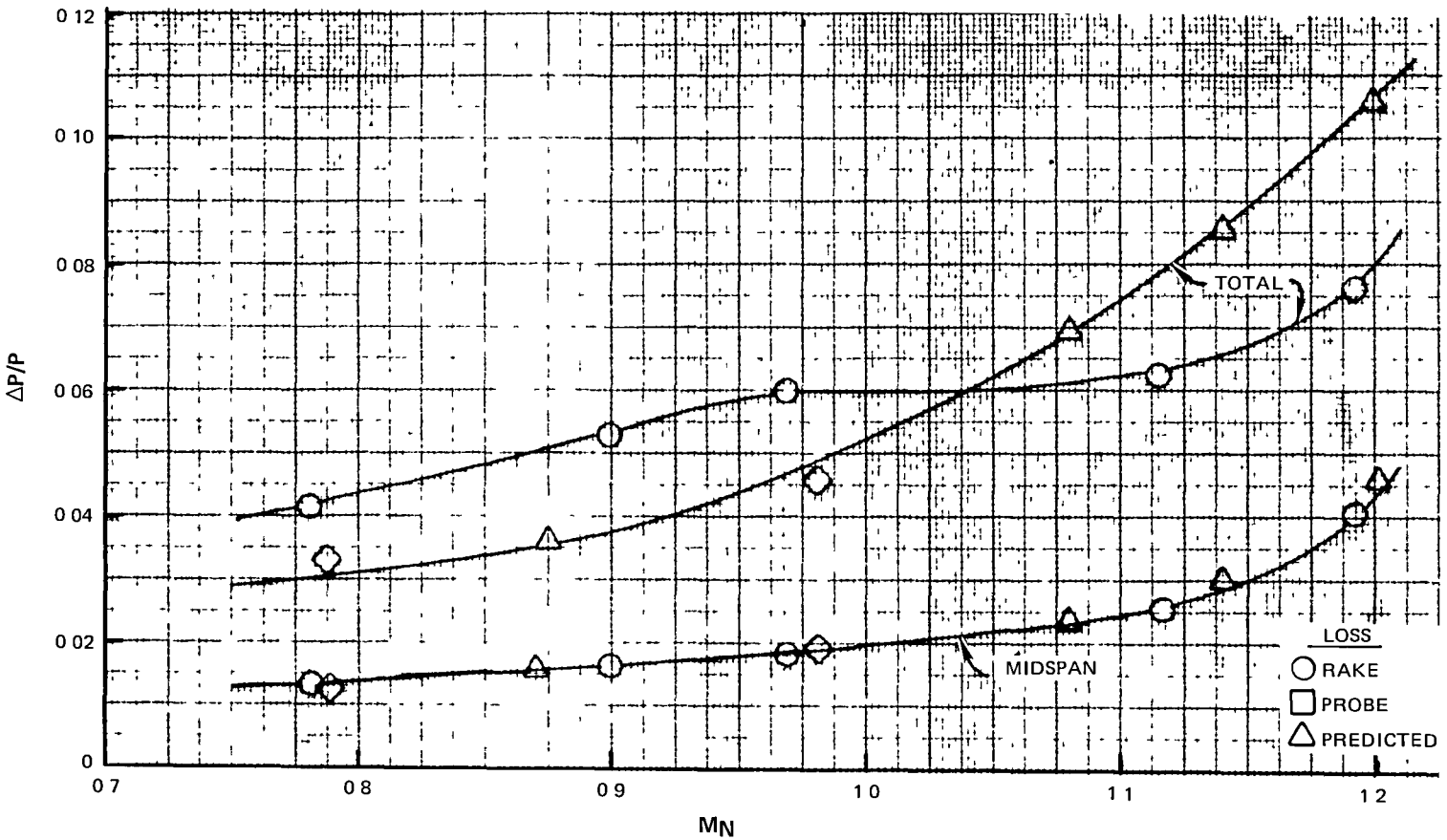

B-1 EEE Uncooled Rig 36% Reaction Annular Cascade Loss vs. Mach Number (Area Averaged)

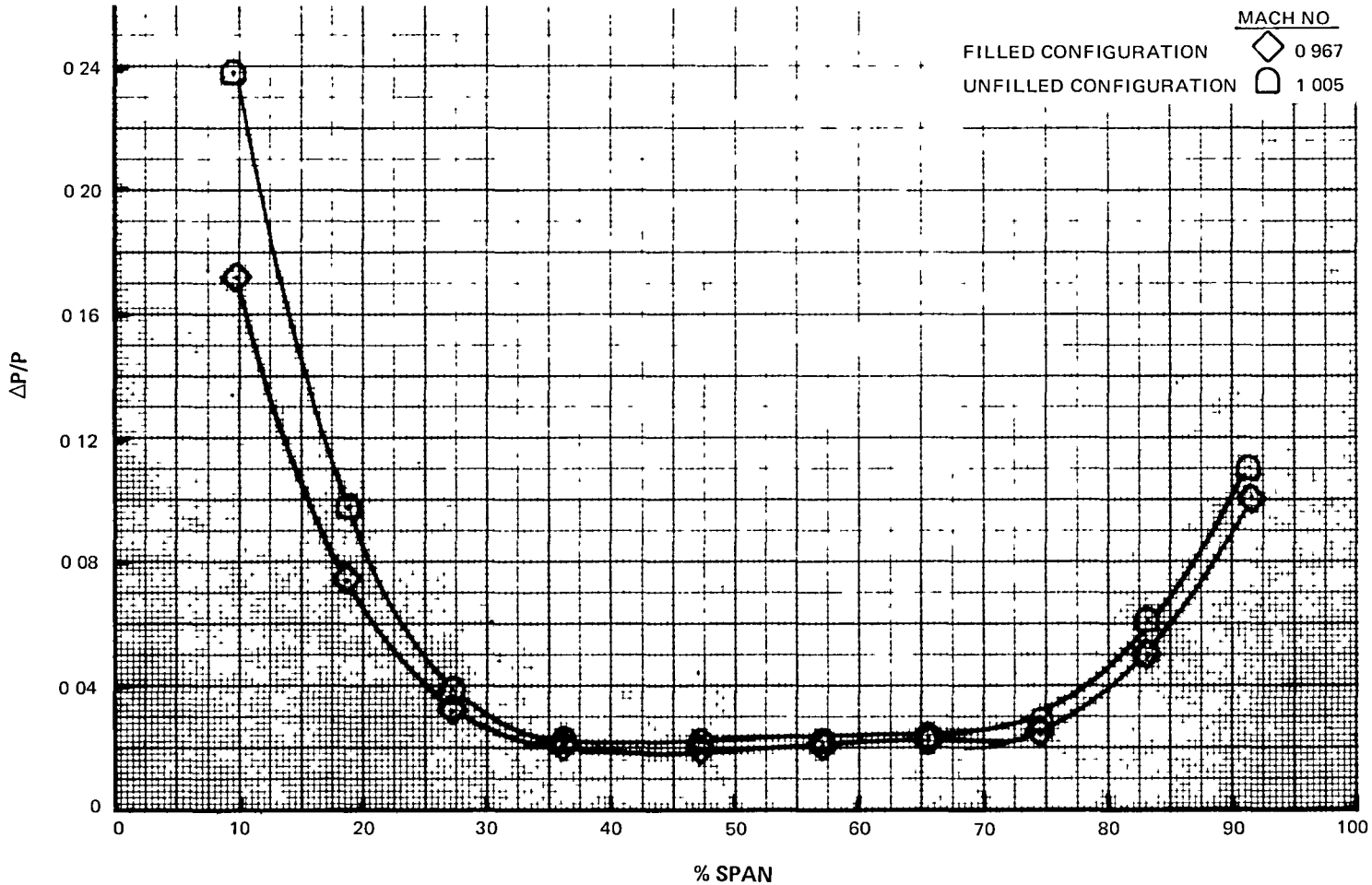

B-2 EEE Uncooled Rig 36% Reaction Annular Cascade Loss vs. % Span Exit Rake Data (Area Averaged)

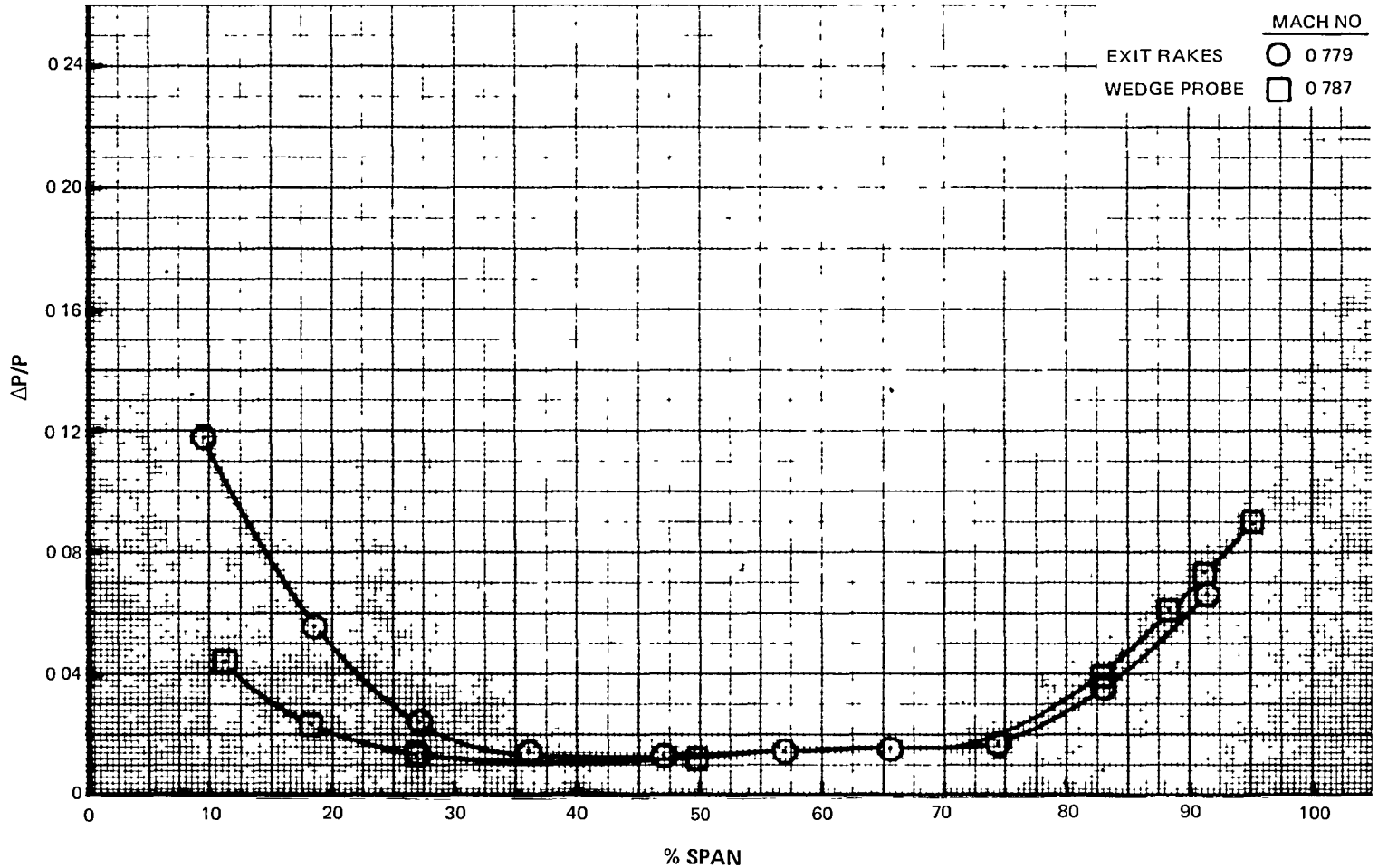

B-3 EEE Uncooled Rig 36% Reaction Annular Cascade Loss vs. % Span (Area Averaged)

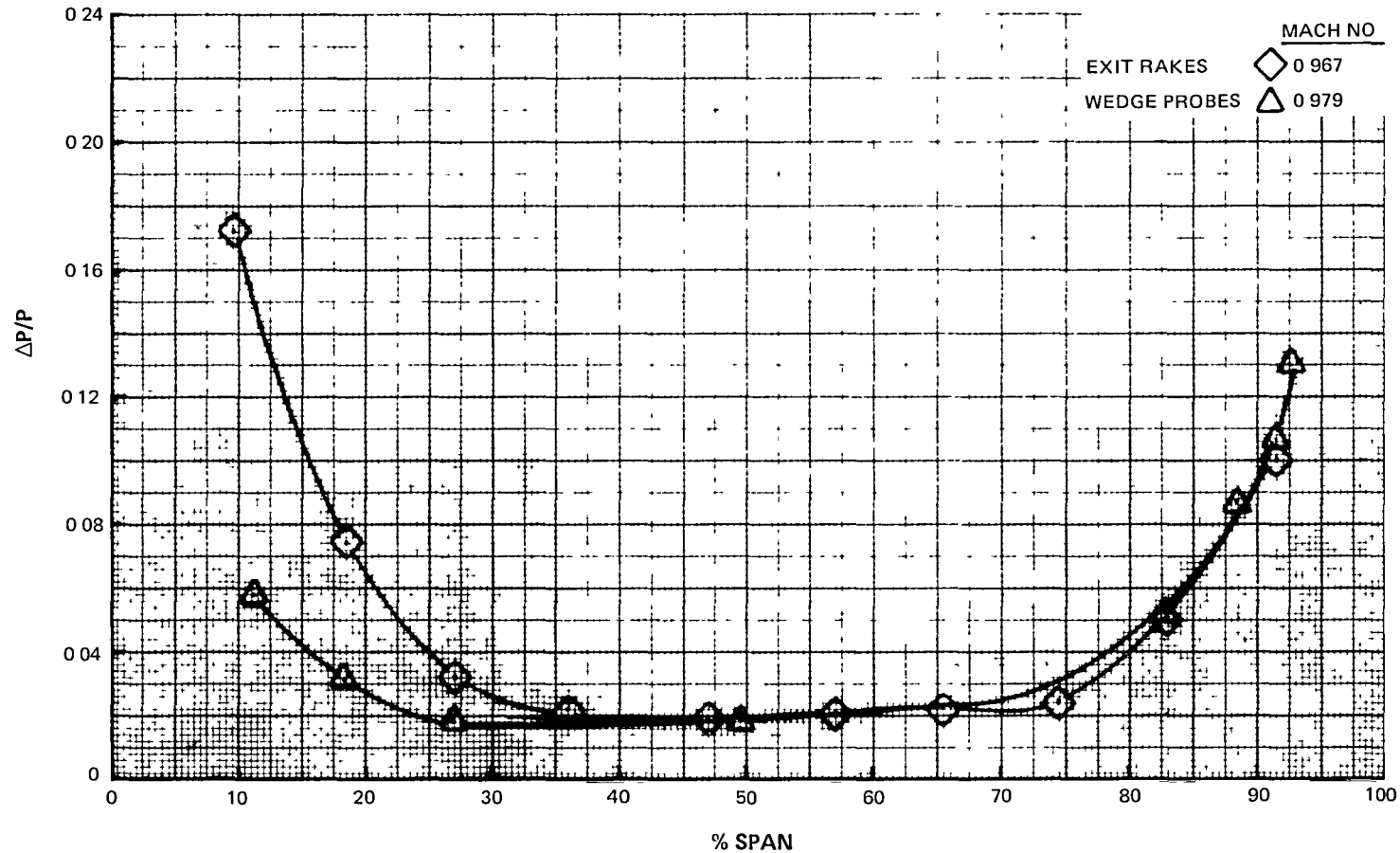

B-4 EEE Uncooled Rig 36% Reaction Annular Cascade Loss vs. % Span (Area Averaged)

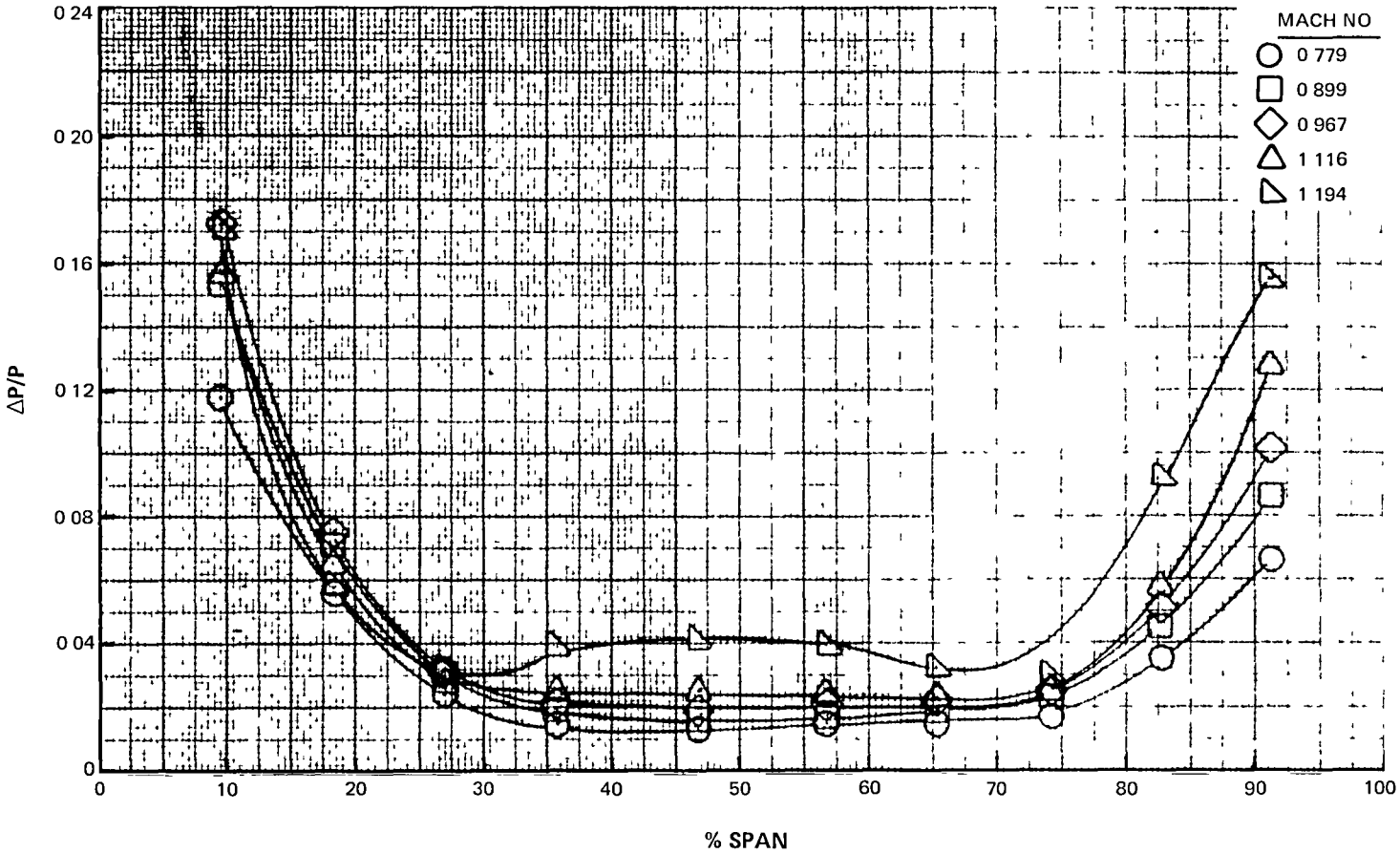

B-5 EEE Uncooled Rig 36% Reaction Annular Cascade Loss vs. % Span (Area Averaged)

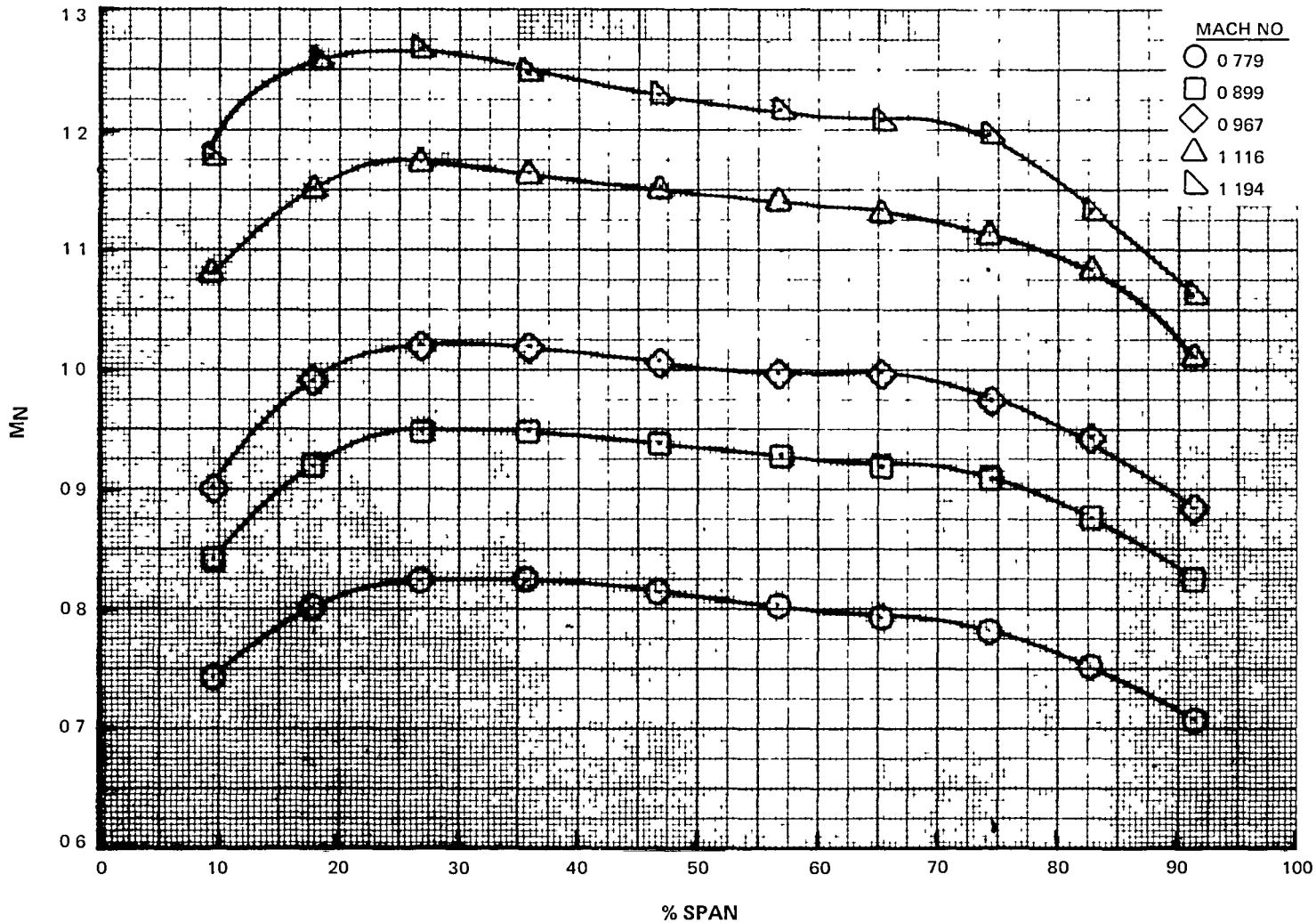

B-6 EEE Uncooled Rig 36% Reaction Annular Cascade Mach Number vs. % Span (Area Averaged)

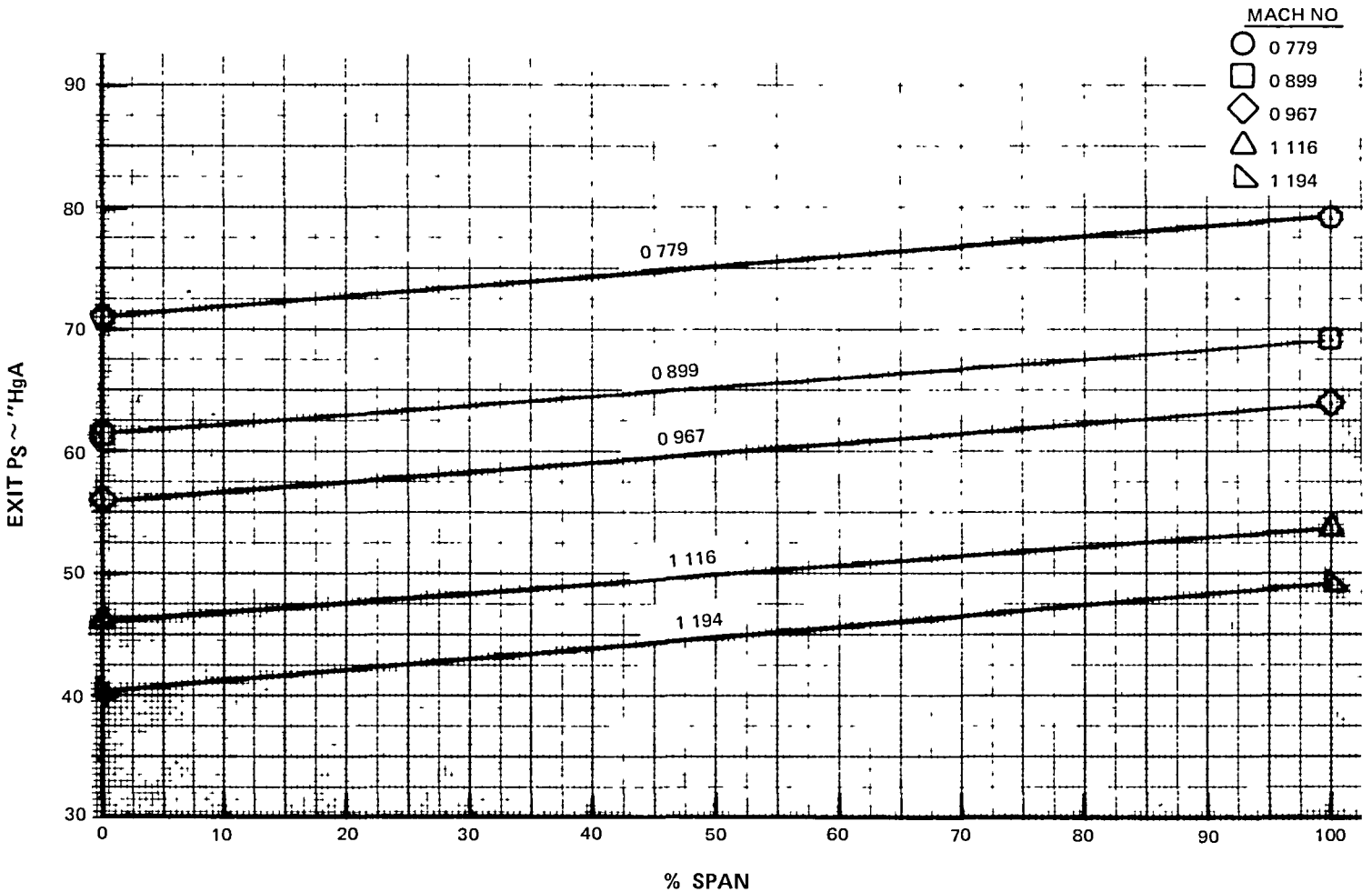

B-7 EEE Uncooled Rig 36% Reaction Annular Cascade Exit Ps vs. % Span (Area Averaged)

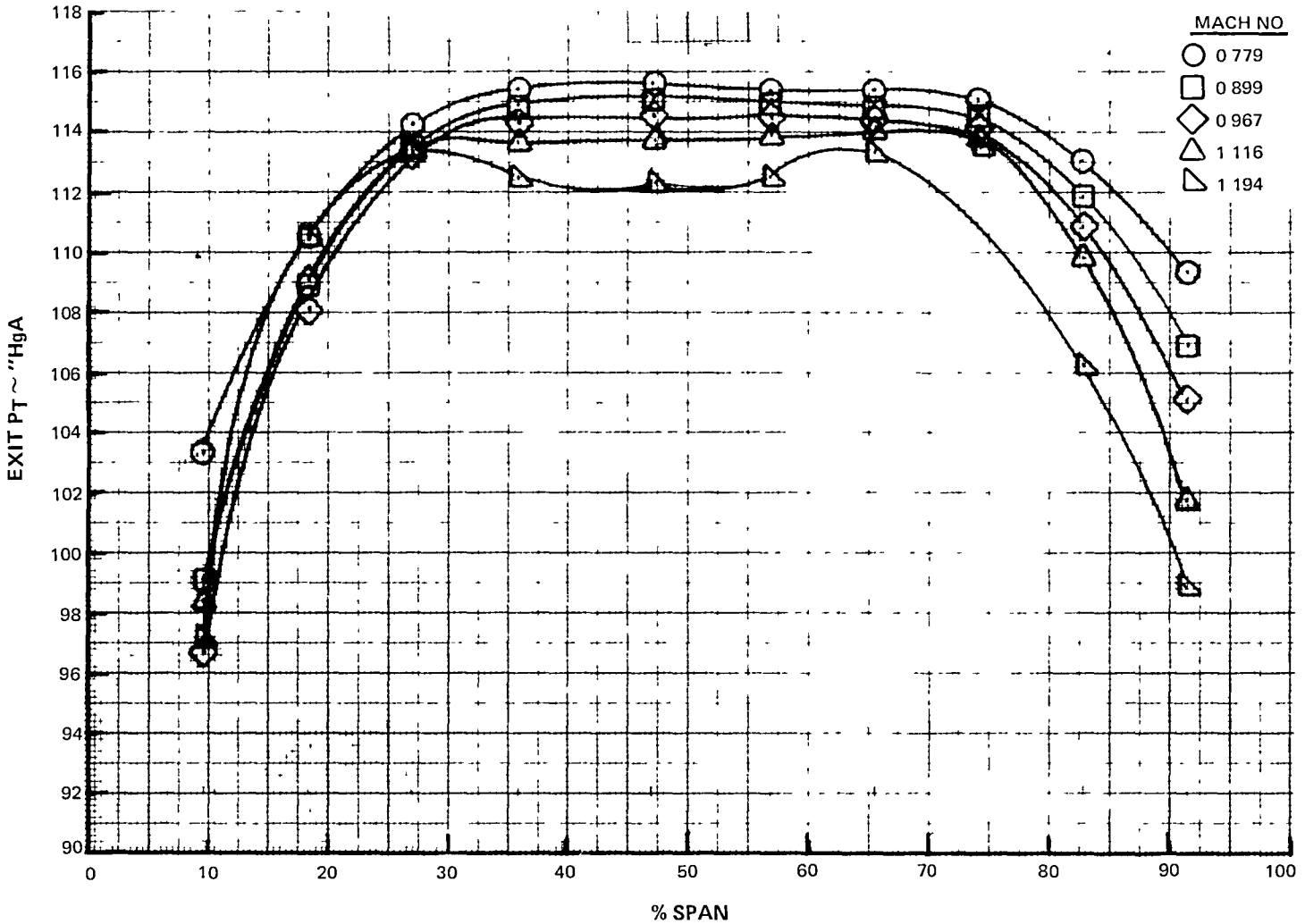

B-8 EEE Uncooled Rig 36% Reaction Annular Cascade Exit Pt vs. % Span (Area Averaged)

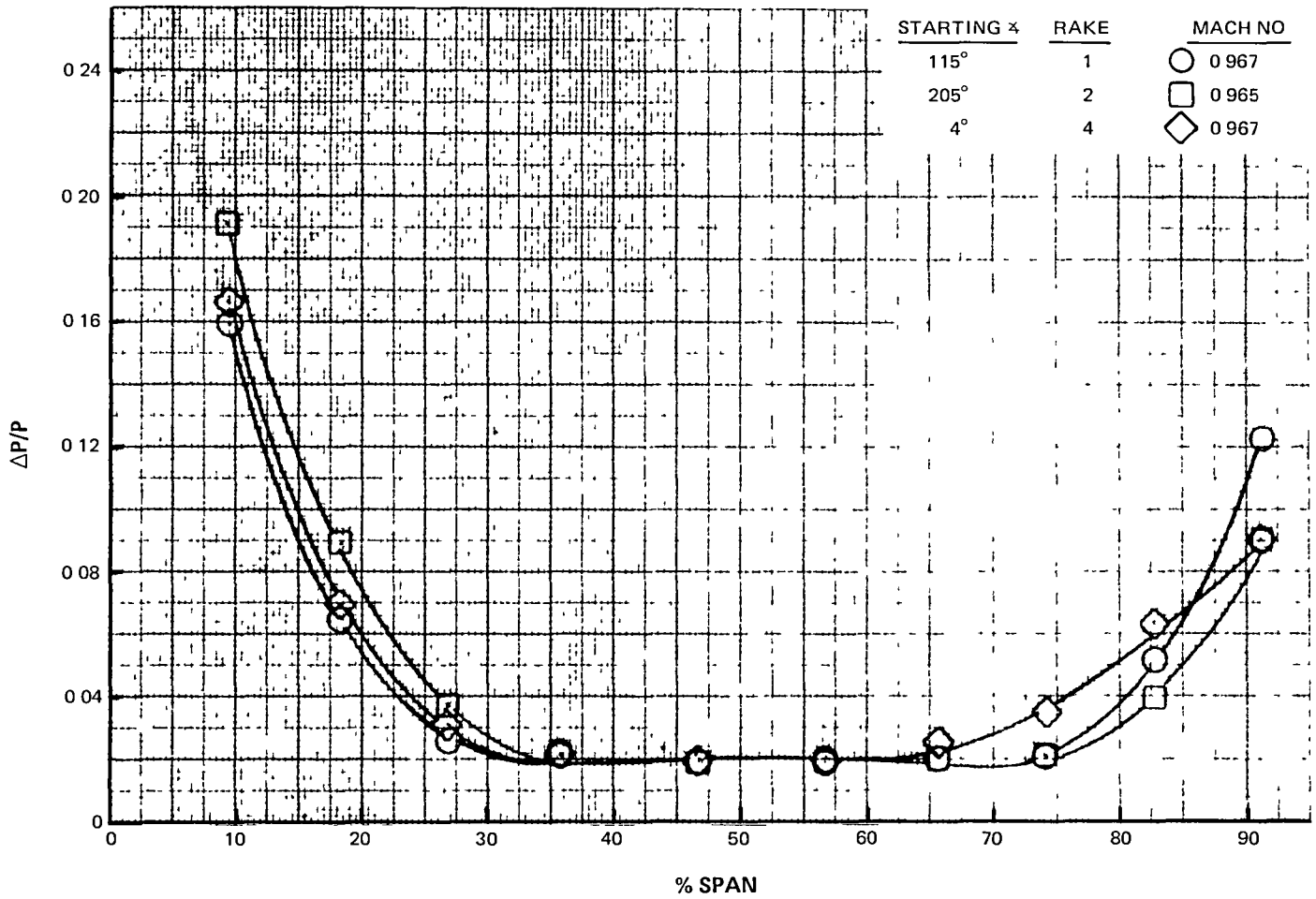

B-9 EEE Uncooled Rig 36% Reaction Annular Cascade Design Point (Area Averaged)

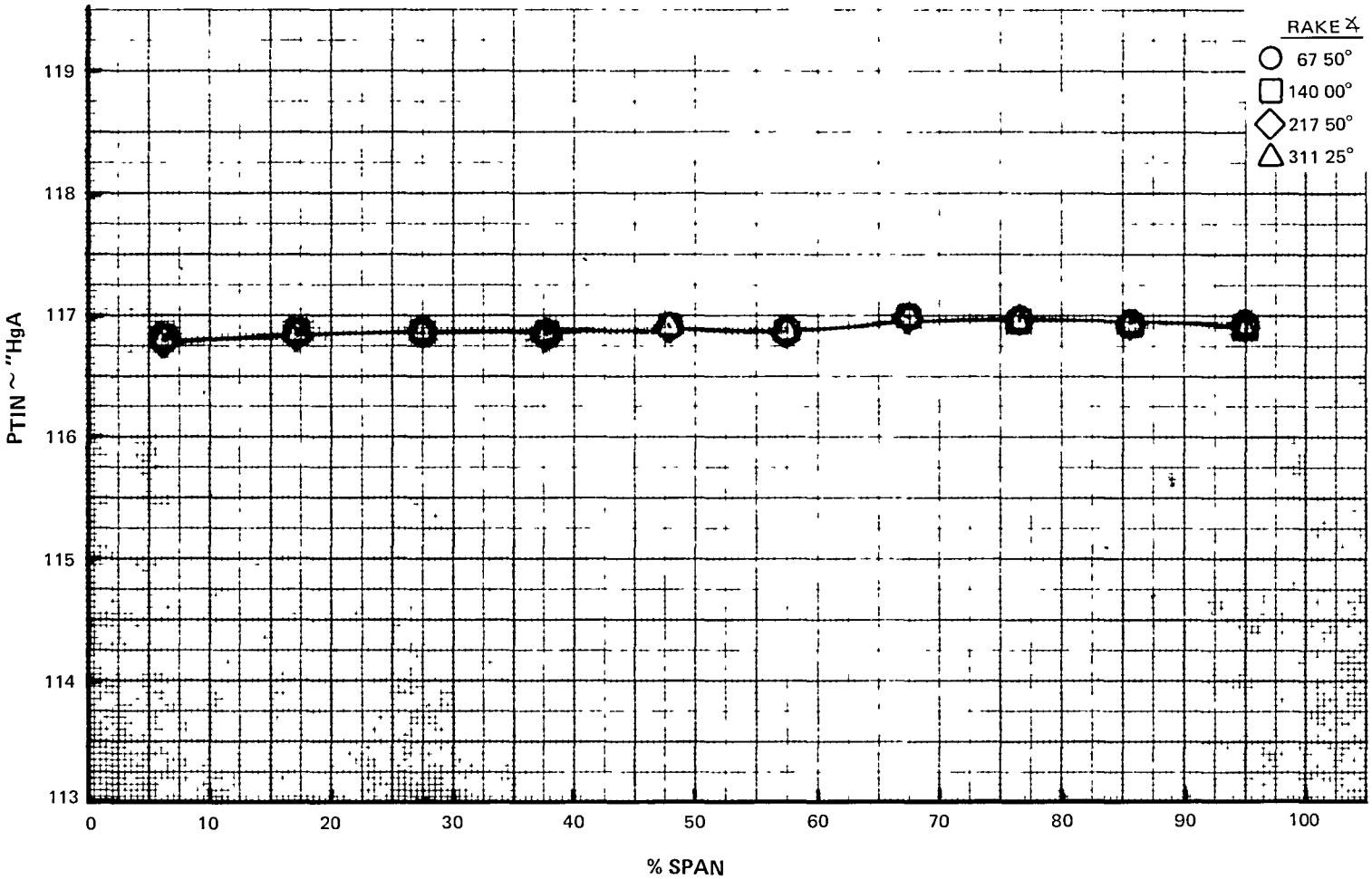

B-10 EEE Uncooled Rig 36% Reaction Annular Cascade Inlet Pt vs. % Span

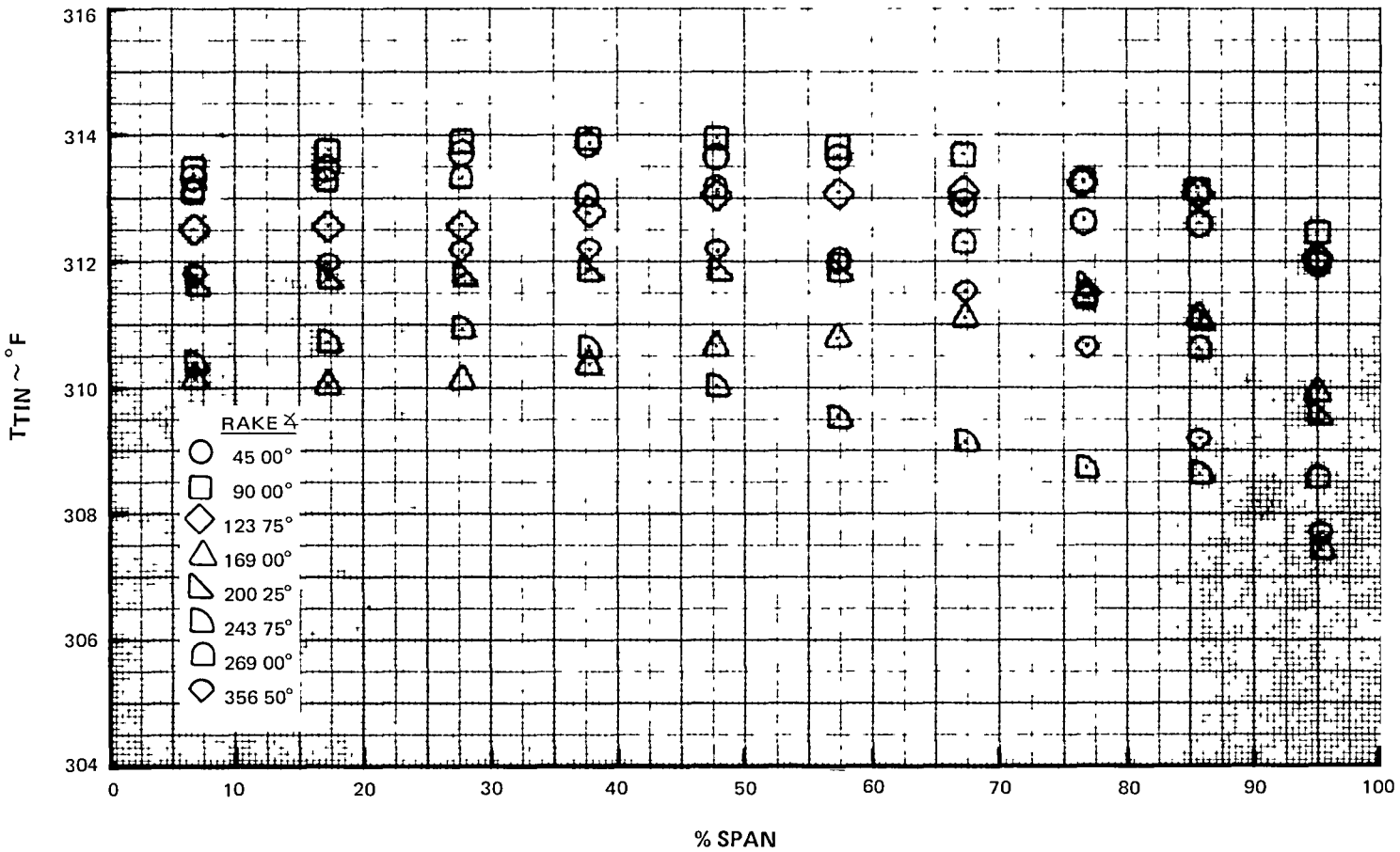

B-11 EEE Uncooled Rig 36% Reaction Annular Cascade Inlet Tt vs. % Span

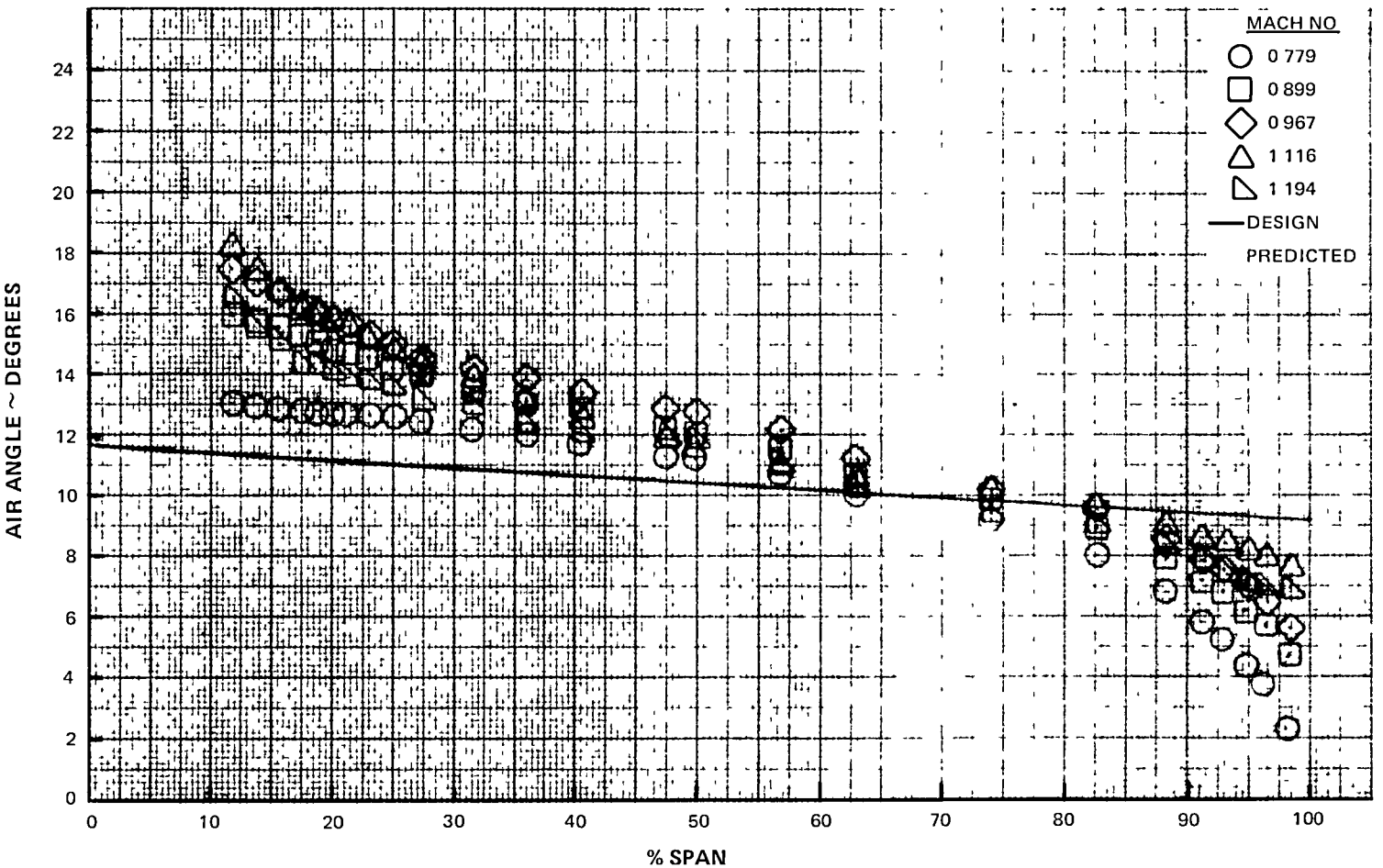

B-12 EEE Uncooled Rig 36% Reaction Annular Cascade Air Angle vs. % Span (Area Averaged)

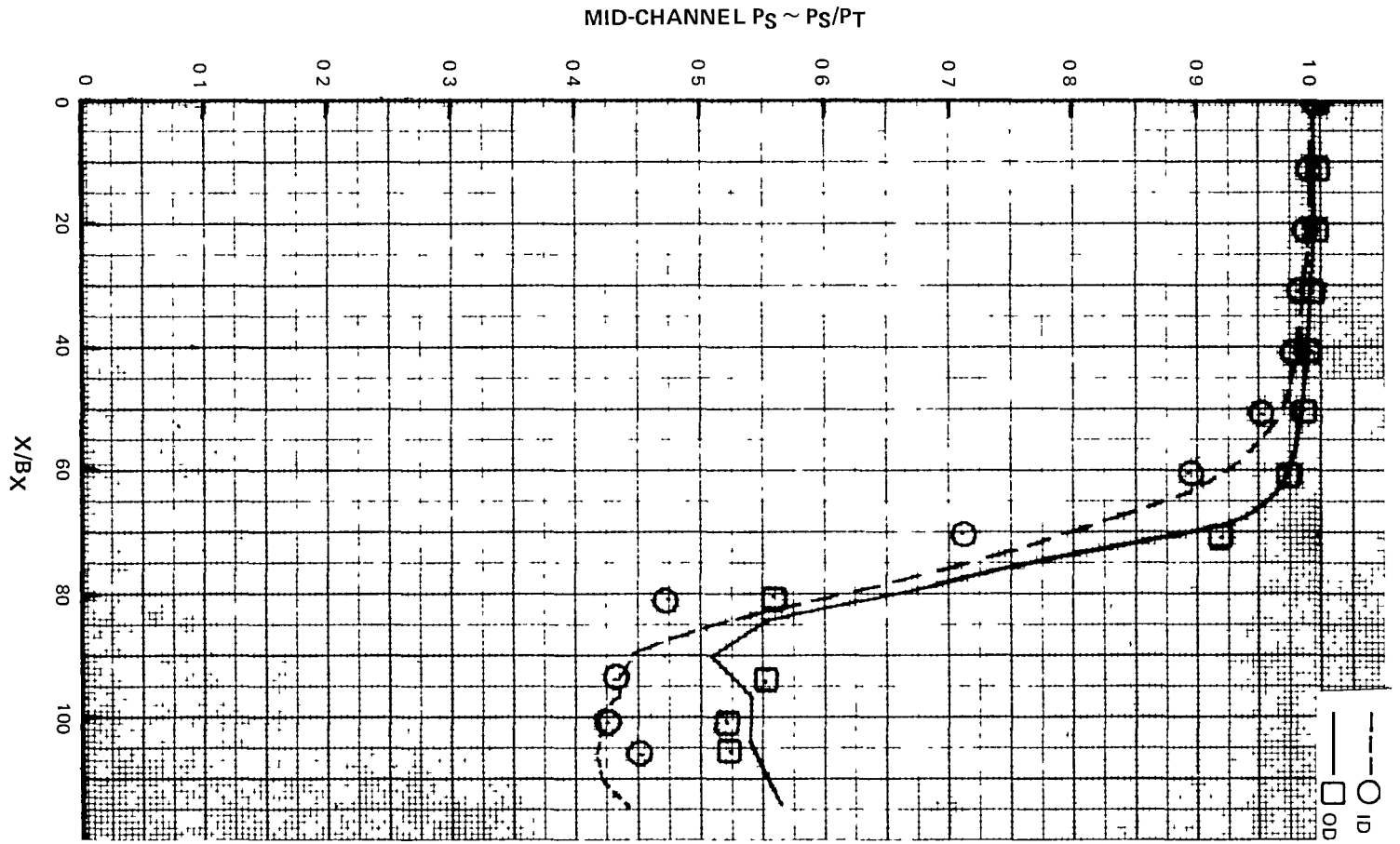

B-13 EEE Uncooled Rig 36% Reaction Annular Cascade Mid-Channel Statics vs. Prediction (Area Averaged)

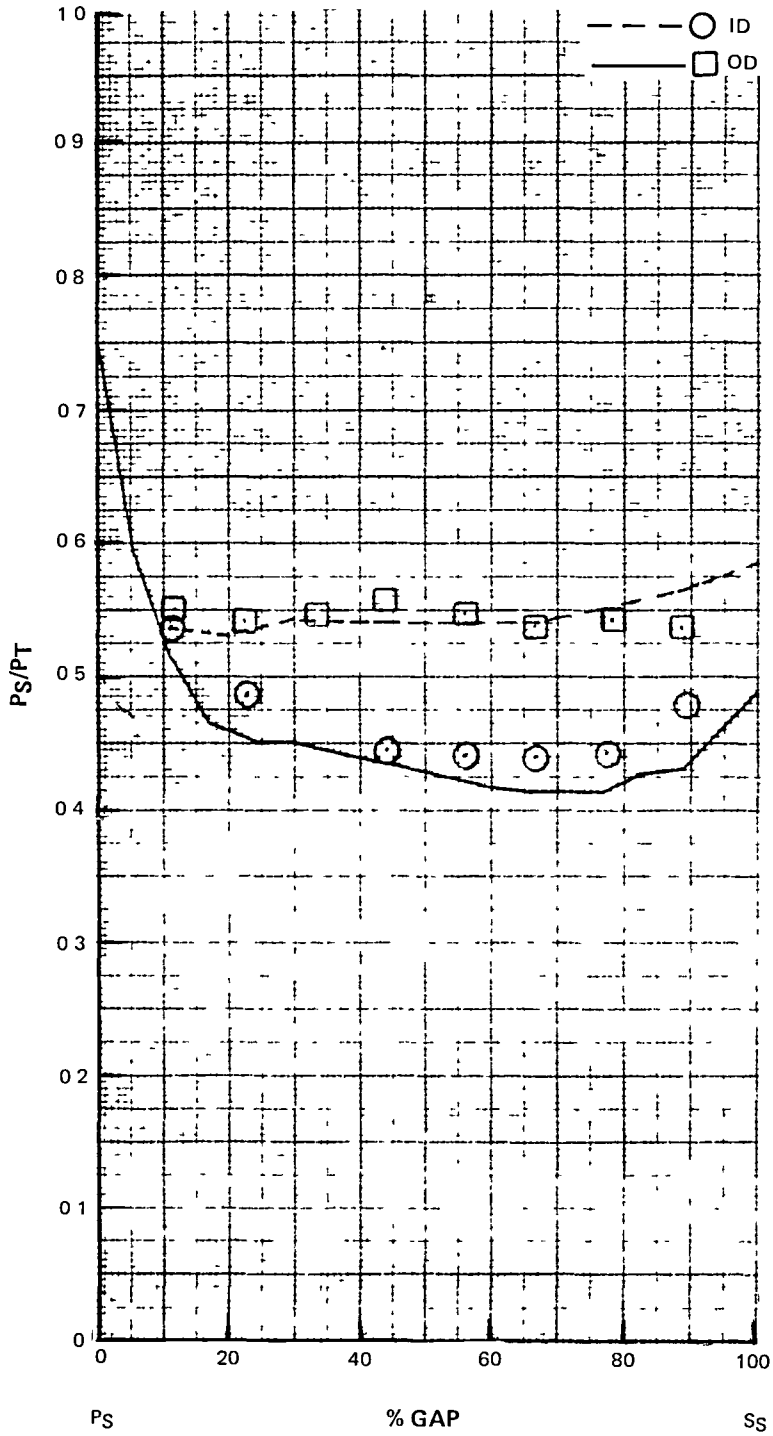

B-14 EEE Uncooled Rig 36% Reaction Annular Cascade T.E. Platform Statics vs. Prediction (Area Averaged)

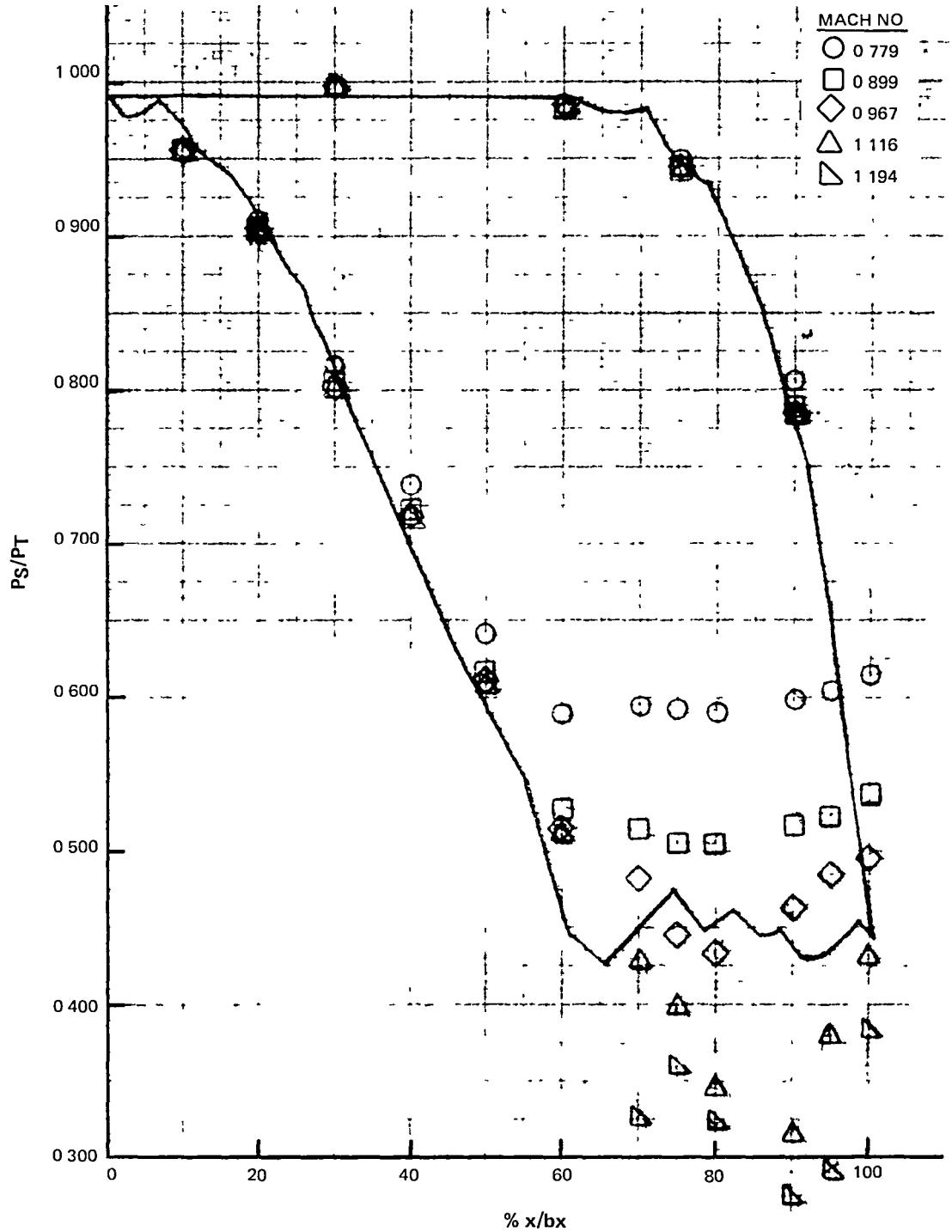

B-15 EEE Uncooled Rig 36% Reaction Airfoil Surface Statics 11% Span (Area Averaged)

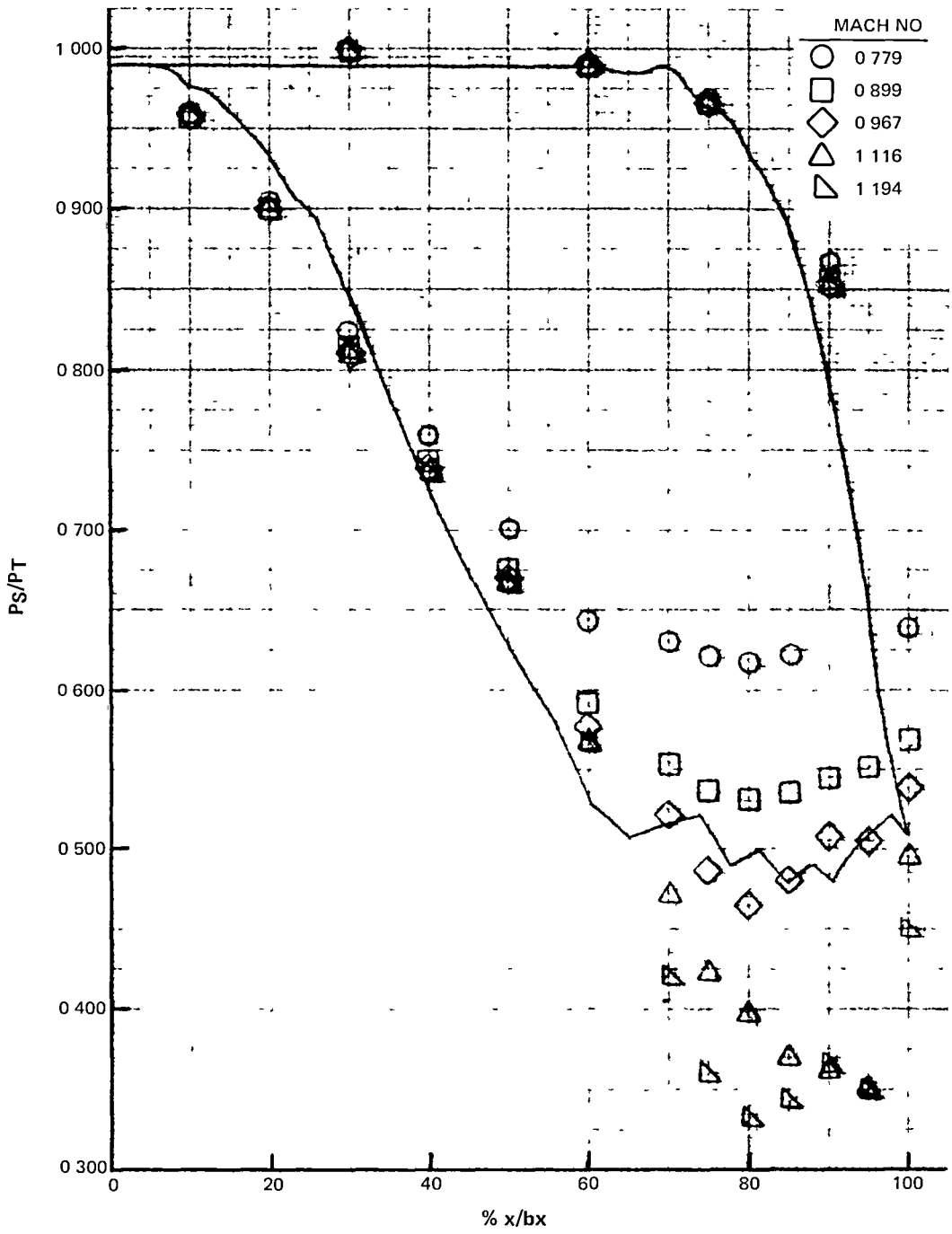

B-16 EEE Uncooled Rig 36% Reaction Airfoil Surface Statics 50% Span (Area Averaged)

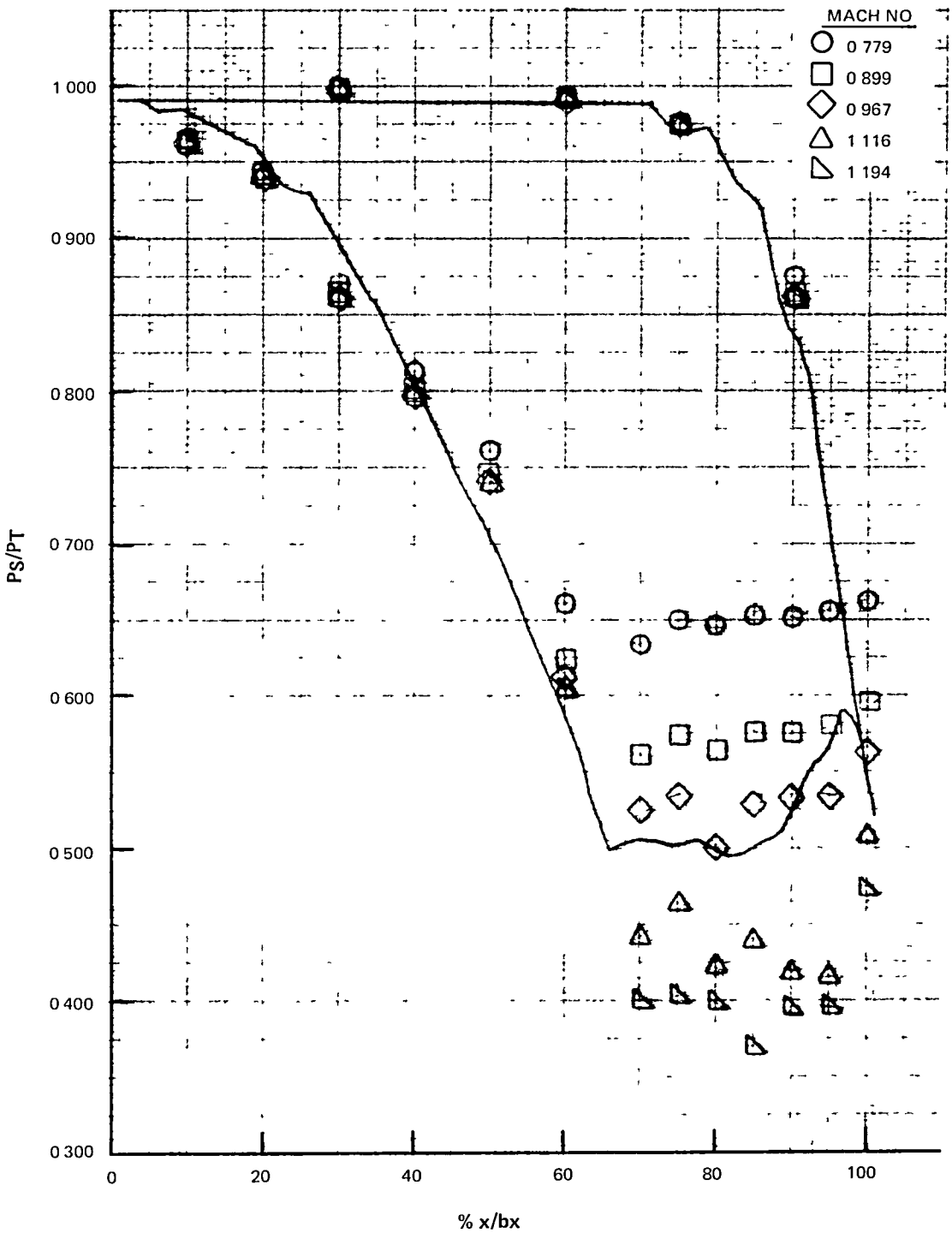

B-17 EEE Uncooled Rig 36% Reaction Airfoil Surface Statics 89% Span (Area Averaged)

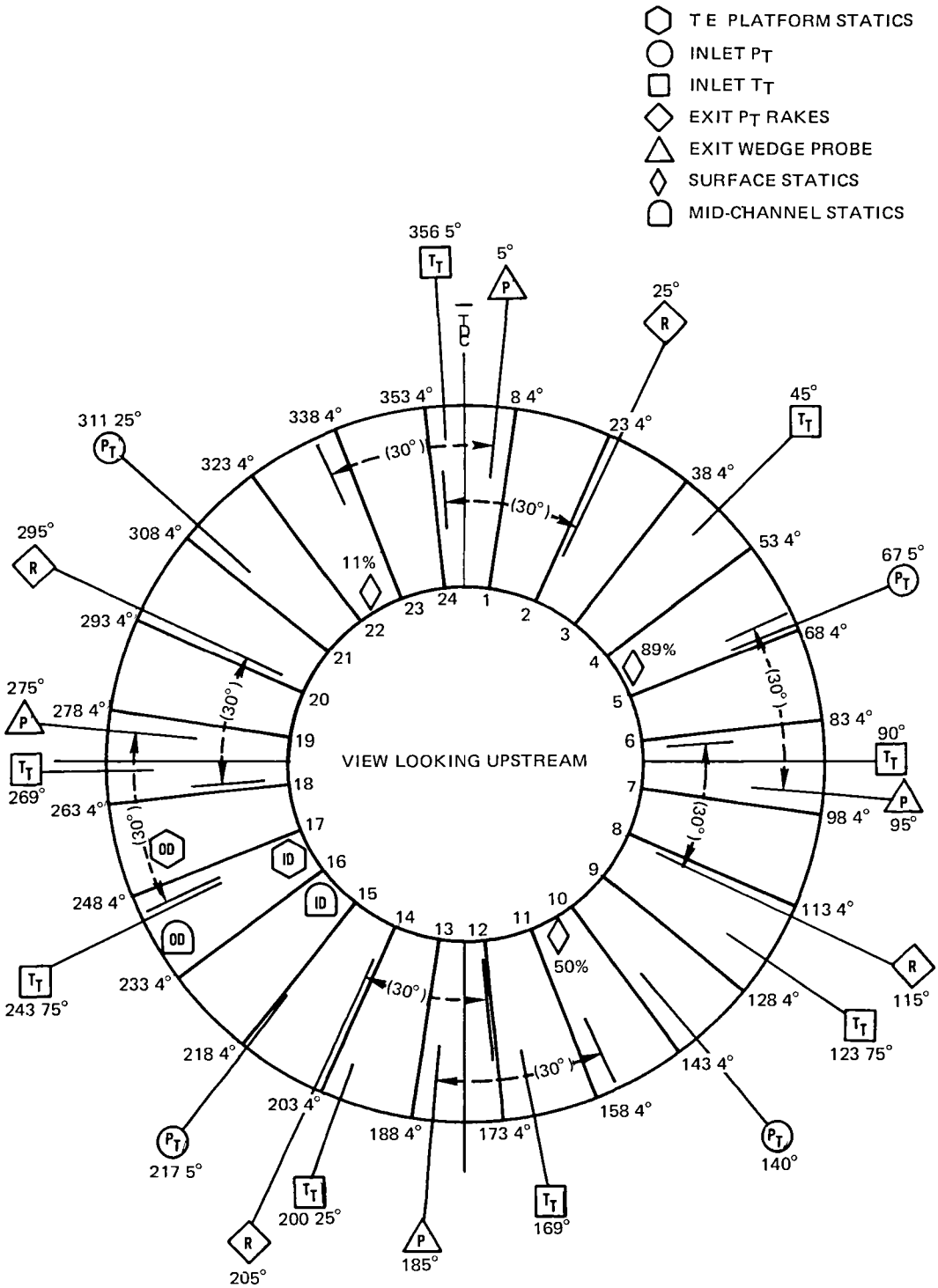

B-18 EEE Build 1 Annular Cascade Circumferential Instrumentation Location

APPENDIX C - BUILD 2 ANNULAR CASCADE DATA

C-16	EEE Uncooled Rig 43% Reaction Annular Cascade Mid-Channel Statics - I.D. (Area Averaged)
C-17	EEE Uncooled Rig 43% Reaction Annular Cascade Mid-Channel Statics - O.D. (Area Averaged)
C-18	EEE Uncooled Rig 43% Reaction Annular Cascade T.E. Platform Statics - I.D. (Area Averaged)
C-19	EEE Uncooled Rig 43% Reaction Annular Cascade T.E. Platform Statics - O.D. (Area Averaged)
C-20	EEE Uncooled Rig 43% Reaction Annular Cascade Airfoil Surface Statics 11% Span (Area Averaged)
C-21	EEE Uncooled Rig 43% Reaction Annular Cascade Airfoil Surface Statics 50% Span (Area Averaged)
C-22	EEE Uncooled Rig 43% Reaction Annular Cascade Airfoil Surface Statics 89% Span (Area Averaged)
C-23	EEE Uncooled Rig 43% Reaction Annular Cascade Circumferential Instrumentation Location

TABLE C-1
DATA SUMMARY

EEE RIG-70709-2
ANNULAR CASCADE DATA SUMMARY

*DESIGN POINT

OPERATING POINT #	STEADY STEADY SCAN #	STEADY STATE DATASET NAME	STEADY STATE JULIAN DAY 1979	STEADY STATE TIME HR:MIN	TRAVERSE SCAN #	TRAVERSE DATASET NAME	PT-IN PSIA	TT-IN °R
1	648	200747010S	24	22:41	967-995	270747012R	57.32	778.6
2	798	200836410S	29	21:39	883-911	270836412R	57.42	796.3
3*	598	200975610S	24	17:07	600-627	270975612R	57.32	779.7
4	366	201064910S	26	10:47	398-426	271064912R	57.37	787.4
5	10	201204110S	25	20:15	12- 42	271204112R	57.32	788.3

OP'TG POINT	W-MAIN LBM/S	RAKE AREA W'TED MACH #	RAKE AREA W'TED TOTAL PT/PT	RAKE MID-SPAN PT/PT	PROBE AREA W'TED MACH #	PROBE AREA W'TED TOTAL PT/PT	PROBE MID-SPAN PT/PT
1	22.23	0.703	0.0328	0.0100	0.706	0.0281	0.0094
2	23.13	0.786	0.0432	0.0128	0.791	0.0363	0.0127
3*	24.10	0.896	0.0538	0.0151	0.911	0.0466	0.0160
4	24.28	0.986	0.0662	0.0200	0.990	0.0571	0.0179
5	24.37	1.105	0.0940	0.0357	1.106	0.0868	0.0428

This Page Intentionally Left Blank

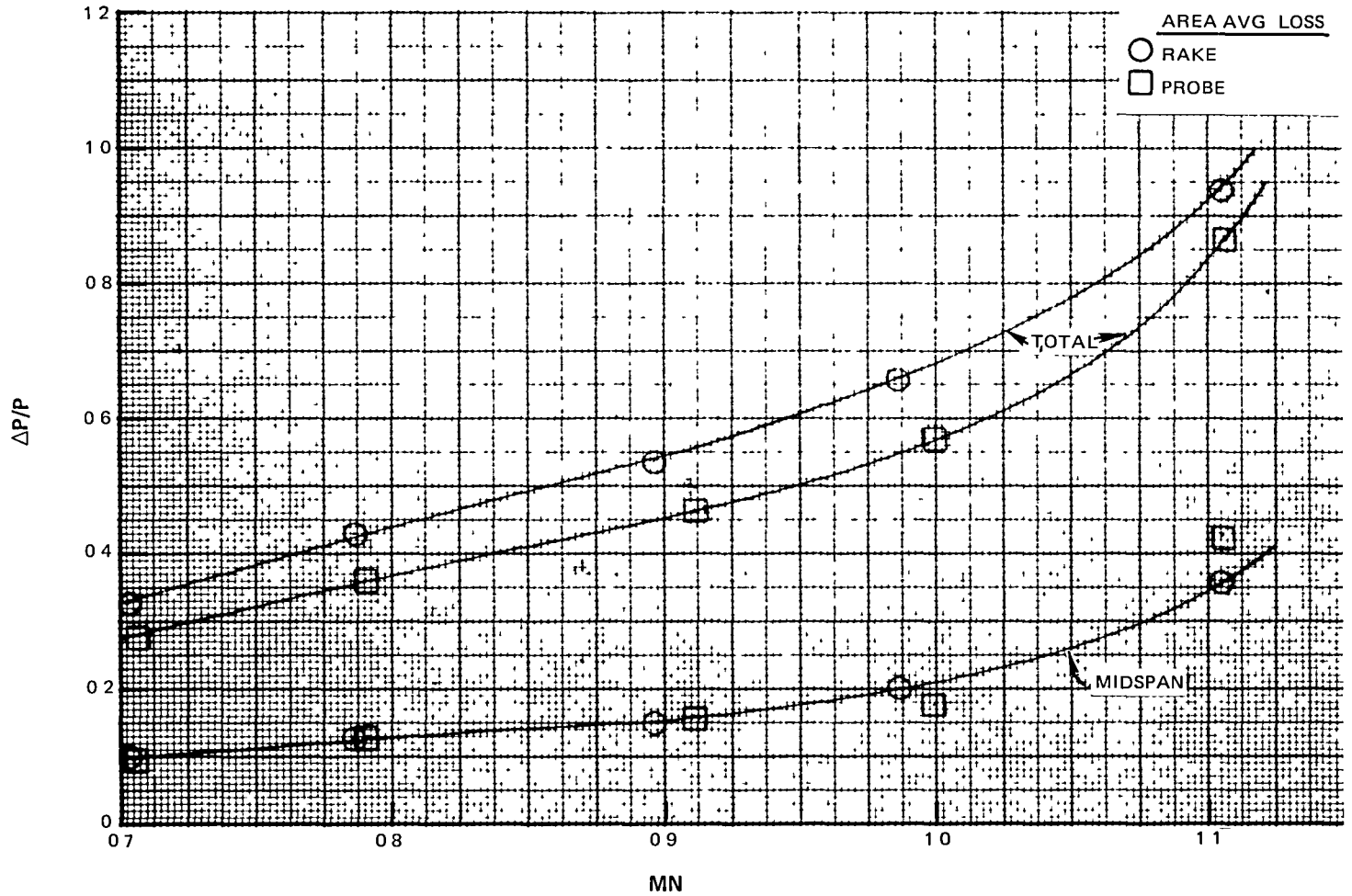

C-1 EEE Uncooled Rig 43% Reaction Annular Cascade Loss vs. Mach Number (Area Averaged)

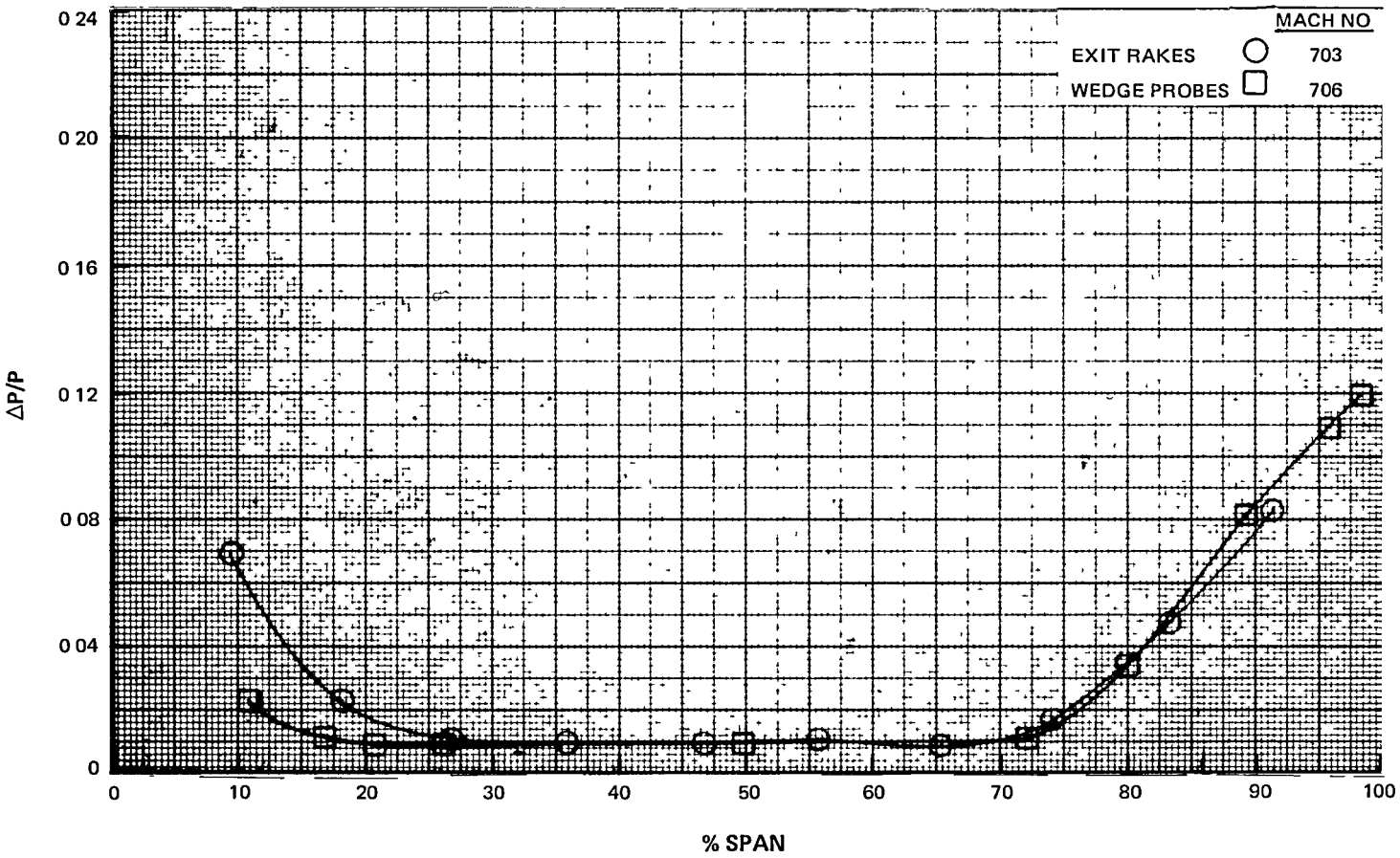

C-2 EEE Uncooled Rig 43% Reaction Annular Cascade Loss vs. % Span (Area Averaged)

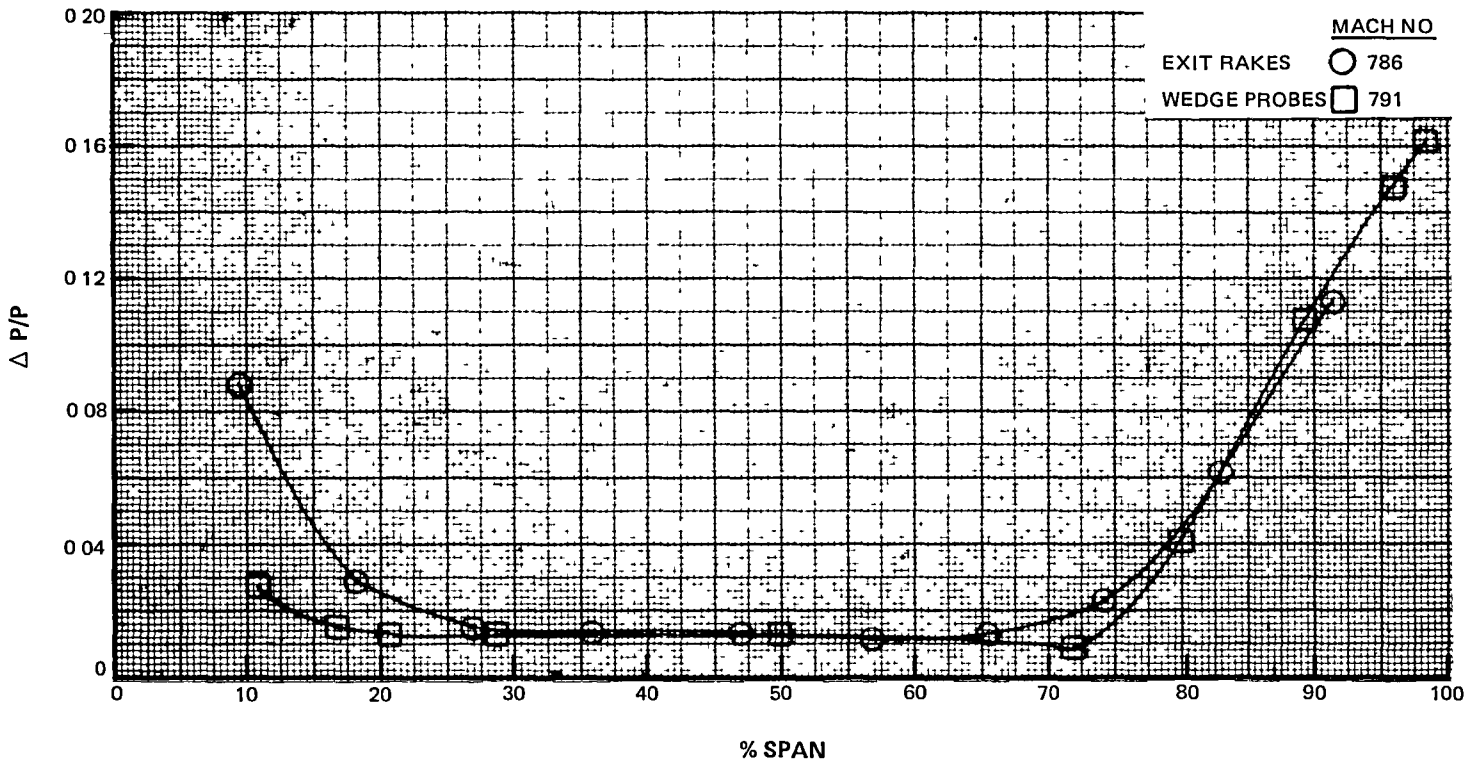

C-3 EEE Uncooled Rig 43% Reaction Annular Cascade Loss vs. % Span (Area Averaged)

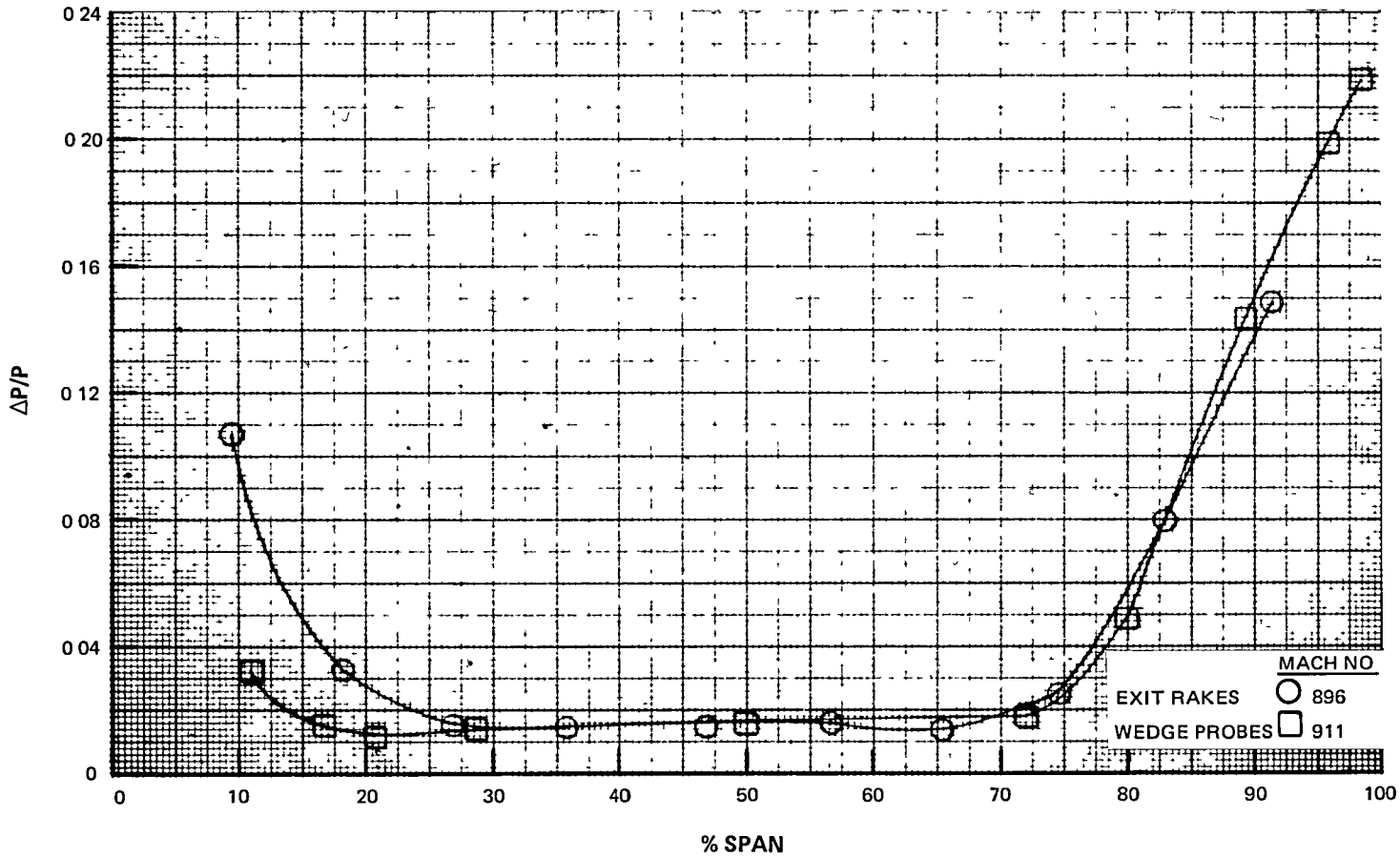

C-4 EEE Uncooled Rig 43% Reaction Annular Cascade Loss vs. % Span (Area Averaged)

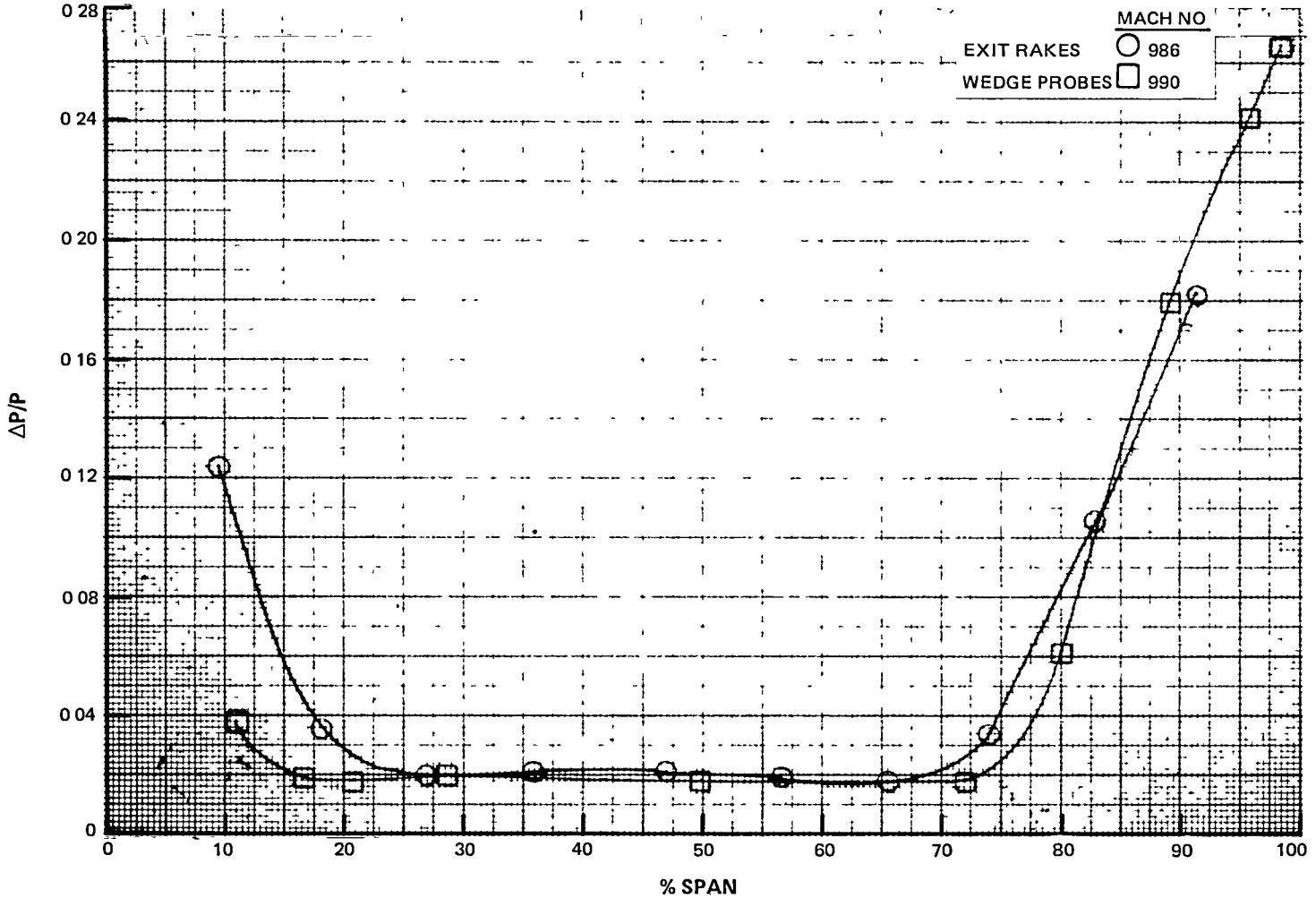

C-5 EEE Uncooled Rig 43% Reaction Annular Cascade Loss vs. % Span (Area Averaged)

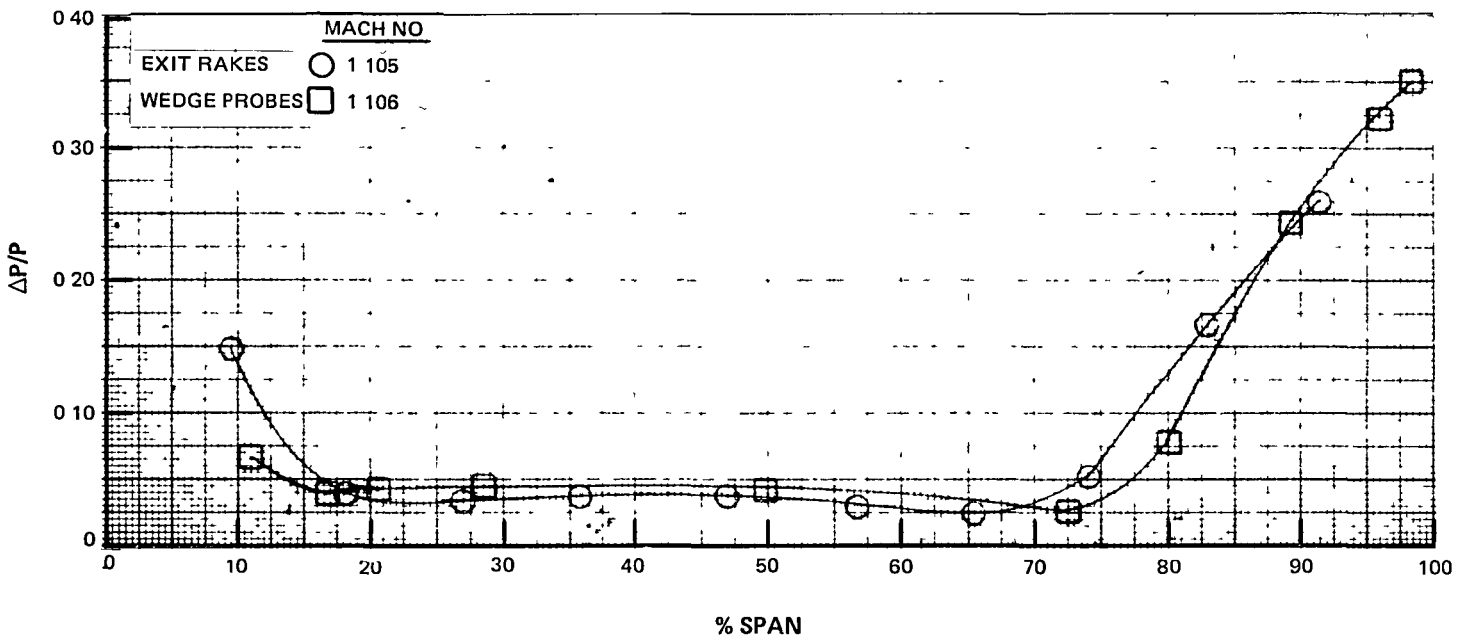

C-6 EEE Uncooled Rig 43% Reaction Annular Cascade Loss vs. % Span (Area Averaged)

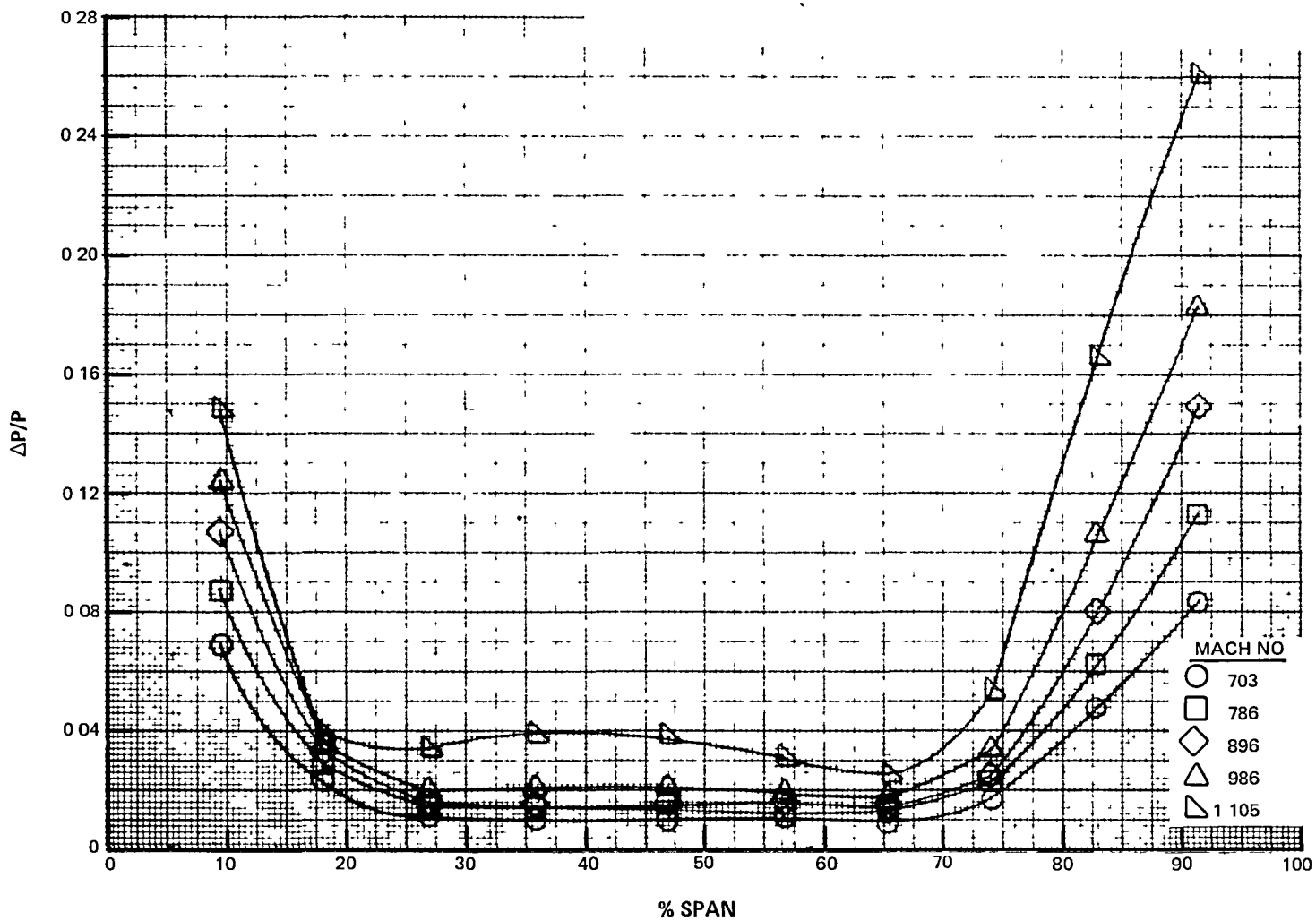

C-7 EEE Uncooled Rig 43% Reaction Annular Cascade Loss vs. % Span (Area Averaged)

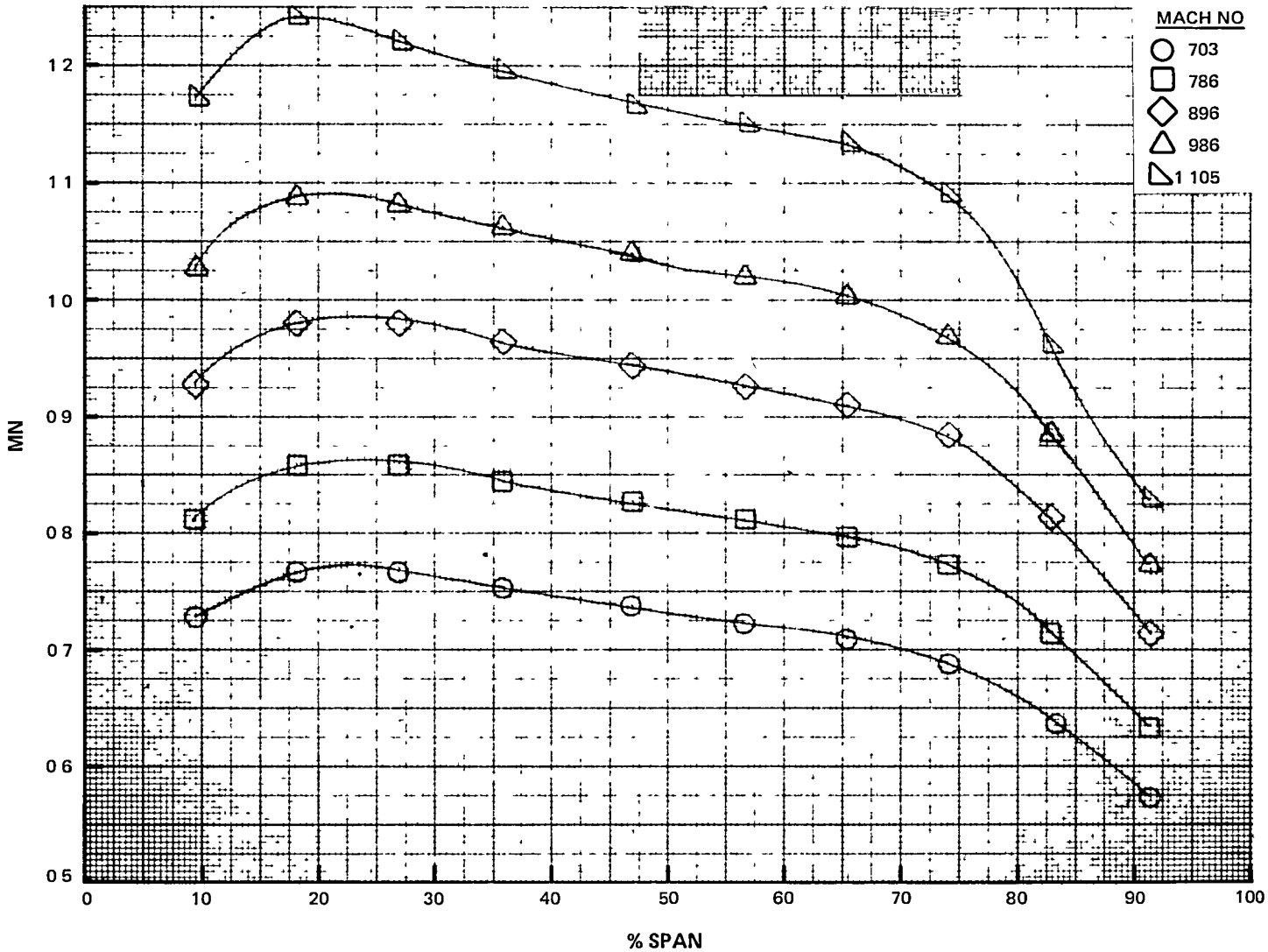

C-8 EEE Uncooled Rig 43% Reaction Annular Cascade Mach Number vs. % Span (Area Averaged)

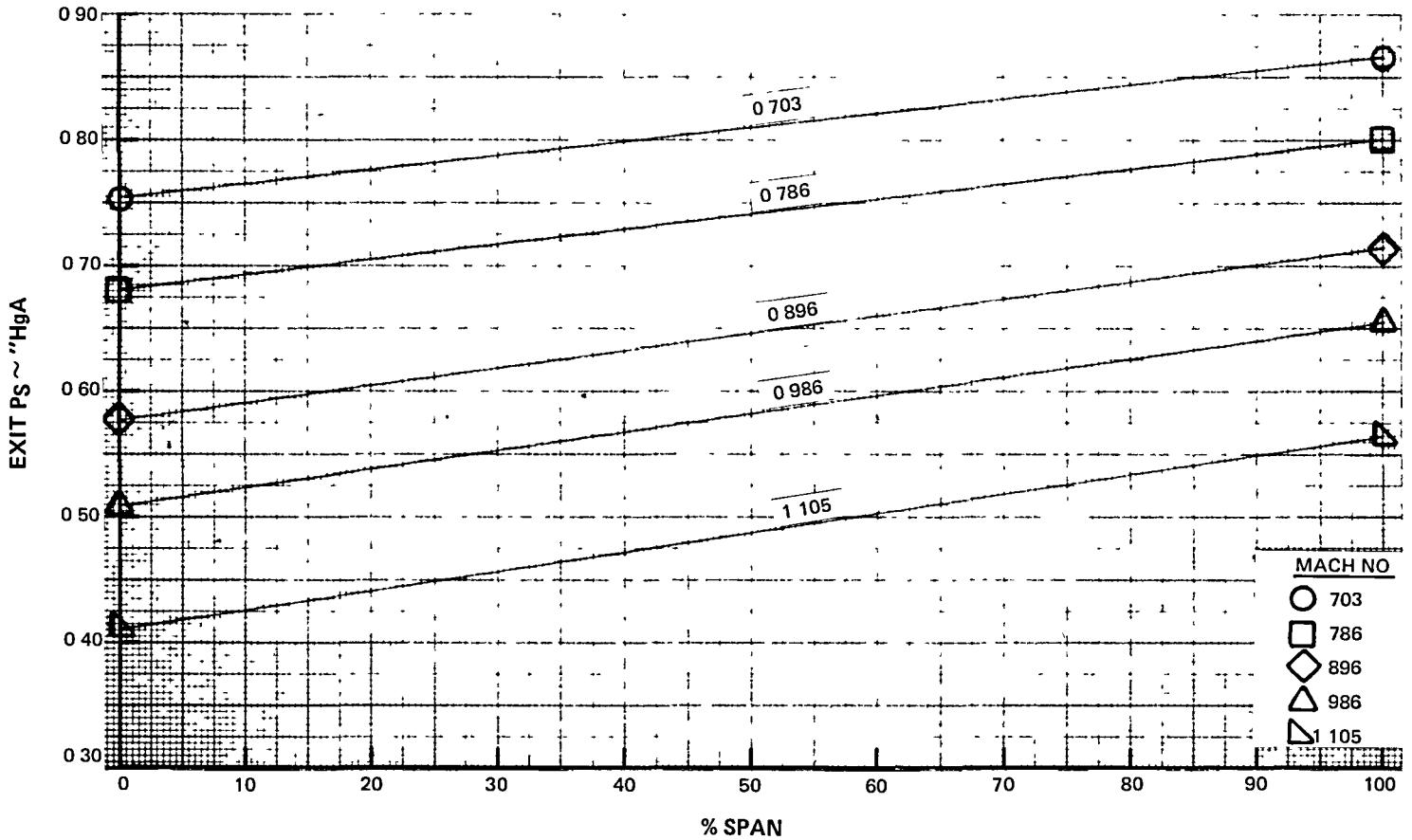

C-9 EEE Uncooled Rig 43% Reaction Annular Cascade Exit Ps vs. % Span (Area Averaged)

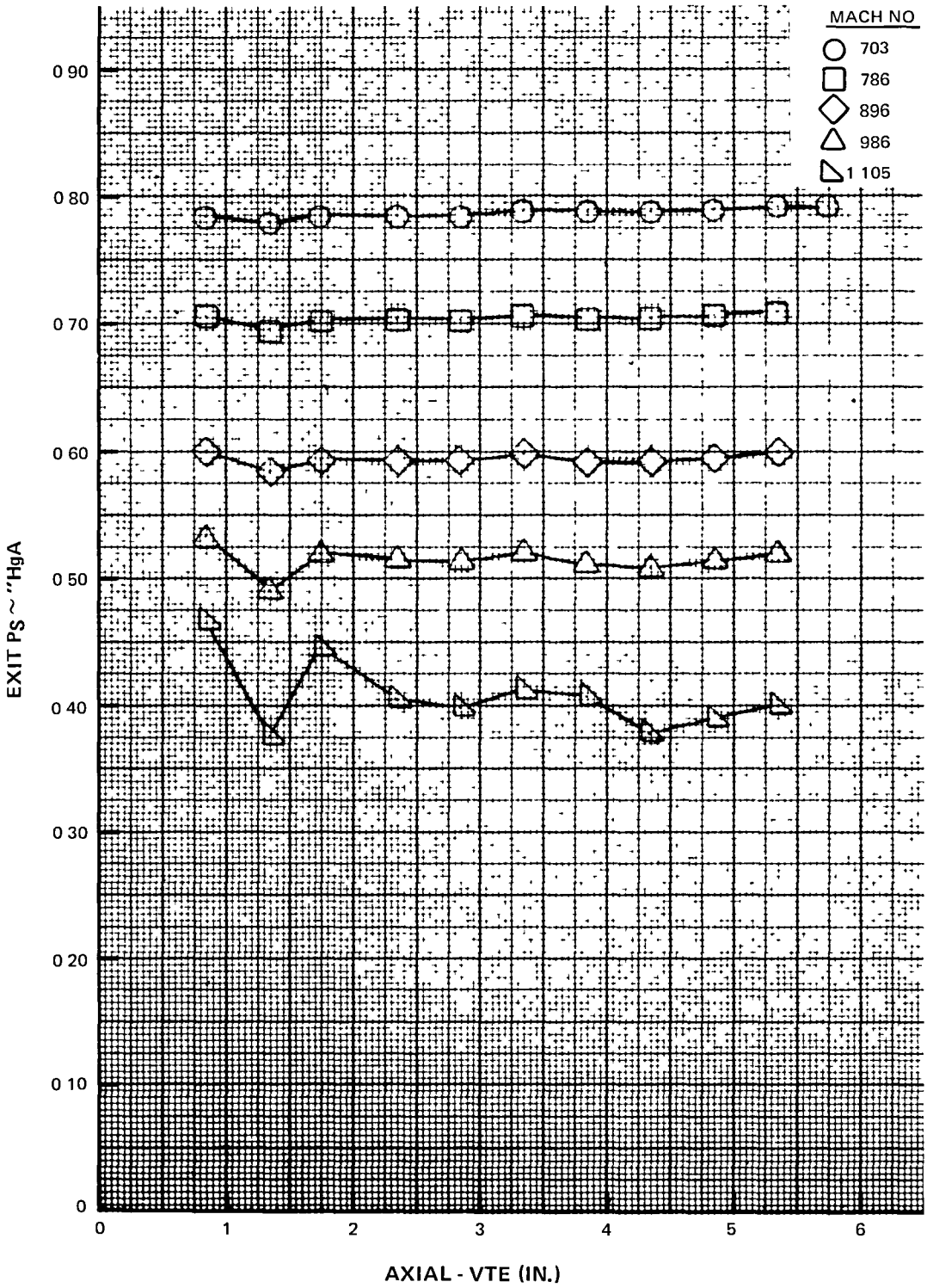

C-10 EEE Uncooled Rig 43% Reaction Annular Cascade Exhaust Case I.D. Static Pressures (Area Averaged)

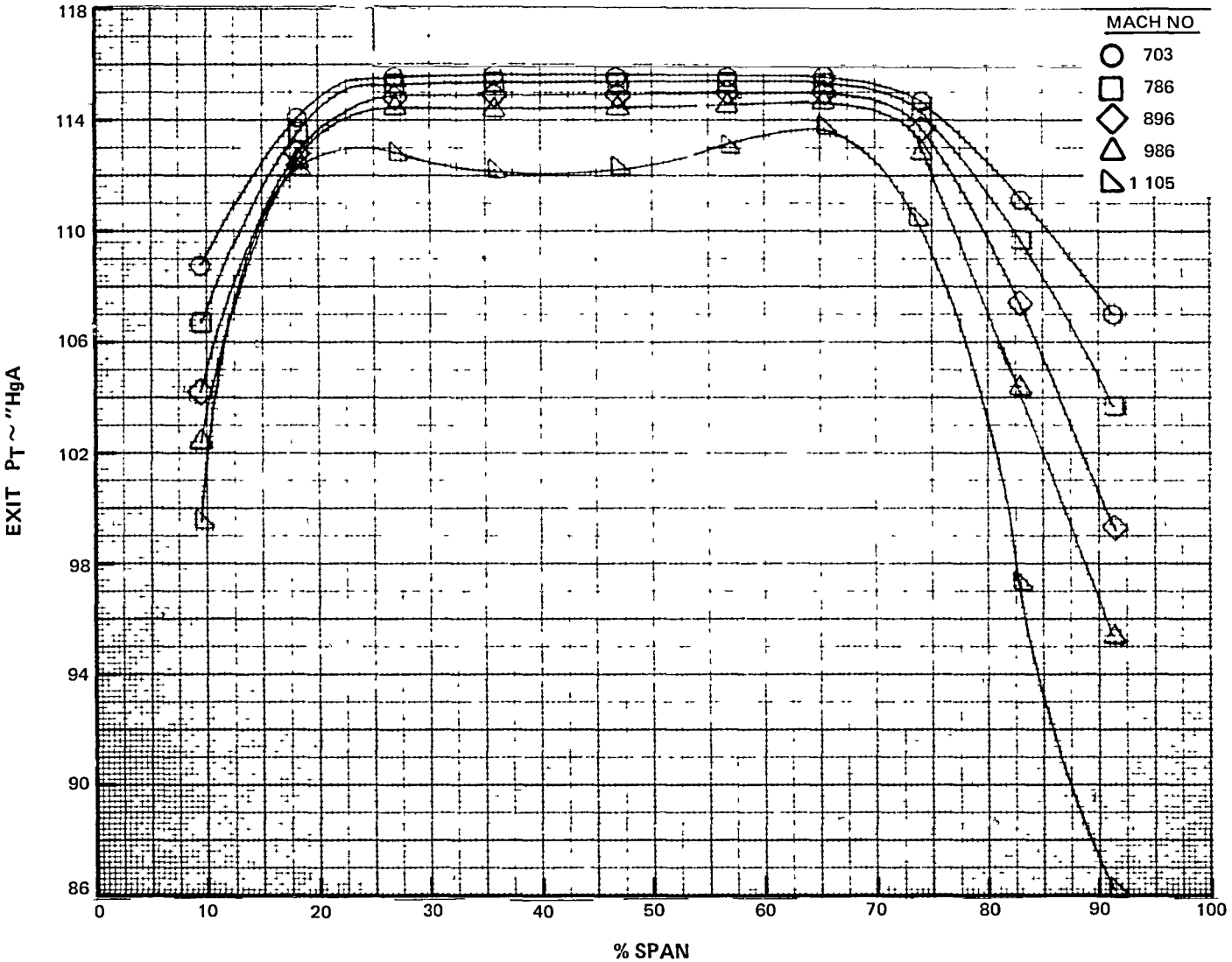

C-11 EEE Uncooled Rig 43% Reaction Annular Cascade Exit Pt vs. % Span (Area Averaged)

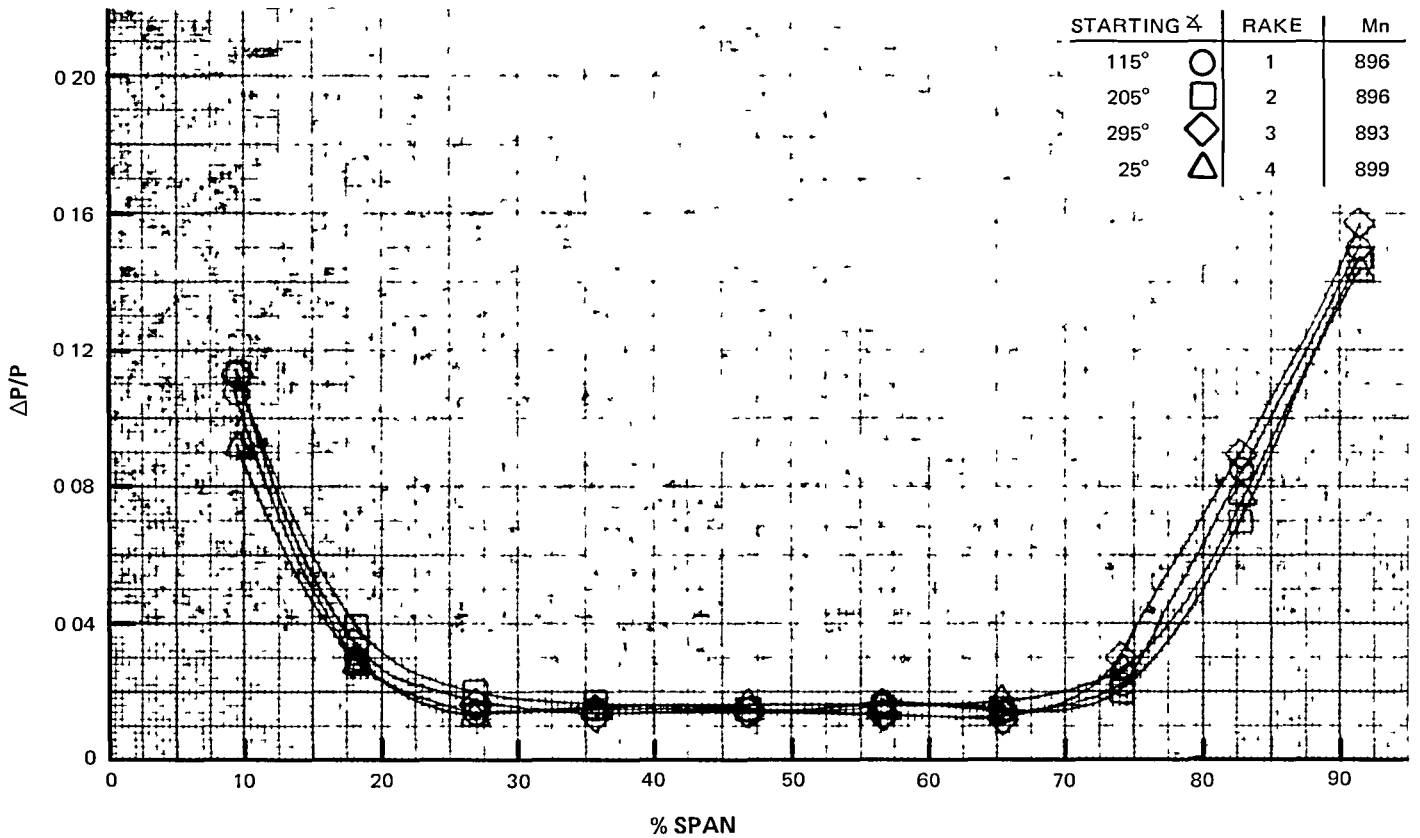

C-12 EEE Uncooled Rig 43% Reaction Annular Cascade Design Point (Area Averaged)

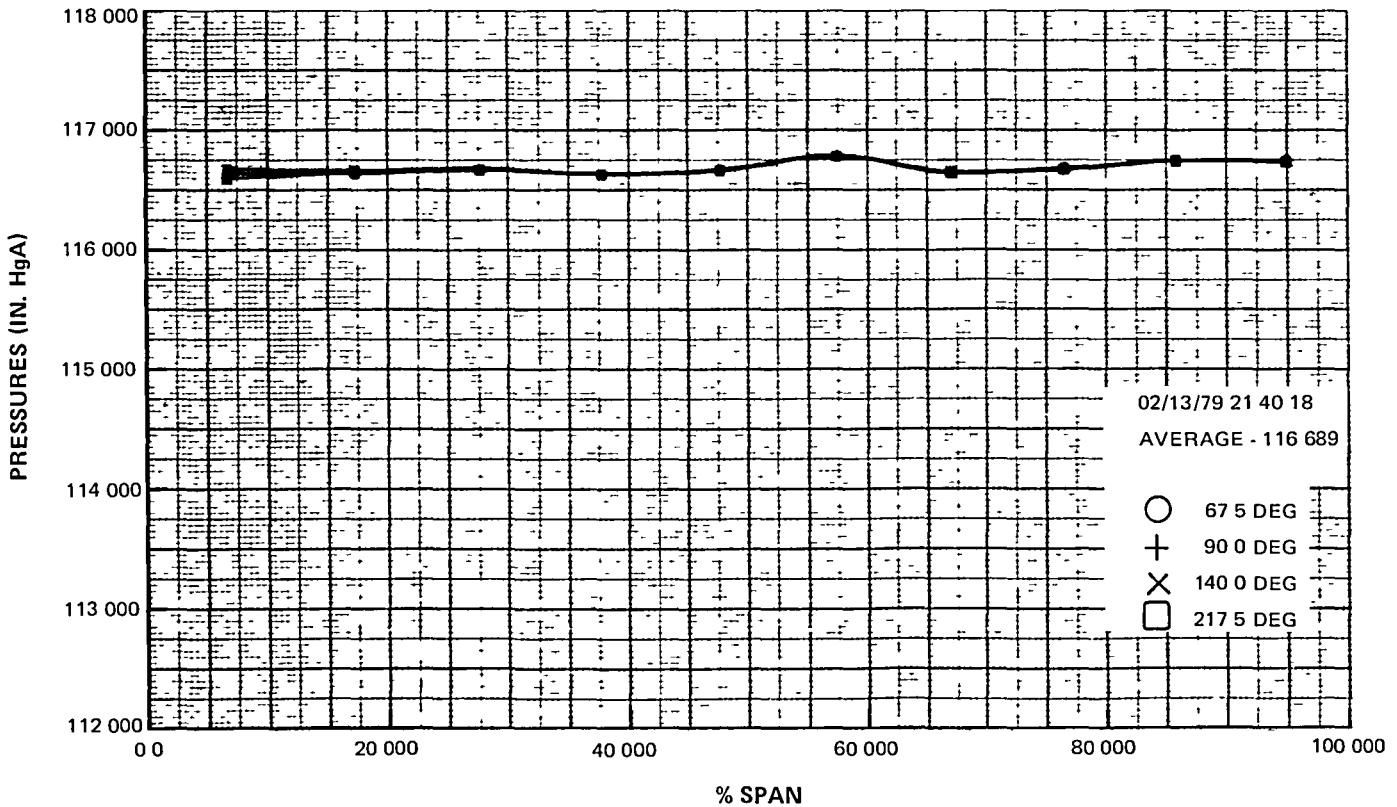

C-13 EEE Uncooled Rig 43% Reaction Annular Cascade Design Point Inlet Pressure

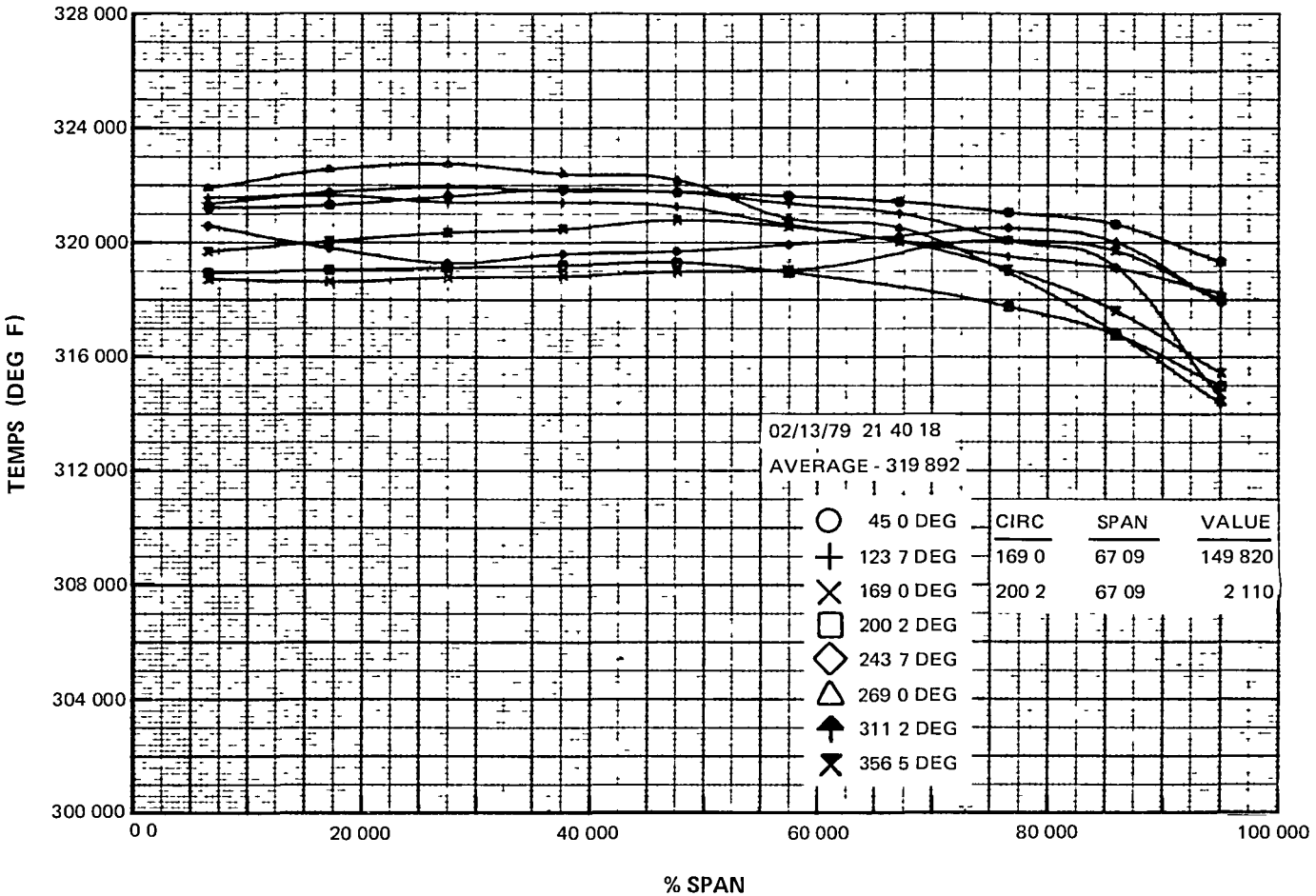

C-14 EEE Uncooled Rig 43% Reaction Annular Cascade Design Point Inlet Temperature

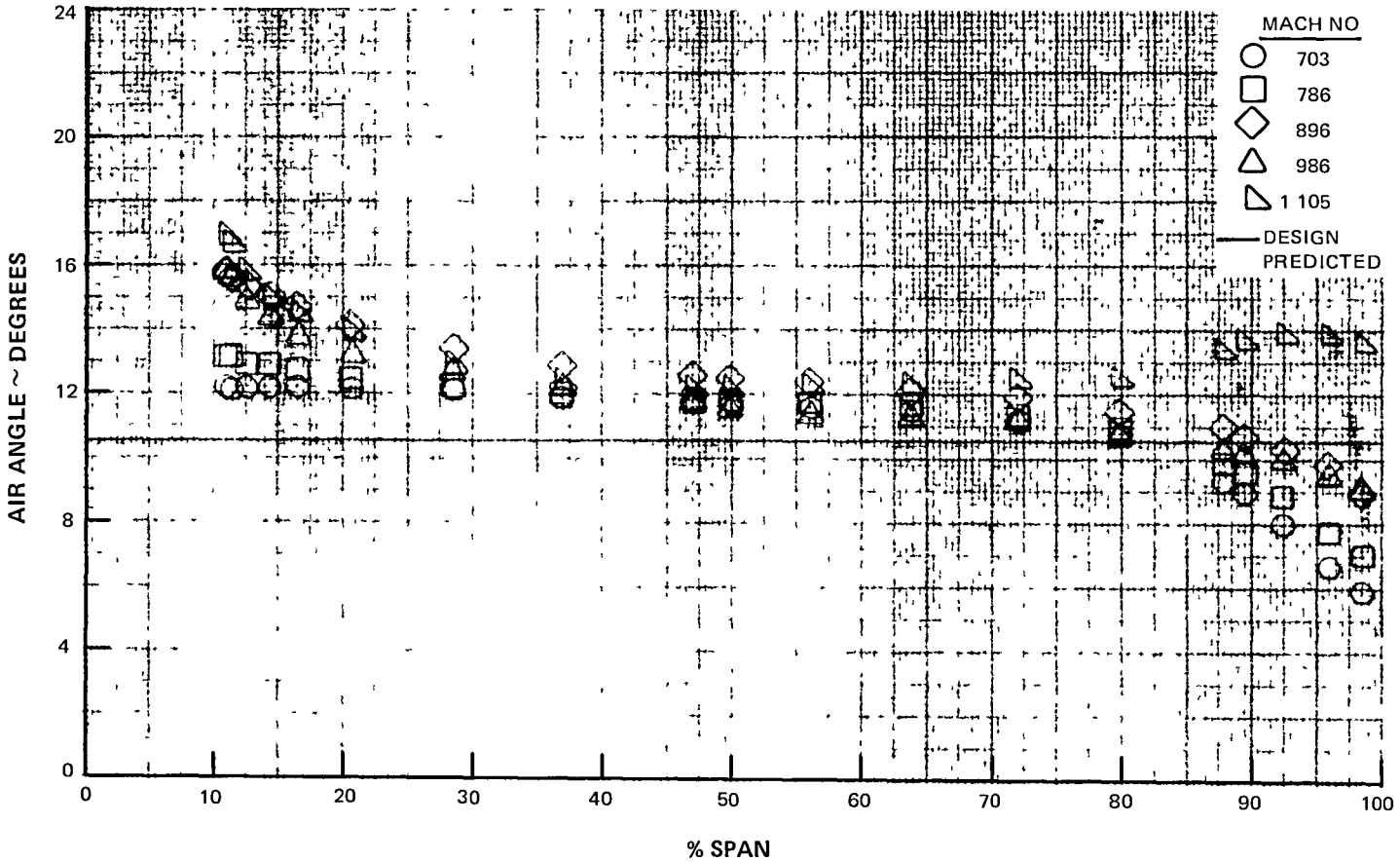

C-15 EEE Uncooled Rig 43% Reaction Annular Cascade Average Air Angle vs. % Span (Area Averaged)

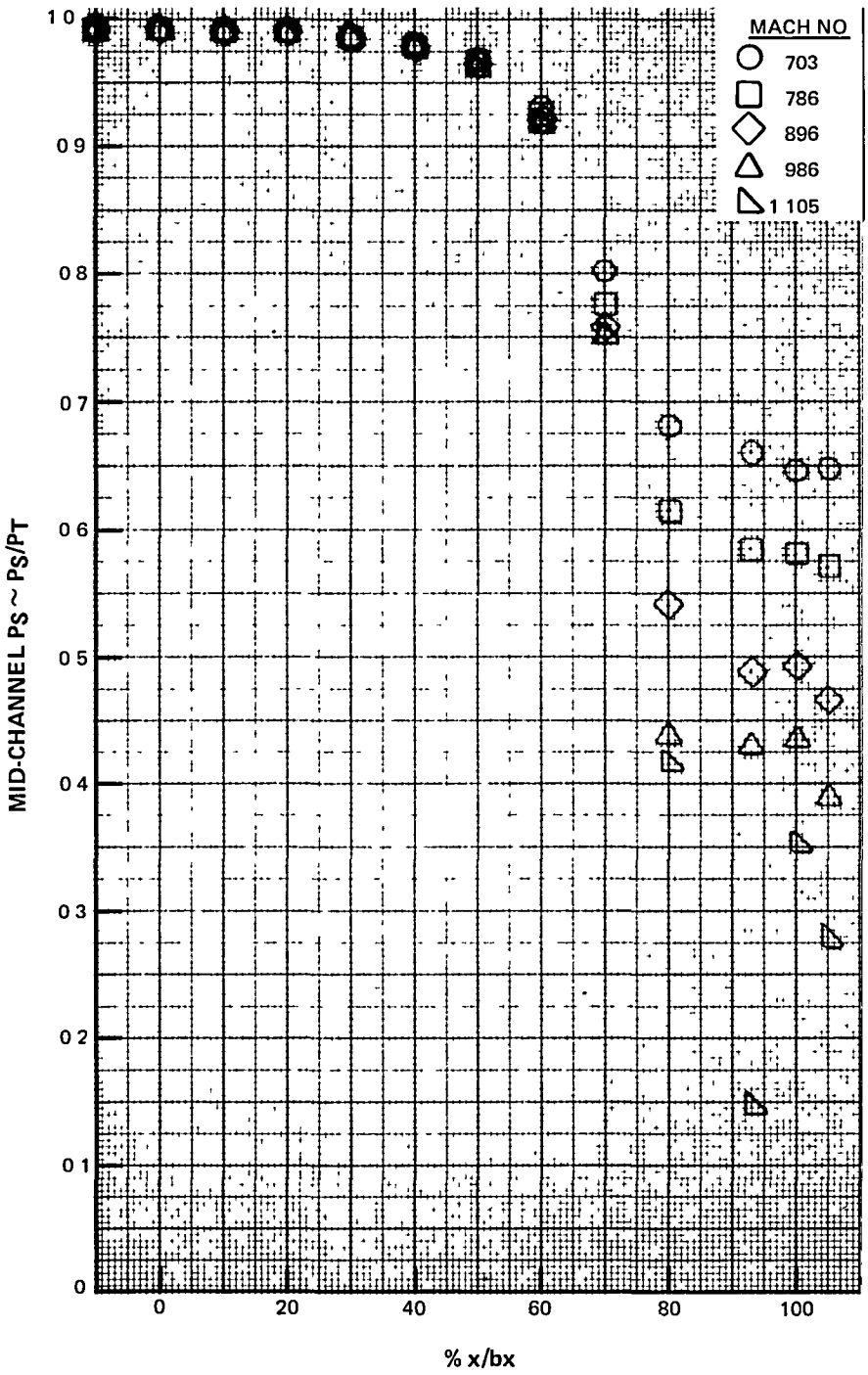

C-16 EEE Uncooled Rig 43% Reaction Annular Cascade Mid-Channel Statics - I.D. (Area Averaged)

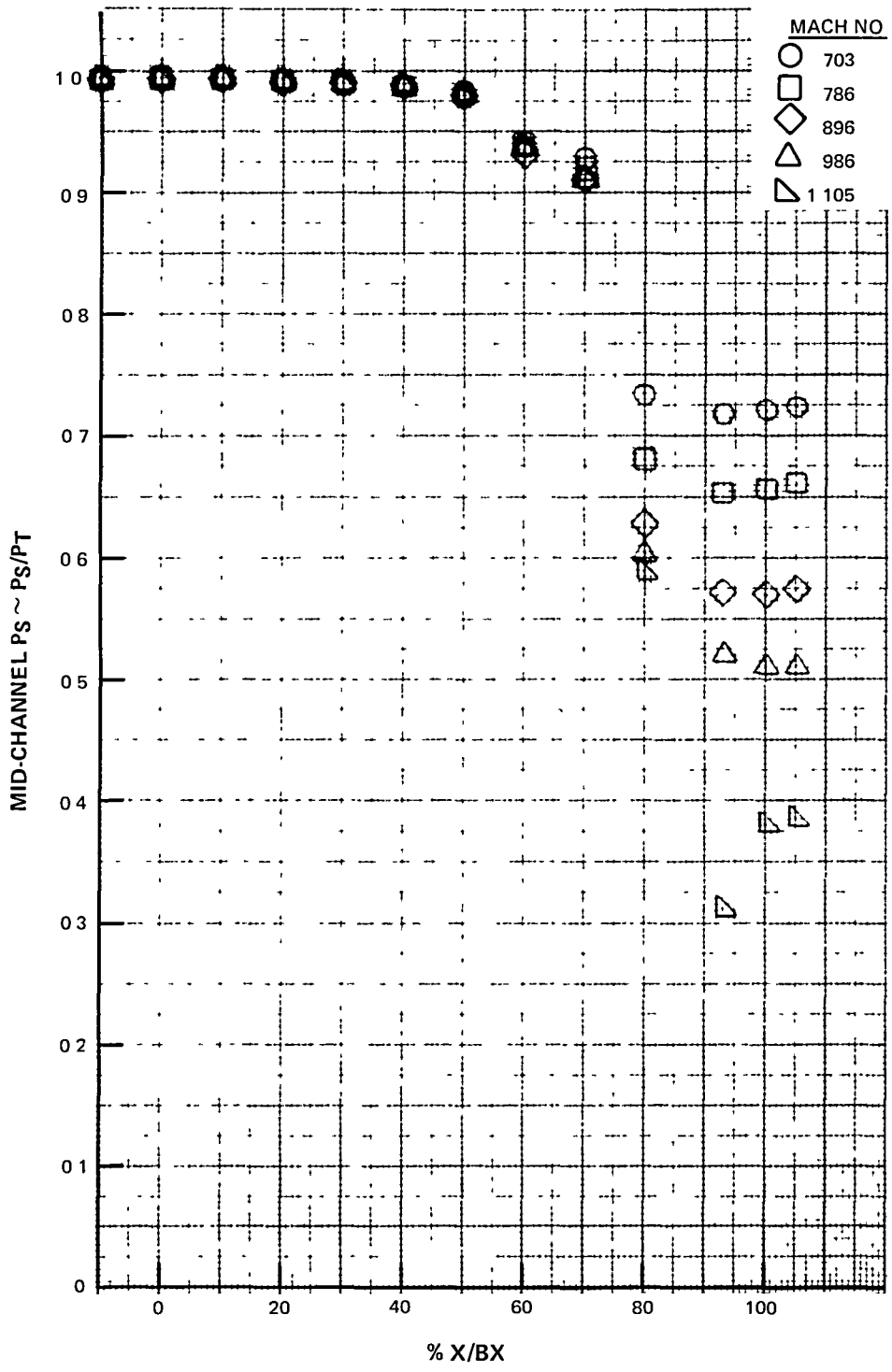

C-17 EEE Uncooled Rig 43% Reaction Annular Cascade Mid-Channel Statics - O.D. (Area Averaged)

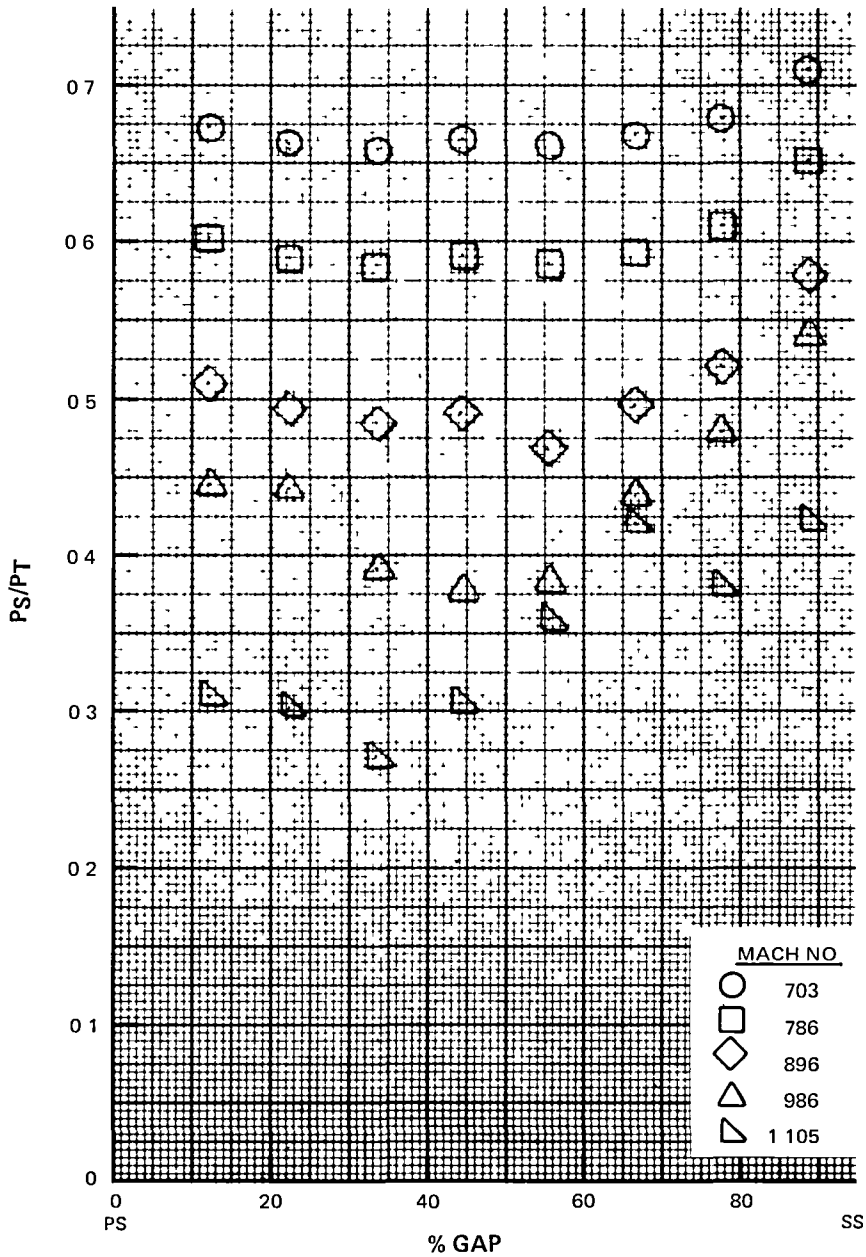

C-18 EEE Uncooled Rig 43% Reaction Annular Cascade T.E. Platform Statics - I.D. (Area Averaged)

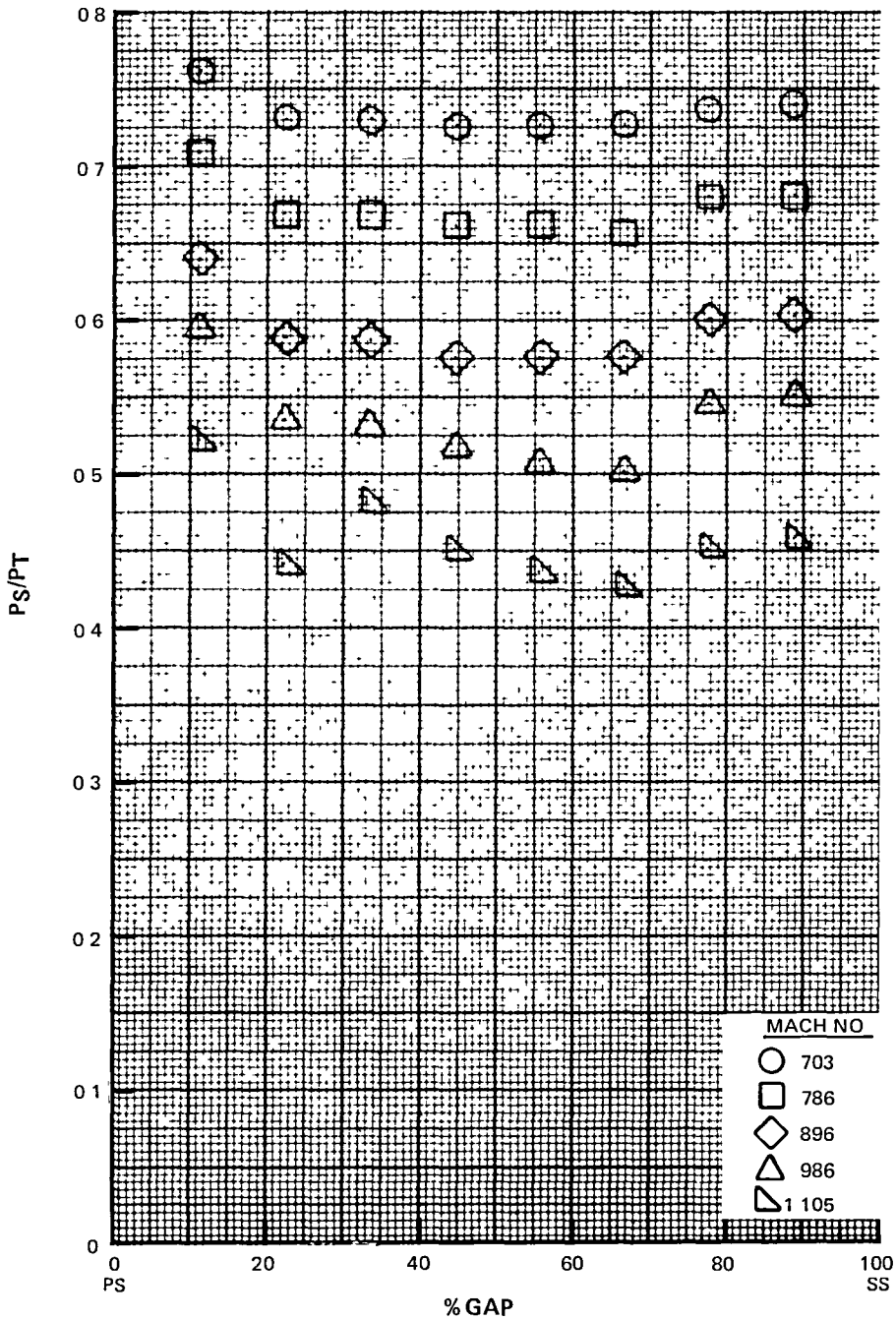

C-19 EEE Uncooled Rig 43% Reaction Annular Cascade T.E. Platform Statics - O.D. (Area Averaged)

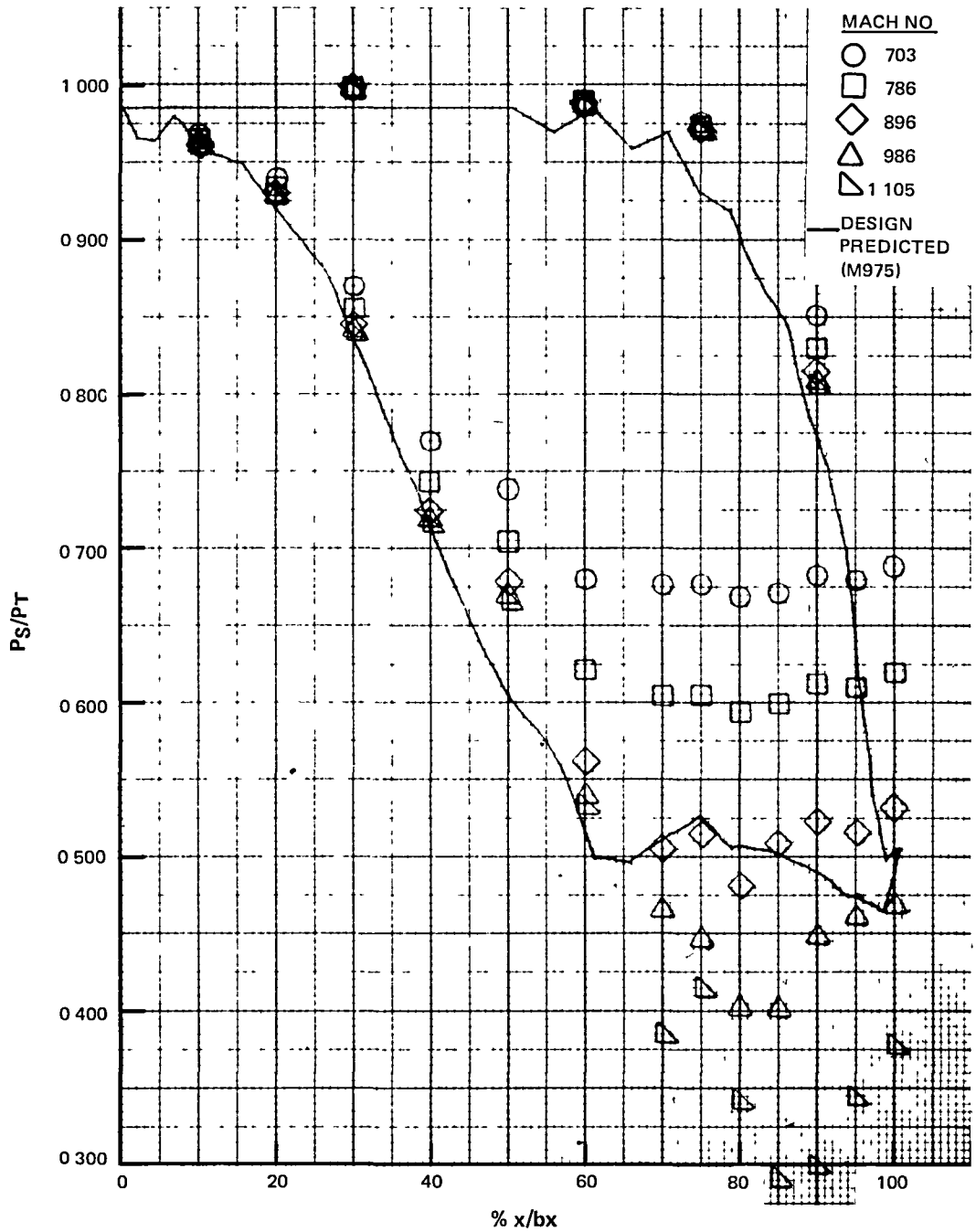

C-20 EEE Uncooled Rig 43% Reaction Annular Cascade Airfoil Surface Statics 11% Span (Area Averaged)

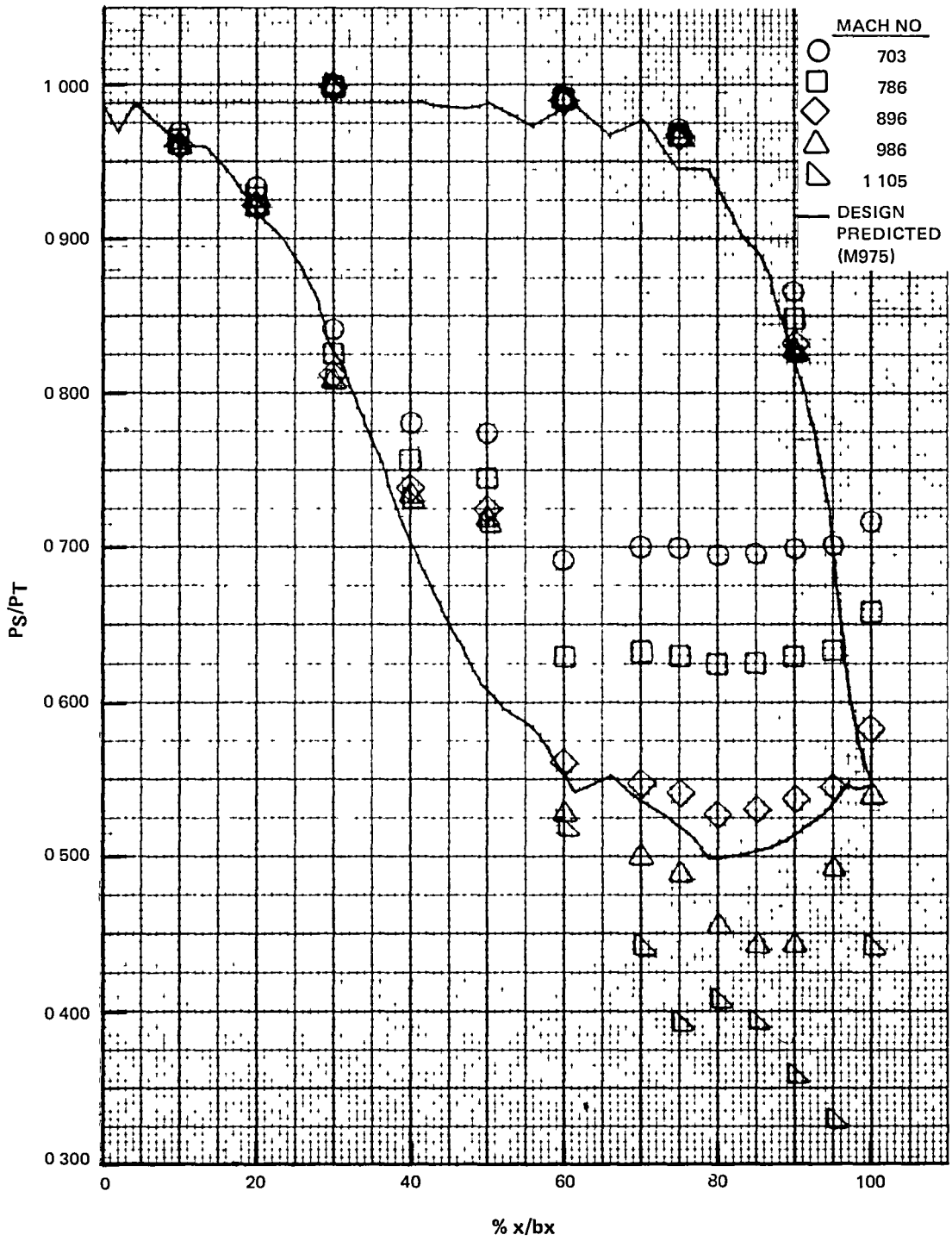

C-21 EEE Uncooled Rig 43% Reaction Annular Cascade Airfoil Surface Statics 50% Span (Area Averaged)

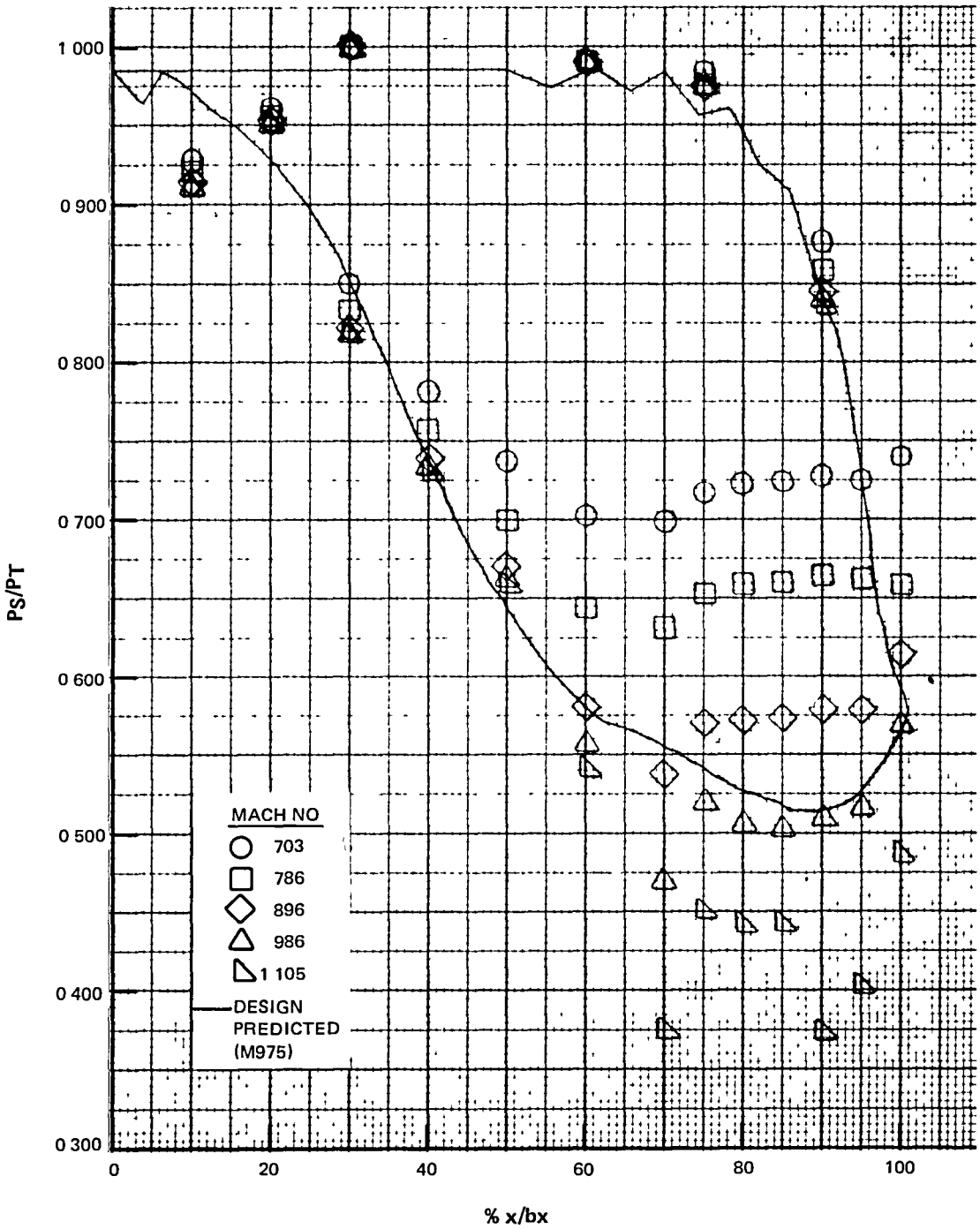

C-22 EEE Uncooled Rig 43% Reaction Annular Cascade Airfoil Surface Statics 89% Span (Area Averaged)

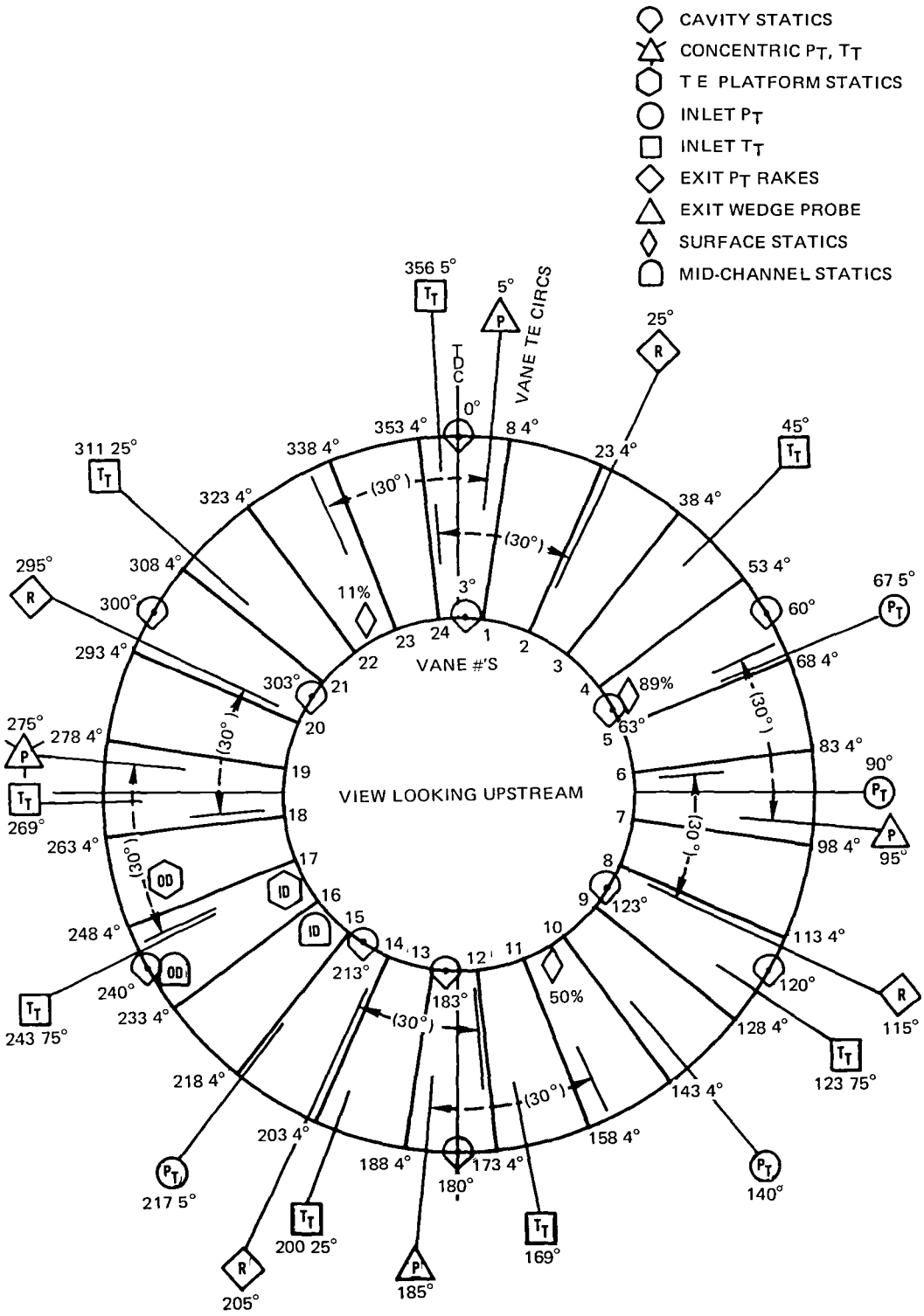

C-23 EEE Uncooled Rig 43% Reaction Annular Cascade Circumferential Instrumentation Location

This Page Intentionally Left Blank

APPENDIX D - BUILD 3 ANNULAR CASCADE DATA

TABLE D-1
DATA SUMMARY

EEE RIG-70709-3
ANNULAR CASCADE DATA SUMMARY

*DESIGN POINT

OPERATING POINT #	STEADY STEADY SCAN #	STEADY STATE DATASET NAME	STEADY STATE JULIAN DAY	STEADY STATE TIME	TRAVERSE SCAN #	TRAVERSE DATASET NAME	PT-IN PSIA	TT-IN °R
			1979	HR:MIN				
1	566	200757010V	65	07:46	568-596	270757012V	57.51	777.4
2	967	200836410V	65	23:07	969-997	270836412V	57.47	784.3
3*	53	200985610V	59	07:07	3- 31	270985612V	57.37	773.2
4	121	201064910V	61	06:04	123-151	271064912V	57.47	787.2
5	900	201204110V	65	20:19	902-930	271204112V	57.42	792.3

OP'TG POINT	W-MAIN LBM/S	RAKE AREA W'TED MACH #	RAKE AREA W'TED TOTAL PT/PT	RAKE MID-SPAN PT/PT	PROBE AREA W'TED MACH #	PROBE AREA W'TED TOTAL PT/PT	PROBE MID-SPAN PT/PT
1	23.29	0.710	0.0303	0.0135	0.712	0.0284	0.0127
2	24.08	0.793	0.0368	0.0167			
*3	24.94	0.914	0.0487	0.0203	0.911	0.0496	0.0177
4	24.96	1.001	0.0623	0.0242	1.003	0.0588	0.0213
5	24.93	1.133	0.0744	0.0352			

This Page Intentionally Left Blank

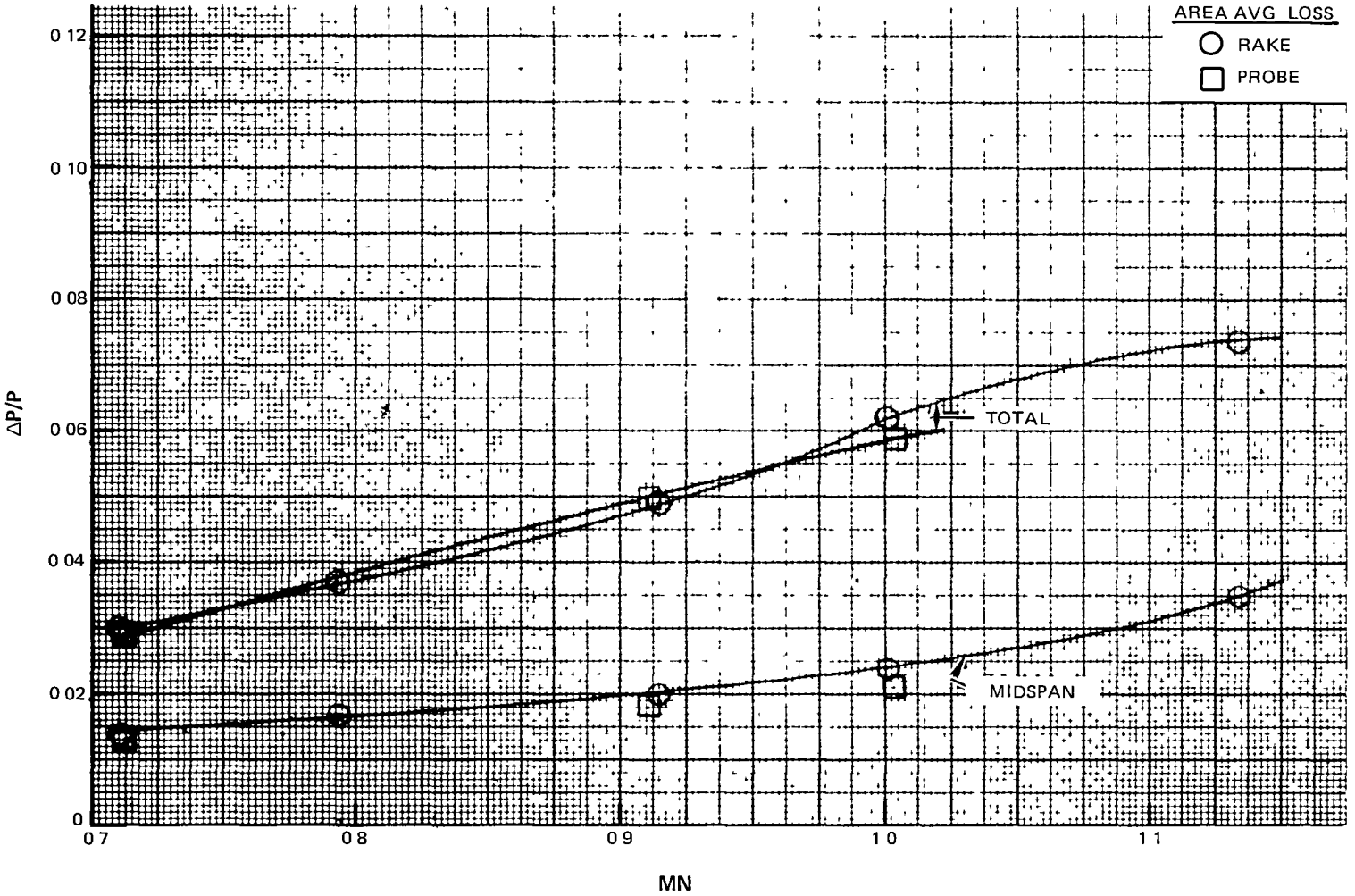

D-1 EEE Uncooled Rig Build 1 Canted Vane Annular Cascade Loss vs. Mach Number (Area Averaged)

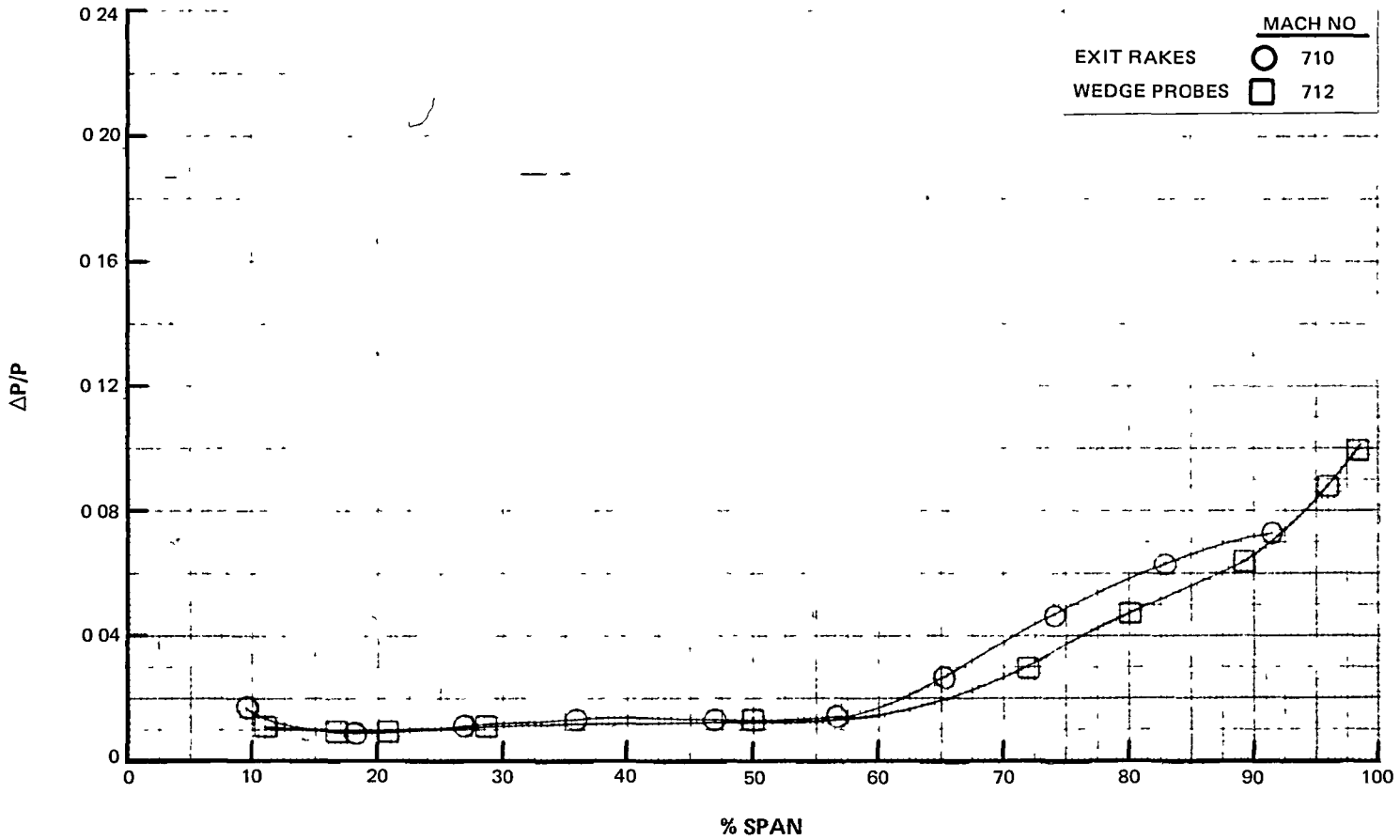

D-2 EEE Uncooled Rig Build 1 Canted Vane Annular Cascade Loss vs. % Span (Area Averaged)

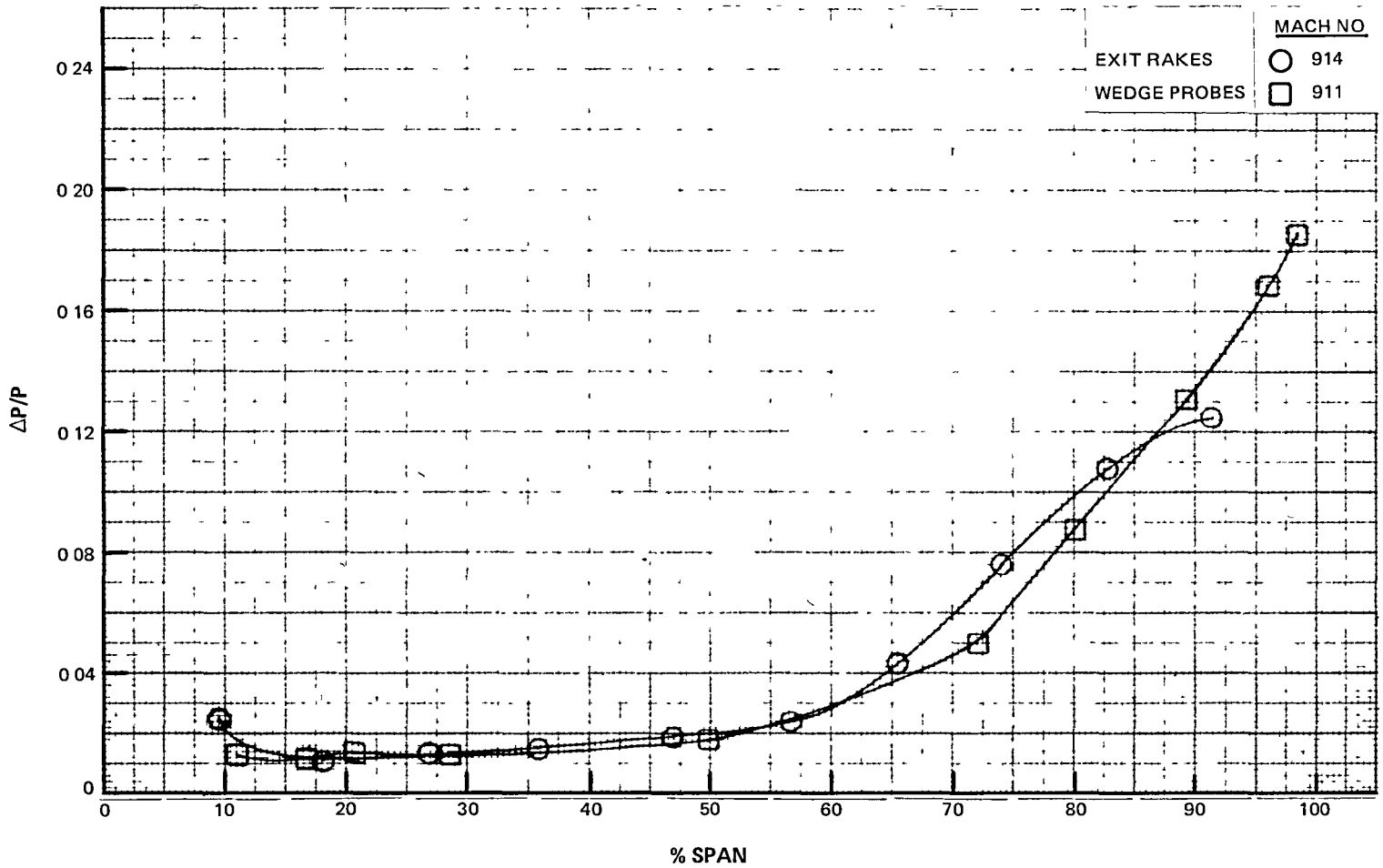

D-3 EEE Uncooled Rig Build 1 Canted Vane Annular Cascade Loss vs. % Span (Area Averaged)

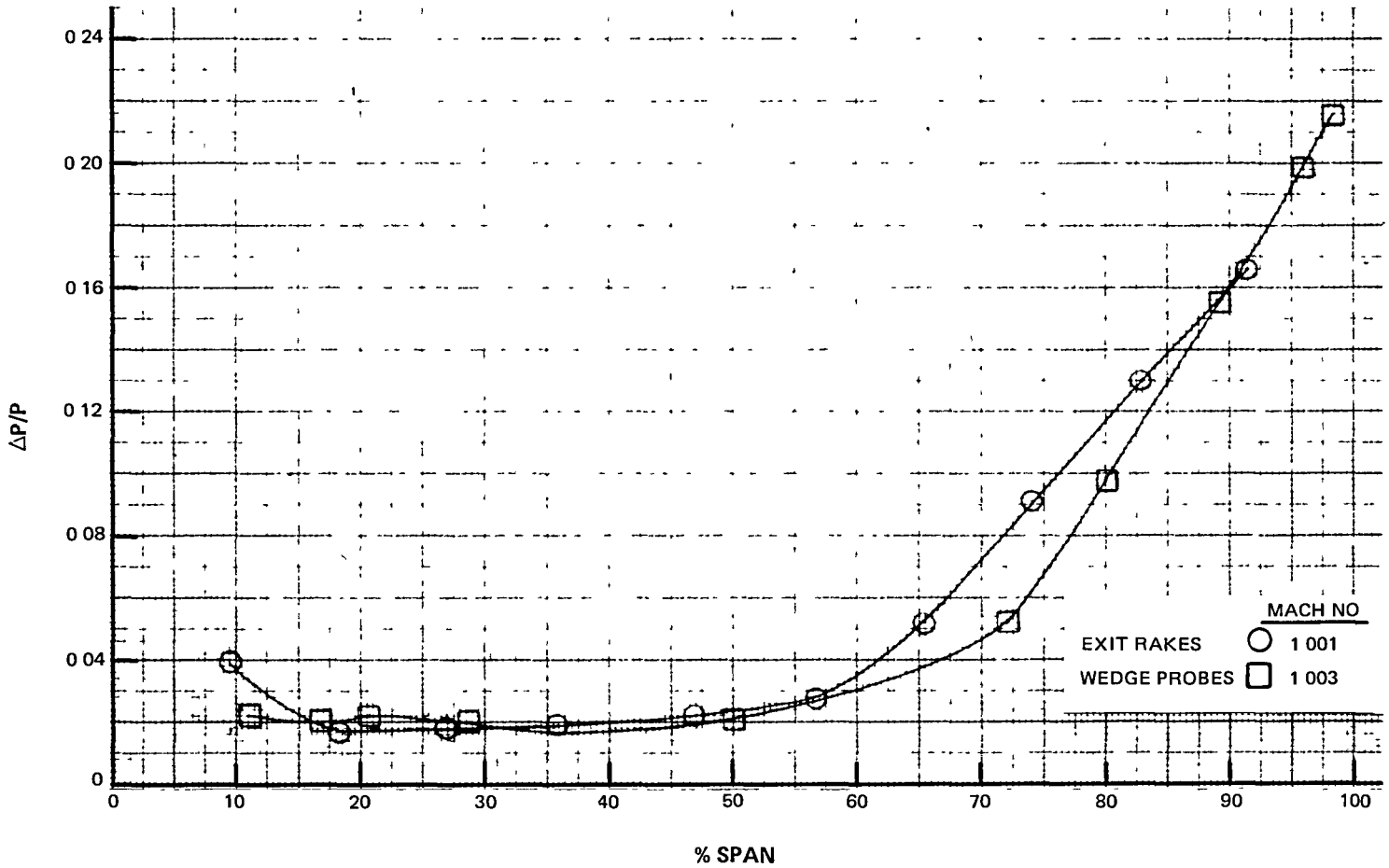

D-4 EEE Uncooled Rig Build 1 Canted Vane Annular Cascade Loss vs. % Span (Area Averaged)

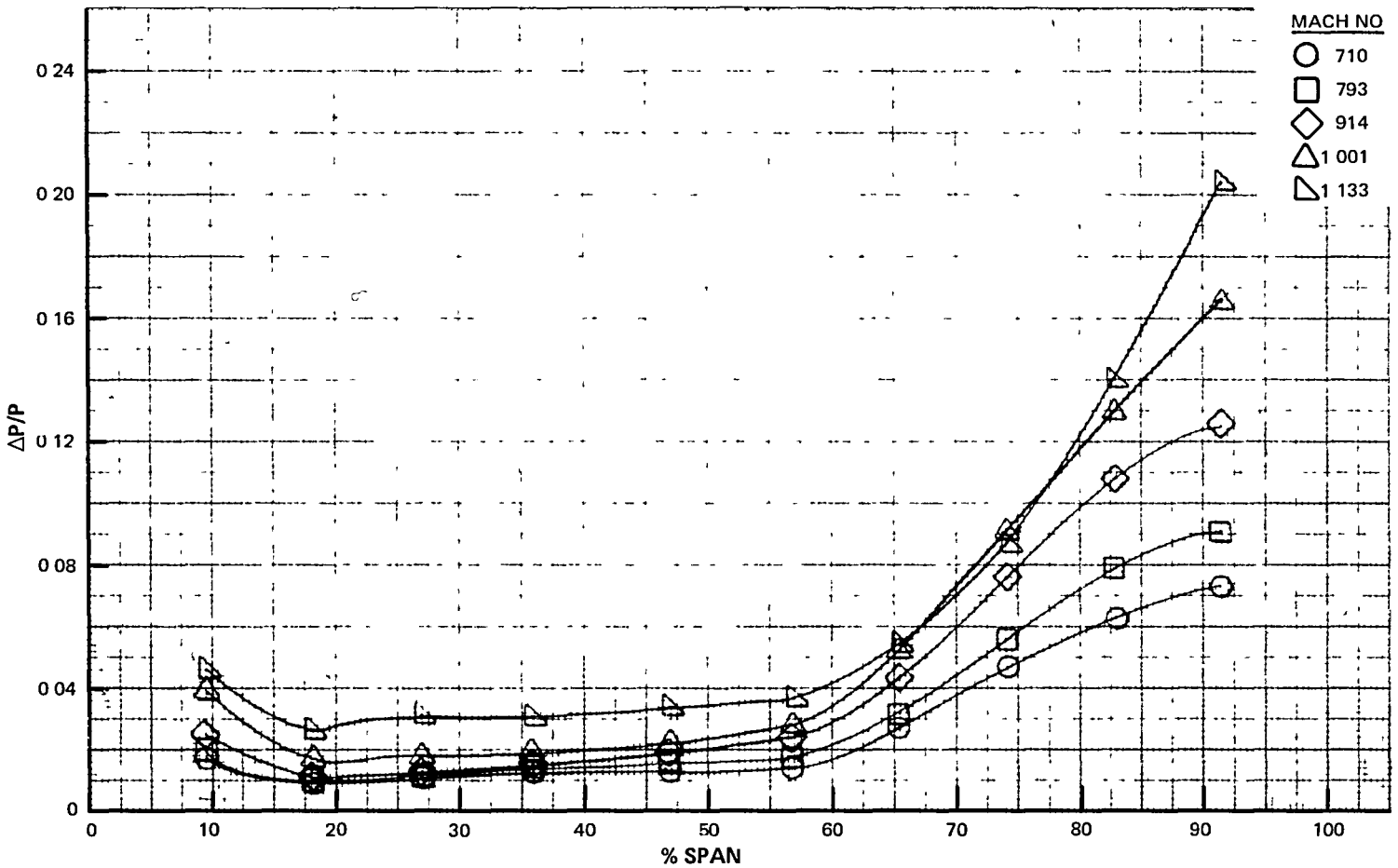

D-5 EEE Uncooled Rig Build 1 Canted Vane Annular Cascade Loss vs. % Span (Area Averaged)

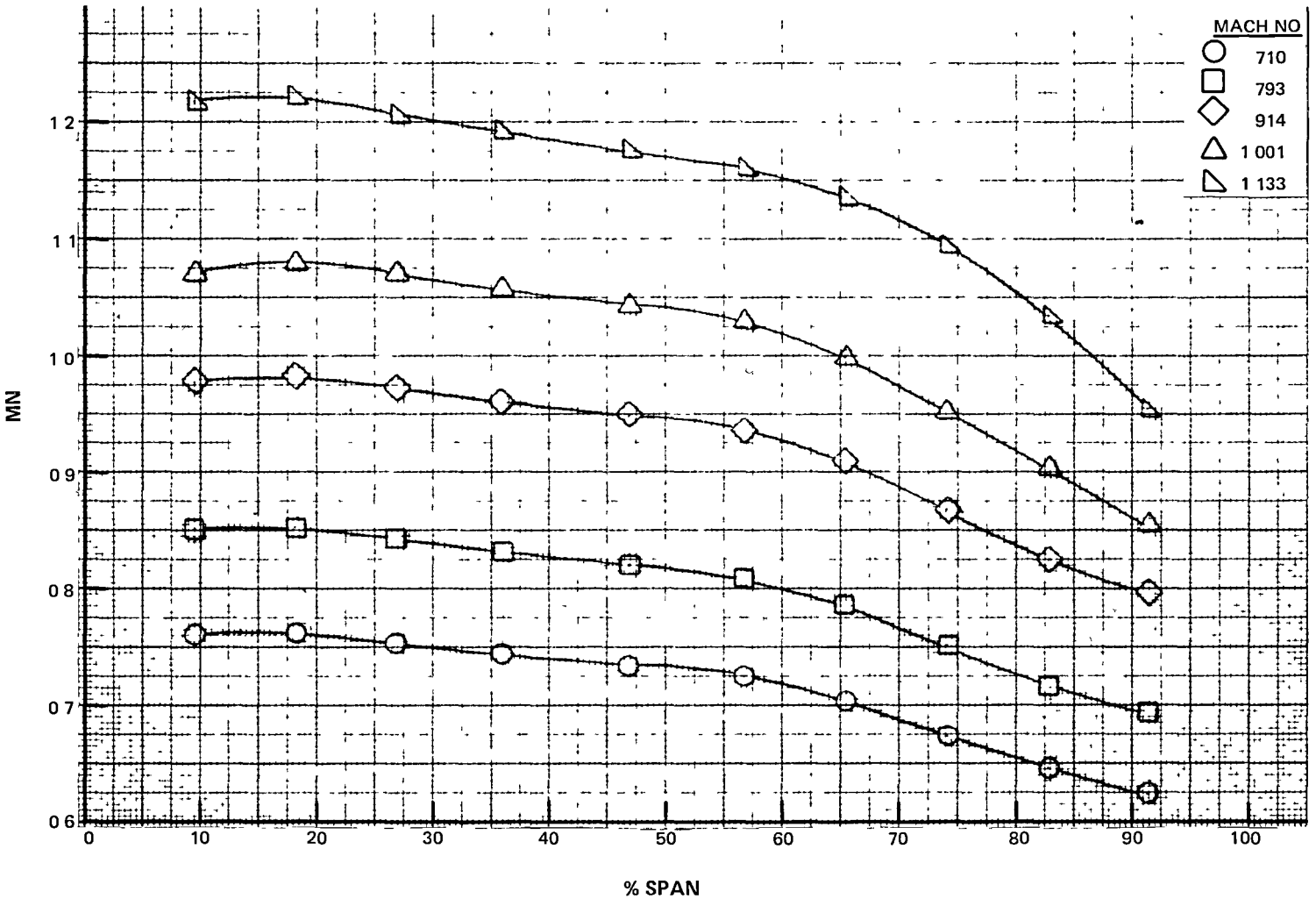

D-6 EEE Uncooled Rig Build 1 Canted Vane Annular Cascade Mach Number vs. % Span (Area Averaged)

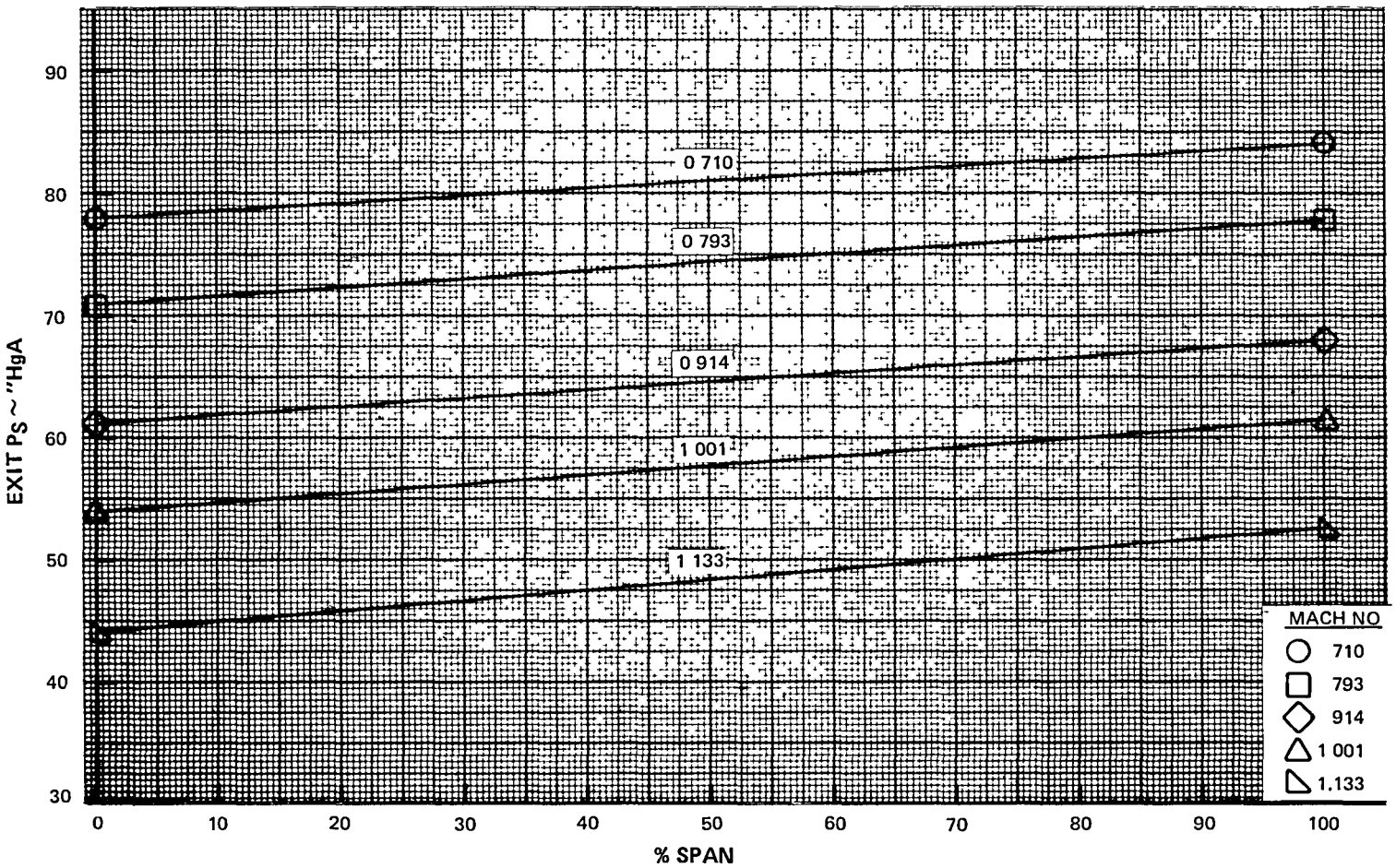

D-7 EEE Uncooled Rig Build 1 Canted Vane Annular Cascade Exit Ps vs. % Span (Area Averaged)

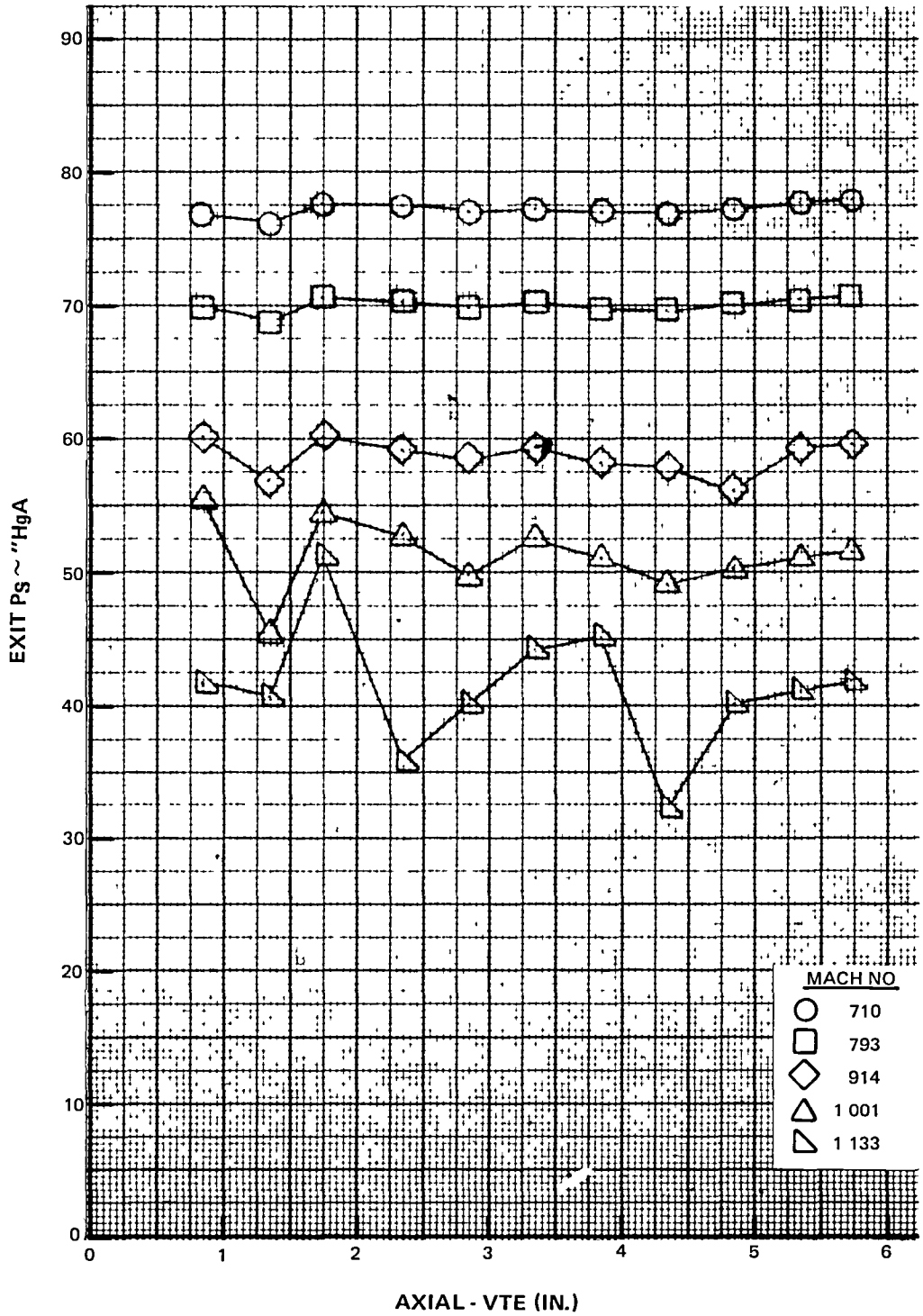

D-8 EEE Uncooled Rig Build 1 Canted Vane Annular Cascade Exhaust Case I.D. Static Pressures (Area Averaged)

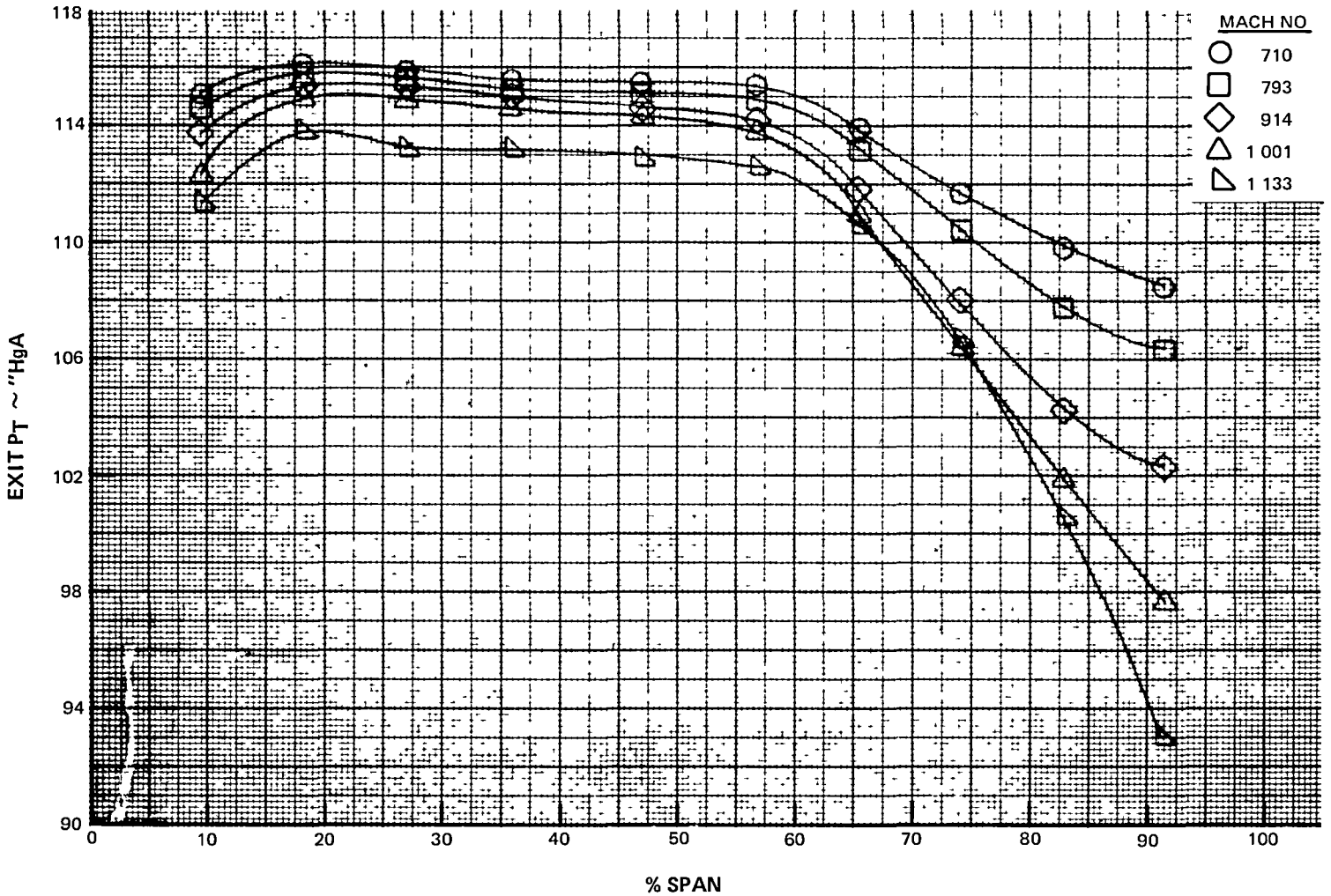

D-9 EEE Uncooled Rig Build 1 Canted Vane Annular Cascade Exit Pt vs. % Span (Area Averaged)

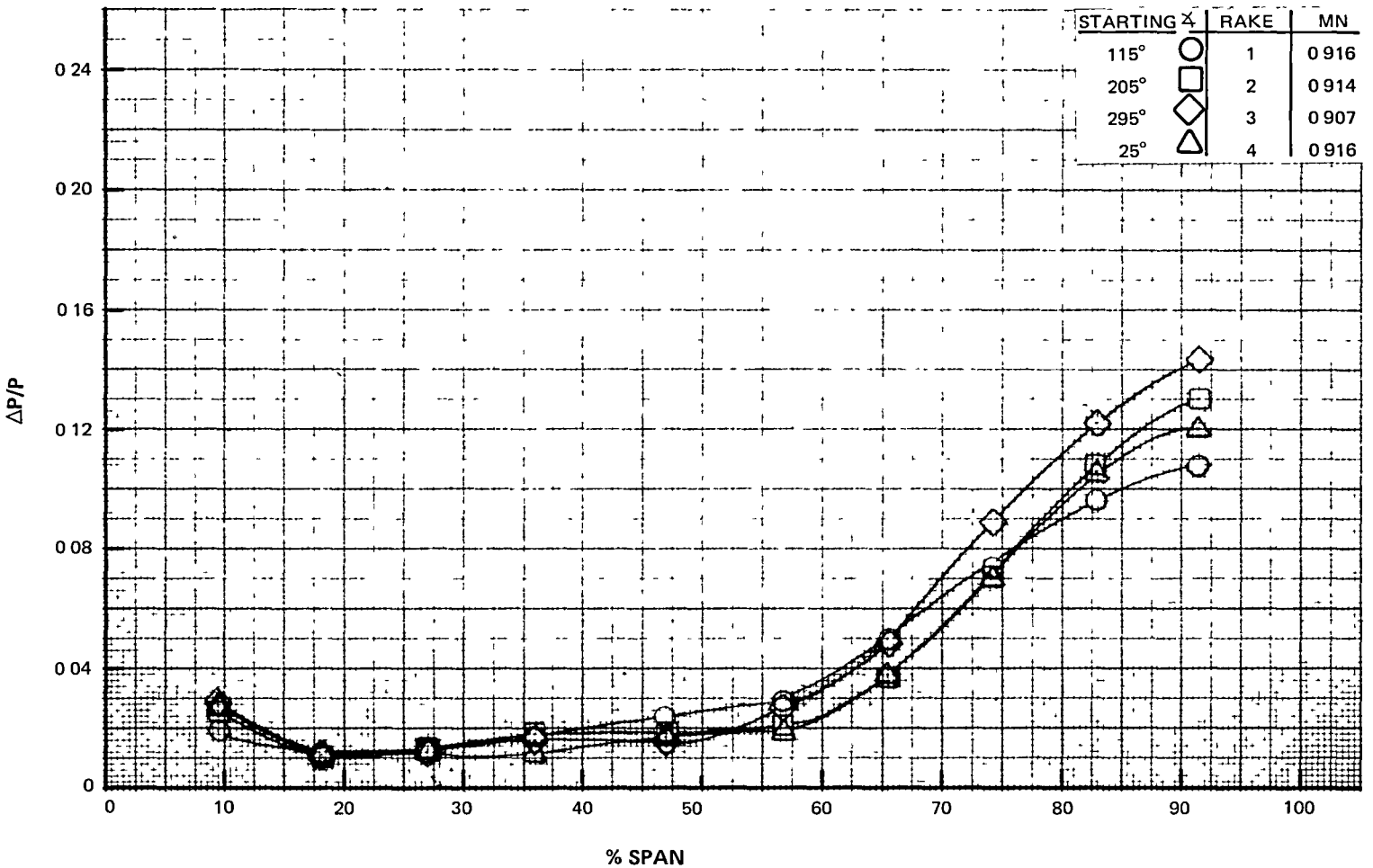

D-10 EEE Uncooled Rig Build 1 Canted Vane Annular Cascade Design Point (Area Averaged)

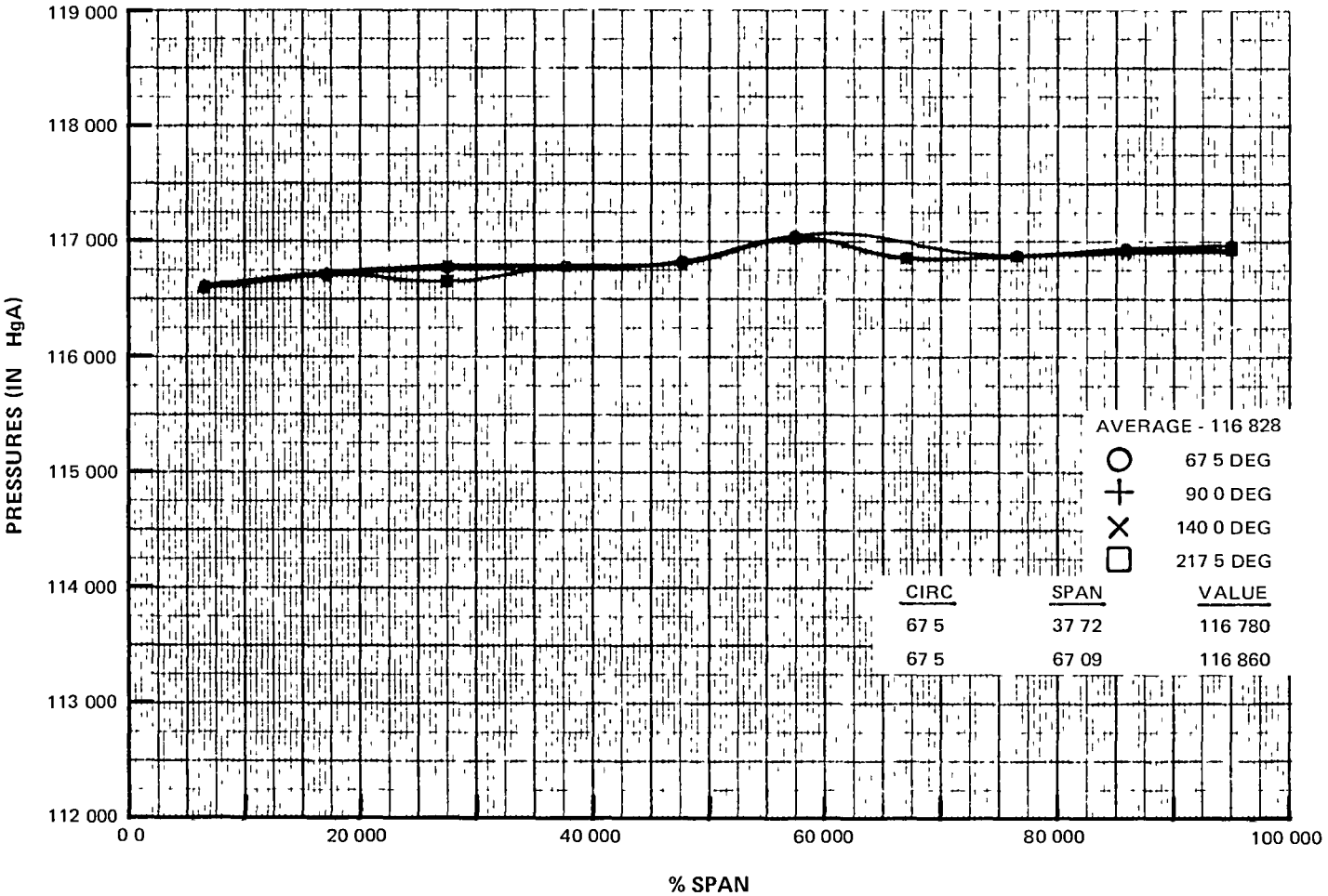

D-11 EEE Uncooled Rig Build 1 Canted Vane Annular Cascade Design Point Inlet Total Pressure

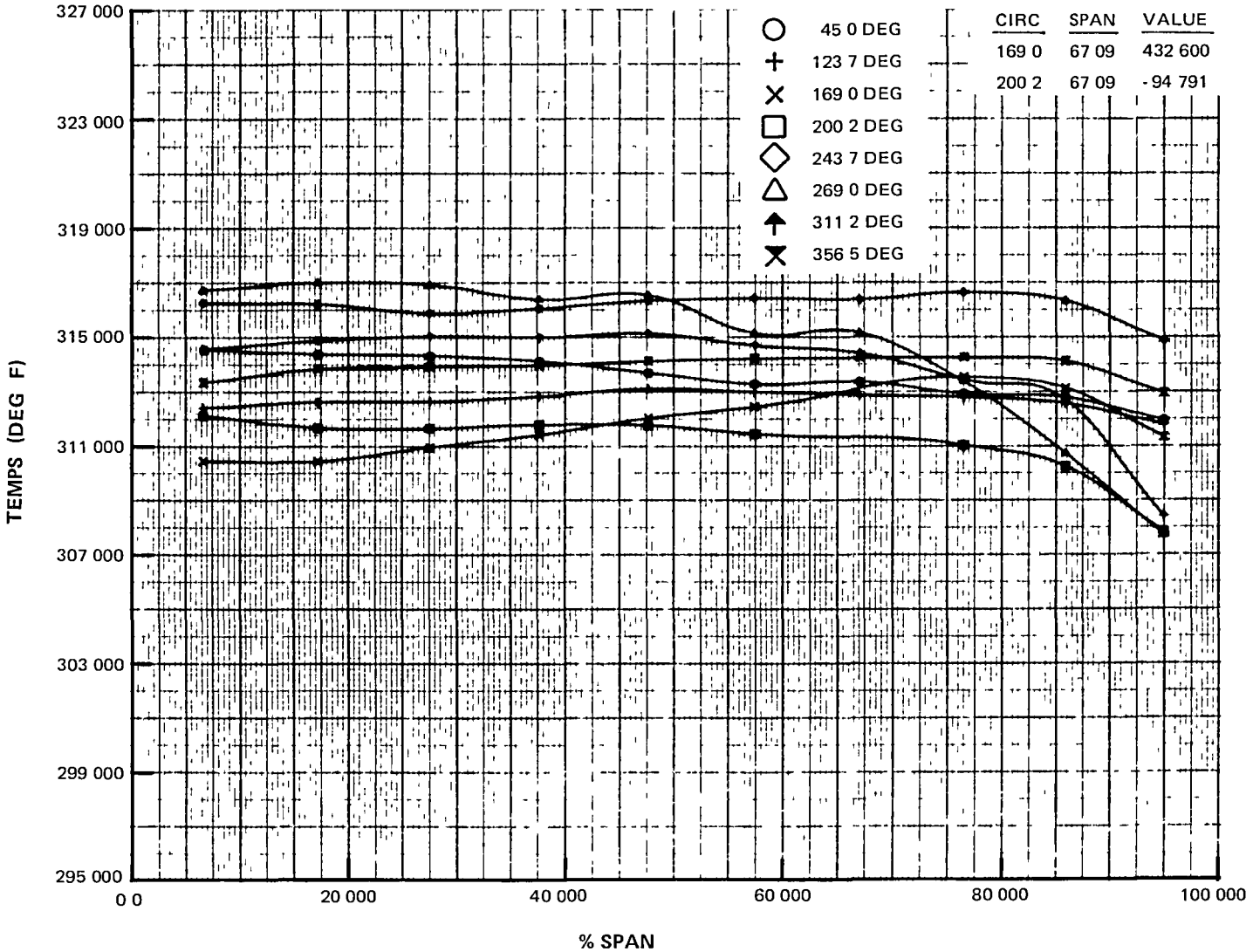

D-12 EEE Uncooled Rig Build 1 Canted Vane Annular Cascade Design Point Inlet Temperature

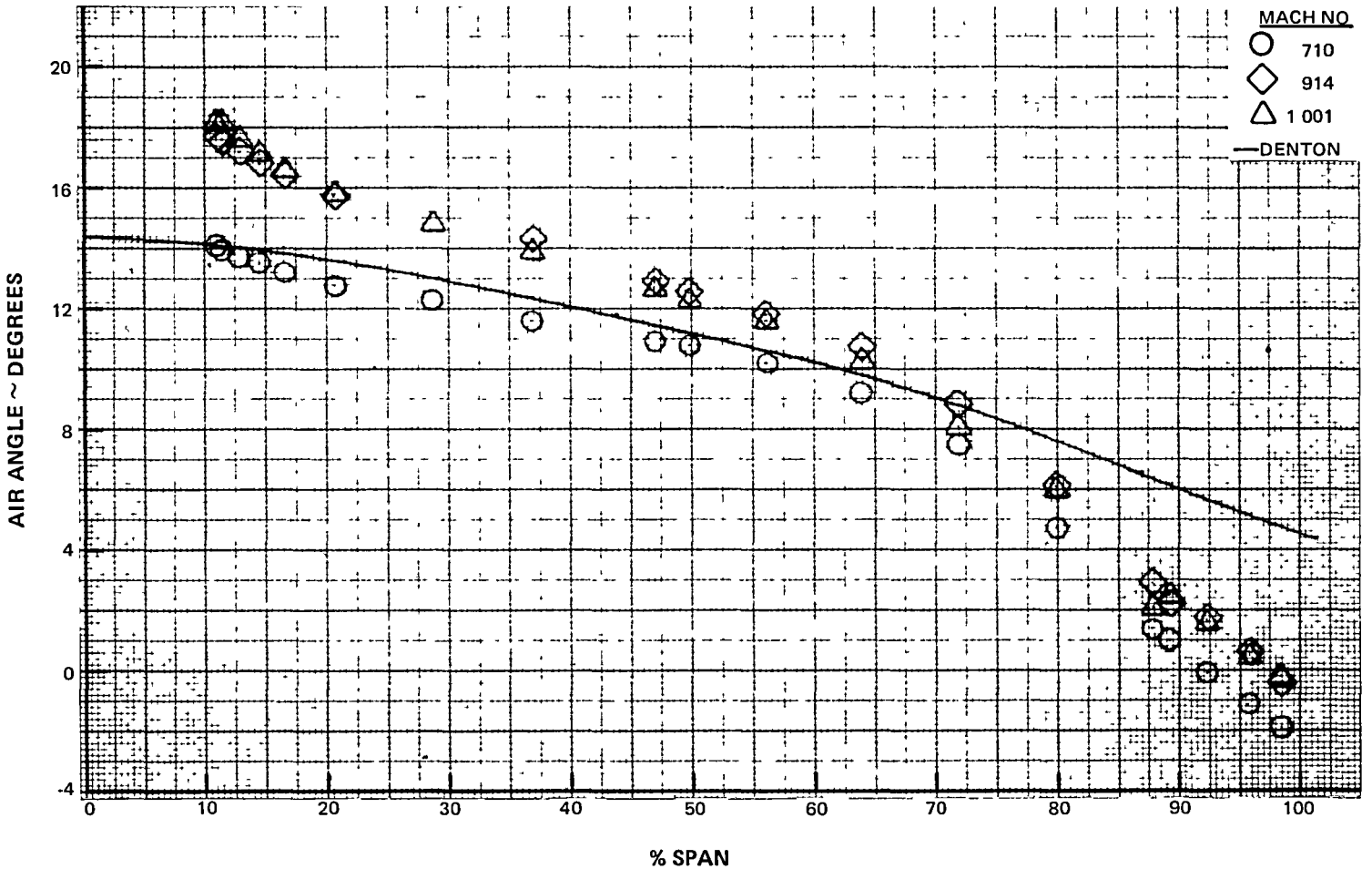

D-13 EEE Uncooled Rig Build 1 Canted Vane Annular Cascade Average Air Angle vs. % Span (Area Averaged)

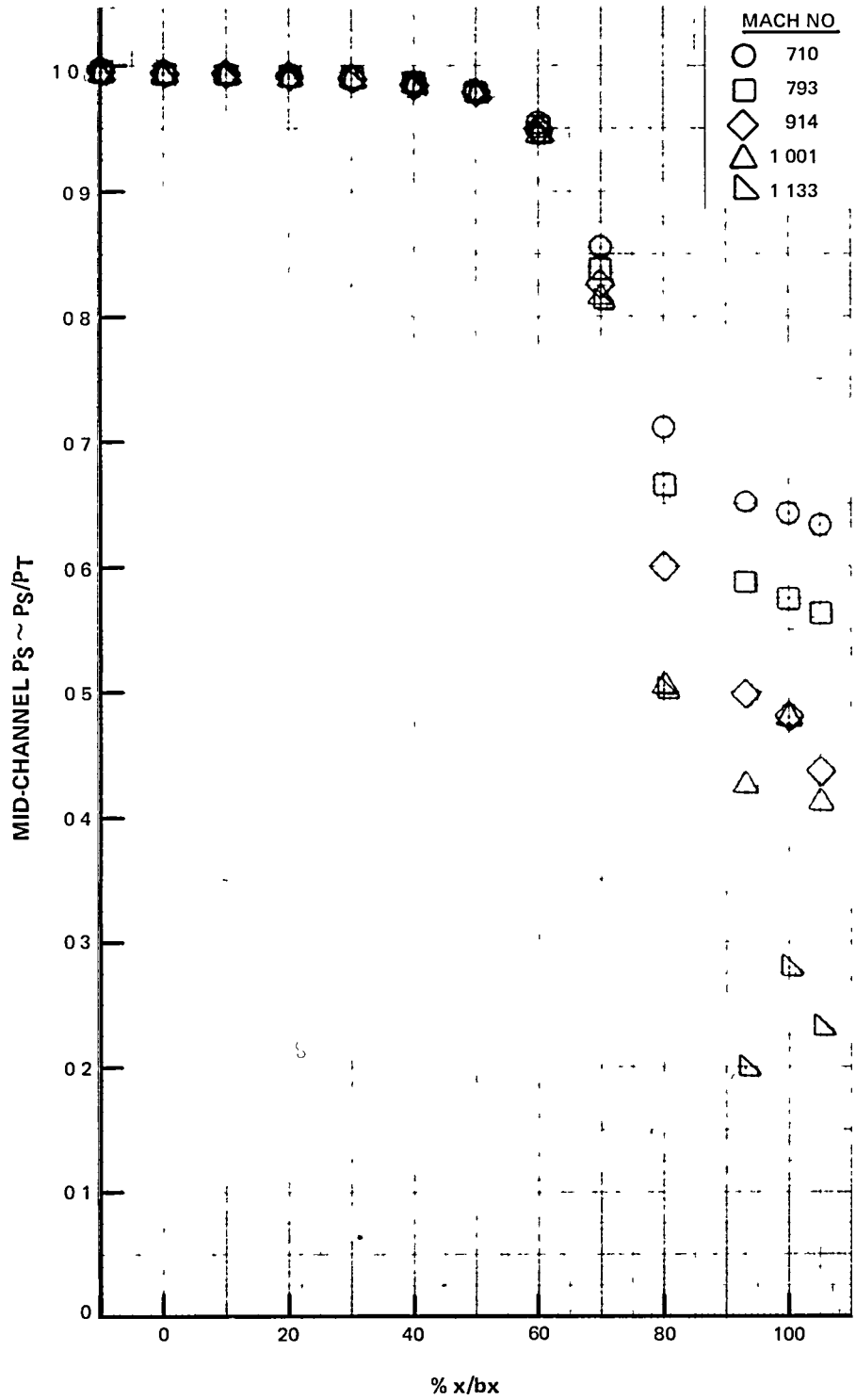

D-14 EEE Uncooled Rig Build 1 Canted Vane Annular Cascade Mid-Channel Statics - I.D. (Area Averaged)

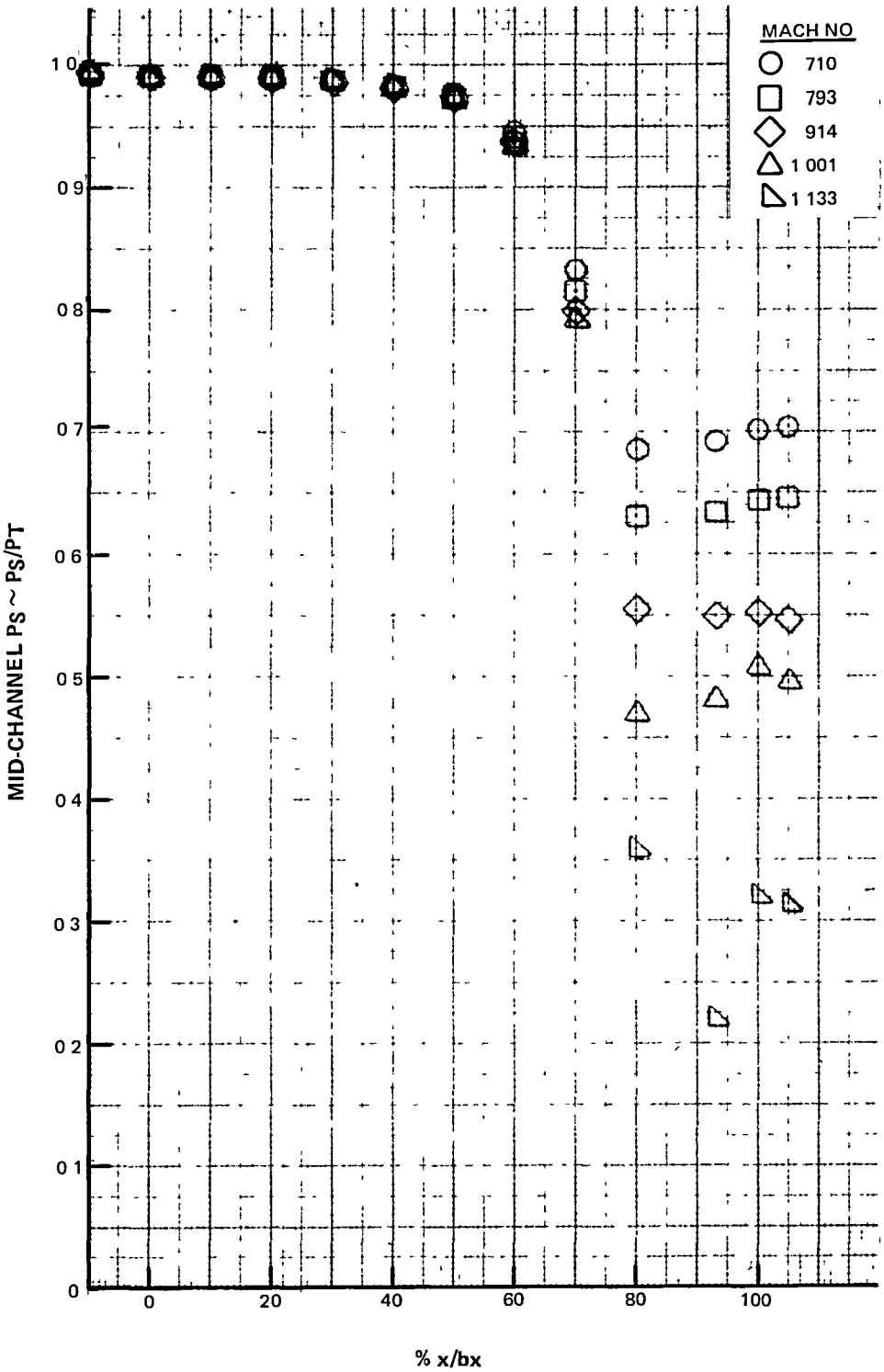

D-15 EEE Uncooled Rig Build 1 Canted Vane Annular Cascade Mid-Channel Statics - O.D. (Area Averaged)

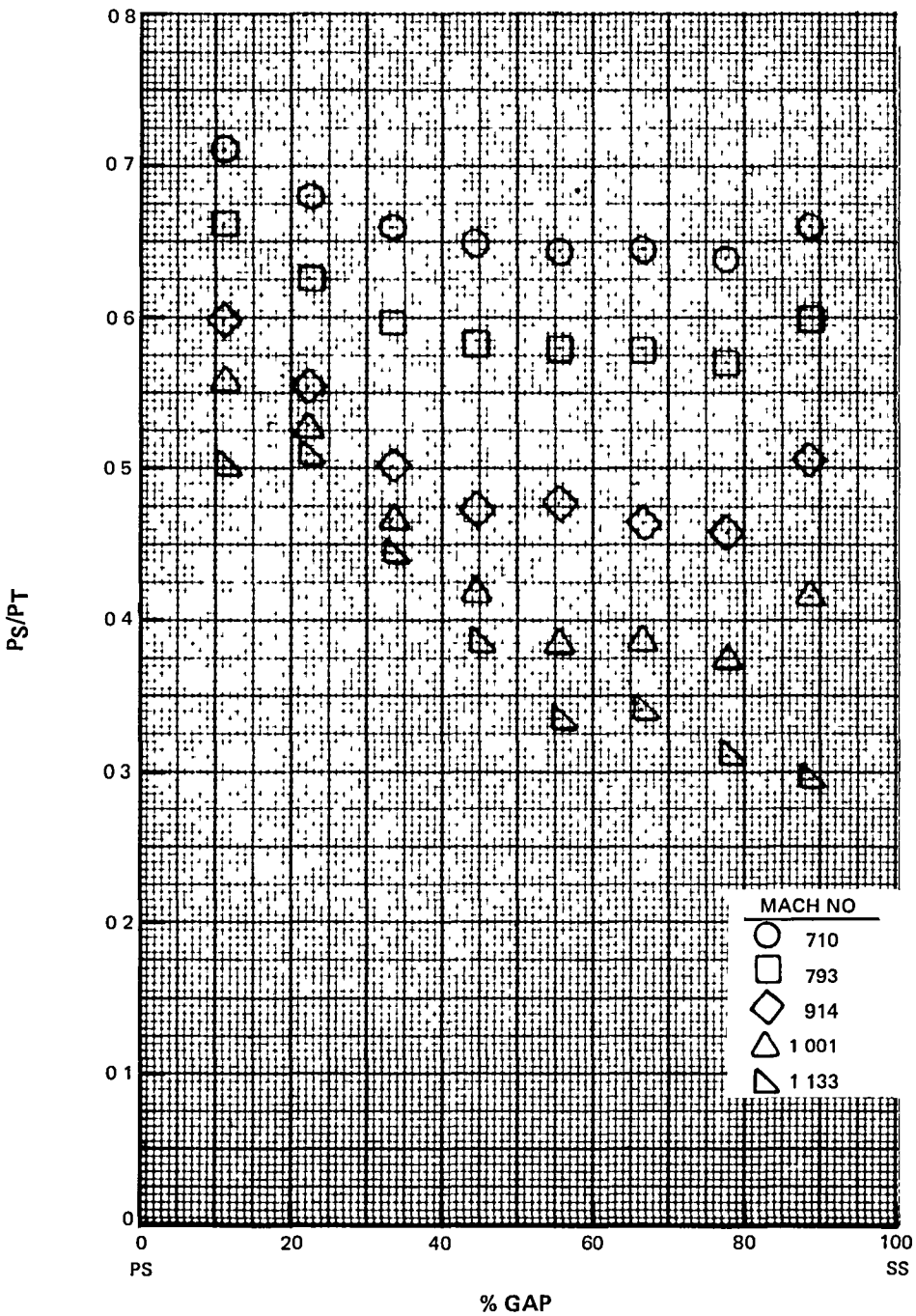

D-16 EEE Uncooled Rig Build 1 Canted Vane Annular Cascade T.E. Platform Statics - I.D. (Area Averaged)

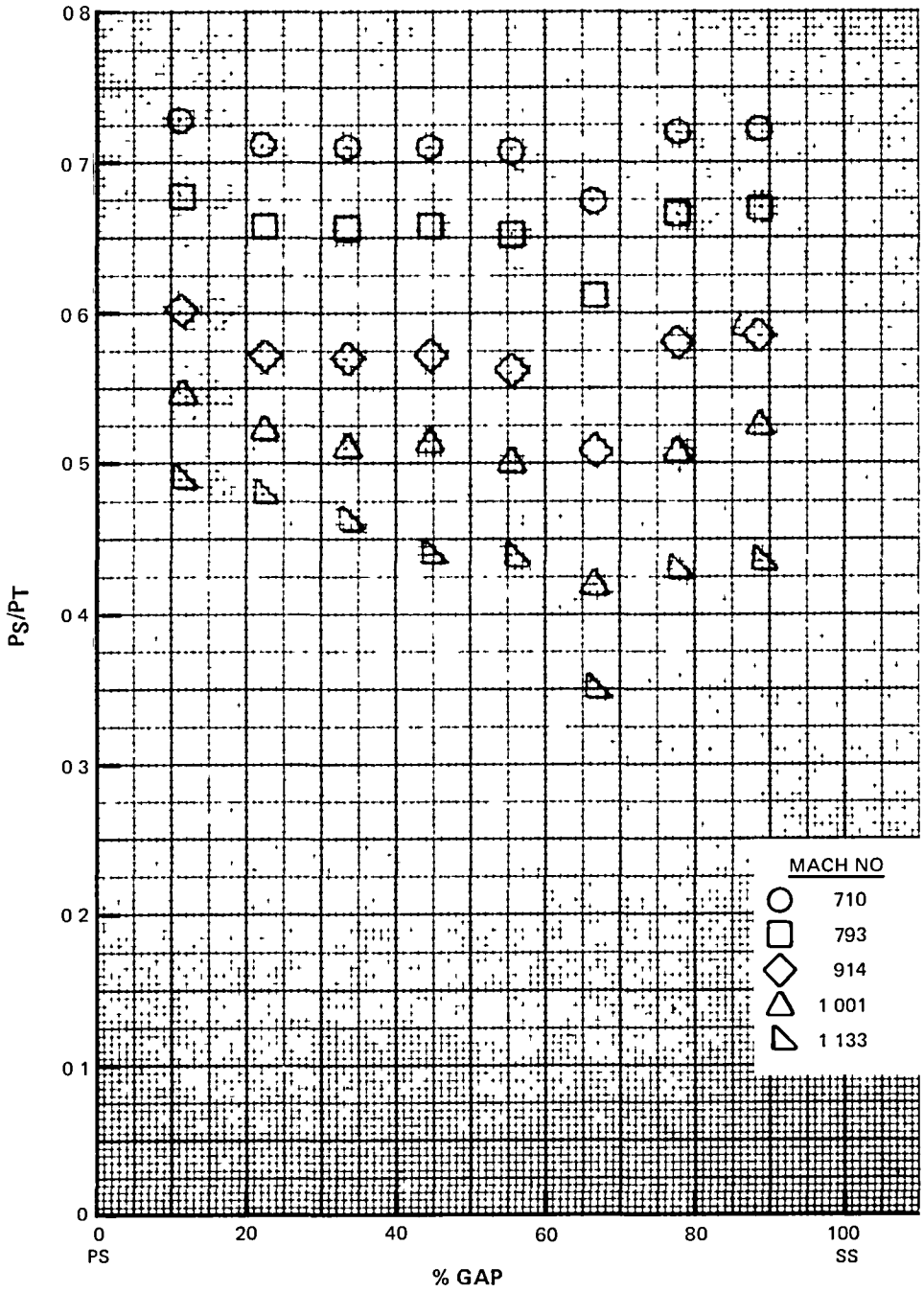

D-17 EEE Uncooled Rig Build 1 Canted Vane Annular Cascade T.E. Platform Statics - O.D. (Area Averaged)

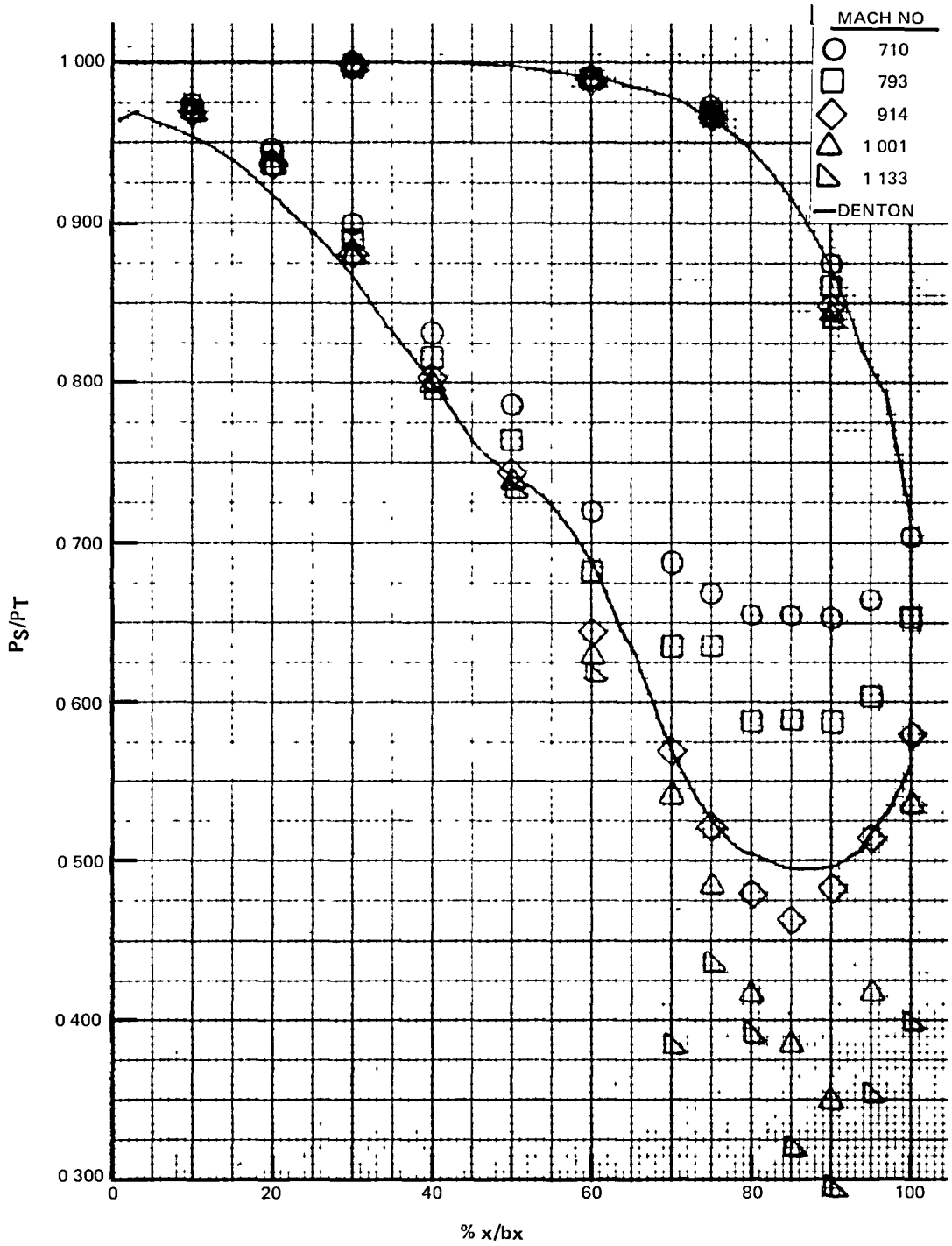

D-18 EEE Uncooled Rig Build 1 Canted Vane Annular Cascade Airfoil Surface Statics 11% Span (Area Averaged)

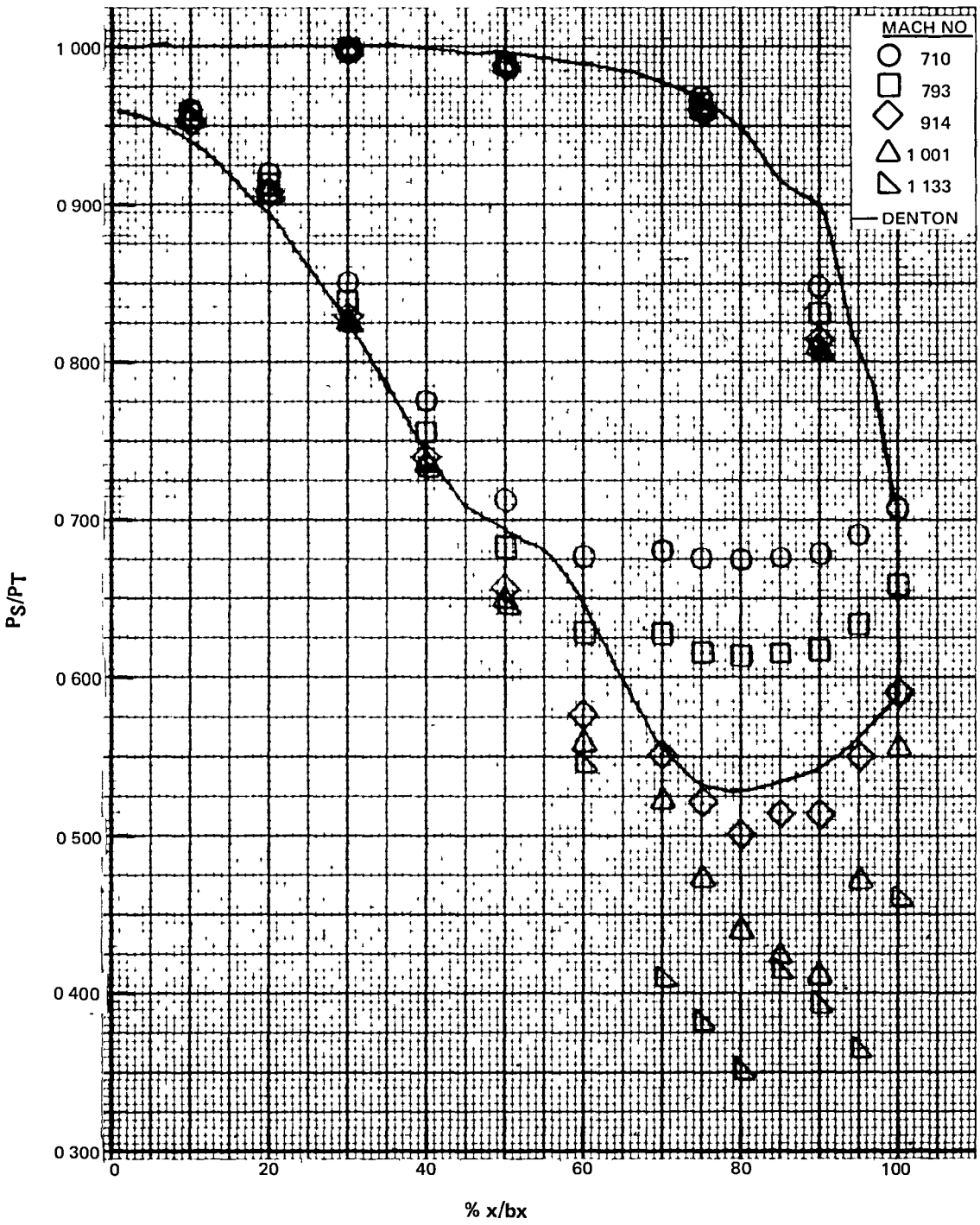

D-19 EEE Uncooled Rig Build 1 Canted Vane Annular Cascade Airfoil Surface Statics 50% Span (Area Averaged)

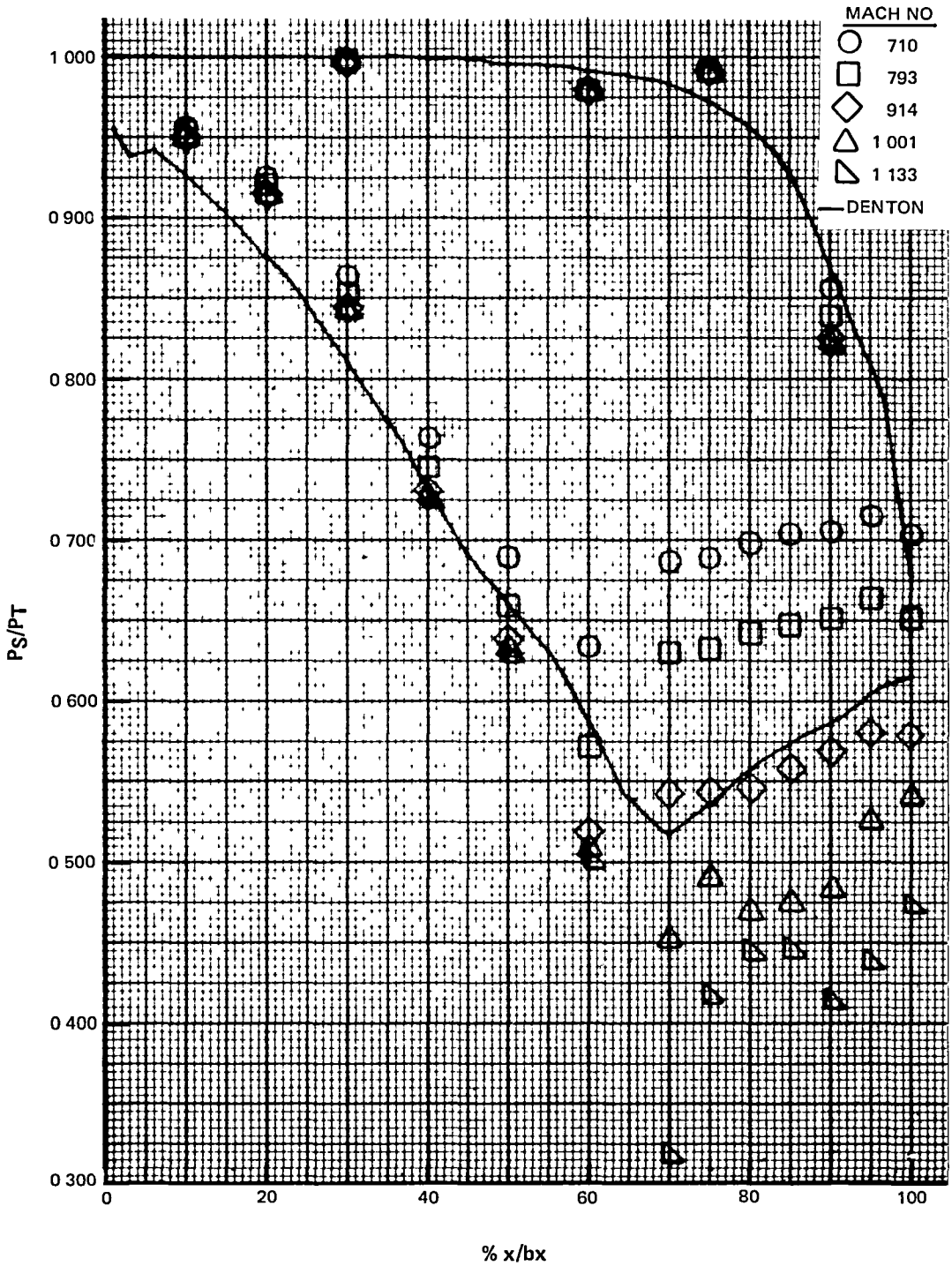

D-20 EEE Uncooled Rig Build 1 Canted Vane Annular Cascade Airfoil Surface Statics 89% Span (Area Averaged)

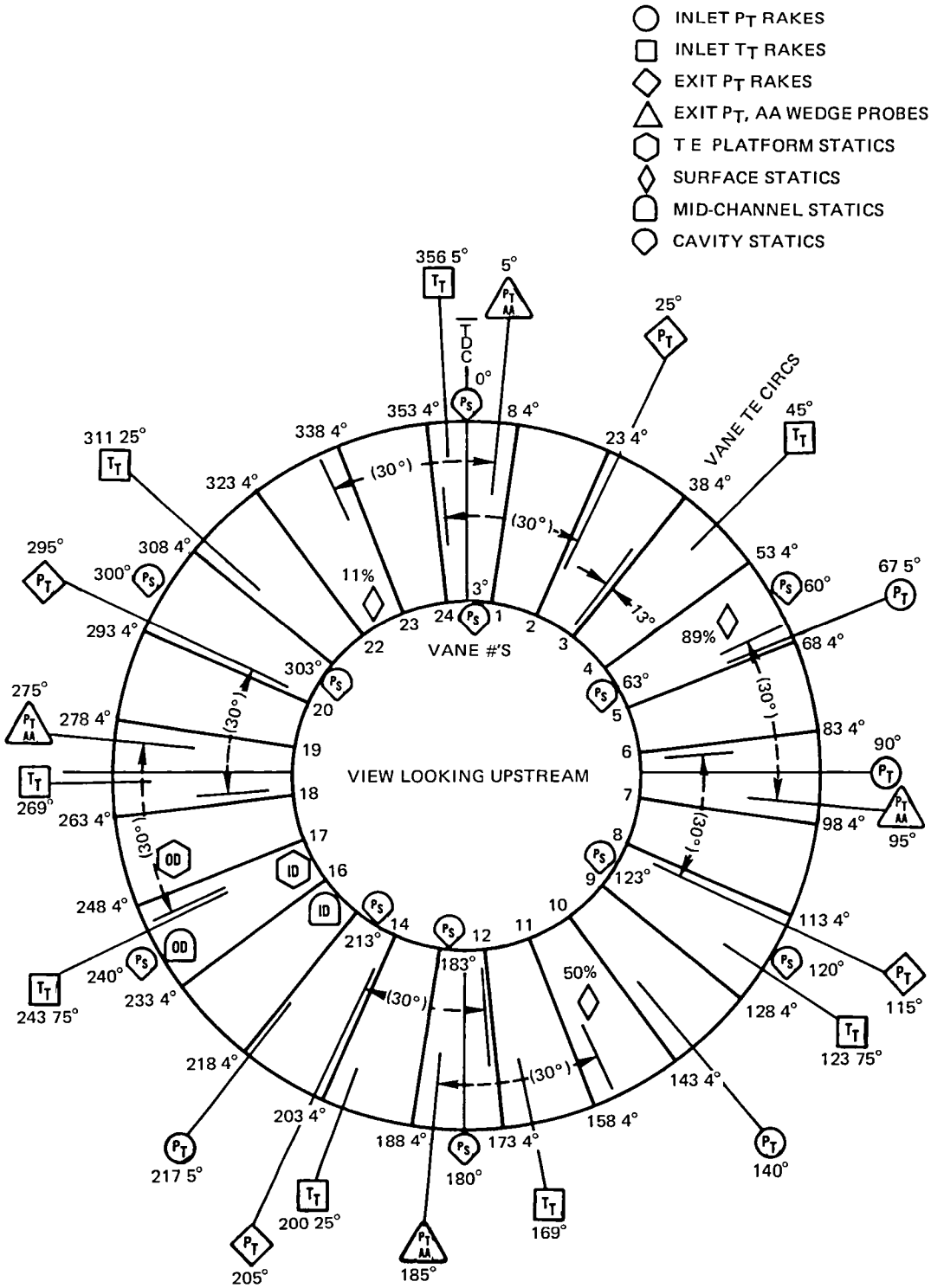

D-21 EEE Uncooled Rig Build 1 Canted Vane Annular Cascade Circumferential Instrumentation Location

This Page Intentionally Left Blank

APPENDIX E - BUILD 1 ROTATING RIG DATA

E-16	EEE Uncooled Rig 36% Reaction Rotating Rig 50% Span Vane Surface Statics
E-17	EEE Uncooled Rig 36% Reaction Rotating Rig 89% Span Vane Surface Statics
E-18	EEE Uncooled Rig 36% Reaction Rotating Rig Mid Gap O.D. Statics vs. % x/bx
E-19	EEE Uncooled Rig 36% Reaction Rotating Rig Mid Gap O.D. Statics vs. % x/bx
E-20	EEE Uncooled Rig 36% Reaction Rotating Rig I.D. Platform Ps vs. % Gap
E-21	EEE Uncooled Rig 36% Reaction Rotating Rig O.D. Platform Ps vs. % Gap
E-22	EEE Uncooled Rig 36% Reaction Rotating Rig Vane Exit Cav vs. % Span
E-23	EEE Uncooled Rig 36% Reaction Rotating Rig Vane Blade Exit Cavity Static vs. % Span

TABLE E-1
DATA SUMMARY

EEE RIG-70709-1
ROTATING RIG
DATA SUMMARY

*DESIGN POINT

STEADY STATE SCAN N^2	STEADY STATE DATA SET NAME	STEADY STATE JULIAN DAY	STEADY STATE TIME	TRAVERSE SCAN N^2's		TRAVERSE DATA SET NAME	P_T IN PSIA	T_T IN ^{OR}	N RPM	W_{MAIN} LBM/ SEC	W_{COOL} LBM/SEC	% W_{COOL} W_{MAIN}	REAC-TION	VR MEAN	N/ T_{TIN}	PRES-SURE RATIO	AREA WGT'D	AVG. CLR INCHES	COR-RECT-ED AREA WGT'D
		1978	HR:MIN: SEC																
134	603503520	310	16.16·48	136	164	873503524N	57.43	769.93	9801.	23.45			0.2845	0.5959	353.2	3.531	90.40	0.0136	90.31
*101	603504120	293	12·40:16	313	341	873504124N	57.48	770.26	9737	23.45			0.3290	0.5631	350.8	4.184	90.19	0.0131	90.06
276	603504620	299	22:54·25	279	307	873504624N	57.31	778.44	9814	23.26			0.3606	0.5487	351.7	4.707	89.36	0.0131	89.23
419	603505020	300	6:41:45	421	449	873505024N	57.53	772.74	9709	23.43			0.3792	0.5371	349.3	5.179	88.17	0.0141	88.12
562	603505520	300	17:37:36	564	592	873505524N	57.37	782.02	7818	23.25			0.4000	0.5308	351.1	5.773	86.86	0.0141	86.81
* 24	603444120	307	8:09:49	26	54	873444124N	57.24	766.64	9819	23.40			0.3308	0.5656	354.6	4.178	90.15	0.0131	90.02
274	603414120	307	17·50·04	278	306	873414124N	57.39	775.83	9733	23.31	0.090	0.386		0.5623	349.4	4.208	89.77	0.0156	89.84
330	603424120	307	20:15·45	335	363	873424124N	57.37	772.03	9754	23.37	0.180	0.770		0.5642	351.1	4.209	89.60	0.0166	89.75
165	603434120	307	13:19:34	182	210	873434124N	57.45	775.96	9812	23.34	0.277	1.189		0.5675	352.2	2.239	88.93	0.0181	89.20
746	602804120	306	14:21·45	748	776	872804124N	57.31	772.54	7880	23.37			0.3412	0.4699	283.5	4.010	86.86	0.0191	87.21
888	602804620	306	20:28·48	890	918	872804624N	57.44	772.48	7779	23.42			0.3779	0.4530	279.9	4.514	85.24	0.191	85.59
316	603503020	311	0:28:43	318	346	873503024N	57.38	771.45	9804	23.38			0.2404	0.6317	352.9	2.959	91.20		
352	603502320	311	1:49:03	354	382	873502524N	57.57	771.24	9750	23.38			0.2167	0.6783	351.1	2.574	87.87	0.0116	87.63
388	602452920	311	3:59:39	390	418	872452920N	57.50	768.20	6873	23.50			0.2472	0.4704	248.0	2.919	81.19	0.0206	81.66

This Page Intentionally Left Blank

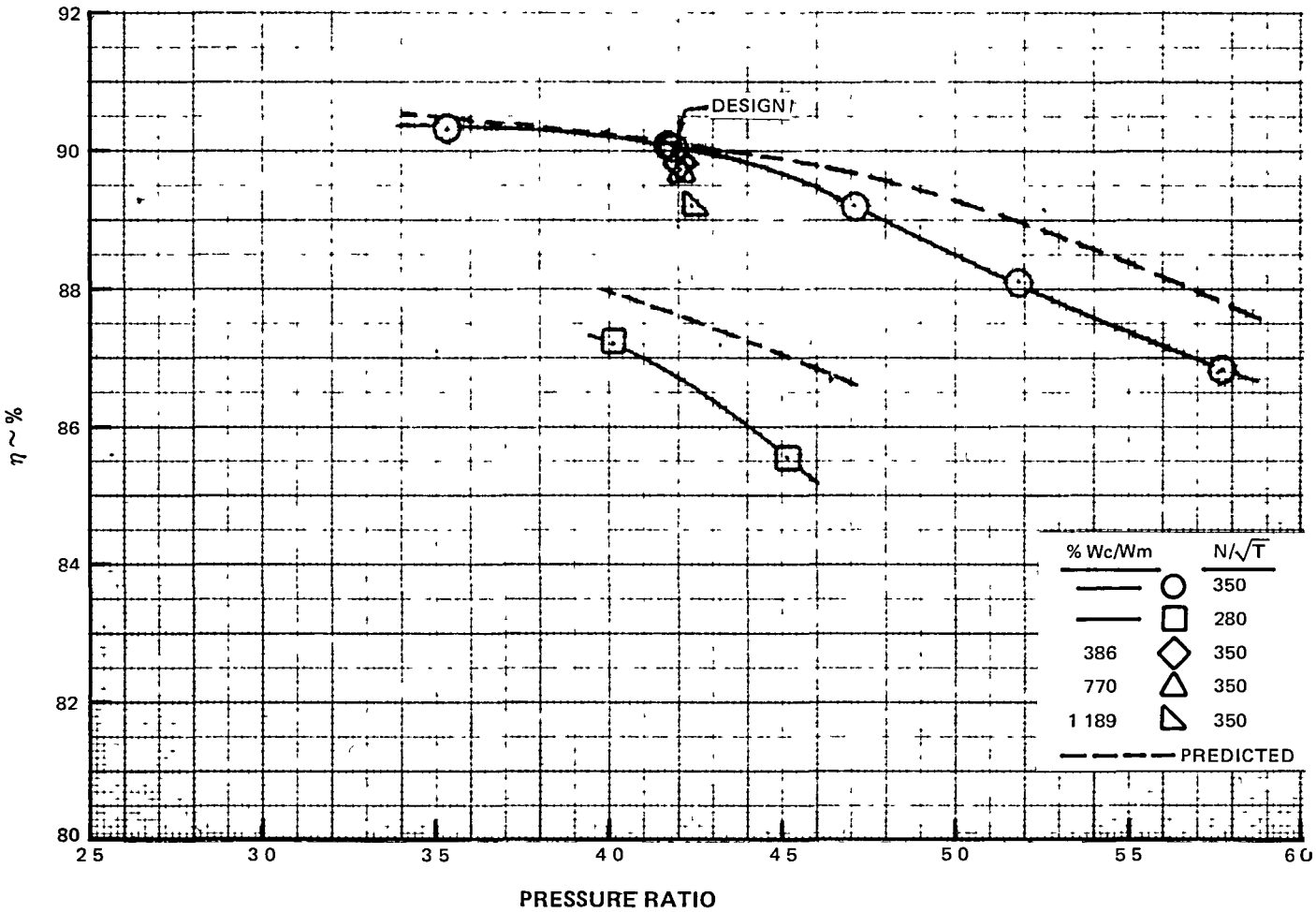

E-1 EEE Uncooled Rig 36% Reaction Rotating Rig Efficiency vs. Pressure Ratio (Area Averaged)

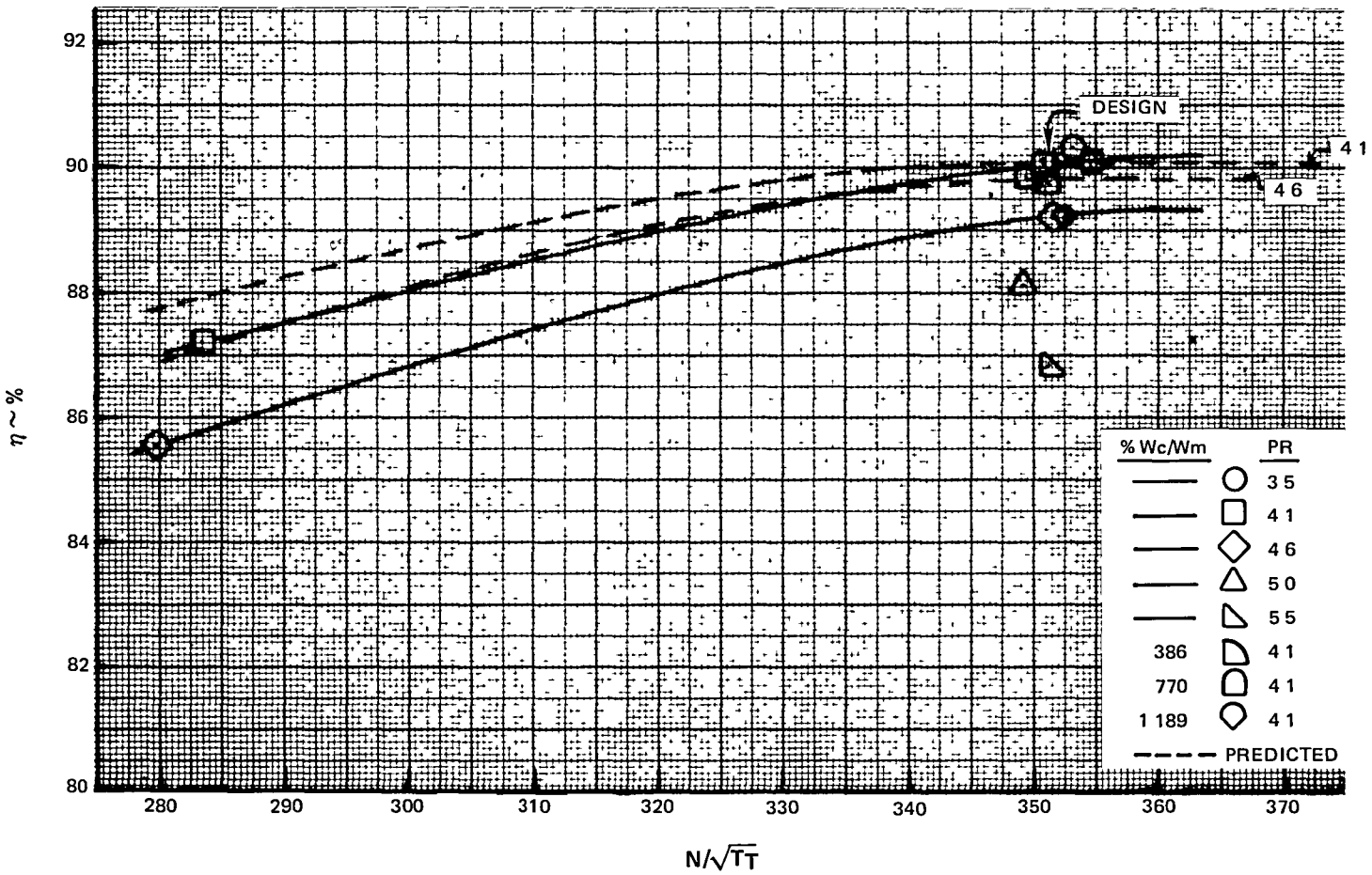

E-2 EEE Uncooled Rig 36% Reaction Rotating Rig Efficiency vs. Speed Parameter (Area Averaged)

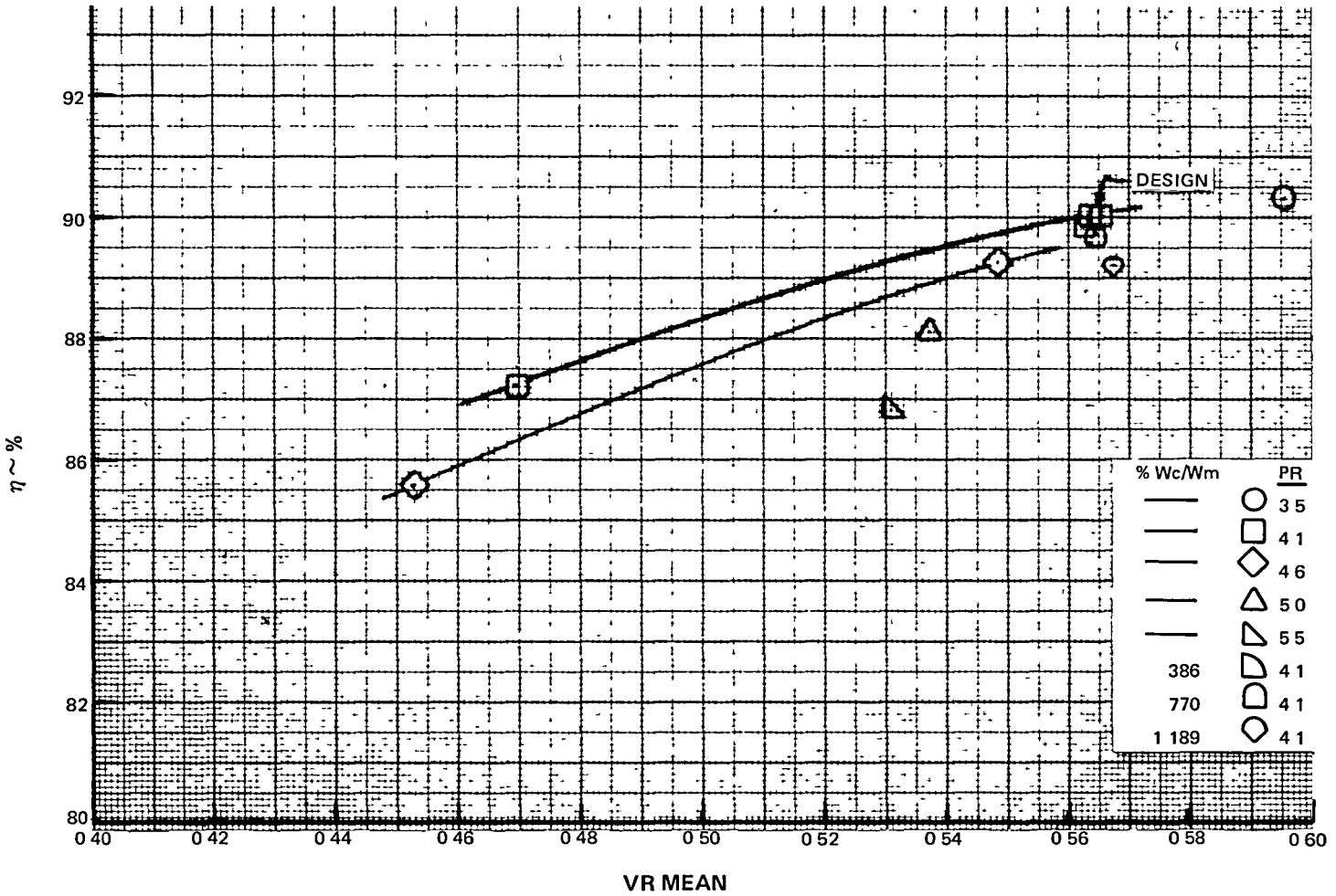

E-3 EEE Uncooled Rig 36% Reaction Rotating Rig Efficiency vs. Mean Velocity Ratio (Area Averaged)

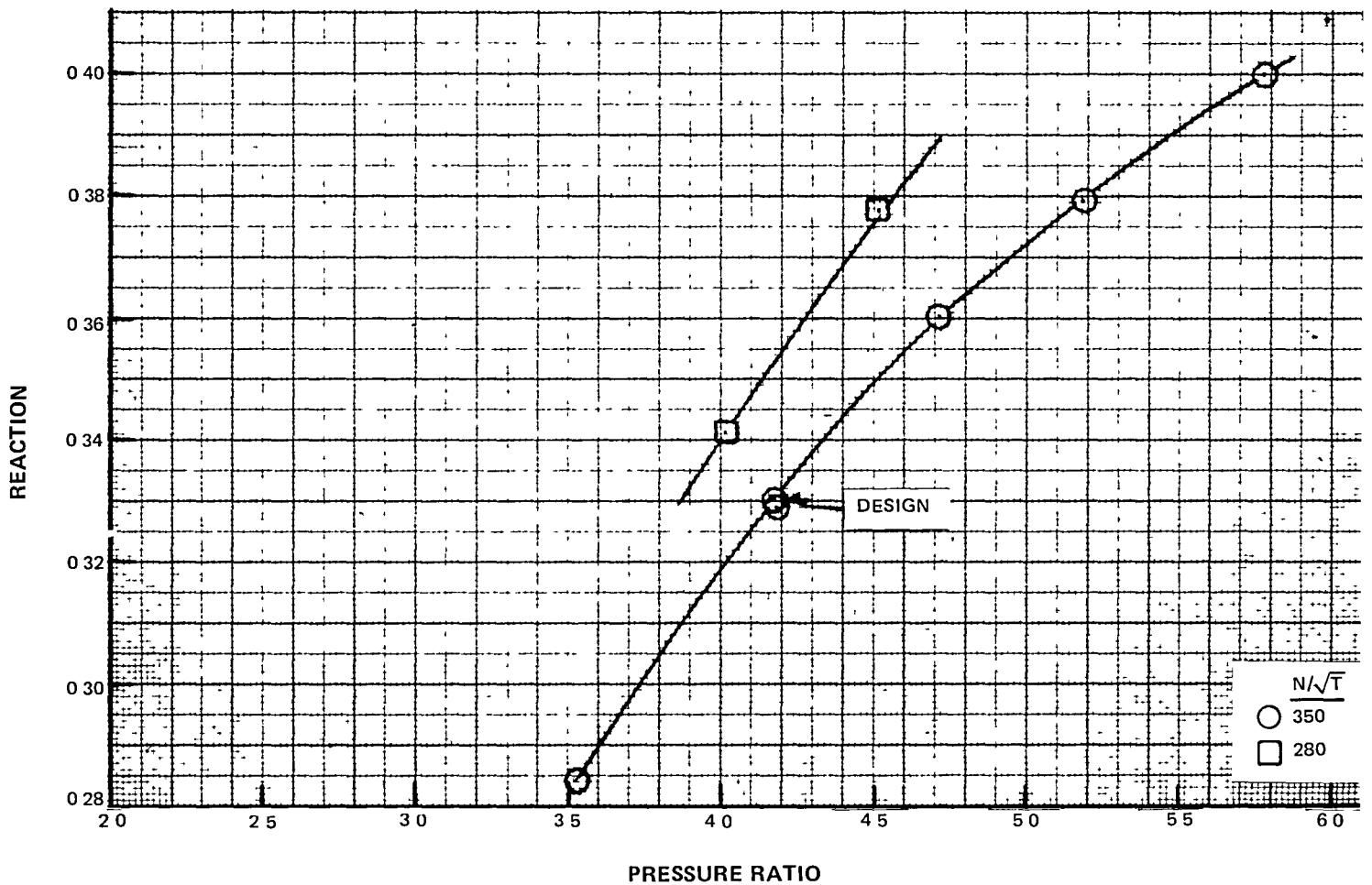

E-4 EEE Uncooled Rig 36% Reaction Rotating Rig Reaction vs. Pressure Ratio

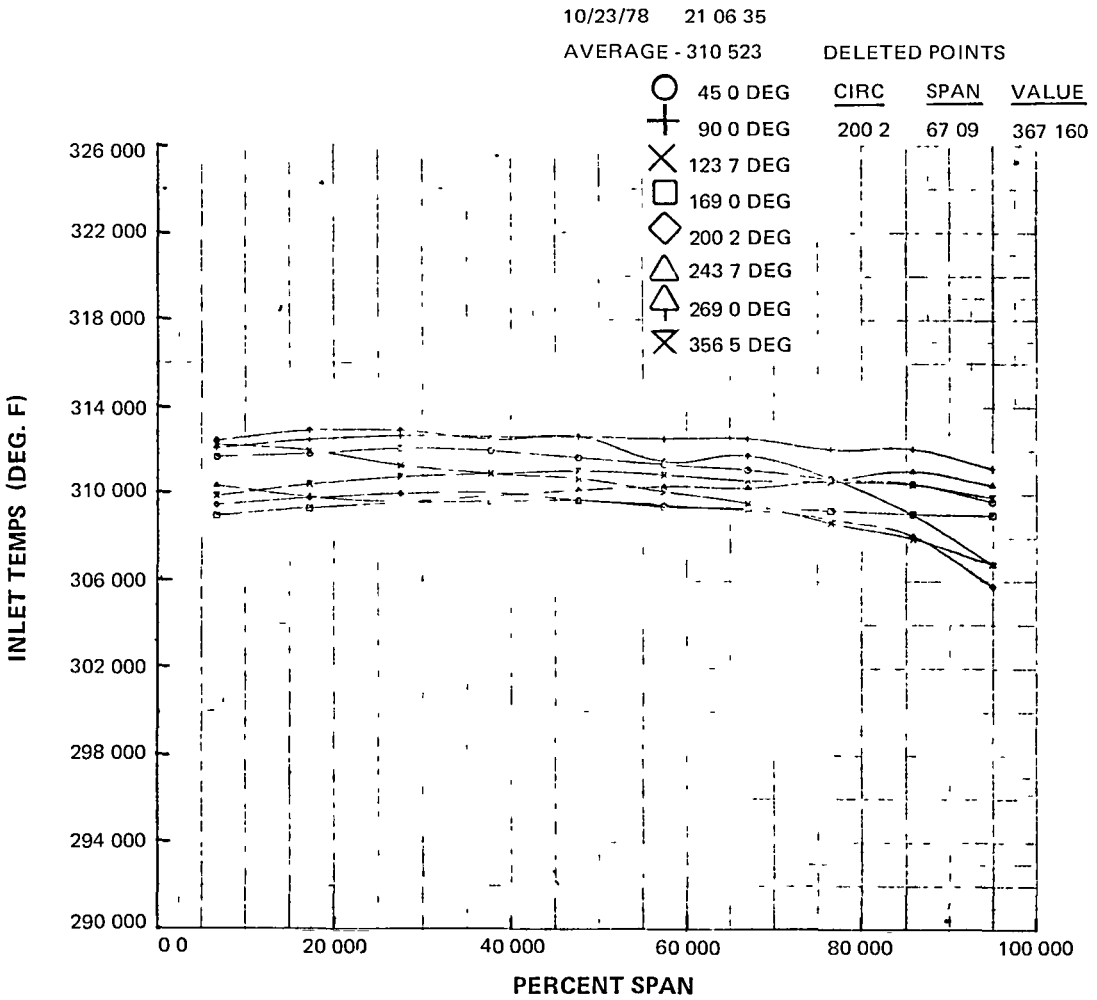

E-5 EEE Uncooled Rig 36% Reaction Rotating Rig Inlet Temperature vs. Span

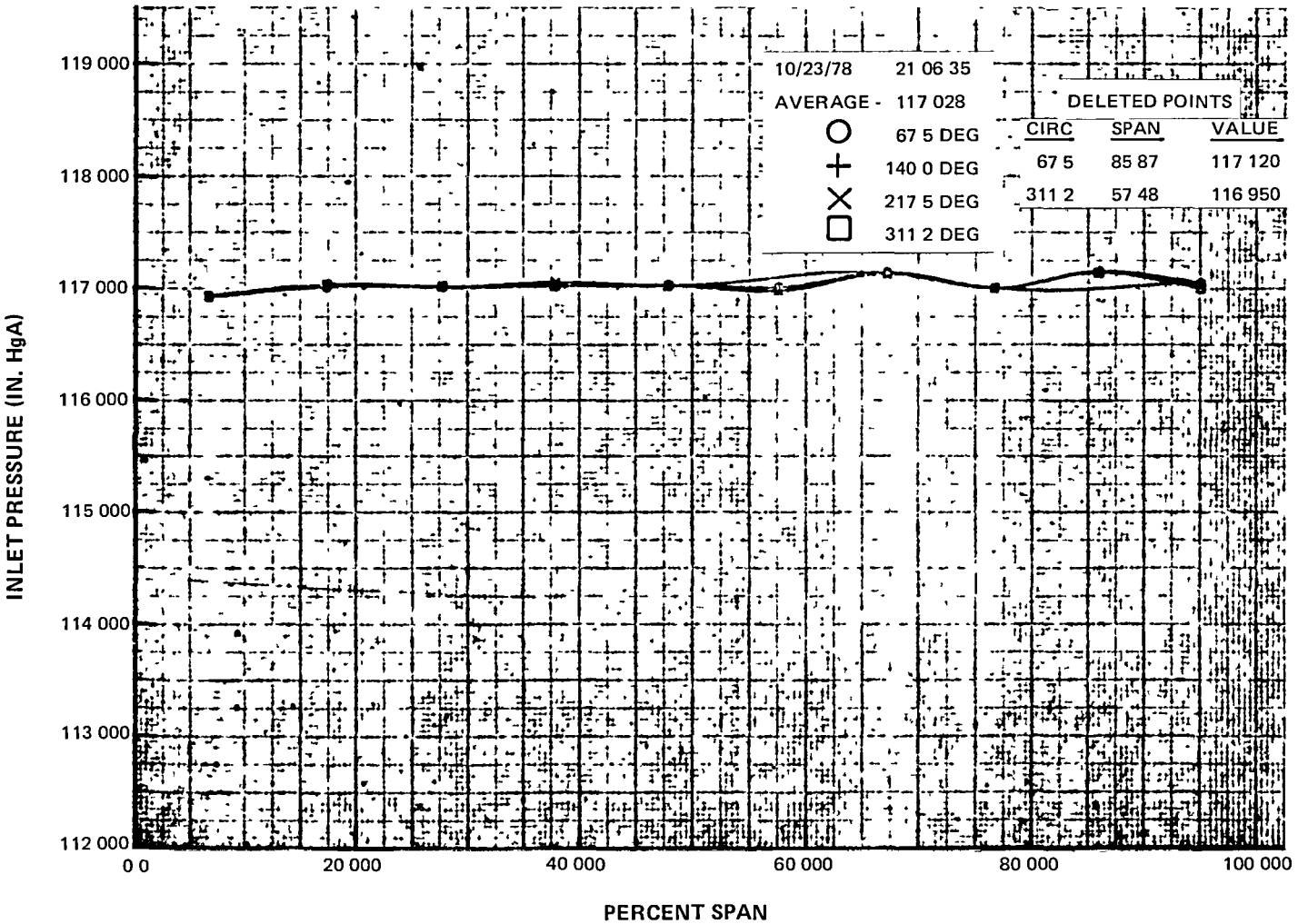

E-6 EEE Uncooled Rig 36% Reaction Rotating Rig Inlet Pressure vs. Span

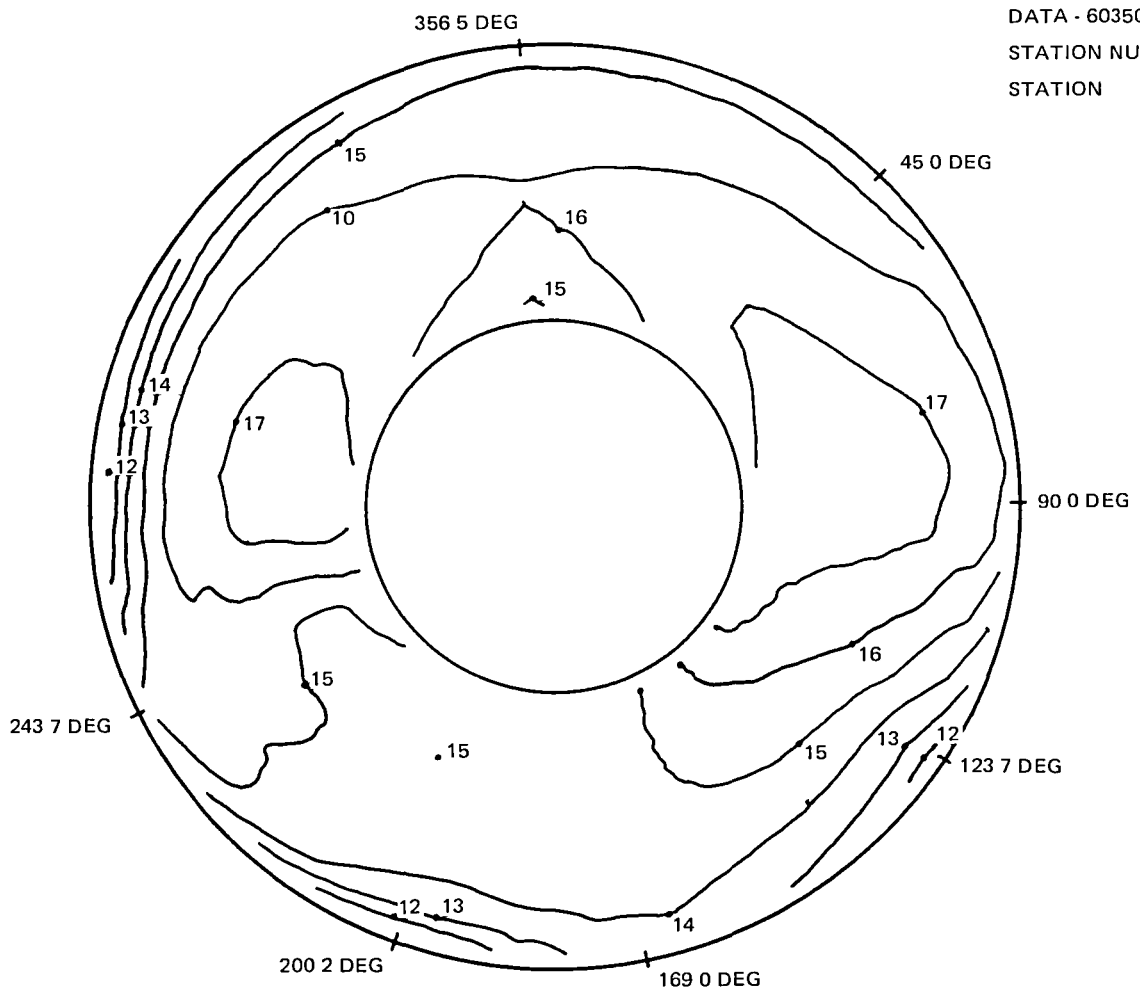

E-7 EEE Uncooled Rig 36% Reaction Rotating Rig Inlet Temperture Contours

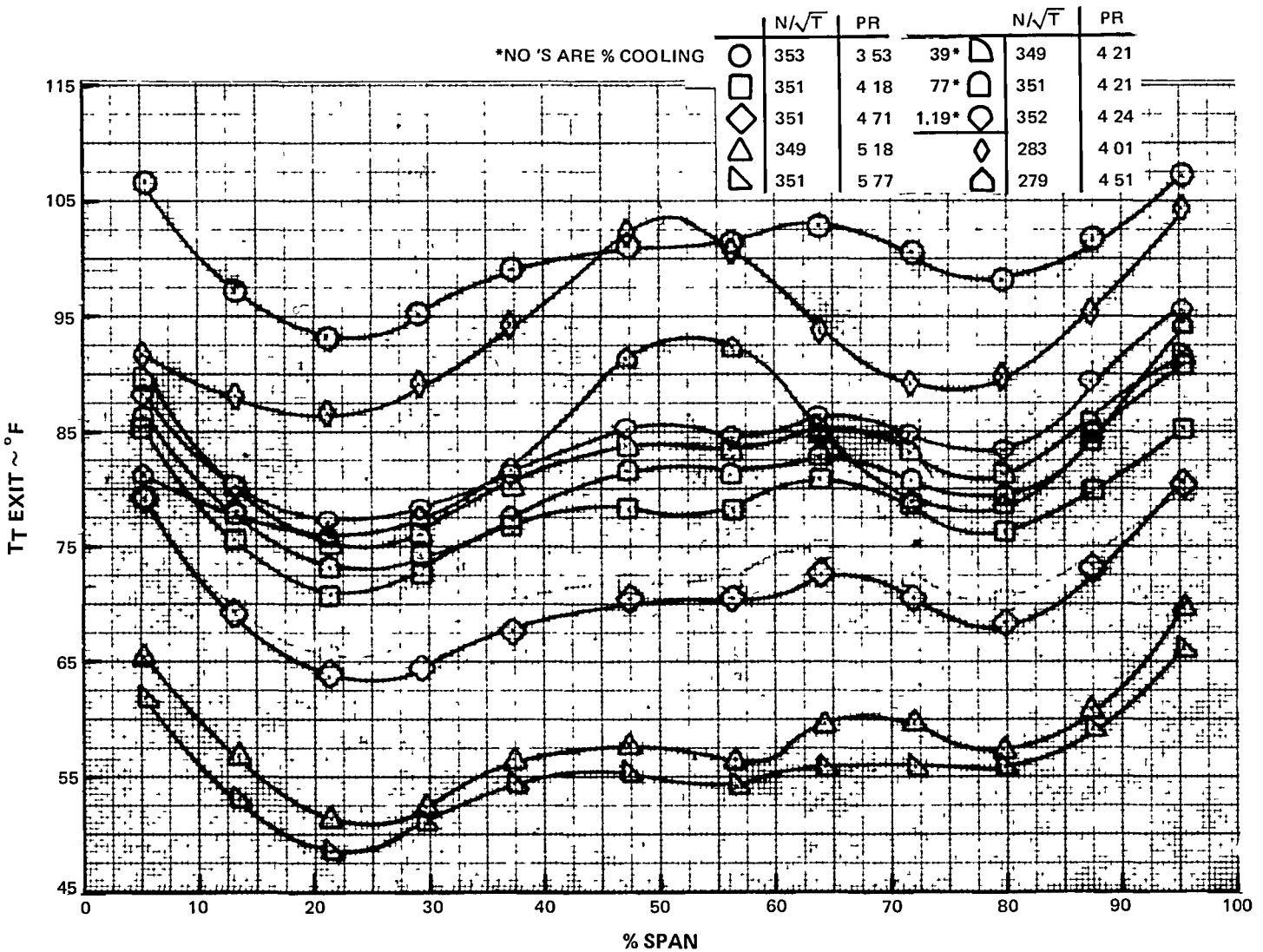

E-8 EEE Uncooled Rig 36% Reaction Rotating Rig Exit Temperture vs. Span

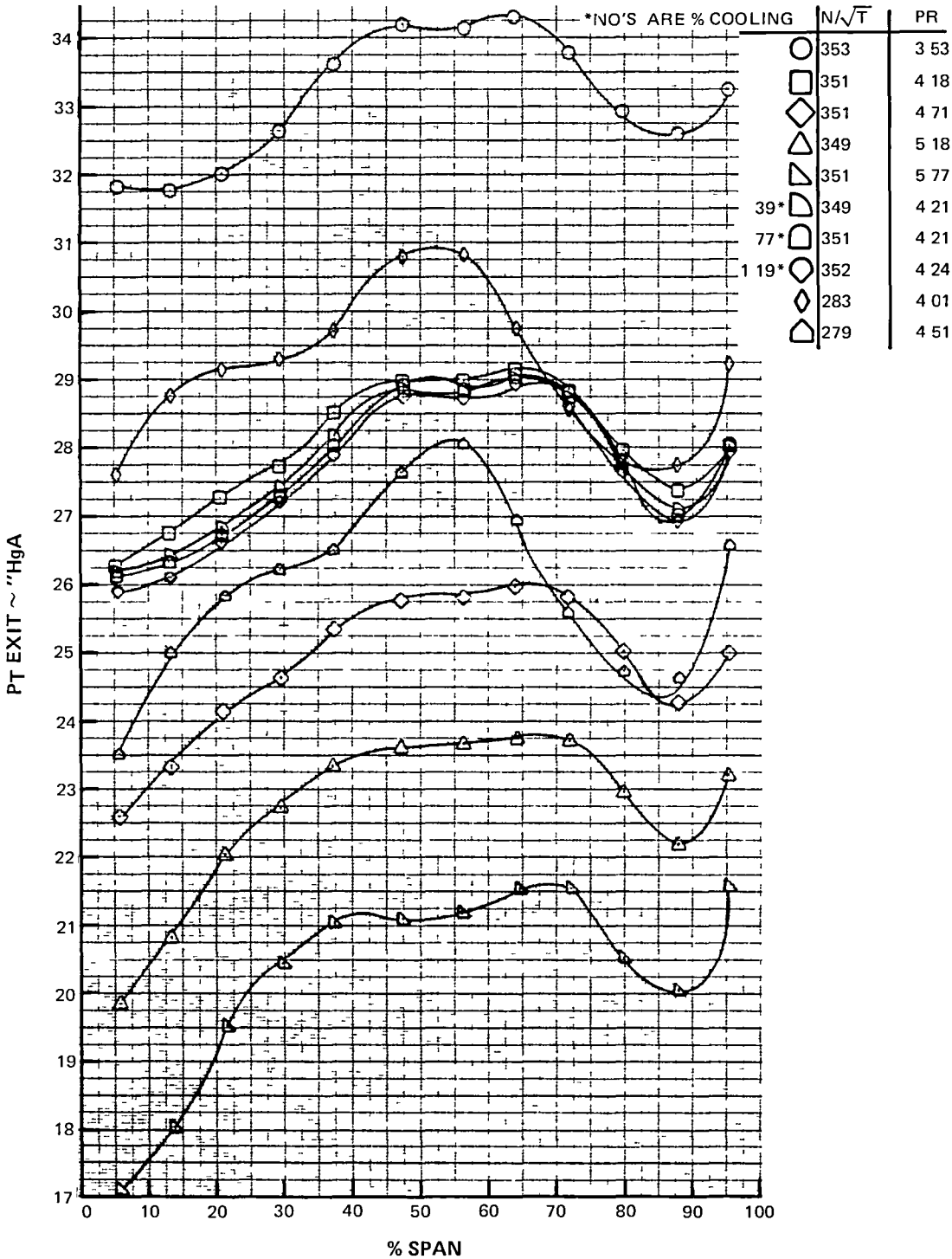

E-9 EEE Uncooled Rig 36% Reaction Rotating Rig Exit Pressures vs. Span

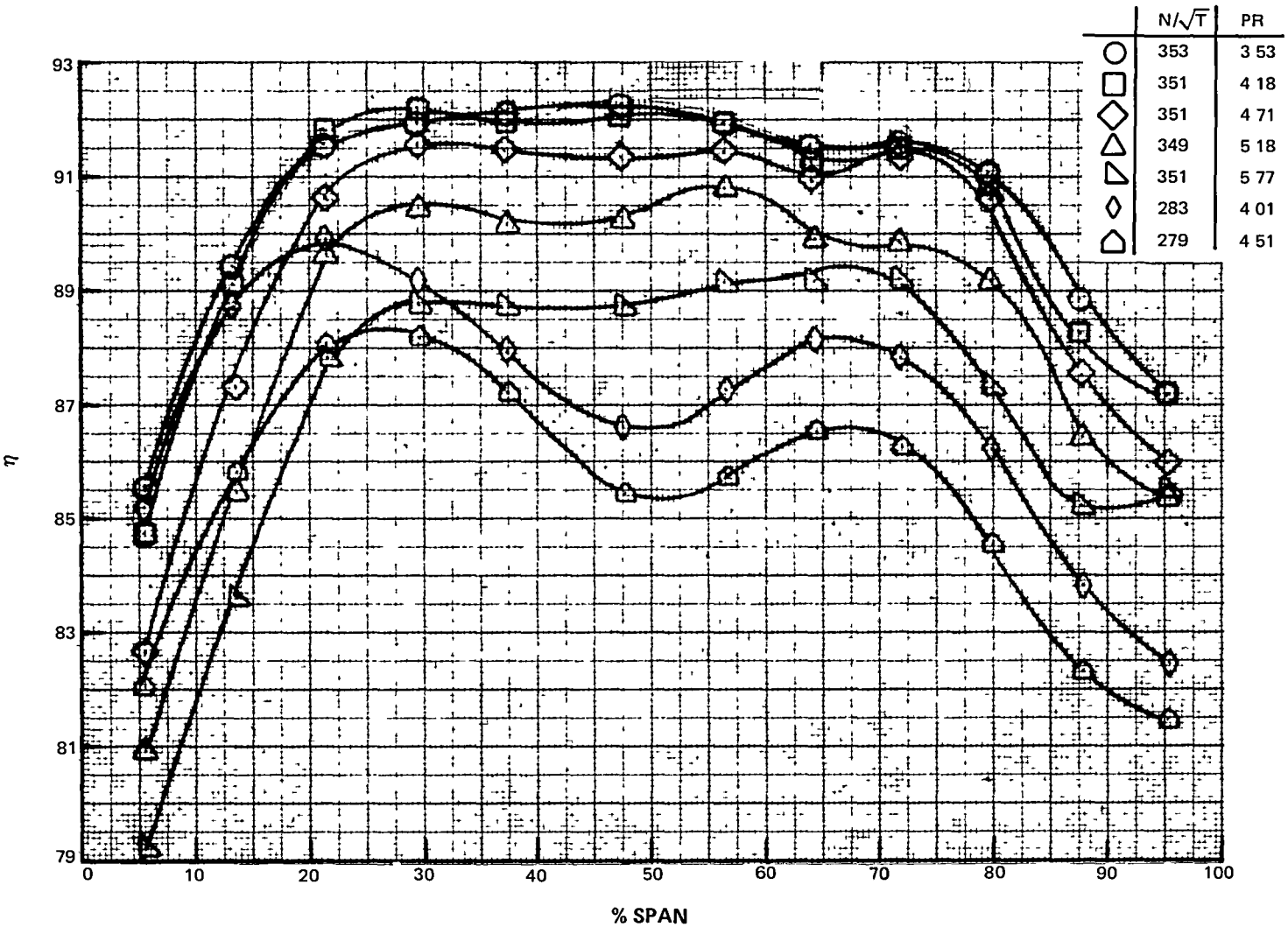

E-10 EEE Uncooled Rig 36% Reaction Rotating Rig Area Averaged Spanwise Efficiency

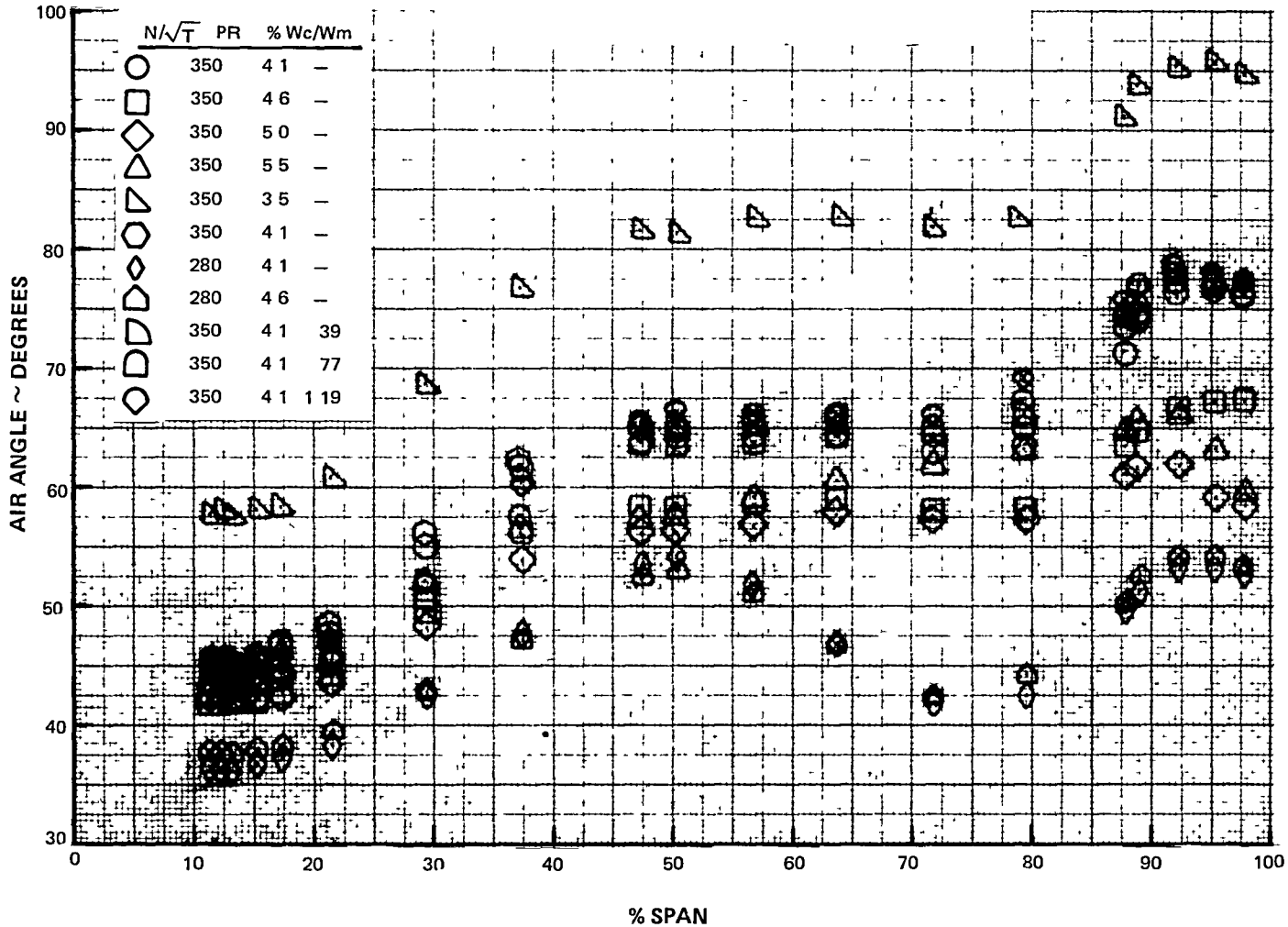

E-11 EEE Uncooled Rig 36% Reaction Rotating Rig Exit Air Angle vs. % Span at Circ. = 155.2 degrees

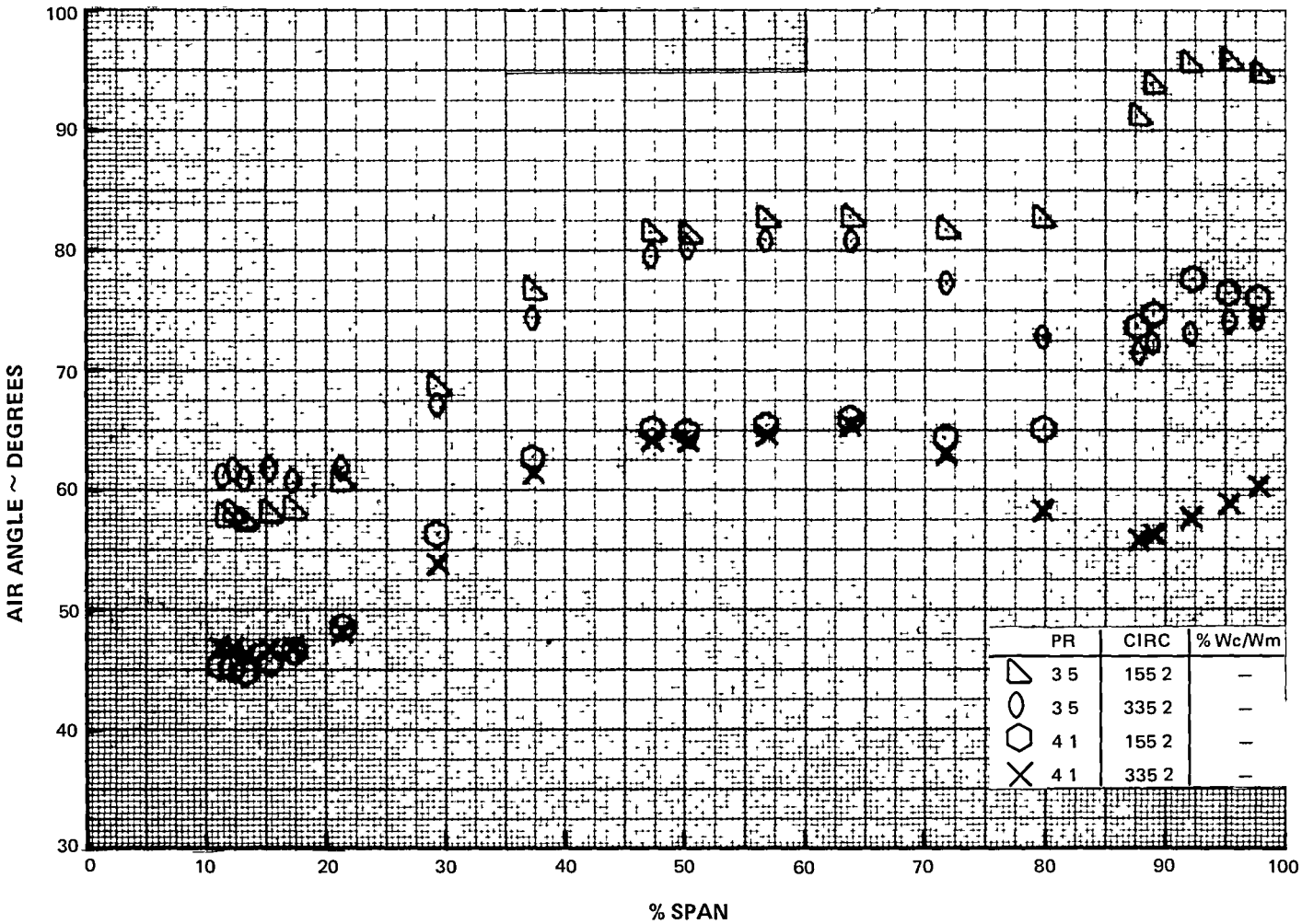

E-12 EEE Uncooled Rig 36% Reaction Rotating Rig Exit Air Angle vs. % Span at N sq. rt. T = 350

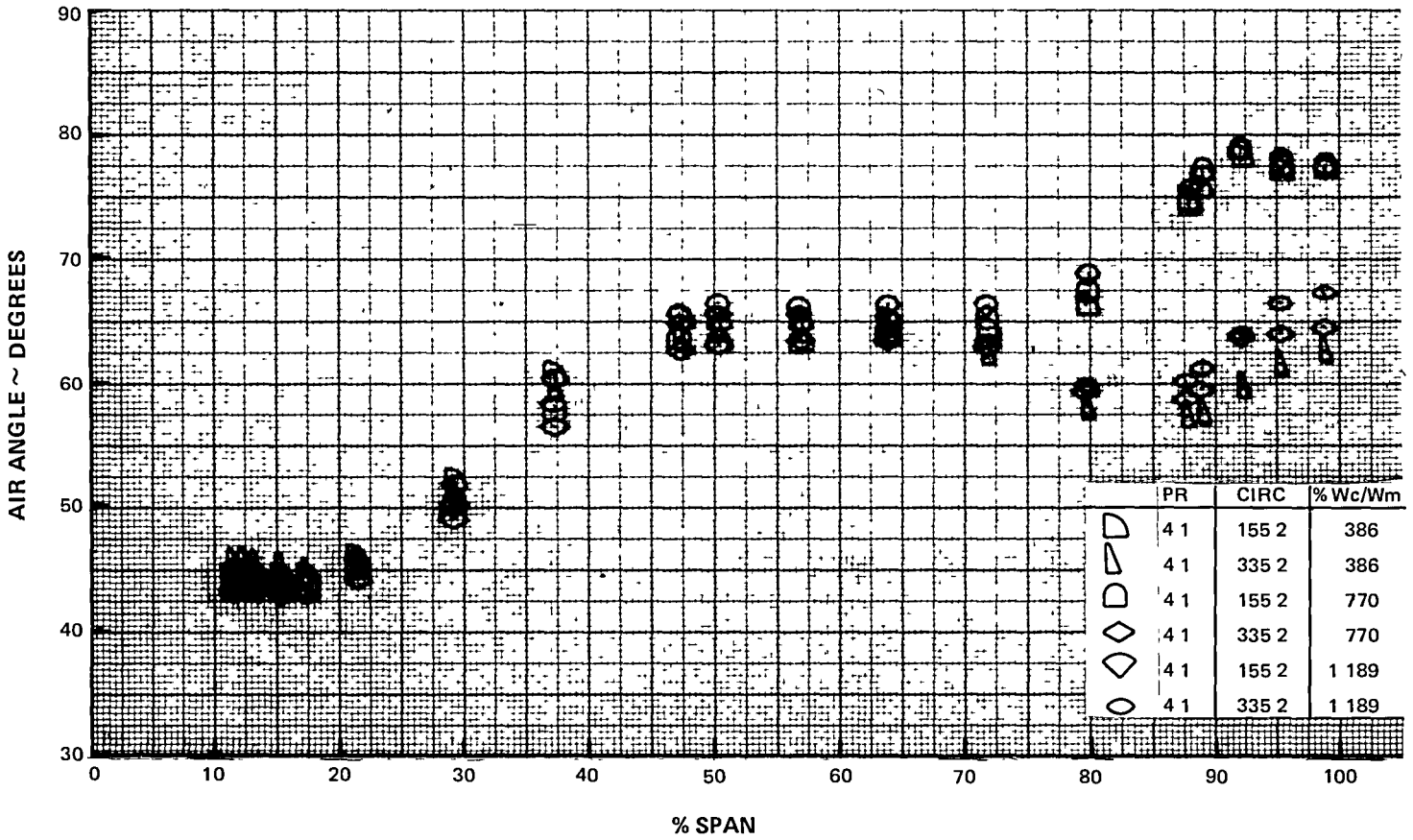

E-13 EEE Uncooled Rig 36% Reaction Rotating Rig Exit Air Angle vs. % Span at N sq. rt. T = 350

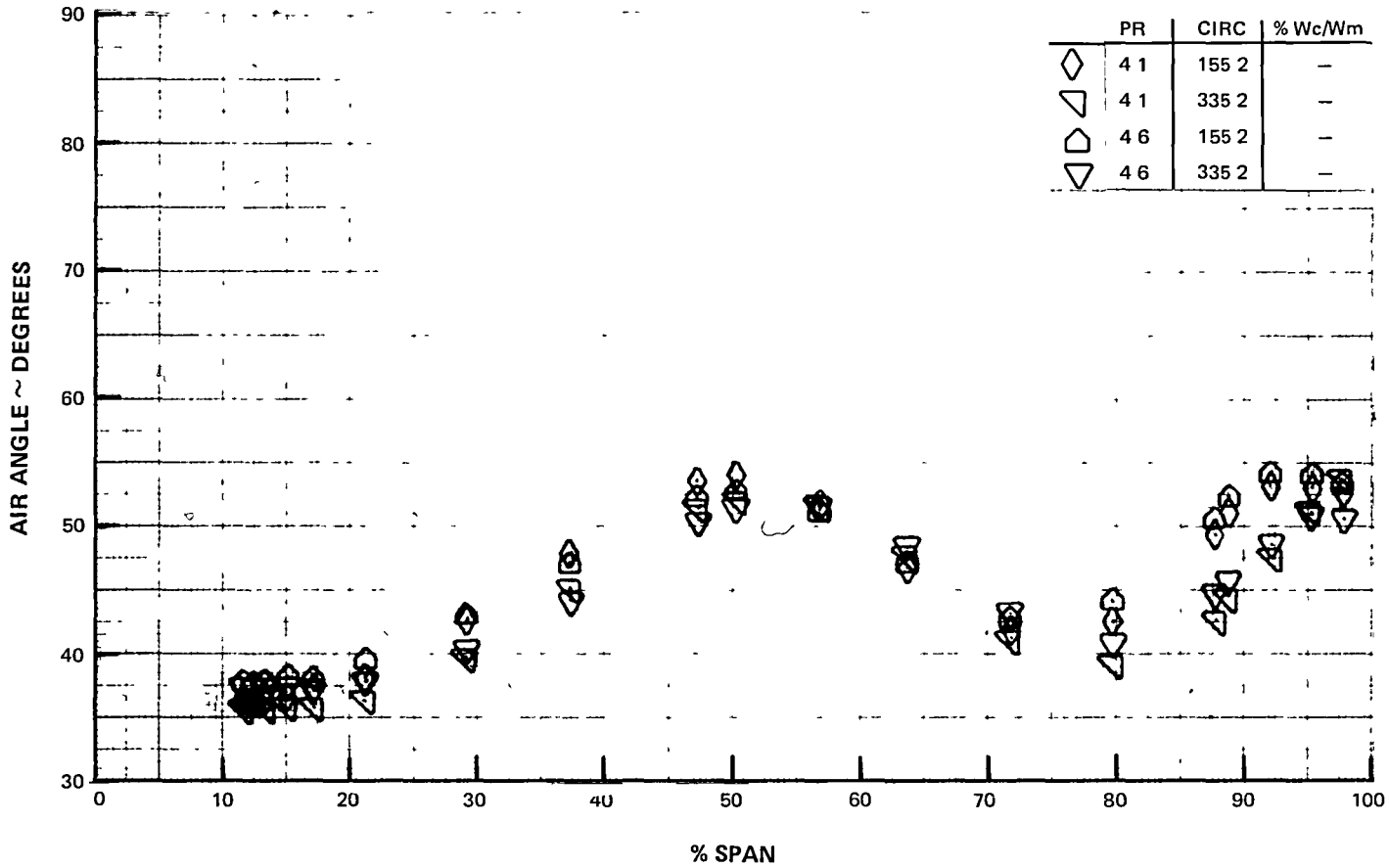

E-14 EEE Uncooled Rig 36% Reaction Rotating Rig Exit Air Angle vs. % Span at N sq. rt. T = 280

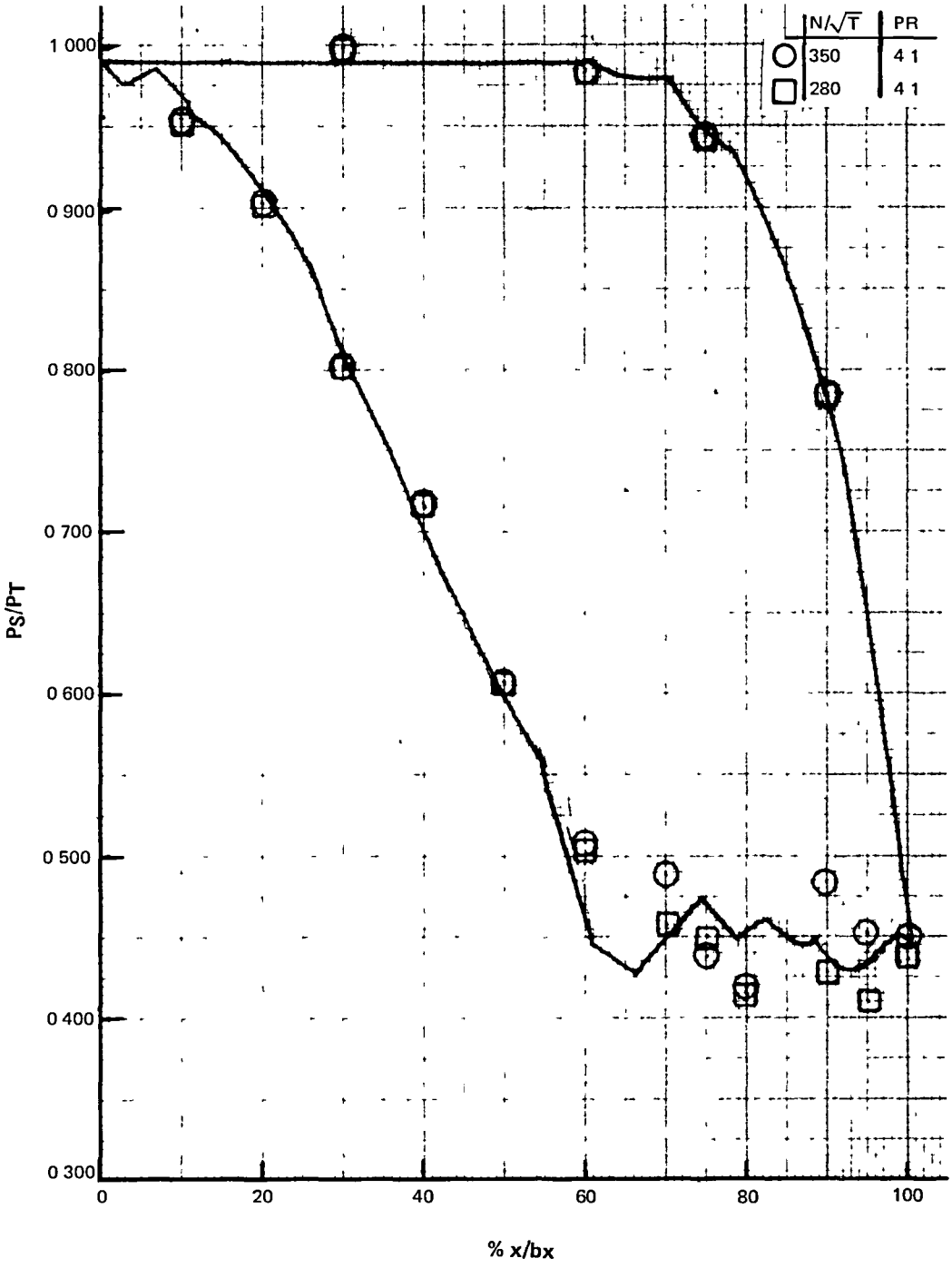

E-15 EEE Uncooled Rig 36% Reaction Rotating Rig 11% Span Vane Surface Statics

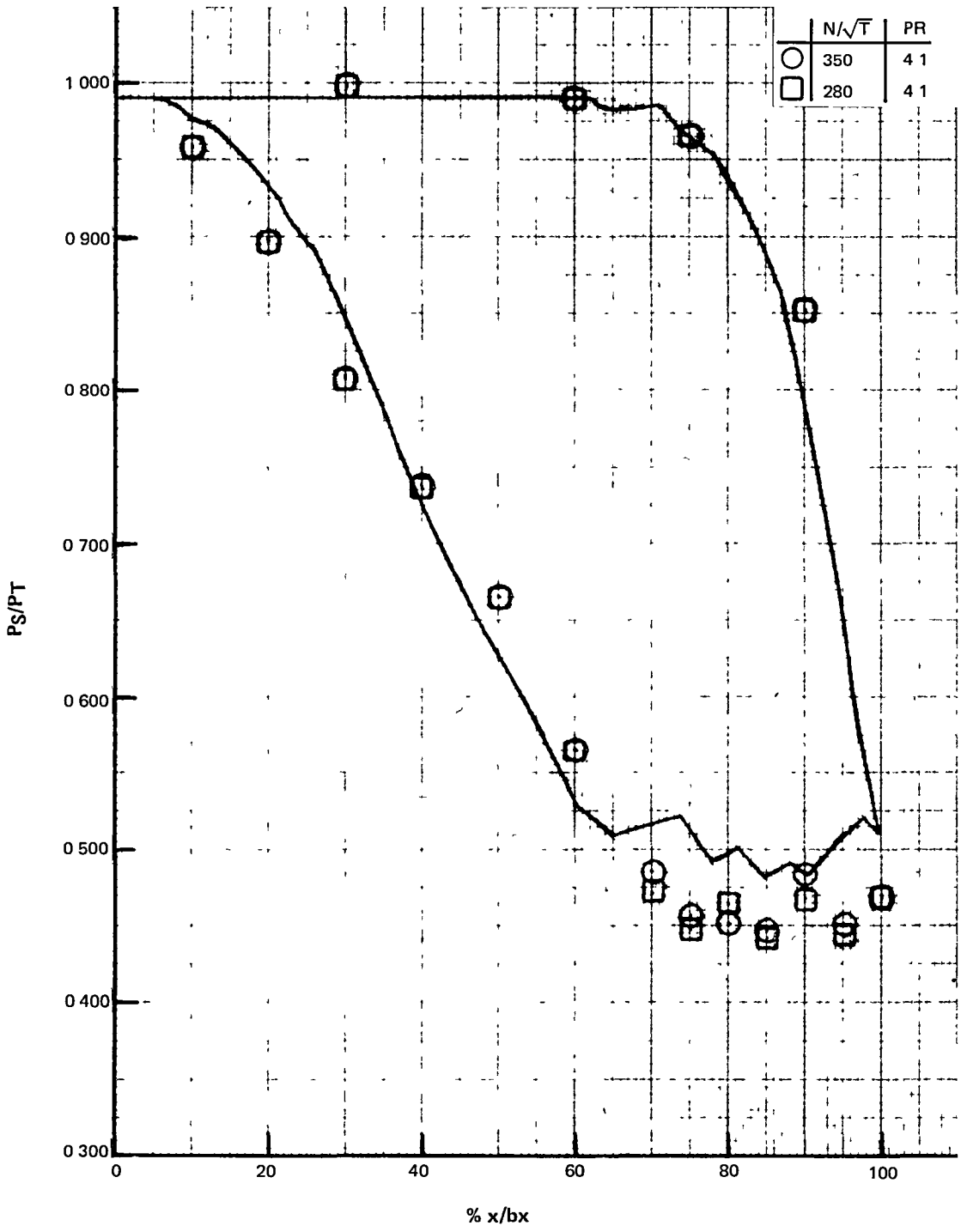

E-16 EEE Uncooled Rig 36% Reaction Rotating Rig 50% Span Vane Surface Statics

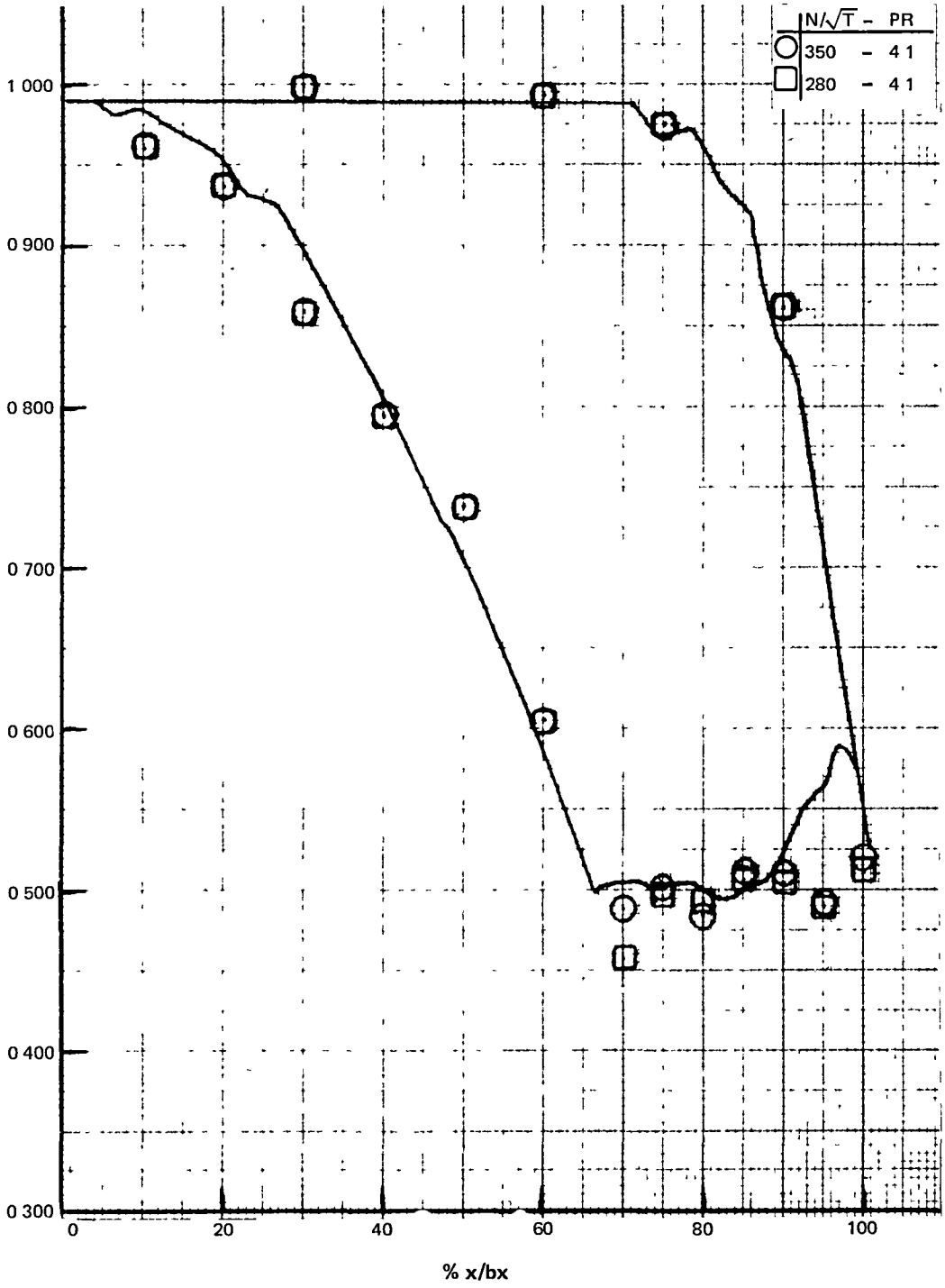

E-17 EEE Uncooled Rig 36% Reaction Rotating Rig 89% Span Vane Surface Statics

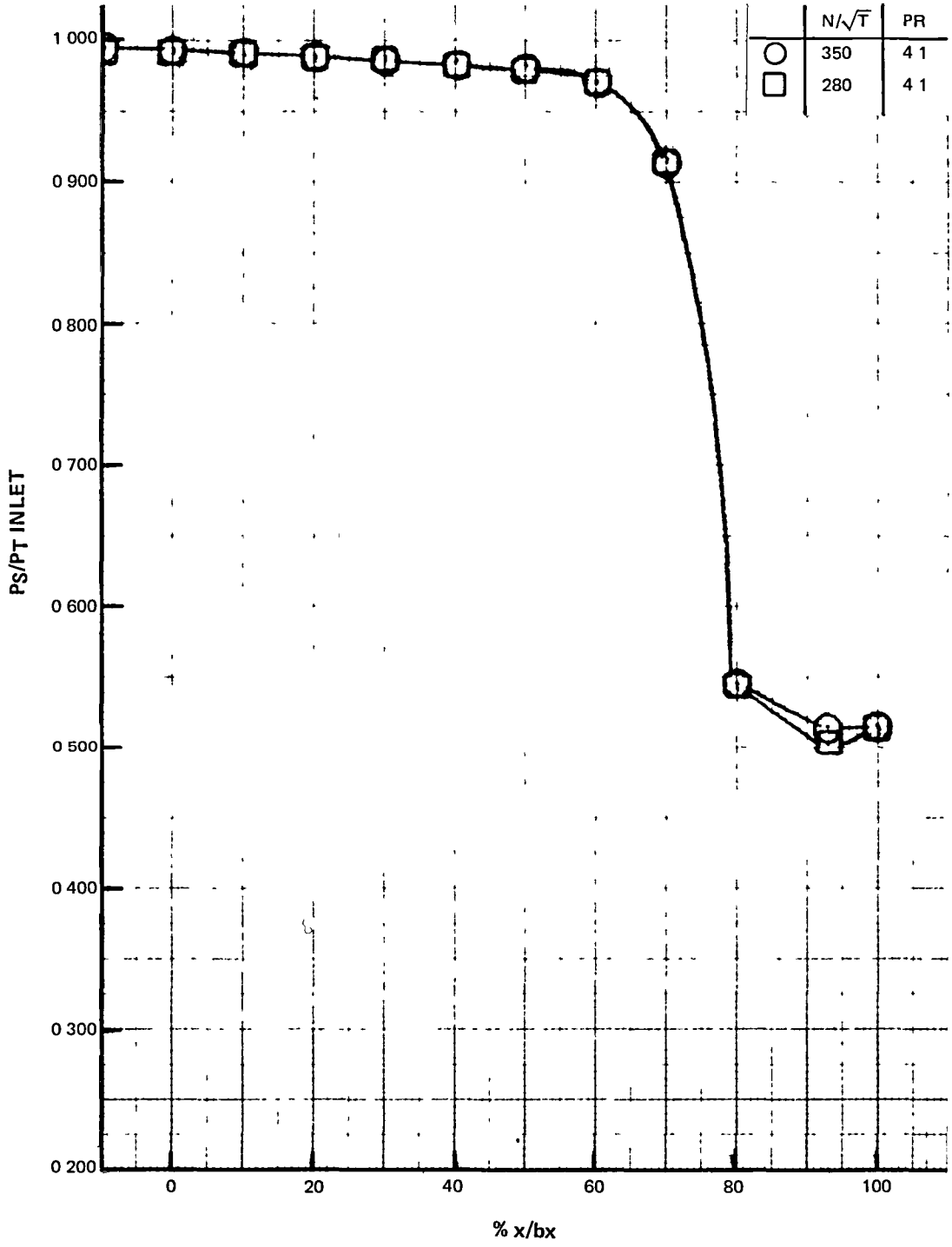

E-18 EEE Uncooled Rig 36% Reaction Rotating Rig Mid Gap O.D. Statics vs. % x/bx

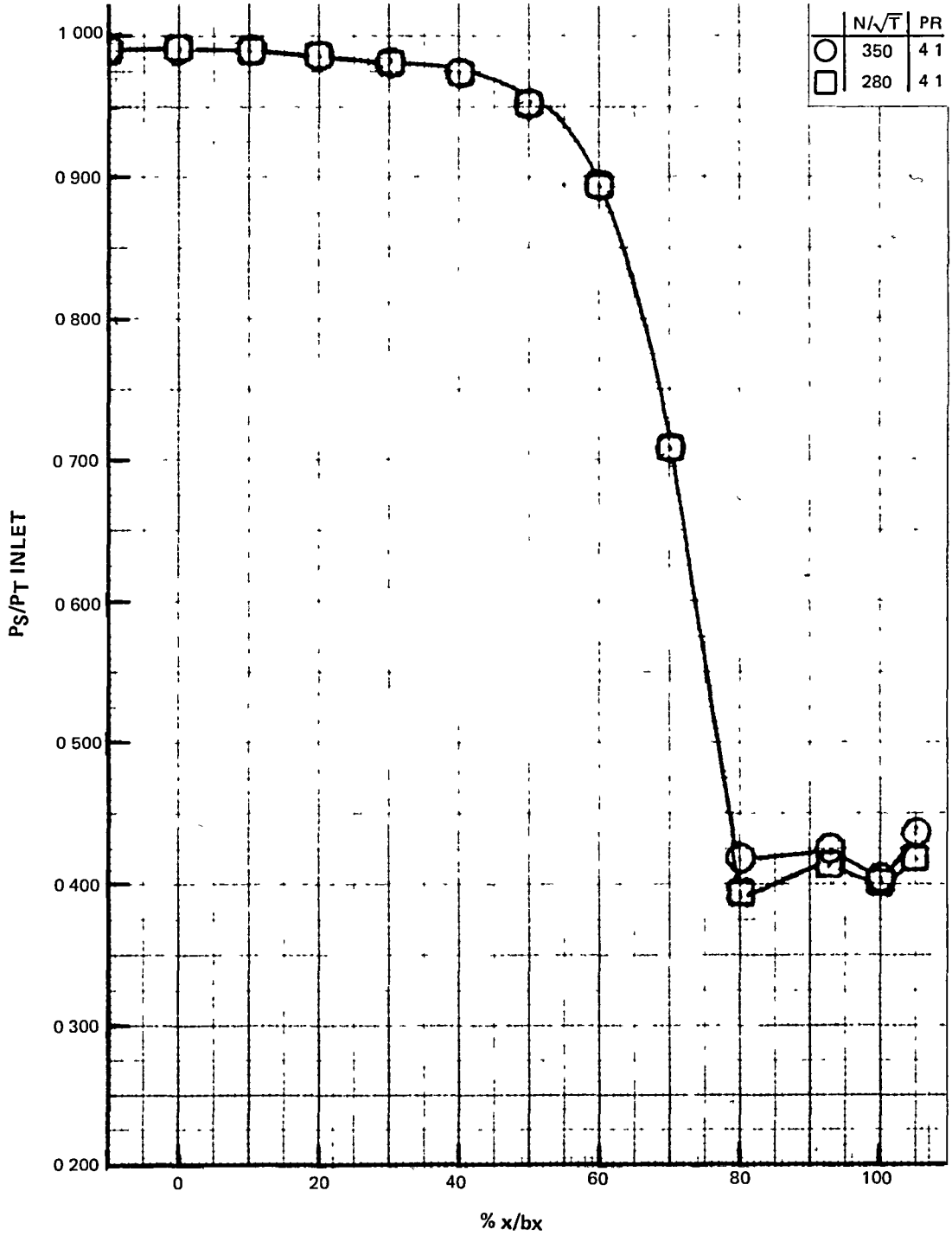

E-19 EEE Uncooled Rig 36% Reaction Rotating Rig Mid O.D. Statics vs. % x/bx

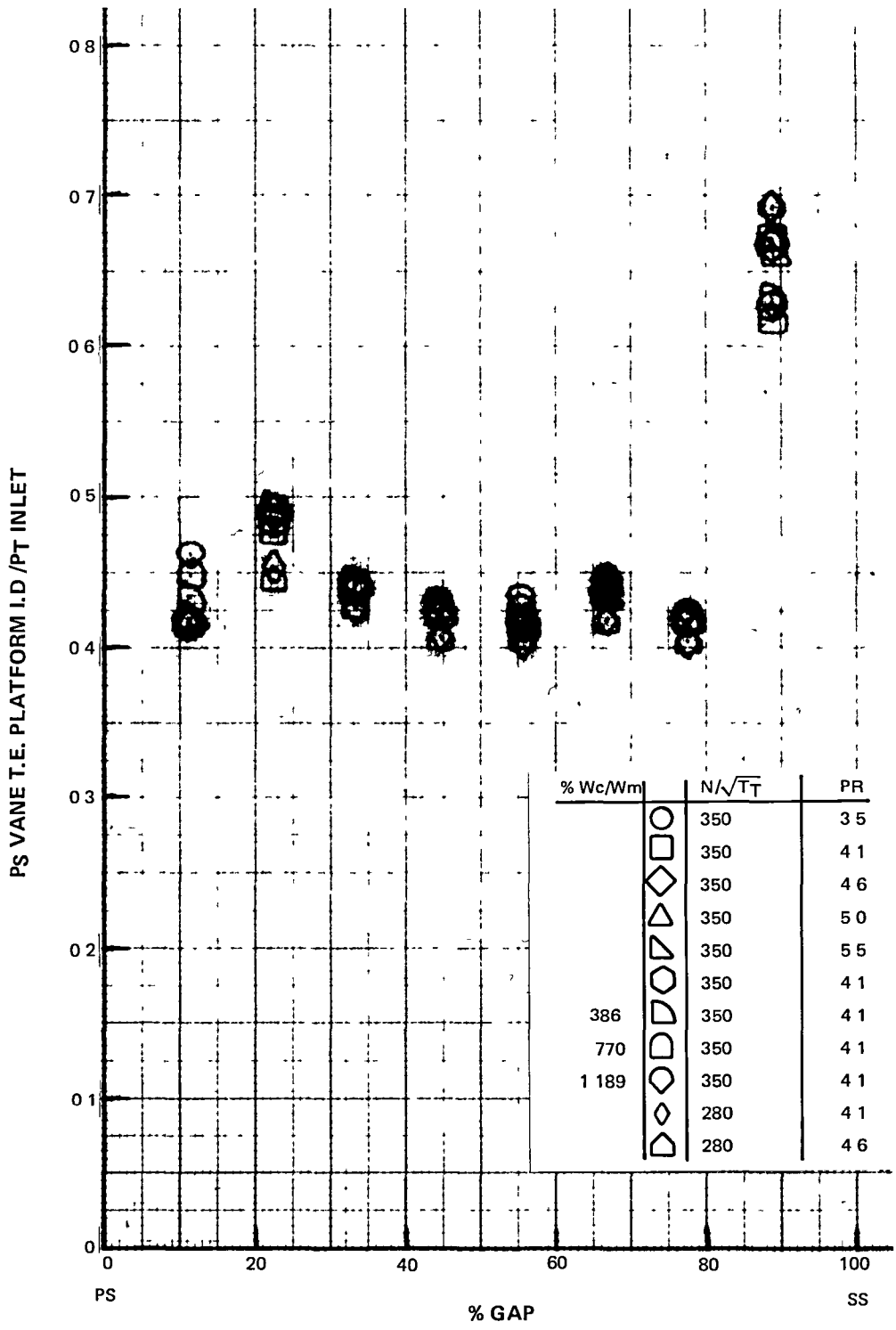

E-20 EEE Uncooled Rig 36% Reaction Rotating Rig I.D. Platform Ps vs. % Gap

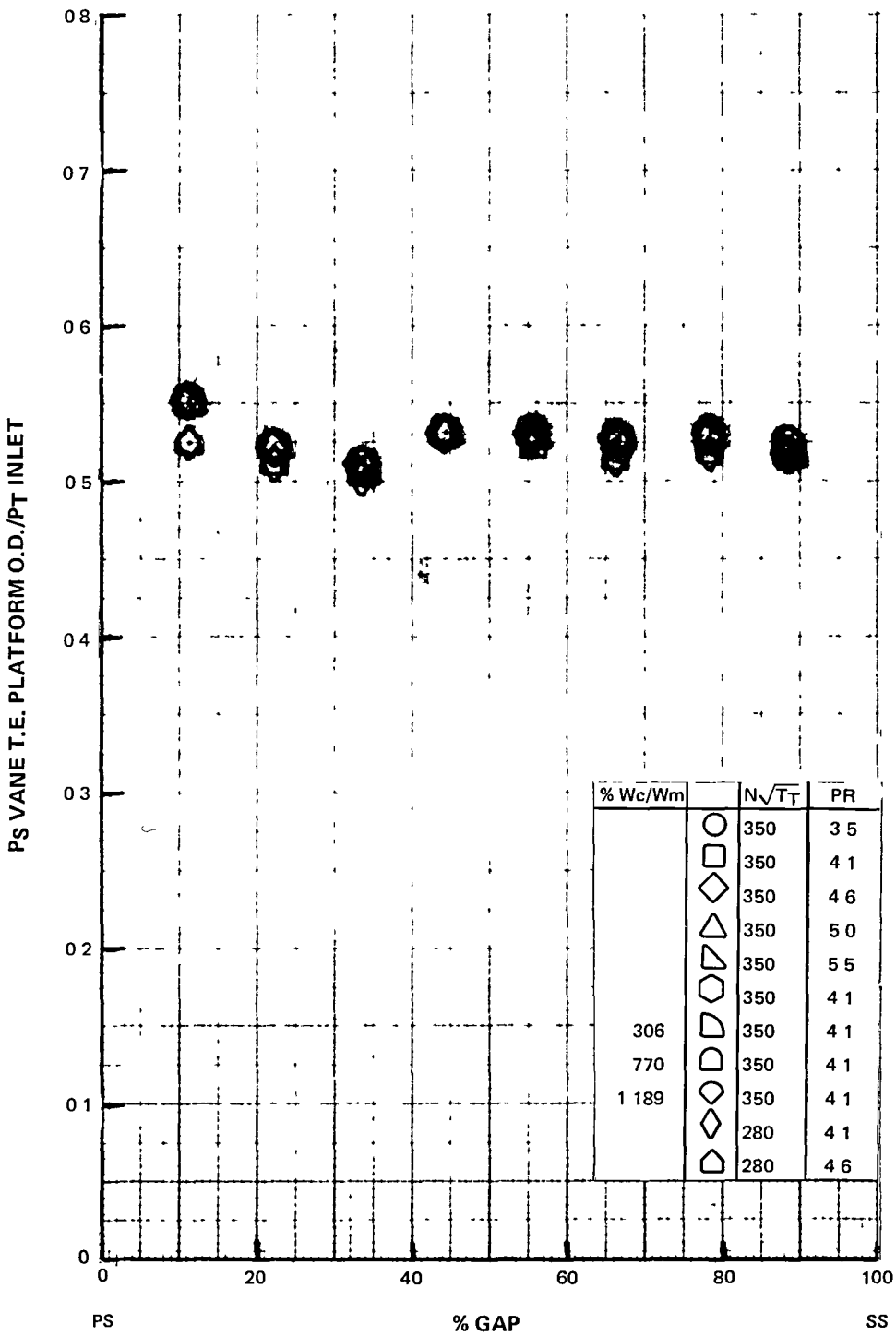

E-21 EEE Uncooled Rig 36% Reaction Rotating Rig O.D. Platform Ps vs. % Gap

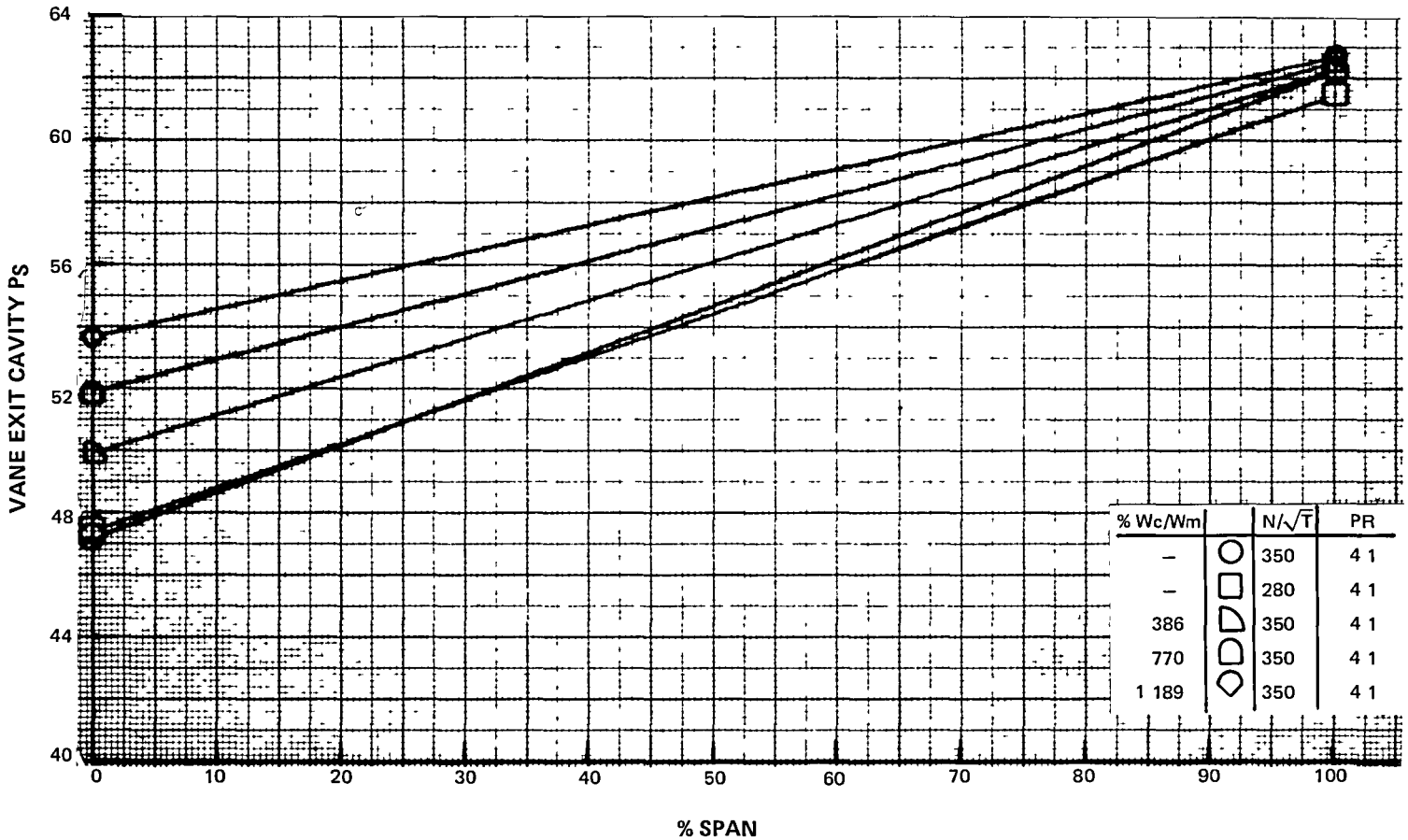

E-22 EEE Uncooled Rig 36% Reaction Rotating Rig Vane Exit Cav vs. % Span

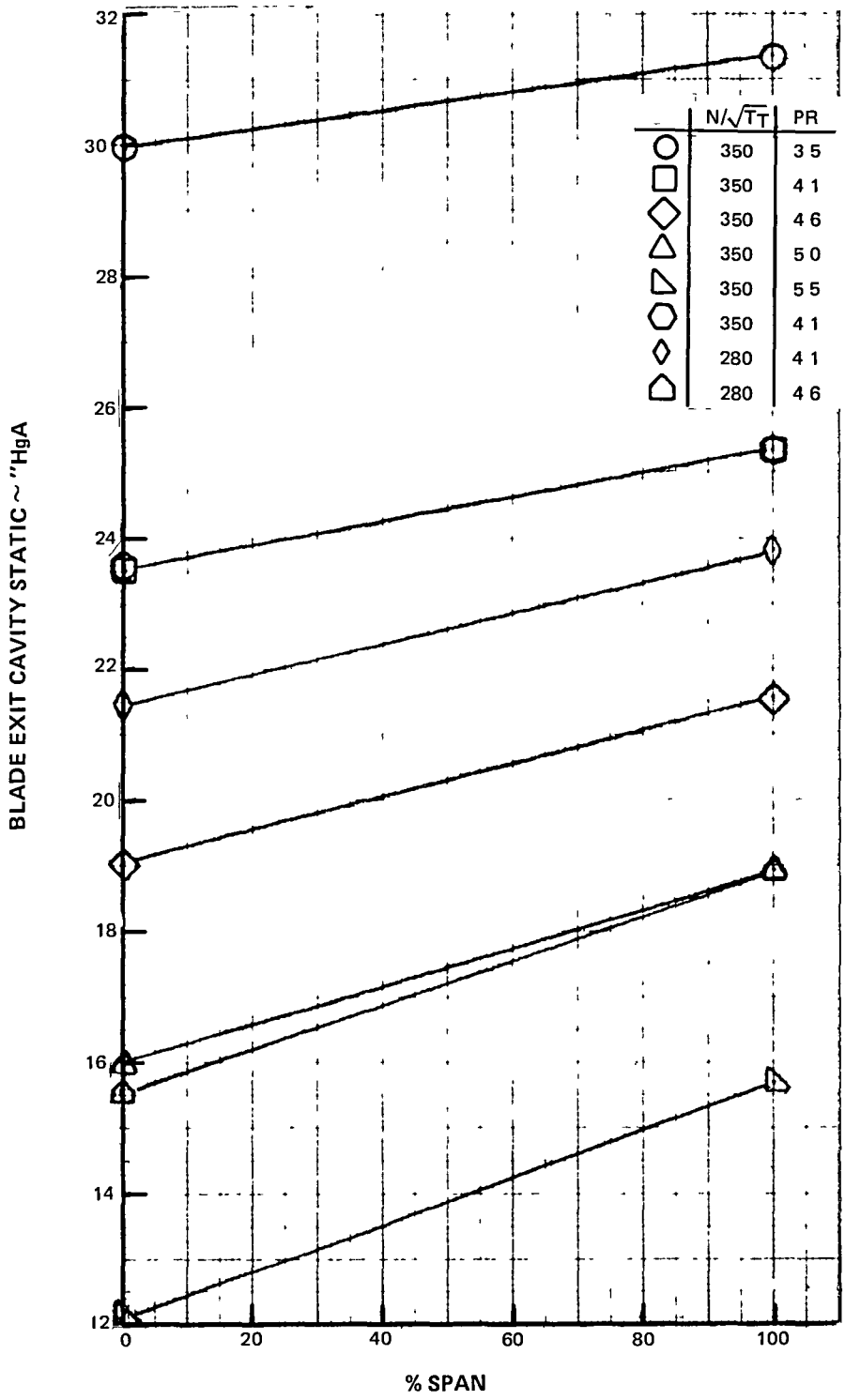

E-23 EEE Uncooled Rig 36% Reaction Rotating Rig Vane Blade Exit Cavity Static vs. % Span

This Page Intentionally Left Blank

APPENDIX F - BUILD 2 ROTATING RIG DATA

TABLE F-1
ECE RIG-70709-2

ROTATING RIG DATA SUMMARY

*DESIGN POINT

OPERATING POINT #	STEADY STEADY SCAN #	STEADY STATE DATASET NAME	STEADY STATE JULIAN DAY	STEADY STATE TIME	TRAVERSE SCAN #	TRAVERSE DATASET NAME	PT-IN PSIA	TT-IN °R	N RPM
			78-79	HR MIN					
*55	473	6035541200	4	17.36	511-539	873554124P	54.47	776.1	9789
2	34	6035046200	355	04·40	36- 65	873504624P	57.51	772.8	9783
3	177	6035050200	355	12·02	179-206	873505024P	57.47	782.8	9798
4	326	6035055200	355	20 54	328-355	873505524Q	57.42	779.1	9796
5	410	6035035200	11	13 51	412-440	873503524P	57.42	791.5	9846
10	435	6028141200	356	02 07	437-464	8728141240	57.51	781 4	7842
11	538	6028046200	356	06 28	540-568	872804624P	57.61	780 3	7806
13	514	6037541200	11	21 25	516-543	873754124P	57 56	715.2	10003
52	291	6035241200	10	04·42	293-320	873524124P	57.61	790.3	9807
53	635	6035341200	356	11 31	637-664	8735341240	57 51	779.3	9803

OP'TG POINT	W-MAIN LBM/S	W-COOL LBM/S	WCOOL WMAIN (%)	REACTION	VP MEAN	N TT-IN	PRES RATIO	OV AREA WEIGHTED (%)	AVG CLR. INCHES	CORRECTED AREA WEIGHTED (%)
*55	23 94			0 3799	0.5672	351.4	4 12	90 62	0.0145	90 60
2	23 96			0.4078	0.5517	351 9	4 69	89 44	0.0145	89 42
3	23 80			0.4221	0 5411	348 9	5 05	88.52	0 0135	88.43
4	23.81			0.4381	0.5354	351.0	5.65	86.80	0.0135	86.71
5	23 67			0.3421	0.920	350 0	3 55	90.32	0 0135	90.23
10	23.90			0.3859	0 4640	280 5	4 03	86.68	0.0205	87 14
11	23.95			0.4155	0.4507	279 4	4.60	84.49	0.0205	84.95
13	24.93			0.3716	0 6039	374.1	4.08	90 87	0.0115	90 62
52	23.73	0.174	0.733	--	0.5654	384 8	4.12	89.96	0.0165	90.10
53	23.85	0 299	1.254	--	0.5693	351 2	4.12	89 64	0 0195	90.02

This Page Intentionally Left Blank

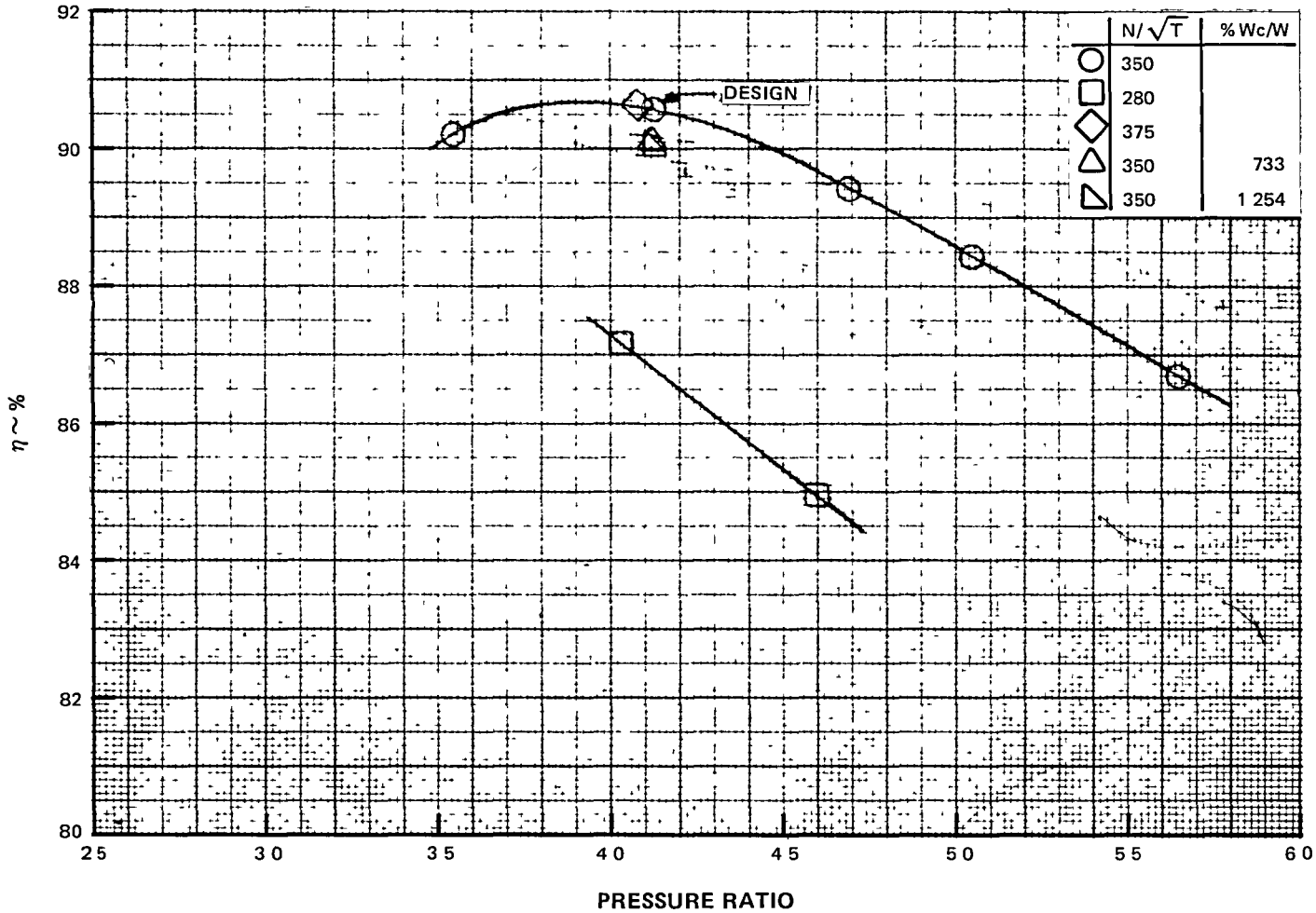

F-1 EEE Uncooled Rig 43% Reaction Rotating Rig Efficiency vs. Pressure Ratio (Area Averaged)

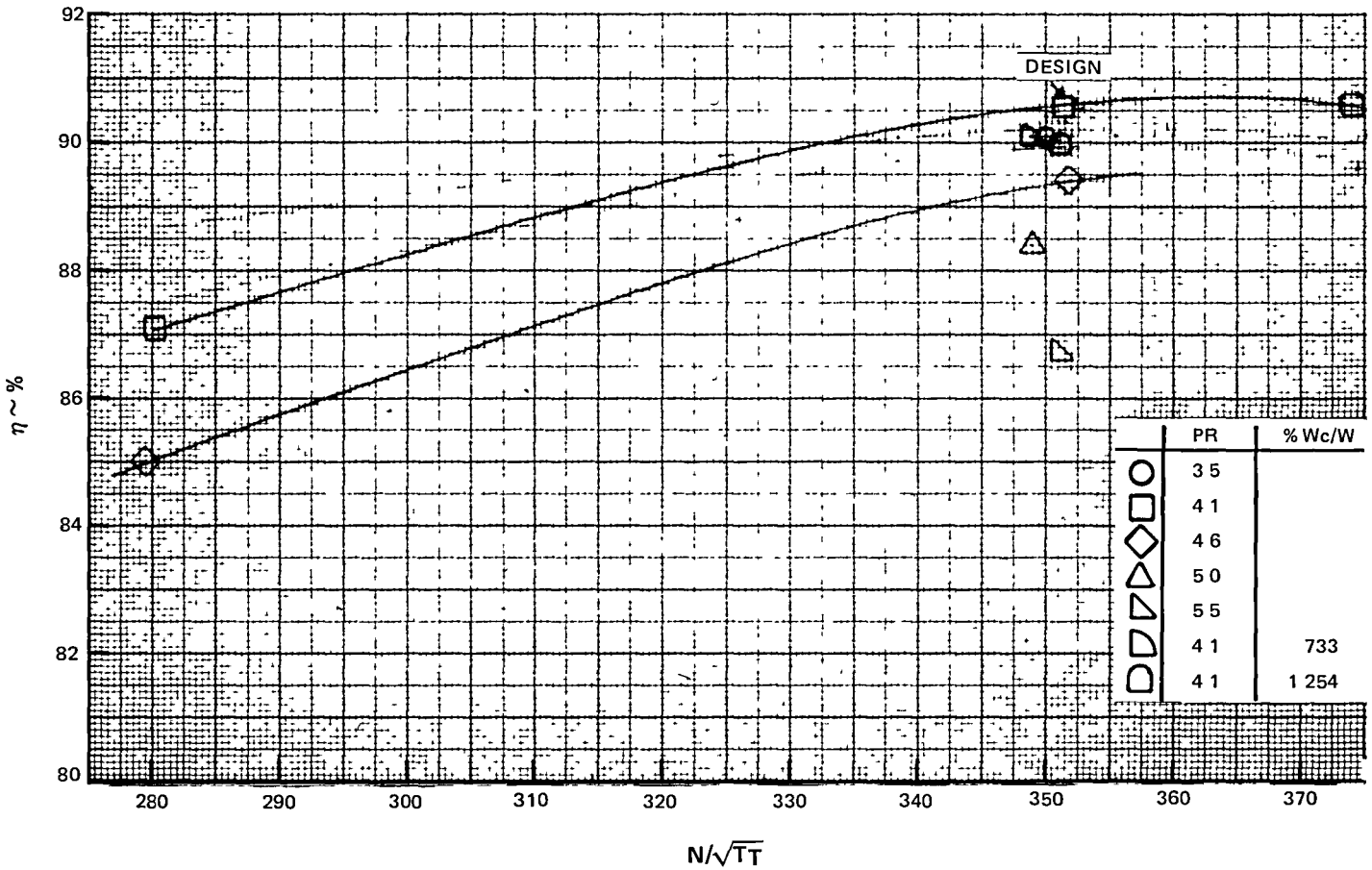

F-2 EEE Uncooled Rig 43% Reaction Rotating Rig Efficiency vs. Speed Parameter (Area Averaged)

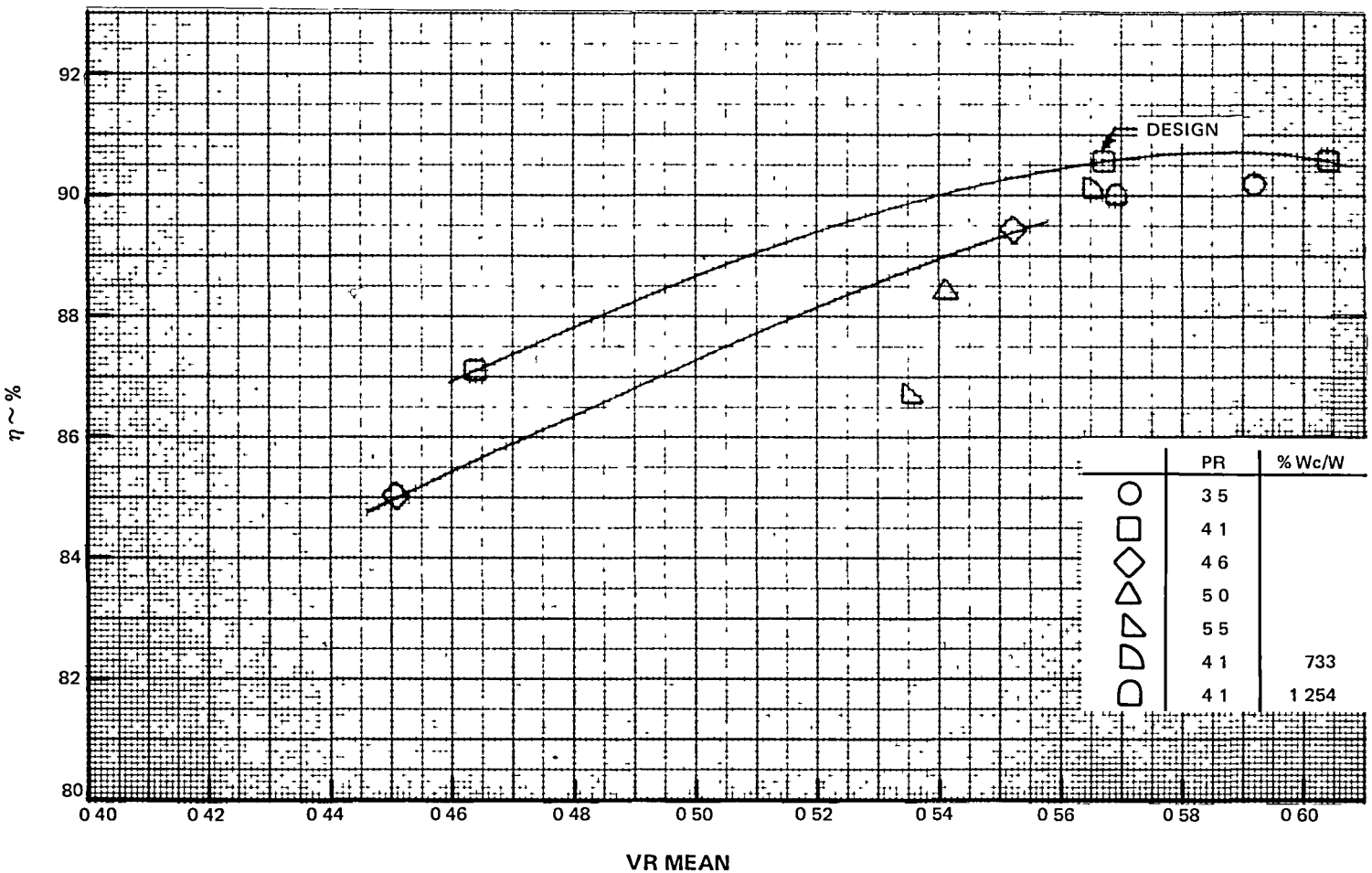

F-3 EEE Uncooled Rig 43% Reaction Rotating Rig Efficiency vs. Mean Velocity Ratio (Area Averaged)

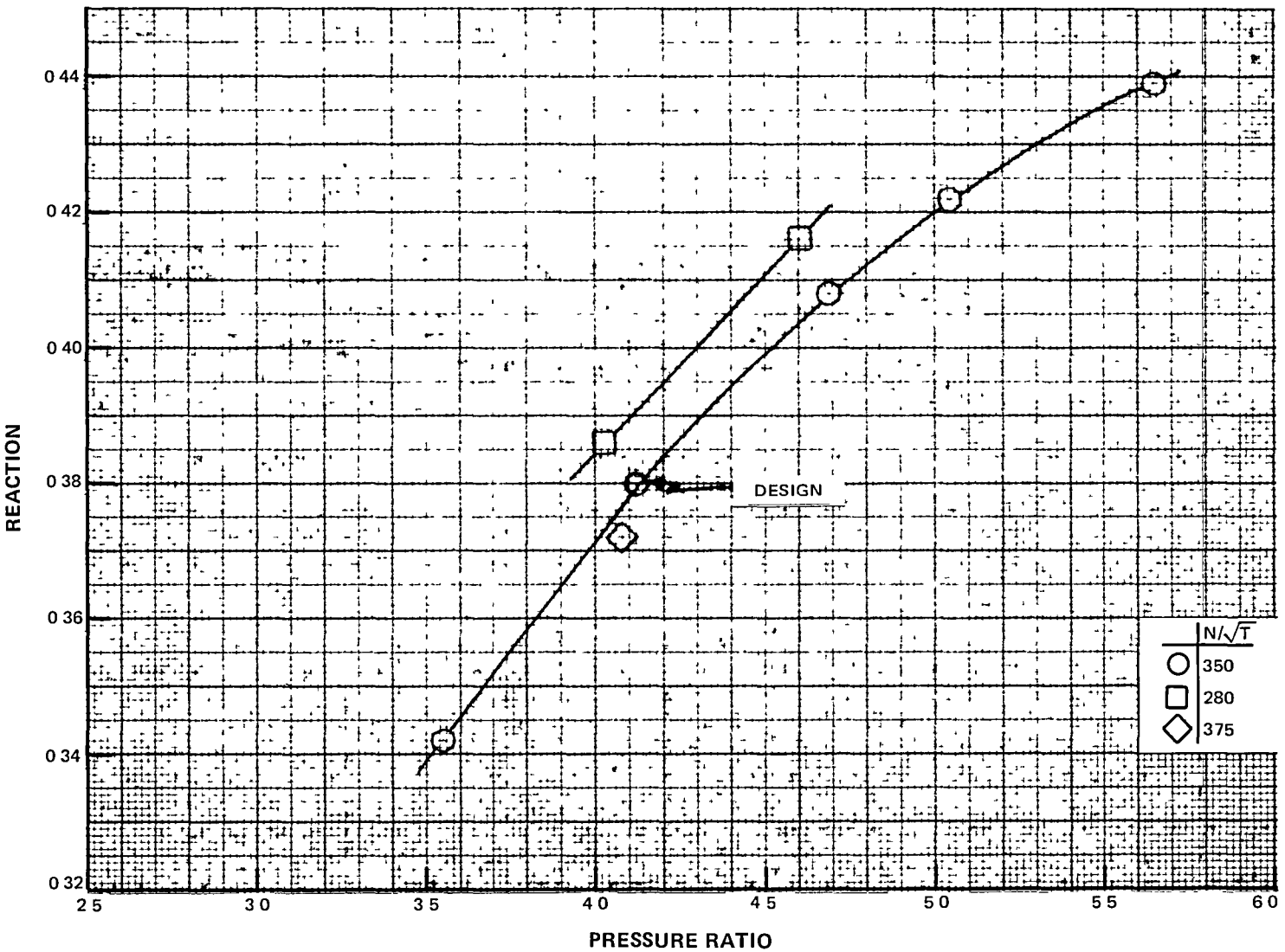

F-4 EEE Uncooled Rig 43% Reaction Rotating Rig Reaction vs. Pressure Ratio (Area Averaged)

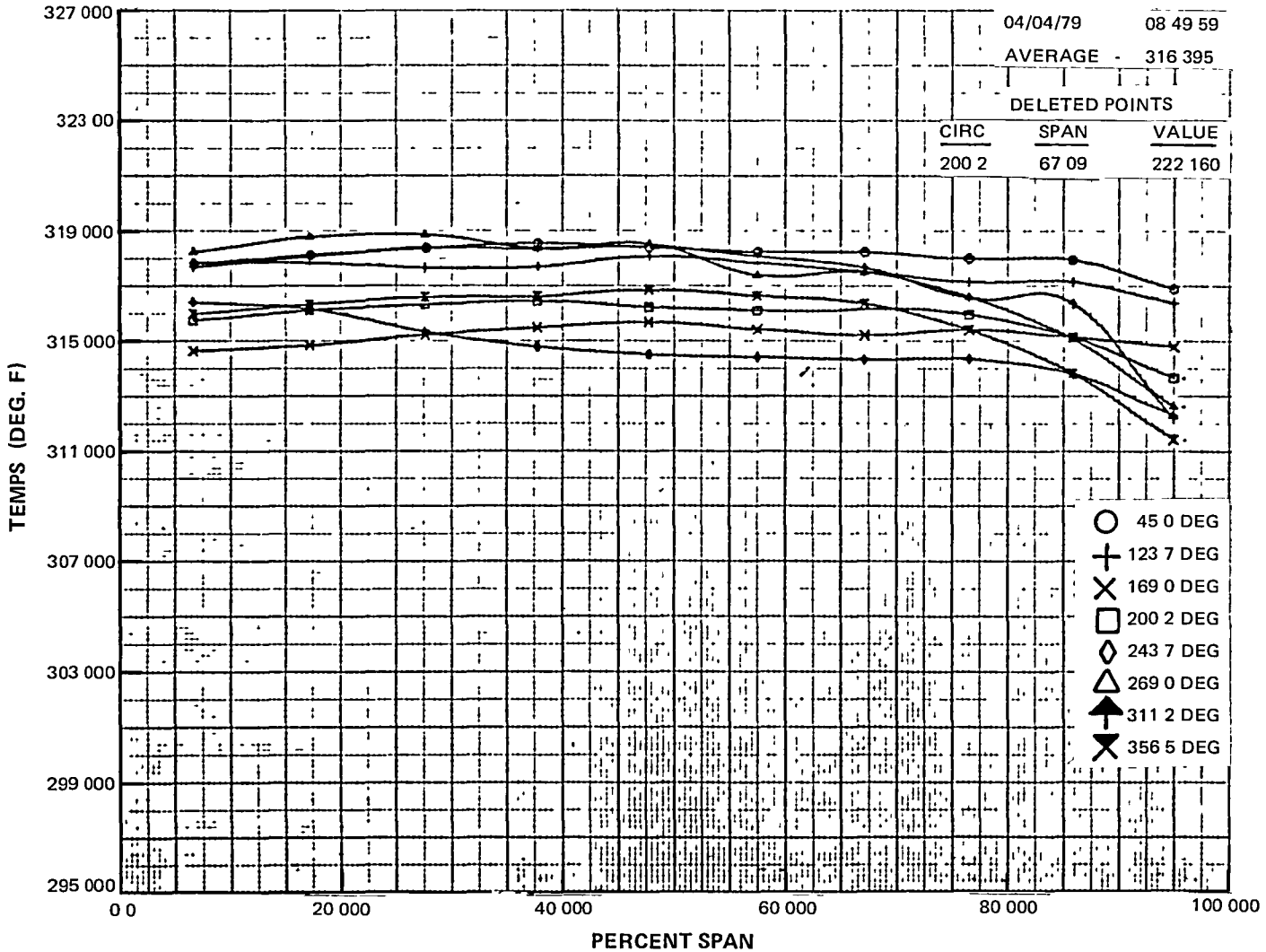

F-5 EEE Uncooled Rig 43% Reaction Rotating Rig Inlet Temperature vs. Span (Area Averaged)

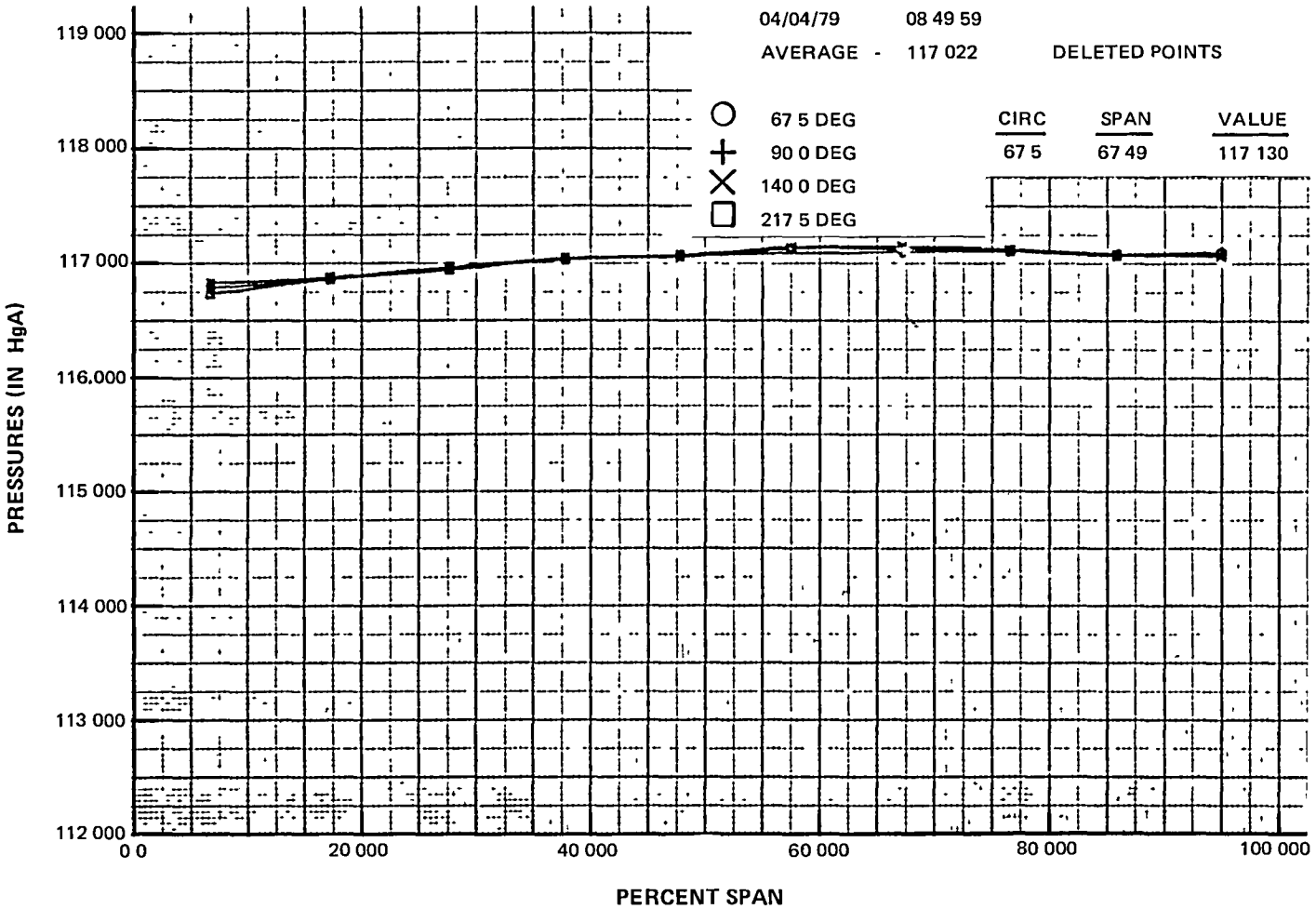

F-6 EEE Uncooled Rig 43% Reaction Rotating Rig Inlet Pressure vs. Span (Area Averaged)

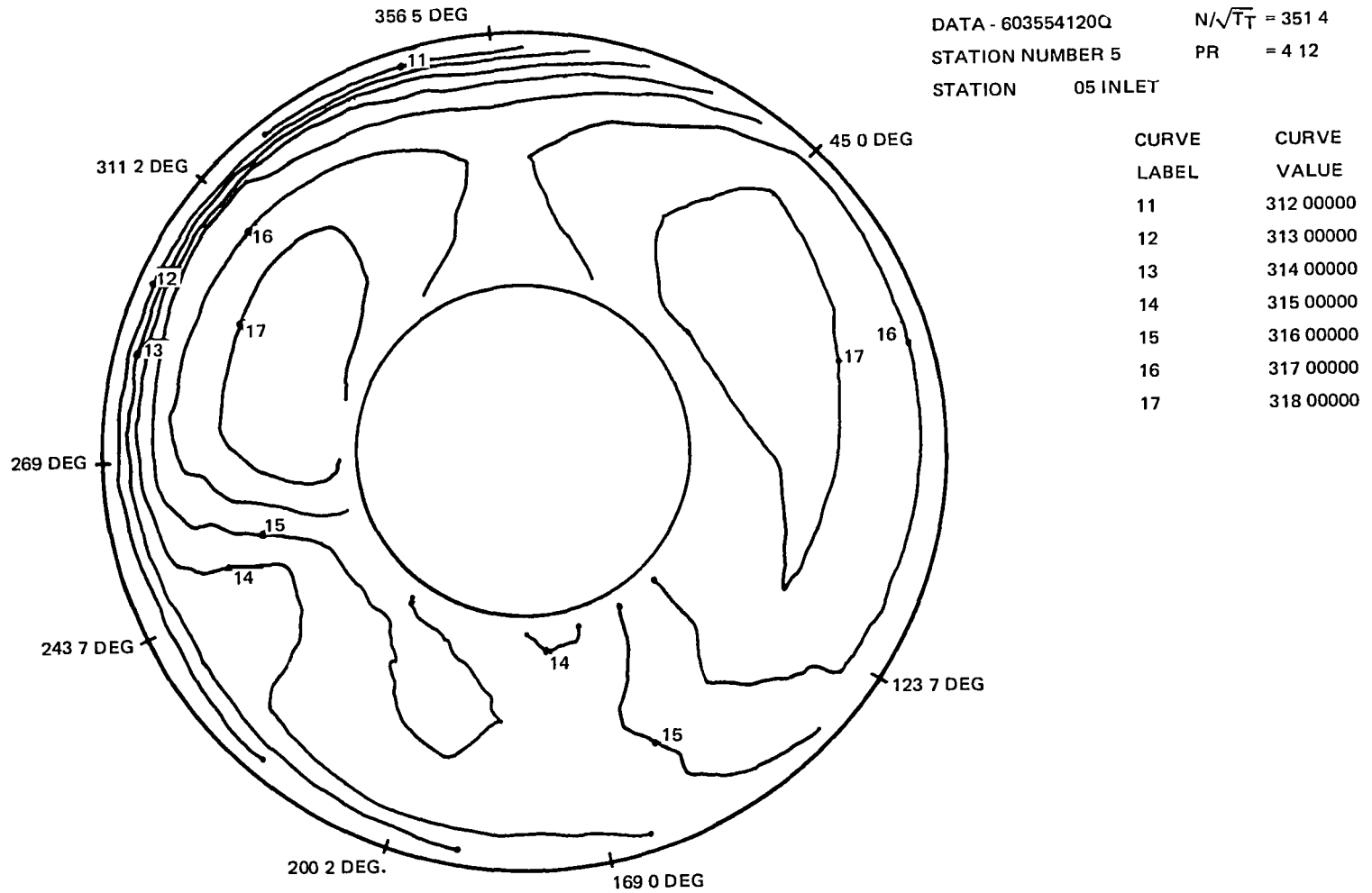

F-7 EEE Uncooled Rig 43% Reaction Rotating Rig Inlet Temperature Contours

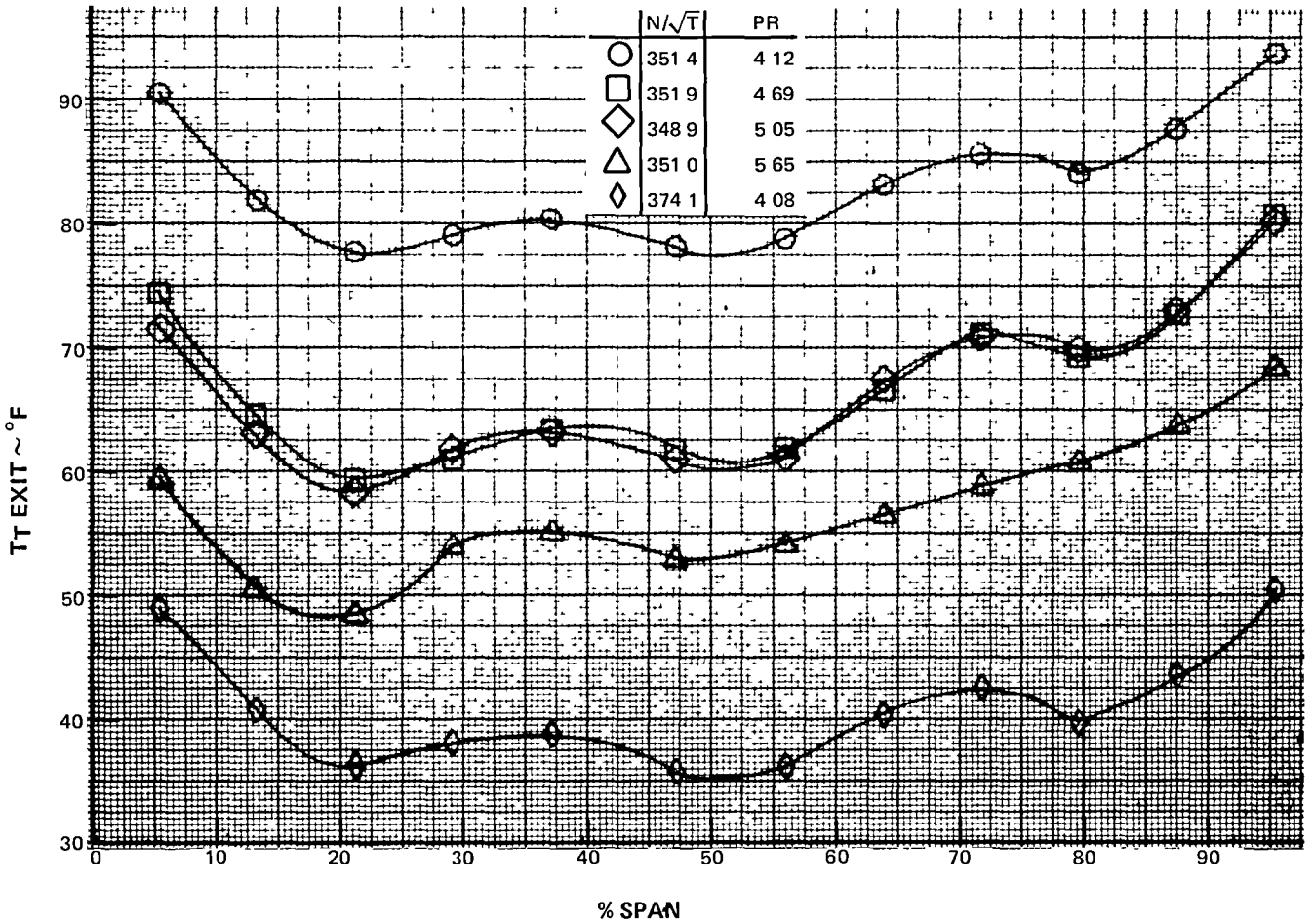

F-8 EEE Uncooled Rig 43% Reaction Rotating Rig Exit Temperature vs. Span

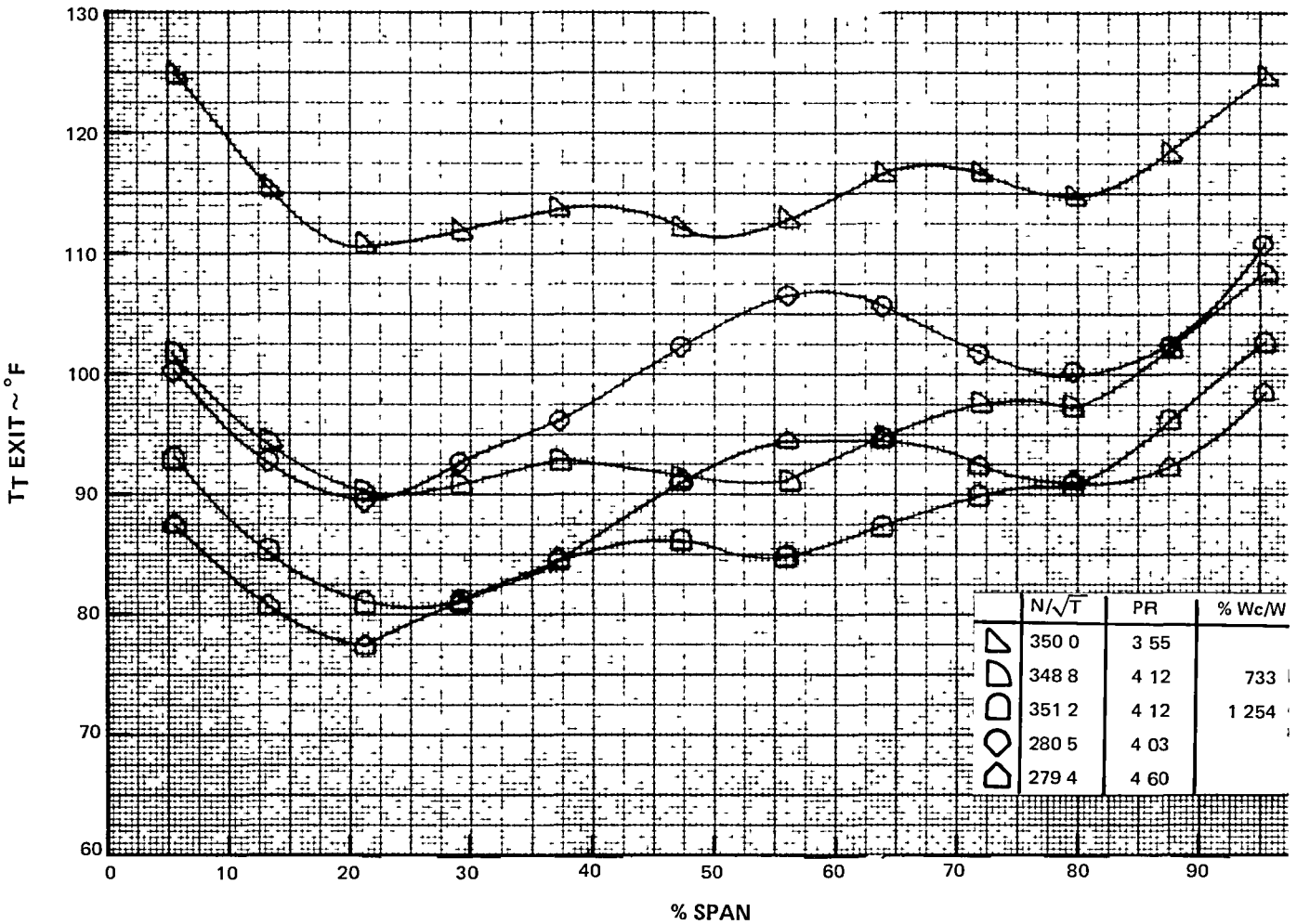

F-9 EEE Uncooled Rig 43% Reaction Rotating Rig Exit Temperature vs. Span

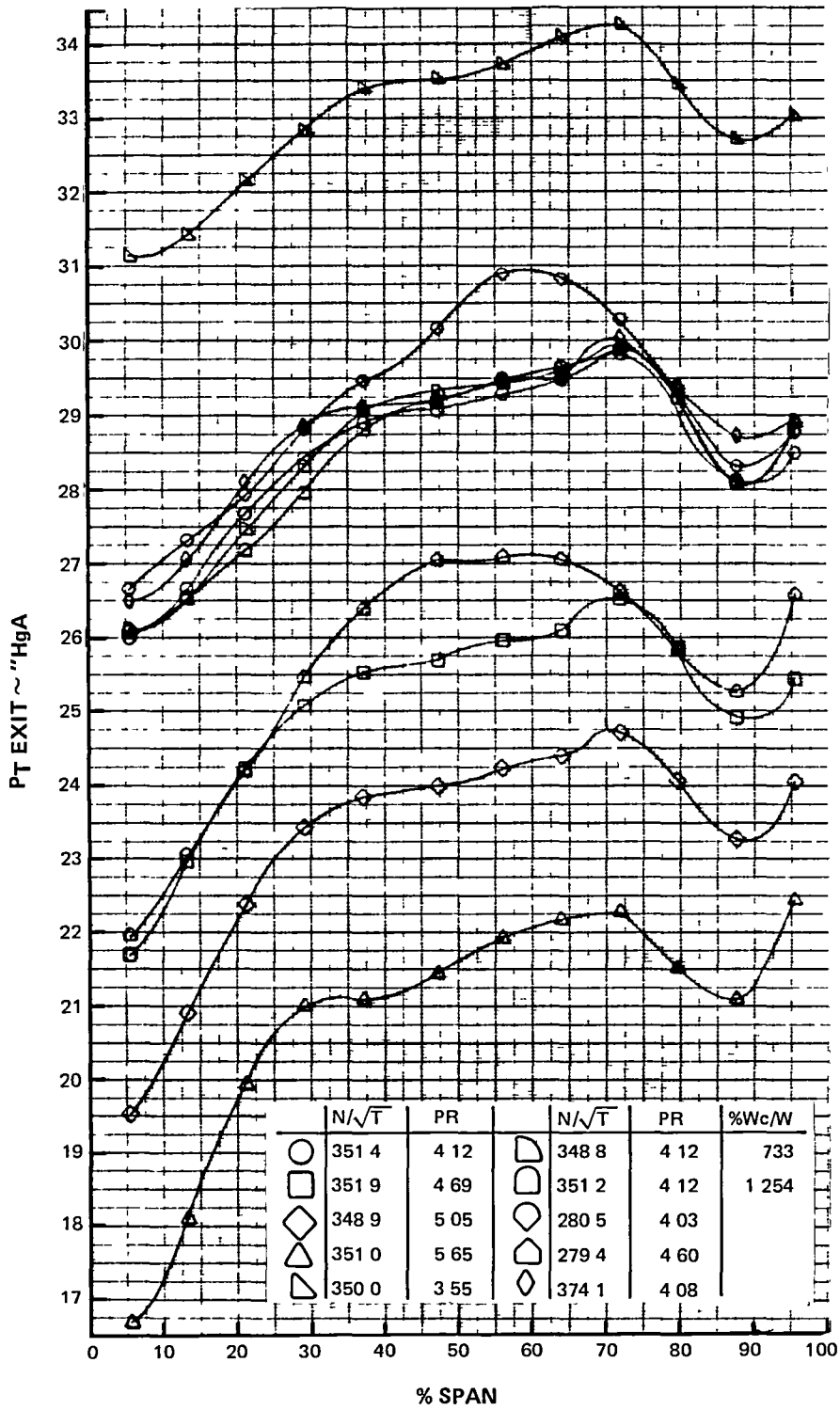

F-10 EEE Uncooled Rig 43% Reaction Rotating Rig Exit Pressure vs. Span

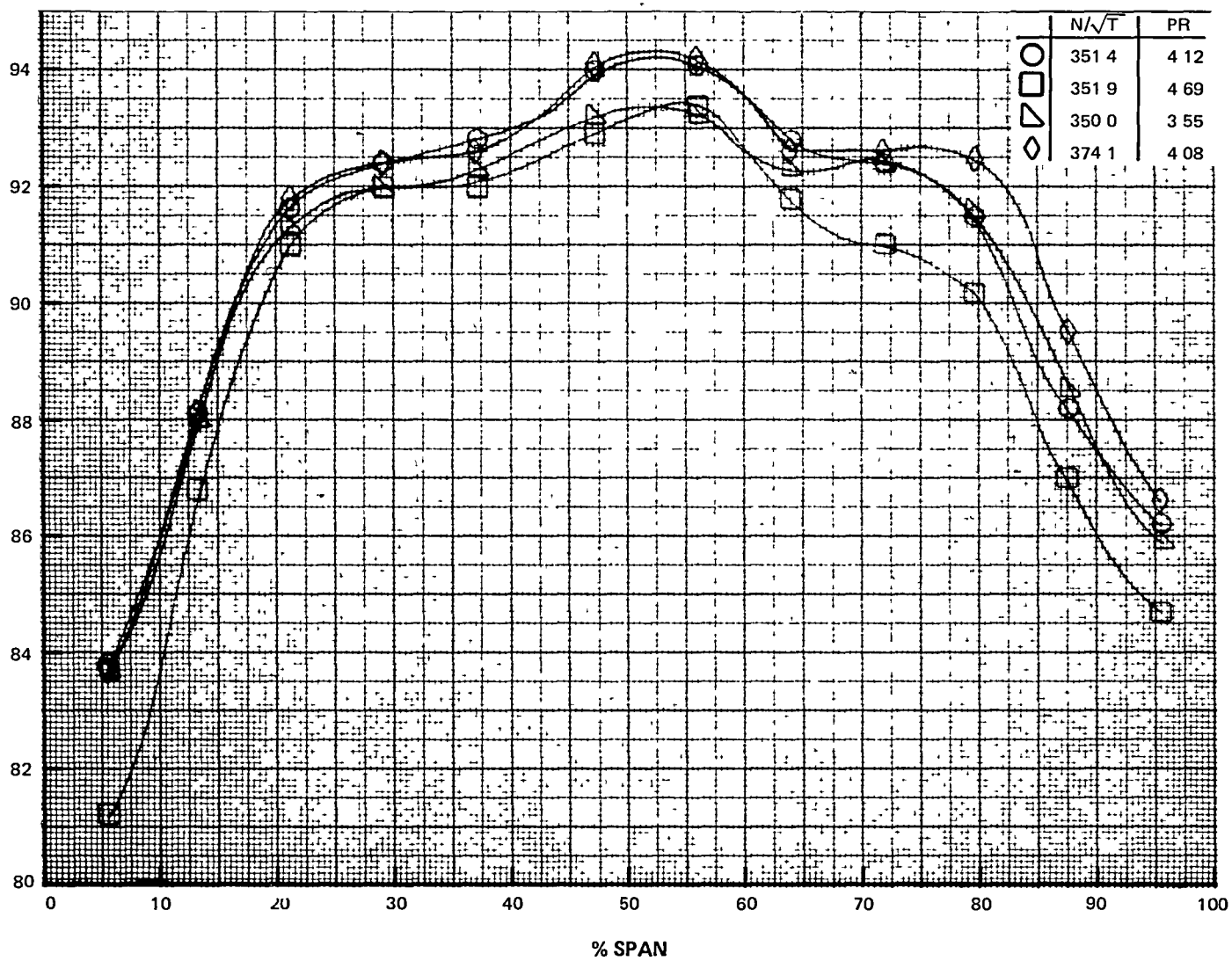

F-11 EEE Uncooled Rig 43% Reaction Rotating Rig Spanwise Efficiency (Area Averaged)

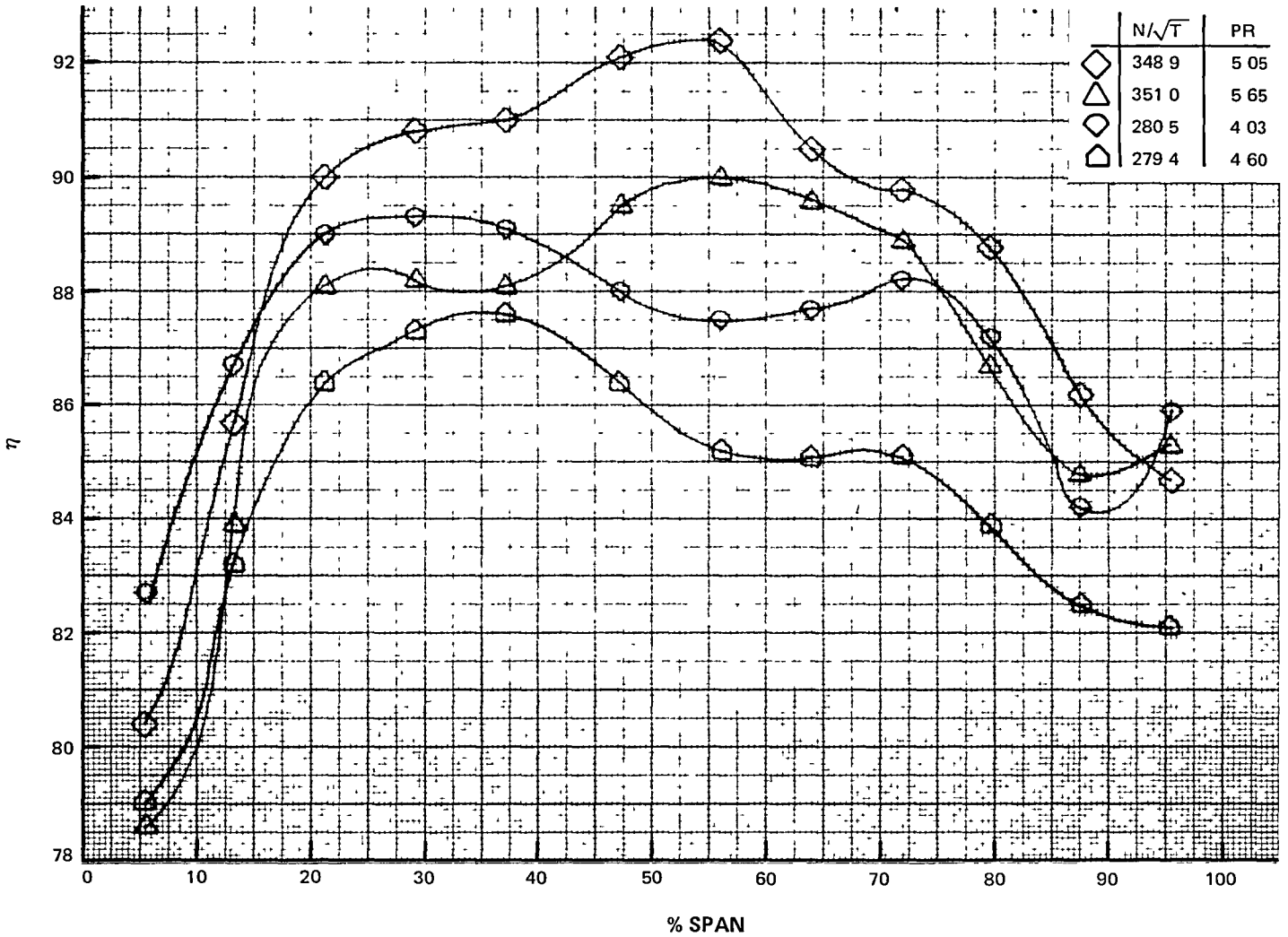

F-12 EEE Uncooled Rig 43% Reaction Rotating Rig Spanwise Efficiency (Area Averaged)

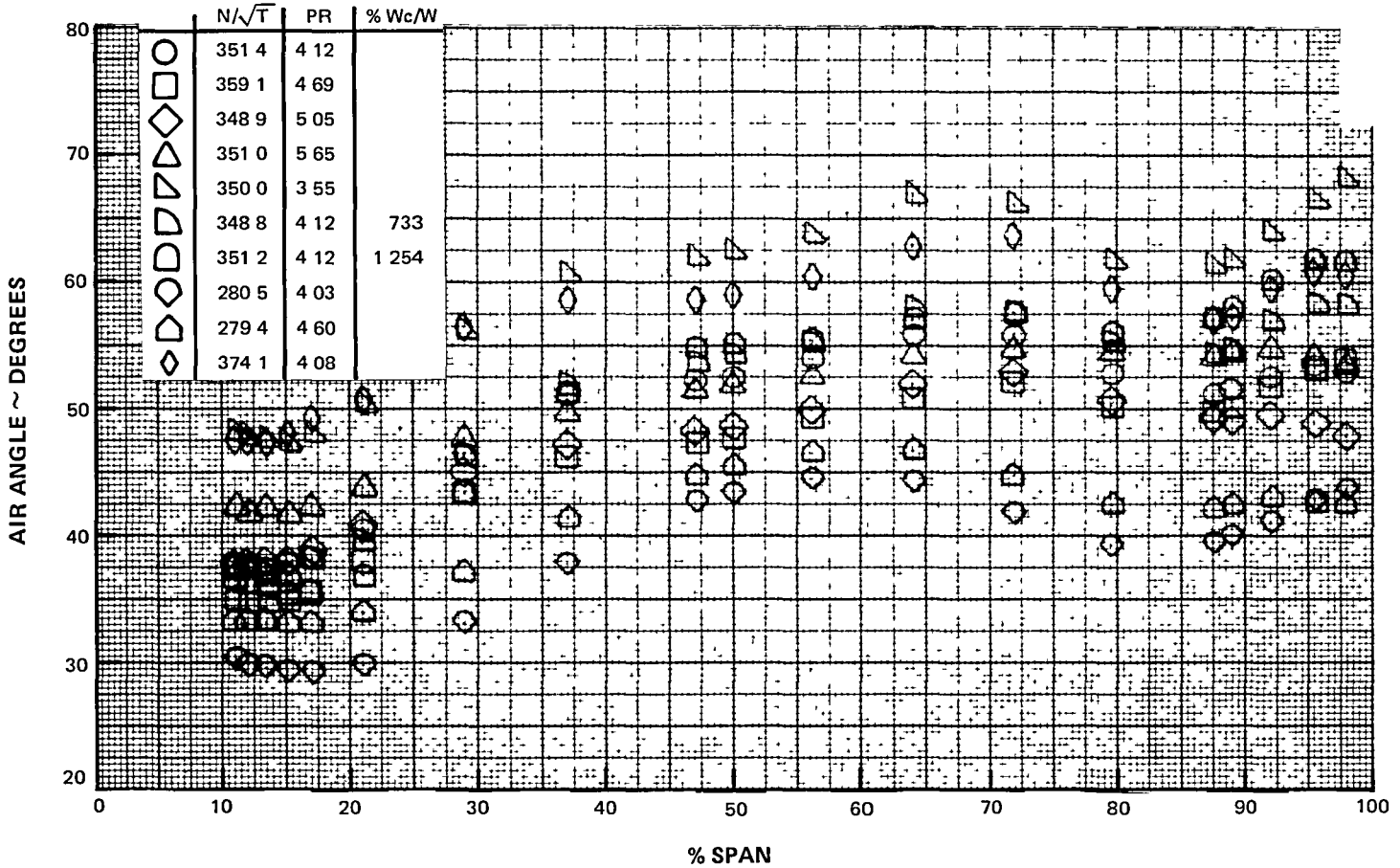

F-13 EEE Uncooled Rig 43% Reaction Rotating Rig Exit Air Angle vs. % Span at Circ. = 91.6 degrees

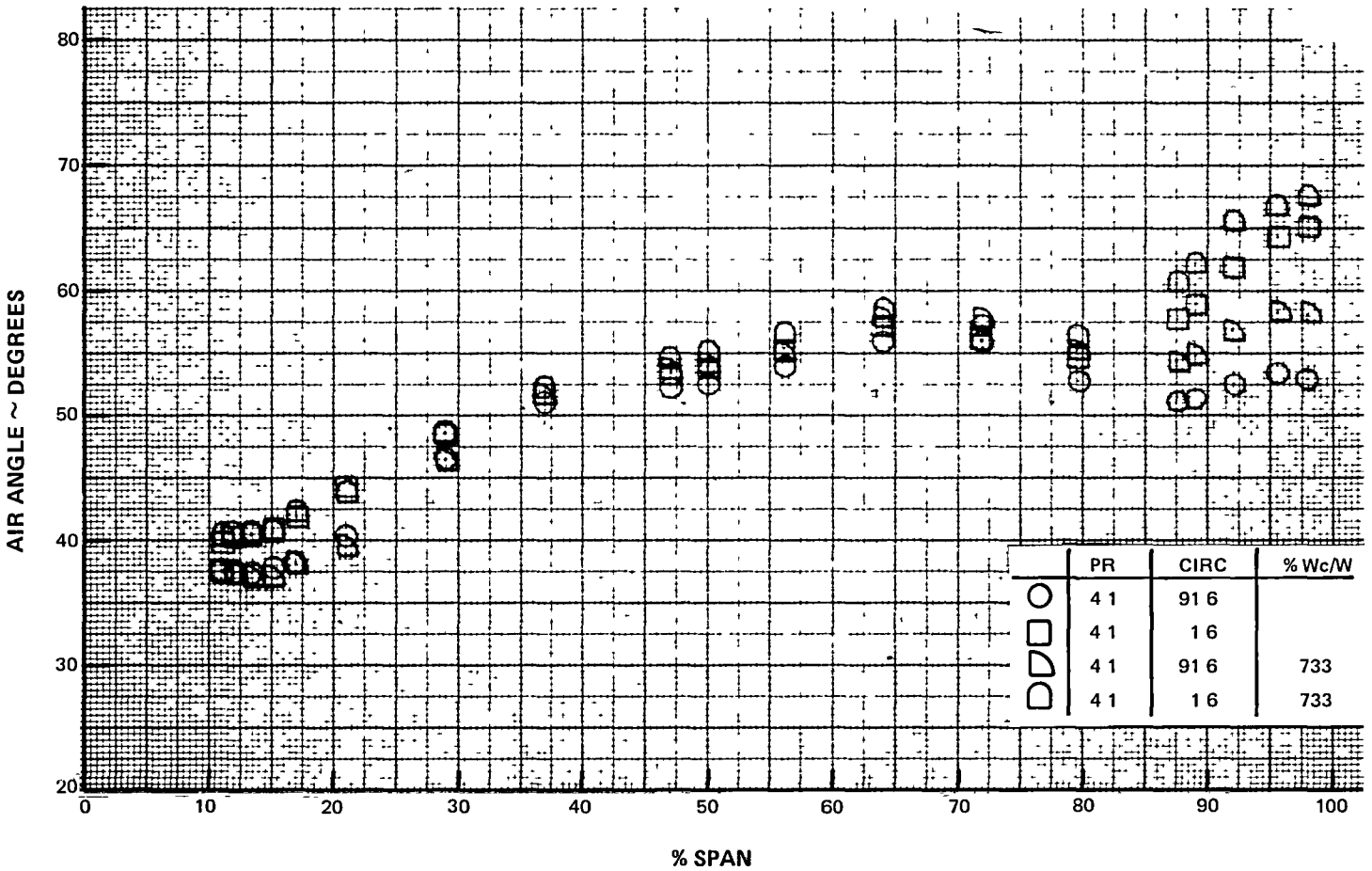

F-14 EEE Uncooled Rig 43% Reaction Rotating Rig Exit Air Angle vs. % Span at N/sq.rt. T = 350

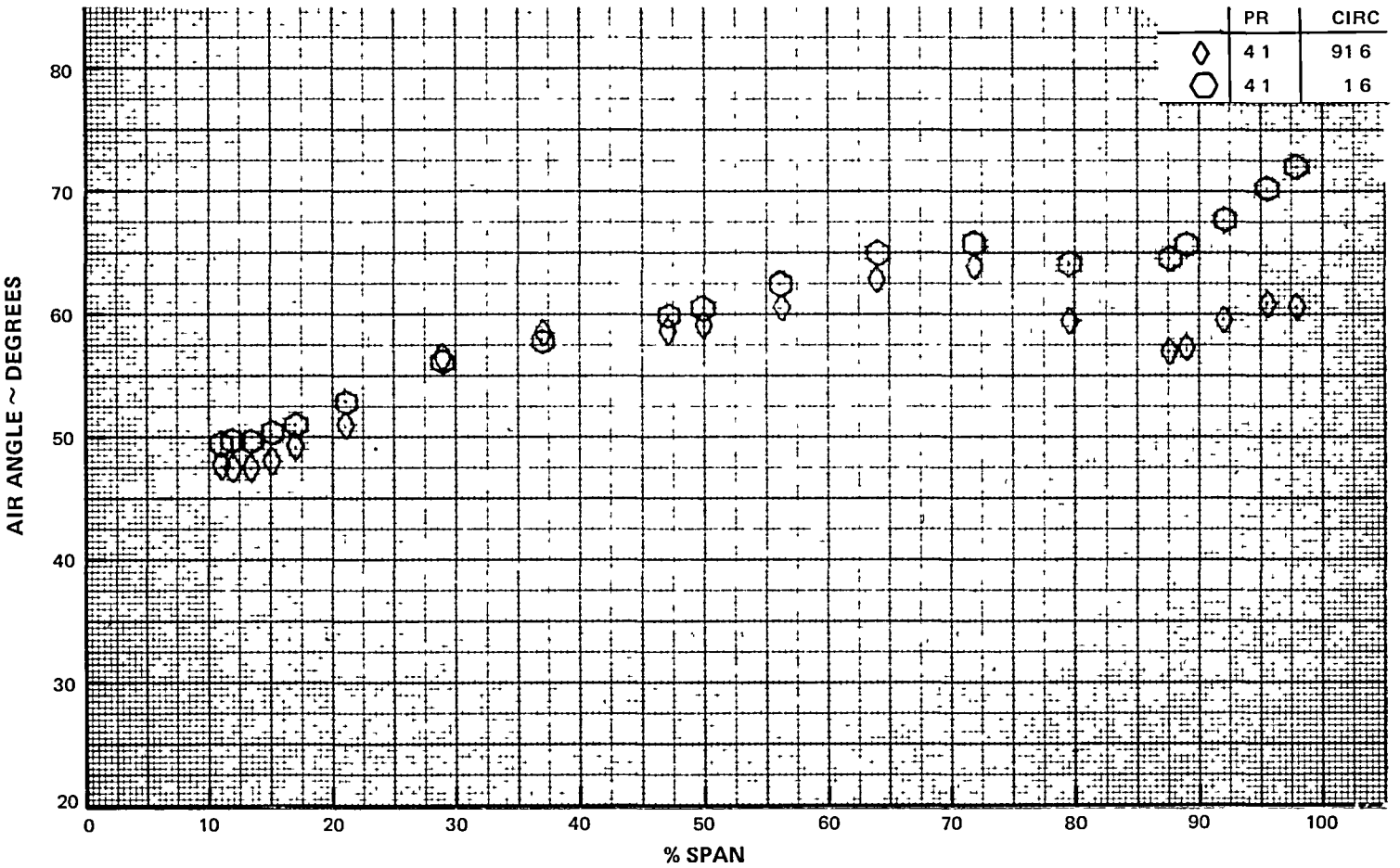

F-15 EEE Uncooled Rig 43% Reaction Rotating Rig Exit Air Angle vs. % Span at N/sq.rt. T = 375

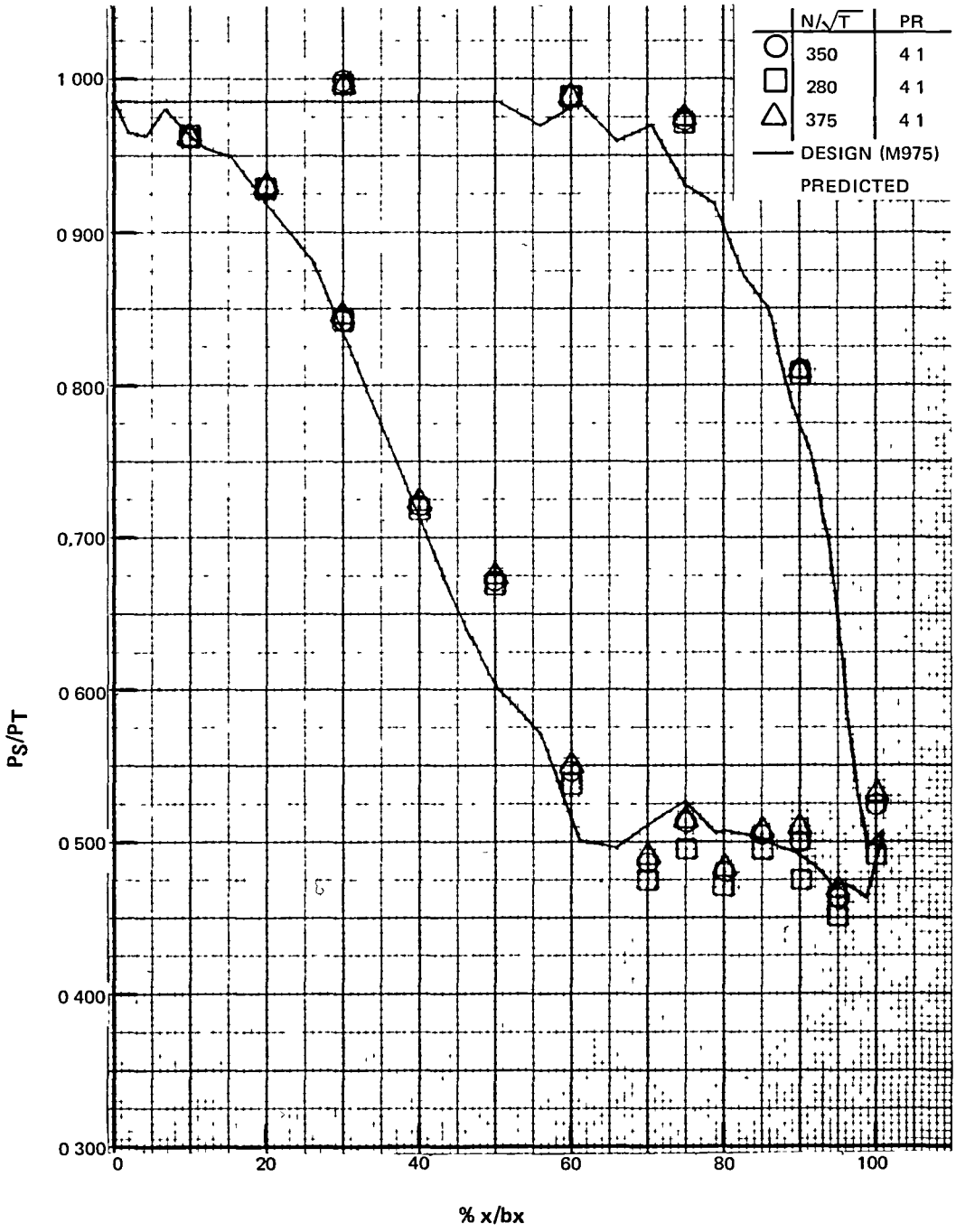

F-16 EEE Uncooled Rig 43% Reaction Rotating Rig Vane Surface Statics - 11% Span

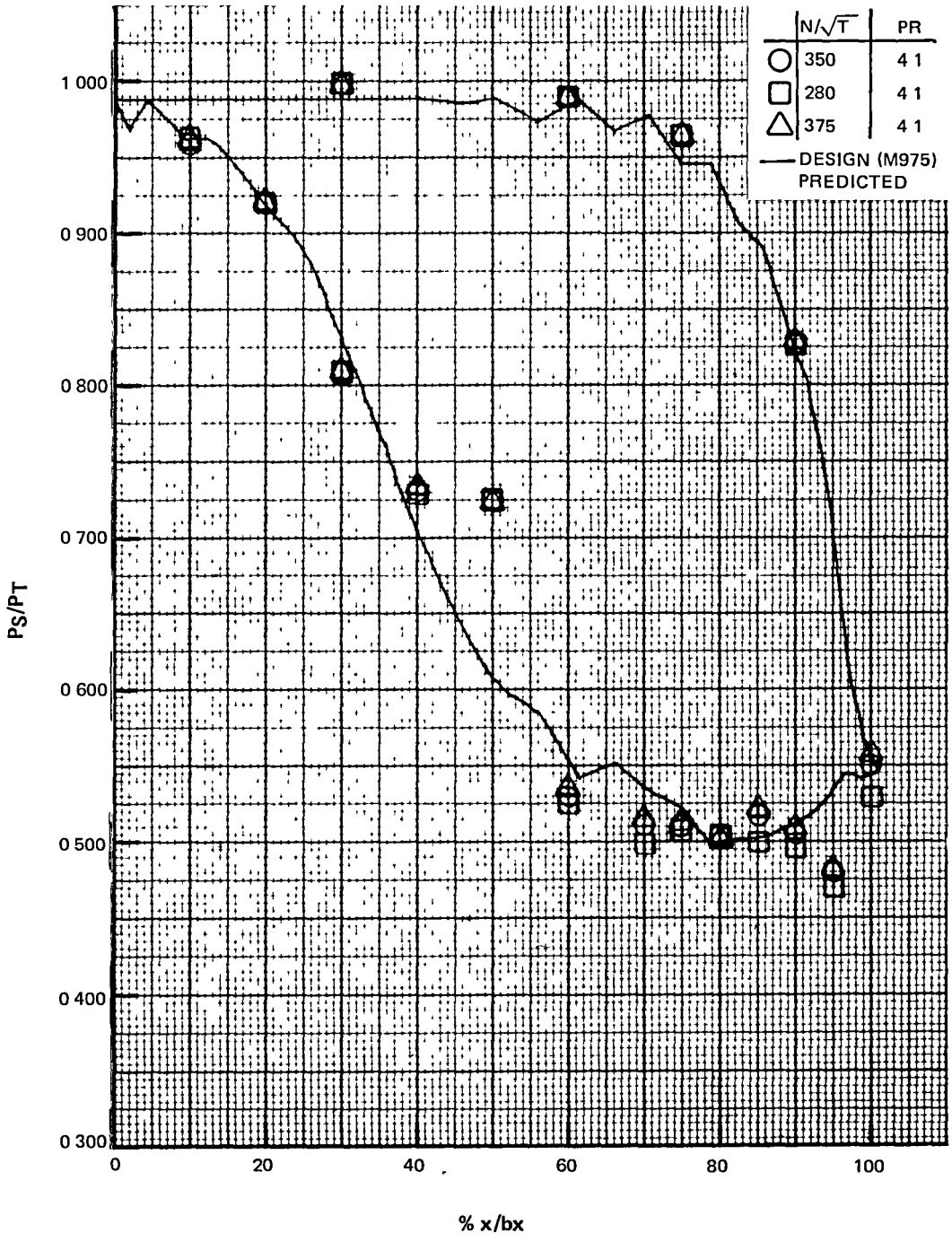

F-17 EEE Uncooled Rig 43% Reaction Rotating Rig Vane Surface Statics - 50% Span

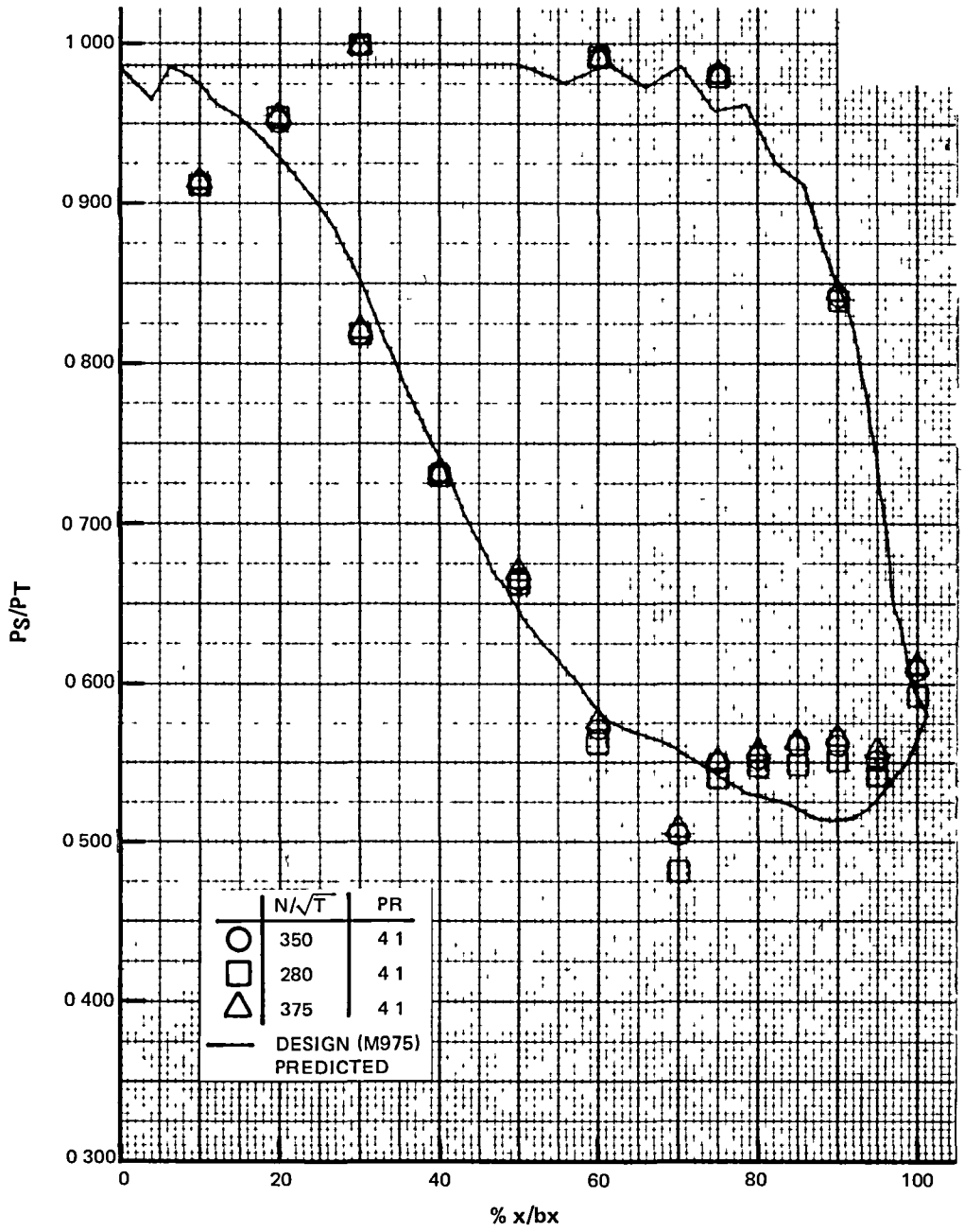

F-18 EEE Uncooled Rig 43% Reaction Rotating Rig Vane Surface Statics - 89% Span

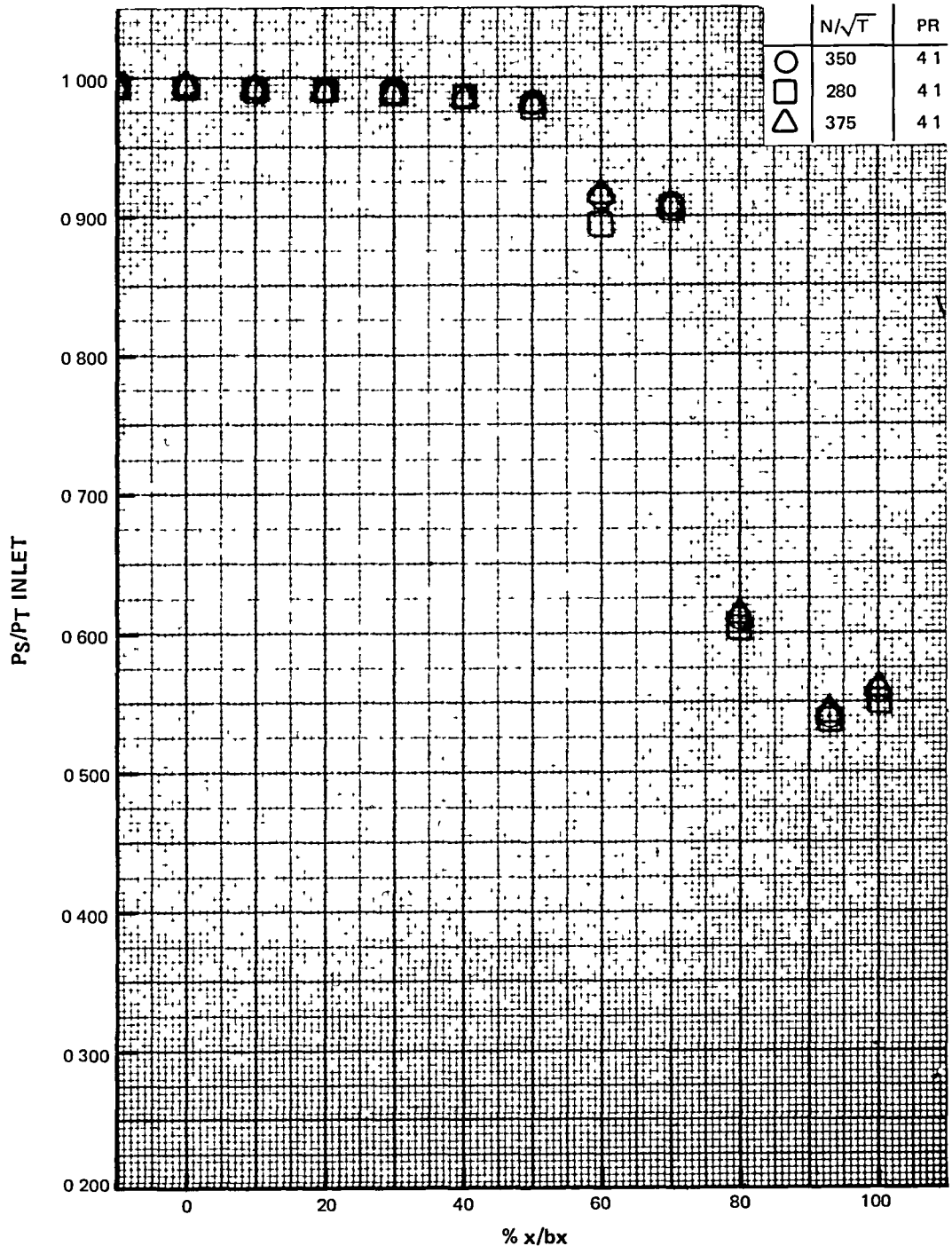

F-19 EEE Uncooled Rig 43% Reaction Rotating Rig Mid Gap O.D. Statics vs. % x/bx

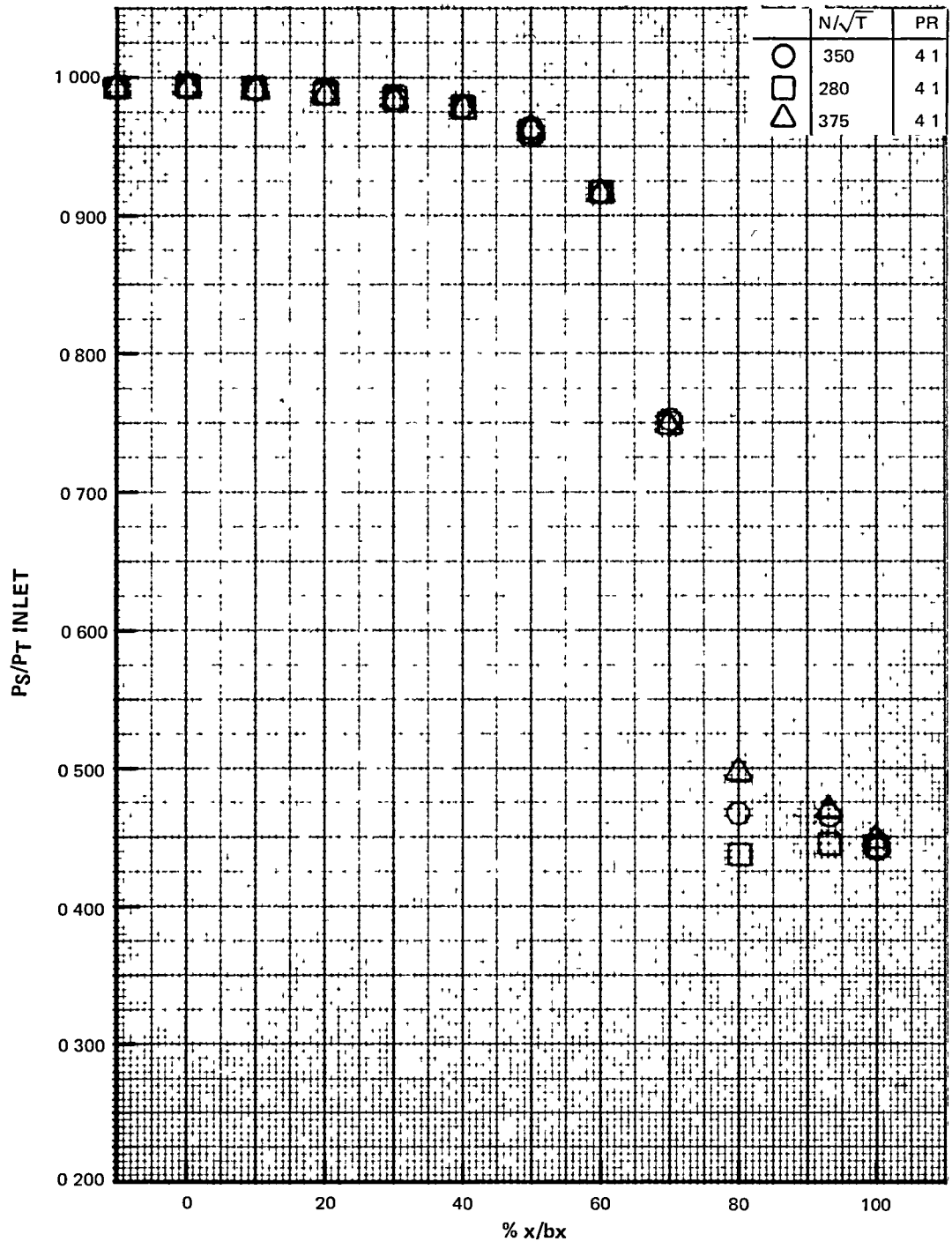

F-20 EEE Uncooled Rig 43% Reaction Rotating Rig Mid Gap O.D. Statics vs. % x/bx

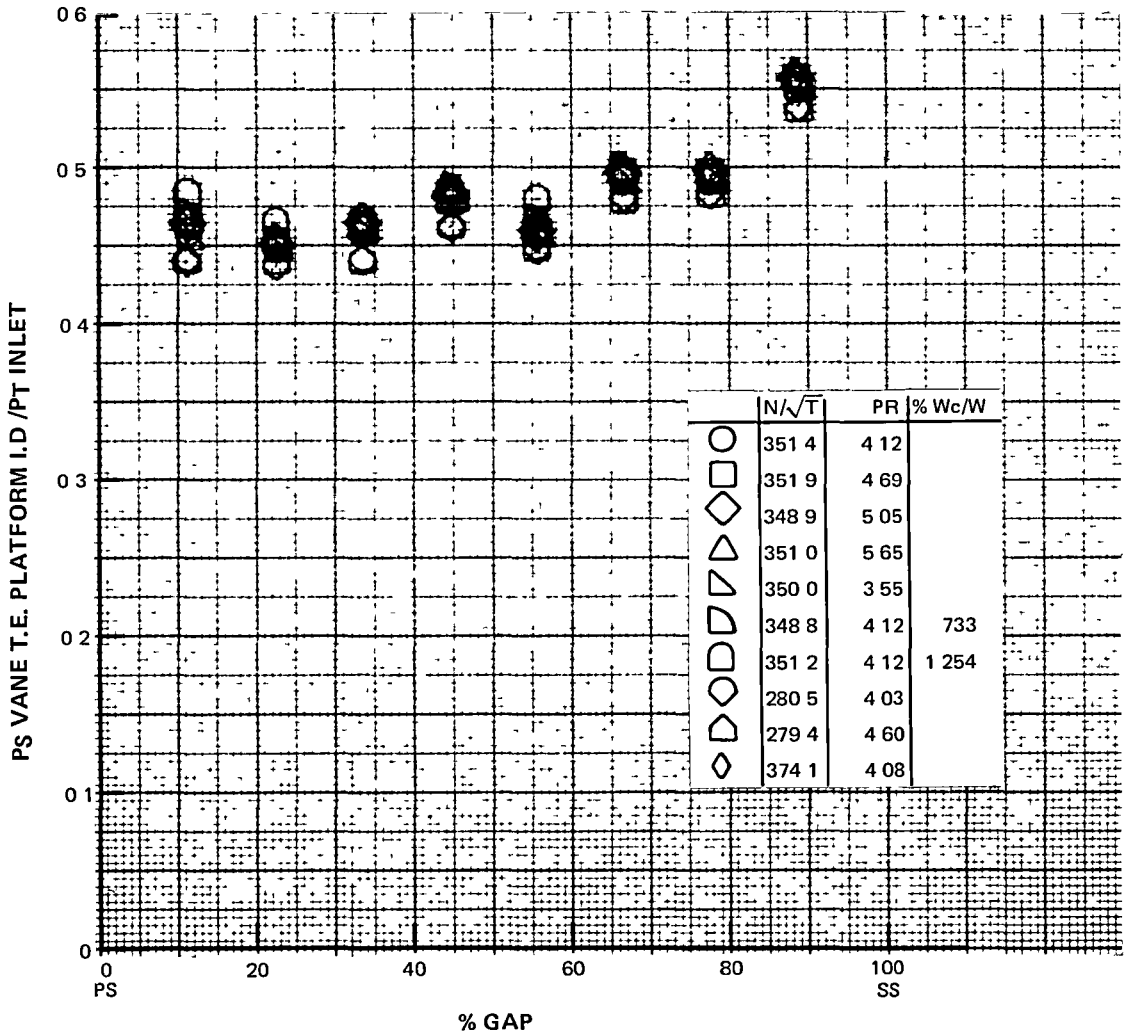

F-21 EEE Uncooled Rig 43% Reaction Rotating Rig I.D. Platform Ps vs. % Gap

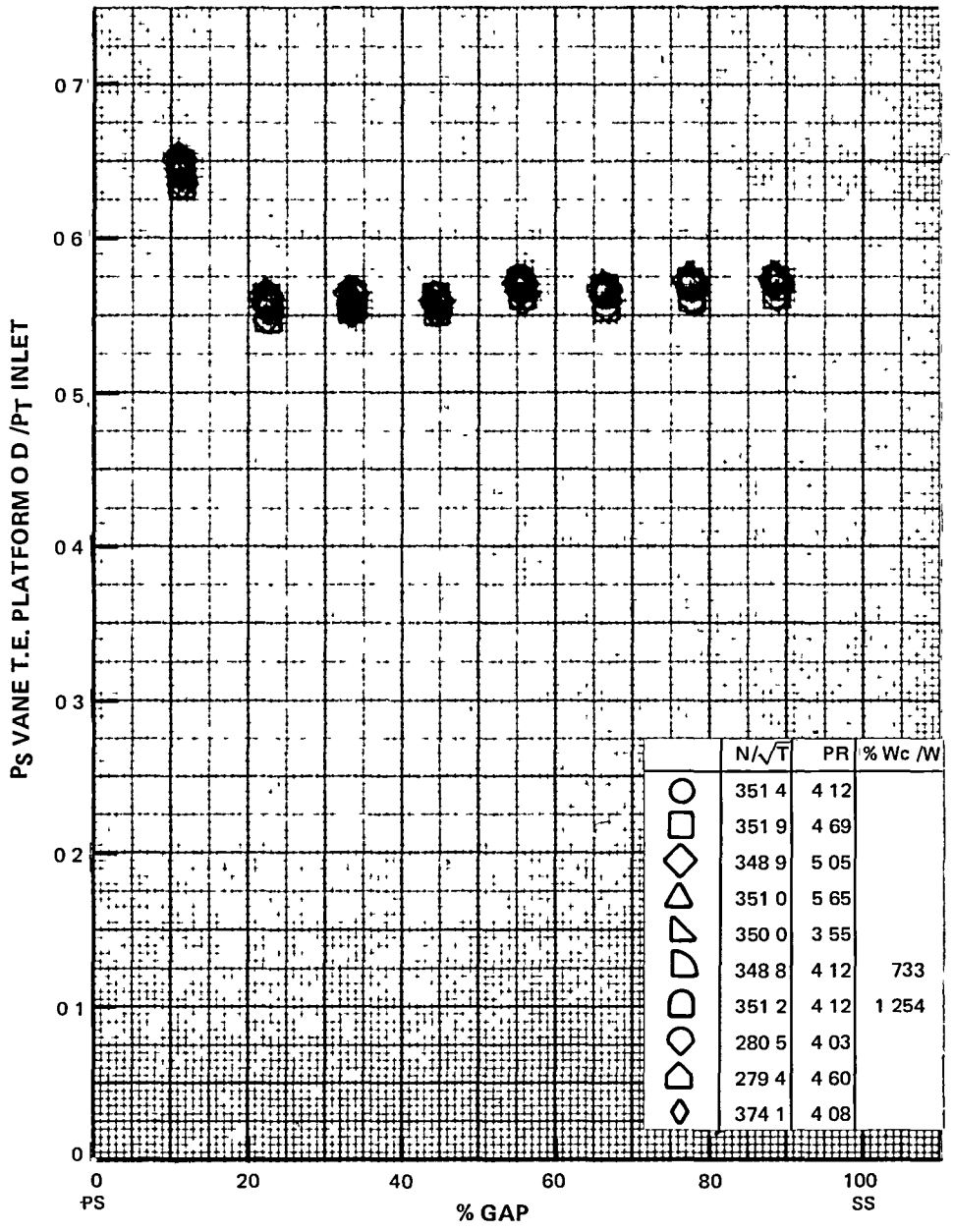

F-22 EEE Uncooled Rig 43% Reaction Rotating Rig O.D. Platform Ps vs. % Gap

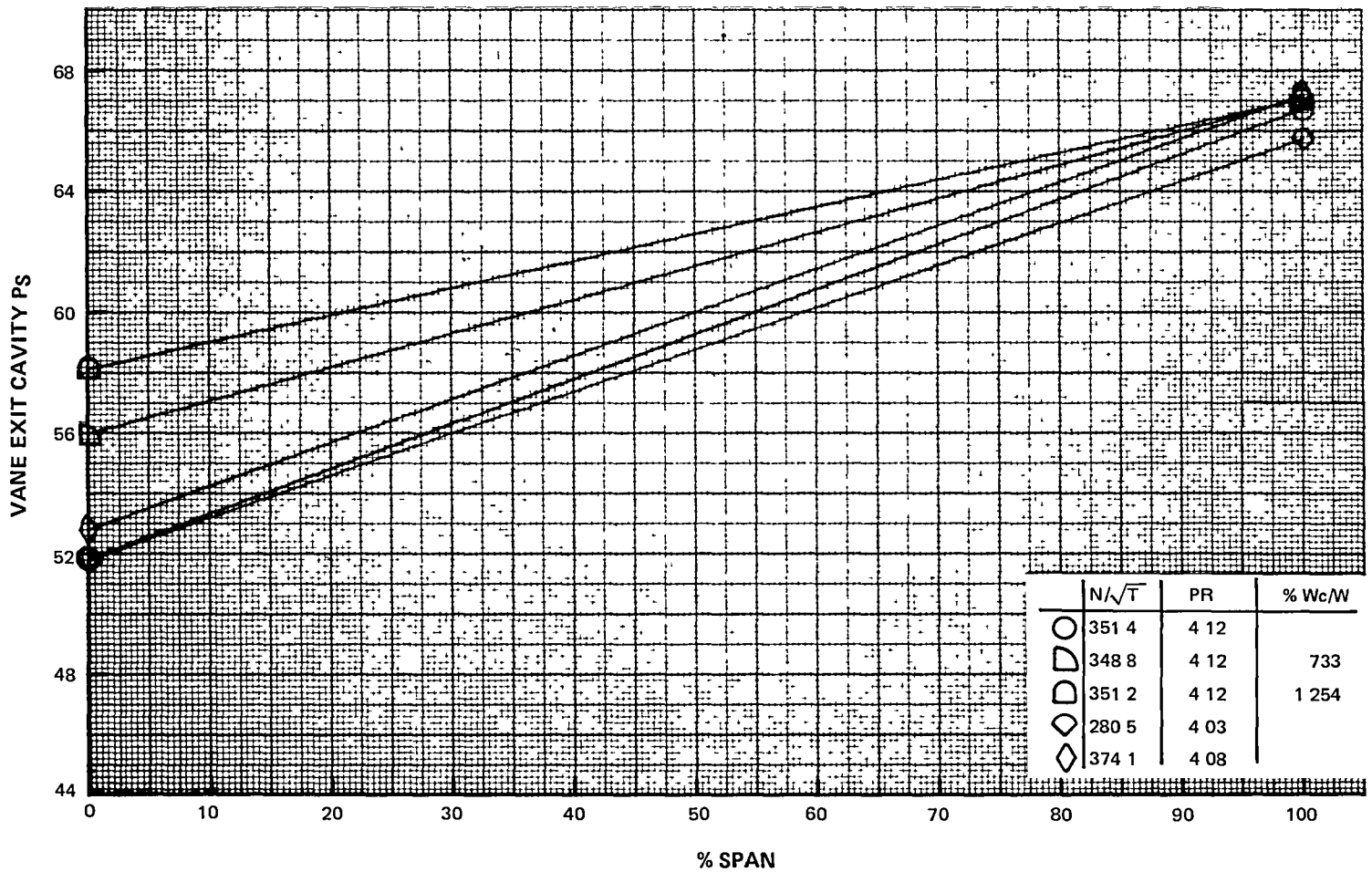

F-23 EEE Uncooled Rig 43% Reaction Rotating Rig Vane Exit Cavity vs. % Span

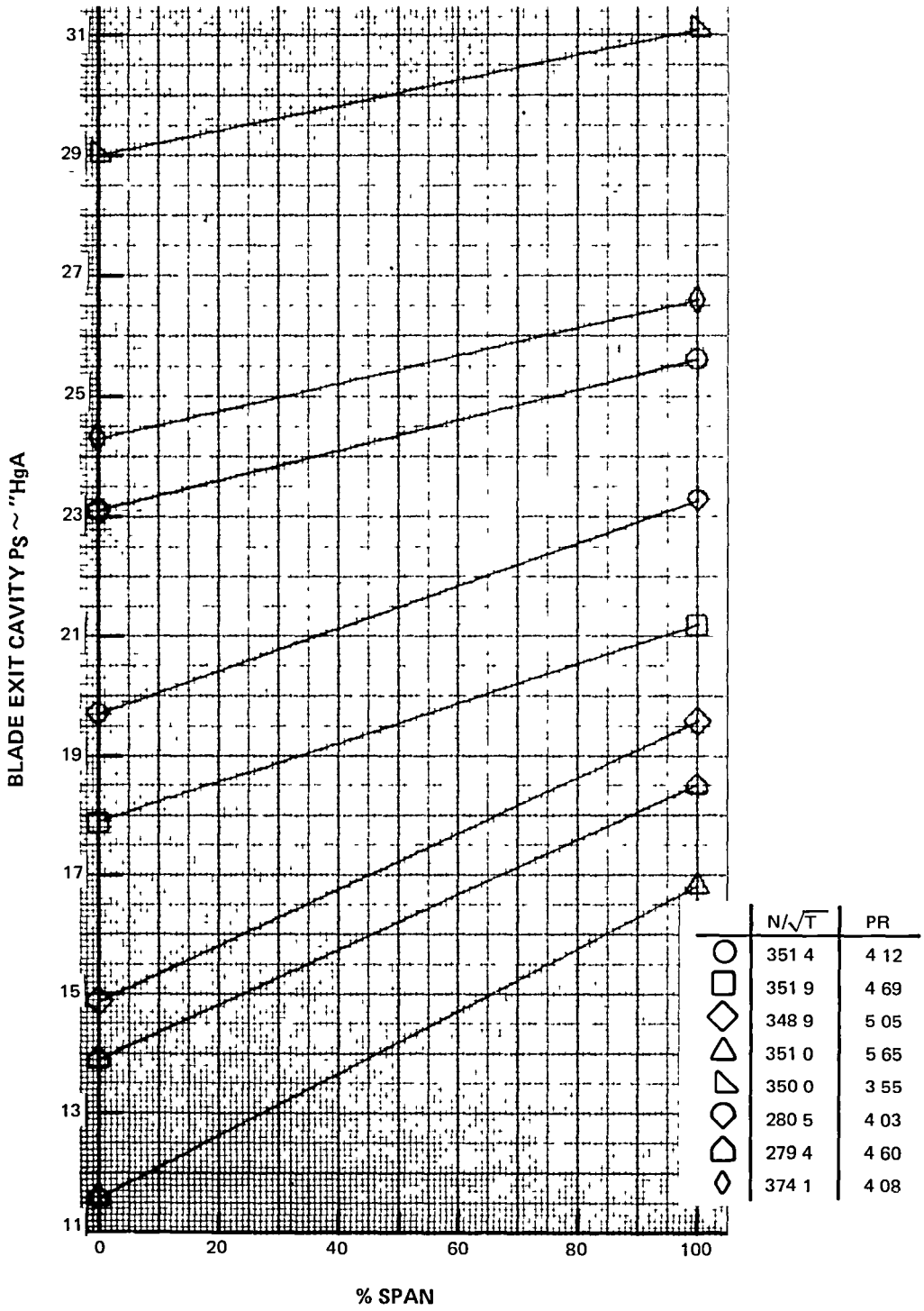

F-24 EEE Uncooled Rig 43% Reaction Rotating Rig Blade Exit Cavity vs. % Span

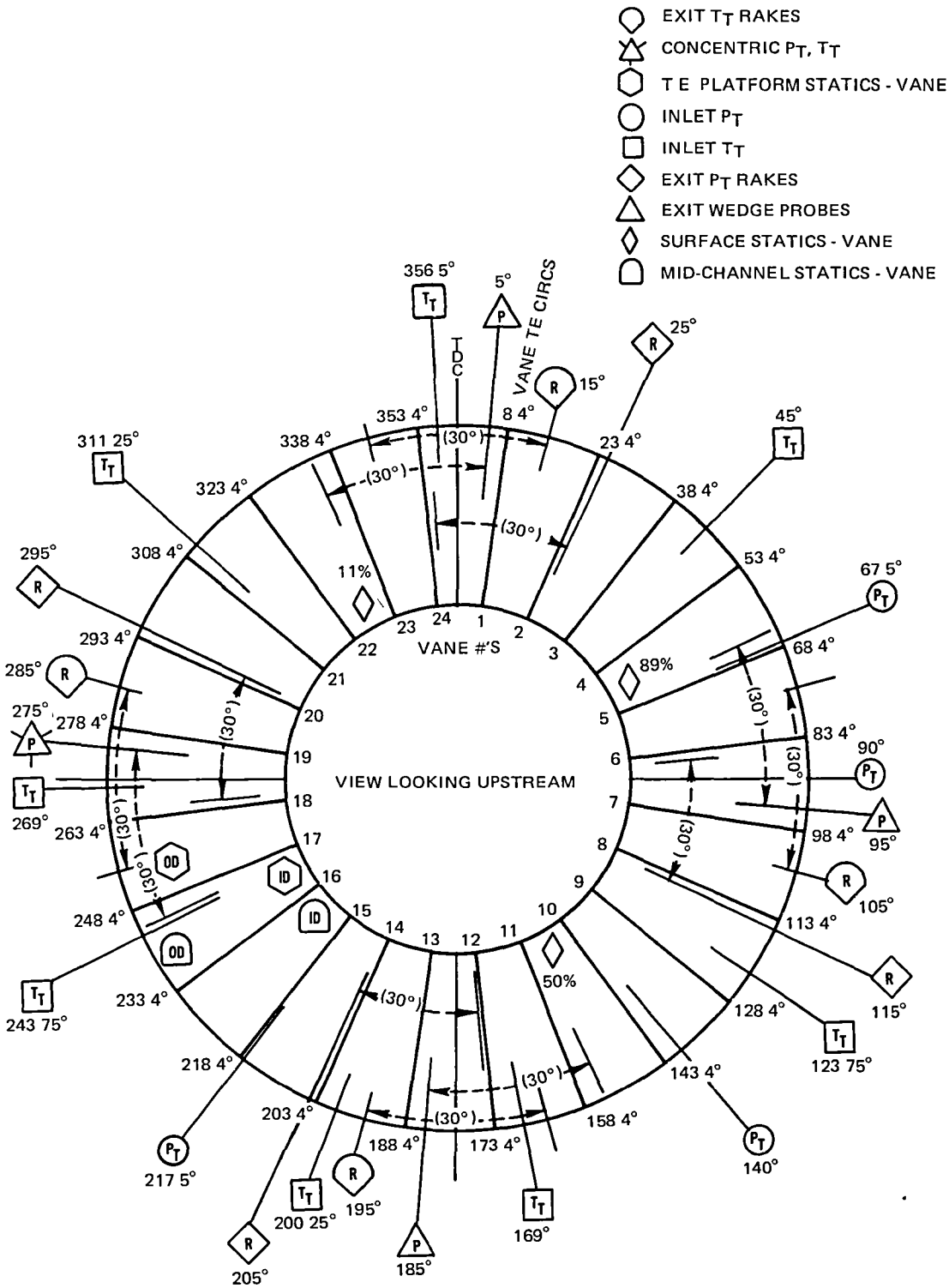

F-25 EEE Uncooled Rig 43% Reaction Rotating Rig Circumferential Instrumentation Location

This Page Intentionally Left Blank

NASA Headquarters
600 Independence Ave , S W
Washington, DC 20546
Attn RTP-6 R S Colladay

NASA-Lewis Research Center
21000 Brookpark Road
Cleveland, OH 44135
C C Ciepluch, MS 301-4 (20 cop)

NASA-Lewis Research Center
21000 Brookpark Road
Cleveland, OH 44135
Library, MS 60-3 (2 copies)

NASA-Lewis Research Center
21000 Brookpark Road
Cleveland, OH 44135
Attn M A Beheim, MS 86-1

NASA-Lewis Research Center
21000 Brookpark Road
Cleveland, OH 44135
Tech Utilization Off , MS 3-19

NASA-Lewis Research Center
21000 Brookpark Road
Cleveland, OH 44135
Attn W M Braithwaite, MS 60-6

NASA-Lewis Research Center
21000 Brookpark Road
Cleveland, OH 44135
Attn J O VanVleet, MS 21-4

NASA Scien and Tech Inf Fac.
P O Box 33
College Park, Maryland 20740
Aquisition Branch (10 Copies)

NASA Dryden Flight Research Ctr
P O Box 273
Edwards, California 93523
Attn Library

Department of Defense
Washington, D C 20301
Attn R Standahar
3D1089 Pentagon

Wright-Patterson Air Force Base
Dayton, OH 45433
Attn E E Bailey (NASA Liaison)
AFAPL/DO

NASA Headquarters
600 Independence Ave , S W
Washington, DC 20546
Attn RJP-2 D J Poferl (2 Cop)

NASA-Lewis Research Center
21000 Brookpark Road
Cleveland, OH 44135
Attn D L Nored, MS 301-2

NASA-Lewis Research Center
21000 Brookpark Road
Cleveland, OH 44135
Report Control Office MS 5-5

NASA-Lewis Research Center
21000 Brookpark Road
Cleveland, OH 44135
Attn R W. Schroeder, MS 500-207

NASA-Lewis Research Center
21000 Brookpark Road
Cleveland, OH 44135
AFSC Liasion Office MS 501-3

NASA-Lewis Research Center
21000 Brookpark Road
Cleveland, OH 44135
Attn A J Glassman, MS 77-2

NASA-Lewis Research Center
21000 Brookpark Road
Cleveland, OH 44135
Attn L Reid, MS 5-9

NASA Ames Research Center
Moffett Field, CA 94035
Attn 202-7/M H Waters

NASA Langley Research Center
Langley Field, VA 23365
Attn Library

Wright-Patterson Air Force Base
Dayton, OH 45433
Attn R P Carmichael
ASD/XRHI

Wright-Patterson Air Force Base
Dayton, OH 45433
Attn H J P VonOhain
AFAPL/CCN

NASA Headquarters
600 Independence Ave , S W
Washington, DC 20546
Attn RTM-6/L Harris

NASA-Lewis Research
21000 Brookpark Road
Cleveland, OH 44135
Attn J W Schaefer, MS 301-4

NASA-Lewis Research Center
21000 Brookpark Road
Cleveland, OH 44135
Attn M J Hartmann MS 5-3

NASA-Lewis Research Center
21000 Brookpark Road
Cleveland, OH 44135
Attn N T Saunders

NASA-Lewis Research Center
21000 Brookpark Road
Cleveland, OH 44135
Attn R J Weber MS 500-127

NASA-Lewis Research Center
21000 Brookpark Road
Cleveland, OH 44135
Attn D C Mikkelson, MS 86-1

NASA-Lewis Research Center
21000 Brookpark Road
Cleveland, OH 44135
Attn R W. Graham, MS 77-2

NASA Ames Research Center
Moffett Field, CA 94035
Attn 202-7/L J Williams

NASA Langley Research Center
Langley Field, VA 23365
Attn D Maiden

Wright-Patterson Air Force Base
Dayton, OH 45433
Attn R Ellis
ASD/YZN

Wright-Patterson Air Force Base
Dayton, OH 45433
Attn E C Simpson
AFAPL/TB

NASA Headquarters
600 Independence Avenue, SW
Washington, DC 20546
Attn Library

NASA-Lewis Research
21000 Brookpark Road
Cleveland, OH 44135
Attn L E Macioce, MS 301-4

NASA-Lewis Research Center
21000 Brookpark Road
Cleveland, OH 44135
Attn W L Stewart, MS 3-5

NASA-Lewis Research Center
21000 Brookpark Road
Cleveland, OH 44135
Attn R A. Rudey, MS 60-4

NASA-Lewis Research Center
21000 Brookpark Road
Cleveland, OH 44135
Attn T P. Moffitt, MS 77-2

NASA-Lewis Research Center
21000 Brookpark Road
Cleveland, OH 44135
Attn K E Skeels, MS 500-305

NASA-Lewis Research Center
21000 Brookpark Road
Cleveland, OH 44135
Attn Army R&T Prop Lab, MS 106-2

NASA Dryden Flight Research Ctr
P O Box 273
Edwards, CA 93523
Attn J A Albers

NASA Langley Research Center
Langley Field, VA 23365
Attn R Leonard

Wright-Patterson Air Force Base
Dayton, OH 45433
Attn Col. C.E Painter
ASD/EN

Wright-Patterson Air Force Base
Dayton, OH 45433
Attn H.I Bush
AFAPL/TB

Boeing Aerospace Co
P O Box 3999
Seattle, Washington 98124
Attn H Higgins

Lockheed California Co
Burbank, CA 91502
Attn R Tullis, Dept 75-21

Boeing Aerospace Co
P O Box 3999
Seattle, WA 98124
Attn H Higgins

Lockheed Georgia Co
Marietta, GA 30060
Attn H S Sweet

General Electric Co /AEG
One Jimson Road
Evendale, OH 45215
Attn T F Donohue

Pan American World Airways, Inc
JFK International Airport
Jamica, NY 11430
Attn J G Borger

United Airlines
San Francisco Int Airport
Maint Operations Cntr
San Francisco, CA 94128

Attn J J Overton

Brunswick Corporation
2000 Brunswick Lane
Deland, Florida 32720
Attn A Erickson

George Shevlin
P O Box 1925
Washington, DC 20013

Boeing Aerospace Co
P O Box 3999
Seattle, WA 98124
Attn D S Miller MS 40-26

Lockheed California Co
Burbank, CA 91502
Attn J I Benson

Gates Learjet Corp
P O. Box 7707
Wichita, KS 67277
Attn E Schiller

Gruman Aerospace Corp
South Oyster Bay Road
Bethpage, NY 11714
Attn C Hoeltzer

American Airlines
Maint & Engr Center
Tulsa, OK 74151
Attn W R Neeley

Pan American World Airways, Inc
JFK International Airport
Jamica, NY 11430
Attn A. MacLarty

General Electric Co /AEG
One Jimson Road
Evendale, OH 45215
Attn B L Koff

FluiDyne Engineering Corp
5900 Olson Memorial Highway
Minneapolis, MN 55422
Attn J S Holdhusen

University of Tennessee
Space Institute
Tullahoma, TN 37388
Attn Fr V. Smith

Gas Dynamics Laboratories
Aerospace Engineering Building
University of Michigan
Ann Arbor, MI 48109

Attn Dr C W Kaufmann

The Boeing Co , Wichita Div
Wichita, KS 67210
Attn D Tarkelson

General Dynamics Covair
P. O Box 80847
San Diego, CA 92138
Attn S Campbell, MZ 632-00

McDonnell Aircraft Co
McDonnel Douglas Corp
P O Box 516
St Louis, MO 63166

Attn F C Claser Dept 243

Eastern Airlines
International Airport
Miami, FL 33148
Attn A E Fishbein

Delta Airlines, Inc
Hartsfield-Atlanta Int Airport
Atlanta, GA 30320
Attn C. C. Davis

Hamilton Standard
Bradley Field
Windsor Locks, CT 06096
Attn P J Dumais, MS 1A-3-1

Rohr Corporation
P O Box 878 - Foot & H Street
Chula Vista, CA 92012
Attn Library

TRW Equipment Corp
TRW Inc
23555 Euclid Ave
Cleveland, OH 44117

Attn I Toth

Massachusetts Inst of Tech
Dept of Structural Mechanics
Cambridge, MA 02139
Attn James Mar

Lockheed California Co
Burbank, CA 91502
Attn J F Stroud, Dept 75-42

Boeing Aerospace Co
P O Box 3999
Seattle, WA 98124
Attn D S Miller MS 40-26

Lockheed Georgia Co
Marietta, GA 30060
Wichita, KS 67277
Attn E Schiller

Rockwell International
International Airport
Los Angeles Division
Los Angelos, CA 90009

Attn A W Martin

TransWorld Airlines
605 Third Avenue
New York, NY 10016
Attn A E. Carrol

Hamilton Standard
Bradley Field
Windsor Locks, CT 06096
Attn A T Reiff, MS 1-2-2

Solar Division
International Harvester
2200 Pacific Highway
San Diego, CA 92112 Library

Iowa State University
Dept of Mechanical Eng
Ames, Iowa 50011
Attn Dr. P Kavanagh

Massachusetts Inst of Tech
Dept of Astronautics and Aero
Cambridge, MA 02139
Attn Jack Kerrebrock

Penn State University
Dept of Aerospace Eng.
233 Hammond Building
University Park, Penn 16802
Attn Dr B Lakshminarayana

USAVRAD Command
PO BOX 209
ST Louis, MO 63166
Attn R M Titus (ASTIO)

Eustis Directorate
U S Army Mobility R&D Laboratory
Fort Eustis, VA 23604
Attn J Lane, SAVDL-EU-Tapp

Federal Aviation Administration
Noise Abatement Division
Washington, DC 20590
Attn J Woodhall

U S Naval Air Test Center
Code SY-53
Patuxent River, MS 20670
Attn E A Lynch

AiResearch Man Co
111 South 34th Street
PO Box 5217
Phoenix, Arizona 85010
Attention C E Corrigan
(93-120/503-4F)

Teledyne CAE, Turbine Engines
1330 Laskey Road
Toledo, OH 43612
Attn W Q Wagner

Williams Research Co.
2280 Maple Road
Walled Lake, MI 48088
Attn R Horn

AVCO/Lycoming
550 S Main Street
Stratford, CT 06497
Attn H Moellmann

Douglas Aircraft Co
McDonnell Douglas Corp
3655 Lakewood Boulevard
Long Beach, CA 90846

Attn R T Kawai, Code 36-41

Environmental Protection Agency
1835 K Street, NW
Attn J Tyler

Federal Aviation Administration
12 New England Executive Park
Burlington, MA 18083
Attn J A Sain, ANE-200

Naval Air Propulsion Test Center
Trenton, NJ 08628
Attn J J Curry

Environmental Protection Agency
2565 Plymouth Road
Ann Arbor, MI 48105
Attn R Munt

Cummins Engine Co Tech Center
500 S Poplar
Columbus, IN 47201
Attn J R Drake

The Garrett Corporation
AiResearch Manufacturing Co
Torrance, CA 90509
Attn F E Faulkner

General Electric Co /AEG
One Jimson Road
Evandale, OH 45215
Attn T Hampton (3 Copies)

General Electric Co /AFG
1000 Western Ave
Lynn, MA 01910
Attn R E Neitzel

The Garrett Corporation
AIResearch Aviation Co
19201 Susana Road
Compton, CA 90221 N J. Palmer

Douglas Aircraft Co
McDonnell Douglas Corp.
3655 Lakewood Boulevard
Long Beach, CA 90846

Attn M Klotzsche

NAVY Department
Naval Air Systems Command
Washington, D C 20361
Attn E A Lichtman, AIR-330E

Navy Department
Naval Air Systems Command
Washington, DC 20361
Attn W Koven, AIR-03E

Naval Air Propulsion Test Center
Trenton, NJ 08628
Attn A A Martino

Curtiss Wright Corporation
Woodridge, NJ 07075
Attn S Lombardo

Detroit Diesel Allison Div GMC
P O Box 894
Indianapolis, IN 46206
Attn W L McIntire

Williams Research Co
2280 W Maple Road
Walled Lake, MI 48088
Attn R Van Nimwegen

Boeing Commercial Airplane Co
P O Box 3707
Seattle, WA 98124
Attn D C Nordstrom

Pratt & Whitney Aircraft Group
Government Products Division
P O Box 2691
West Palm Beach, FL 33402

Attn B A Jones

Aerospace Corporation
R&D Center
Los Angeles, CA 90045
Attn Library

Pratt & Whitney Aircraft Group
400 Main Street
East Hartford, CT 06102
Attn Gardner (3 Cop) and Sons

NAVY Department
Naval Air Systems Command
Washington, D C 20361
Attn G Derderian, AIR-5362C

Navy Department
Naval Air Systems Command
Washington, DC 20361
Attn J L Byers, AIR-53602

Environmental Protection Agency
1835 K Street, NW
Washington, DC 20460
Attn J Schettino

Curtiss Wright Corporation
Woodridge, N J 07075
Attn S Moskowitz

Detroit Diesel Allison Div GMC
333 West First Street
Dayton, OH 45402
Attn F Walters

The Garrett Corporation
AiResearch Manufacturing Co
402 S 36 Street
Phoenix, AZ 85304

Attn F B Wallace

Boeing Commercial Airplane Co
P O Box 3707
Seattle, WA 98124
Attn P Johnson, MS 40-53

Westinghouse Electric Corp
P. O Box 5837
Beulah Road
Pittsburgh, PA 15236
Attn Library

End of Document